University of Southampton

Faculty of Natural & Environmental Sciences

School of Ocean & Earth Sciences

Particle Export and Flux Through the Mesopelagic in the High-Latitude North and South Atlantic

by

Patrick Martin

Thesis for the degree of Doctor of Philosophy

April 2011

UNIVERSITY OF SOUTHAMPTON

ABSTRACT

FACULTY OF NATURAL & ENVIRONMENTAL SCIENCES
SCHOOL OF OCEAN & EARTH SCIENCES

Doctor of Philosophy

PARTICLE EXPORT AND FLUX THROUGH THE MESOPELAGIC IN THE HIGH-LATITUDE NORTH AND SOUTH ATLANTIC

by Patrick Martin

The biological carbon pump (BCP) is a significant part of the global carbon cycle, exporting ∼10 Gt of particulate organic carbon (POC) out of the euphotic zone each year. However, most of the exported POC is remineralized biologically within the upper few hundred metres of the mesopelagic, above the permanent thermocline. Gaining more understanding of the factors controlling the BCP is hence important for understanding and predicting the global carbon cycle better. This thesis investigates the BCP in the Iceland Basin, and during an artificial ocean iron fertilisation experiment in the South Atlantic.

In the Iceland Basin, export during a spring diatom bloom was tracked using Lagrangian sediment traps and thorium-234 disequilibria. A large pulse of diatom detritus was exported suddenly at the end of the bloom, probably upon impending Si-limitation. The particles were rich in transparent exopolymer particles (TEP, sticky polysaccharides secreted by phytoplankton), and a comparatively large proportion (20–40%) of the exported POC sank past 750 m. This shows that diatom blooms can produce rapid pulses of particle sedimentation that are transferred efficiently through the mesopelagic, and suggests that aggregation and sinking are mediated by TEP.

In contrast, alleviating iron limitation in low silicic acid waters of the South Atlantic with very high copepod grazing pressure only caused a modest phytoplankton response and no enhancement of downward particle flux. This was probably primarily due to grazing control and detritus-feeding by copepods, since diatom growth rates were apparently not strongly Si-limited. This suggests that future Fe-fertilisation experiments must investigate the role of zooplankton thoroughly to distinguish beween bottom-up control of export by nutrient concentrations and top-down control by zooplankton. Export measurements based on thorium-234 disequilibria compared well with net community production measured by O_2:Ar ratios over the 39 d experiment, suggesting that these two methods can be meaningfully compared over ∼month-long cruises.

Further work was conducted with a mesoscale array of four time-series sediment traps deployed for eight moths in the Iceland Basin to study particle flux at 2000 m. Large, fast-sinking acantharian cysts contributed up to 48% of POC flux during a specific flux event in early spring, demonstrating that the celestite shells of these protists do not necessarily dissolve in the upper mesopelagic as generally believed. The hypothesis is advanced that deep sinking of acantharian reproductive cysts during spring in this region enables juveniles to feed off seasonally sedimenting phytodetritus in the deep-sea.

Finally, the full time-series of particle flux in the four deep traps was analysed. Fluxes peaked in late spring and again in mid-summer. Over the eight months, cumulative mass flux varied by 30% between traps without corresponding variation in the cumulative flux of thorium-230, implying genuine mesoscale variability in bathypelagic particle flux. Moreover, during any one of the two-week collection intervals total mass flux of particles varied 2–16-fold between traps, although it is unclear how much of this short-term variability was due to differences in collection efficiency between traps. Overall, the traps probably under-collected thorium-230 in absolute terms by at least 50%, but this estimate is very uncertain.

Contents

List of Figures

List of Tables

Declaration of Authorship

I, Patrick Martin, declare that the thesis entitled "*Particle Export and Flux Through the Mesopelagic in the High-Latitude North and South Atlantic*" and the work presented in the thesis are both my own, and have been produced by me as the result of my own original research. I confirm that:

- This work was done wholly or mainly while in candidature for a research degree at this University
- Where any part of this thesis has previously been submitted for a degree or any other qualification at this University or any other institution, this has been clearly stated
- Where I have consulted the published work of others, this is always clearly attributed
- Where I have quoted from the work of others, the source is always given. With the exception of such quotations, this thesis is entirely my own work
- I have acknowledged all main sources of help
- Where the thesis is based on work done by myself jointly with others, I have made clear exactly what was done by others and what I have contributed myself
- Parts of this work have been published as:
  - **Martin P.**, Allen J.T., Cooper M.J., Johns D.G., Lampitt R.S., Sanders R., Teagle D.A.H. (2010). Sedimentation of acan- tharian cysts in the Iceland Basin: Strontium as a ballast for deep ocean parti- cle flux, and implications for acantharian reproductive strategies. *Limnology & Oceanography*, *55*(2), 604–614.
  - **Martin P.**, Lampitt R.S., Perry M.J., Sanders R., Lee C., D'Asaro E. (2011). Export and mesopelagic particle flux during a North Atlantic spring diatom bloom. *Deep-Sea Research I*, *58*, 338-349, doi:10.1016/j.dsr.2011.01.006

Signed:

Date:

Acknowledgements

First of all, I would like to thank my supervisors, Richard Lampitt and Richard Sanders, for all the advice, motivation, inspiration, and help they gave me, and for all the many things they have taught me over the past four years. They were always ready to devote time to me when I needed it. I am also grateful to them for giving me as much freedom as I could possibly have wanted to pursue my own ideas, and for encouraging me to do so.

Paul Morris, Ian Salter, Corinne Pebody, Mark Stinchcombe, Darryl Green, Matt Cooper, and Bob Head all helped with different aspects of lab work and took time to explain and discuss analytical and sample-handling questions.

I am particularly grateful to everyone who helped me set up the $^{230}\mathrm{Th}\,/\,^{231}\mathrm{Pa}$ technique at NOCS. Alfred Aquilina invested a lot of time and effort in the undertaking, even though it felt like a wild goose chase for much of the time; without him, it would probably have been one. Rachel Mills oversaw the project, and her advice and encouragement helped greatly. I am also especially indebted to Andy Milton, who took a lot of time with Alfred and me to set up the mass spectrometry methods and went out of his way to teach me a lot about mass spectrometry. Finally, the project would never have got off the ground without the help of Alex Thomas, Gideon Henderson, and Ben Hickey, who taught me the basics during a highly enjoyable month's visit to Oxford, and answered even the most obvious of my many questions.

Kevin Saw designed and built the PELAGRA traps with Richard Lampitt, and joined me on two cruises to take care of the complex and labour-intensive technical side of deploying them. His efforts ensured many successful PELAGRA deployments, and working together with Kevin was one of the highlights of those cruises, as was unwinding together in Patagonia after LohaFEX.

I would also like to thank the principle scientists of the cruises that contributed to my thesis (John Allen: D321; Mary Jane Perry: NAB'08 on R/V *Knorr*; Victor Smetacek and Wajih Naqvi: LohaFEX on FS *Polarstern*), as well as all the participants, and the captain and crew of each ship, who made the cruises such successful and very enjoyable expeditions.

I am grateful to all developers of LyX for providing such a fantastically easy-to-use GUI front-end for LaTeX, which made writing this thesis far easier — though I have been left with a worrying degree of appreciation for things like thin spaces.

Last, but certainly not least, I would like to thank my family and S. S. T for their help and support.

Abbreviations

BSi	Biogenic silicon (diatom opal-derived Si)
BOS	Biological oxygen saturation
CTD	Conductivity, Temperature, Depth; usually refers to the Niskin rosette used for water sampling, which has an on-board CTD sensor
dpm	Disintegration per minute ($=\frac{1}{60}$ Becquerel); units in which ^{234}Th activity is reported
DIC	Dissolved inorganic carbon
DOC	Dissolved organic carbon
DOM	Dissolved organic matter
FeAX	Artificial iron fertilisation experiment
GX eq	Gum Xanthan equivalents; units in which TEP are measured
ICP-MS	Inductively-coupled plasma mass spectrometer
ICP-OES	Inductively-coupled plasma optical emission spectrometer
MilliQ	Ultra-pure deionised water with conductivity of $18.2\,\mathrm{M\Omega\,cm^{-1}}$
NCP	Net community production ($=$ Net primary production $-$ heterotrophic respiration)
NPP	Net primary production ($=$ Gross primary production $-$ autotrophic respiration)
PIC	Particulate inorganic carbon (only the carbon in $CaCO_3$)
POC	Particulate organic carbon
POM	Particulate organic matter
PON	Particulate organic nitrogen
RSD	Relative standard deviation ($\frac{\text{Standard deviation}}{\text{Mean}}$)
T_{eff}	Transfer efficiency of particle flux ($\frac{\text{deep particle flux}}{\text{shallow particle flux}}$)
TEP	Transparent exopolymer particles; acidic polysaccharides that bind Alcian Blue
^{230}Th; ^{234}Th	Naturally-occurring isotopes of thorium, produced *in situ* from ^{238}U
^{238}U	The most abundant isotope of uranium, occurs naturally in seawater and is conservative

Chapter 1

Introduction

1.1 The Biological Carbon Pump

1.1.1 Role in the global carbon cycle

The oceans play a major role in the carbon cycle, accounting for half the world's photosynthesis and acting as a net sink for anthropogenic CO_2. Human activity since the Industrial Revolution has raised the atmospheric CO_2 concentration from 280 ppmv to 390 ppmv, and anthropogenic CO_2 emissions are currently $\sim$8.5 Pg C y^{-1} (*Friedlingstein et al.* 2010), with profound implications for global climate (*IPCC* 2007). The net ocean sink for CO_2 is around 2.2 Pg C y^{-1} (*Takahashi et al.* 2002; *IPCC* 2007 [p. 511 ff.]), and the main regions for uptake of anthropogenic CO_2 are the North Atlantic and the Southern Ocean between about 50°S and 30°S (*Sabine et al.* 2004). Two main processes are responsible for oceanic CO_2 uptake, the Solubility Pump and the Biological Carbon Pump (*Volk and Hoffert* 1985). The former is the physical dissolution of CO_2 into the ocean, and is currently a net sink due to the anthropogenic increase in atmospheric CO_2. However, it appears as though the ocean sink due to the Solubility Pump may decrease in future (*IPCC* 2007 [pp. 511 ff.]; *Le Quéré et al.* 2007).

The Biological Carbon Pump (BCP), or Soft Tissue Pump, refers to the downward sinking of particulate organic carbon (POC) in the ocean. Throughout the sunlit region of the ocean, the euphotic zone, primary production by phytoplankton lowers fCO_2 and builds up biomass. Most of the biomass is turned over and respired within the euphotic zone, but a small proportion sinks down into intermediate and deep waters as organic particles, and a very small fraction is ultimately buried in deep-sea sediments (*Hedges and Keil* 1995; *Boyd and Trull* 2007). Most of the particles sinking out of the euphotic zone are remineralized by heterotrophic organisms in intermediate and deep waters, which increases the concentrations of CO_2 and nutrients in deeper water masses. This CO_2 is ultimately returned to the atmosphere over the time-scales of ocean mixing (1–1000 y, depending on depth and region), and thus the BCP is currently balanced by the flux of CO_2 back to the atmosphere due to upward transport of deep water, and is not a net sink for CO_2 (*Sarmiento and Gruber* 2006 [pp. 352 ff.]).

While most POC that sinks out of the euphotic zone is thus ultimately returned back to the atmosphere as CO_2, the depth to which the particles sink before being remineralized is very important, as this governs how soon the CO_2 will equilibrate with the atmosphere again. At the high latitudes that are the subject of the present work, the water column stratifies thermally in spring yielding a shallow surface layer that is mixed by winds, and in which primary production occurs over the growing season (often 50–100 m deep initially, and typically stratifying further over the course of the summer). Stratification breaks down again in autumn as the surface layer cools, and convective mixing then takes place from the surface down to the permanent thermocline, establishing the winter mixed layer. Any POC that is remineralized above the depth of winter mixing thus equilibrates again with the atmosphere within at most a year. Conversely, any POC that sinks below the winter mixed layer can only return to the surface on the time-scales of the global thermohaline circulation, usually 100–1000 y (depending on depth and region). The depth of winter mixing varies substantially between regions, and is usually around 1000 m in the temperate and sub-polar North Atlantic (the study site for Chapters 2, 4, and 5), but typically 200–400 m in the Antarctic Polar Frontal Zone (the study site for Chapter 3). In the southern portions of the sub-tropical gyres, the surface ocean tends to be stratified permanently, so particles need to sink only below the upper ∼200 m to be removed from contact with the atmosphere over time-scales of the global thermohaline circulation.

From the point of view of the global carbon cycle, an important distinction therefore needs to be made between particles sinking out of the surface layer of the ocean, and particles sinking past the permanent thermocline. In this study, the flux out of the surface layer will be referred to as "export", while the flux past the permanent thermocline will be termed "sequestration" flux. Two further terms that need defining: "mesopelagic" will here refer to the region located between 100 m and 1000 m, and "bathypelagic" will refer to depths deeper than 1000 m.

Export flux is often measured (or, with models, calculated) at a fixed depth of 100 m. This practice was criticised by *Buesseler and Boyd* (2009), who suggested that export flux should instead be defined as the flux at the base of the euphotic zone (the depth of 1% or 0.1% light penetration), which more accurately represents the depth over which primary production takes place. As the euphotic zone can vary in depth from ∼50 m during phytoplankton blooms to ∼150 m in the oligotrophic ocean gyres (where a significant proportion of phytoplankton biomass may occur as a deep chlorophyll maximum at the base of the euphotic zone, *Cullen* 1982), varying the depth at which export flux is measured is doubtless preferable on theoretical grounds. As shown by *Buesseler and Boyd* (2009), accounting for this variability is potentially very important if particle fluxes are to be compared meaningfully between high and low latitudes. For the present work, export flux was still measured at 100 m depth, but as both study sites were located at high latitudes with similar mixed layer and euphotic zone characteristics, this should not add particular complications in the present case.

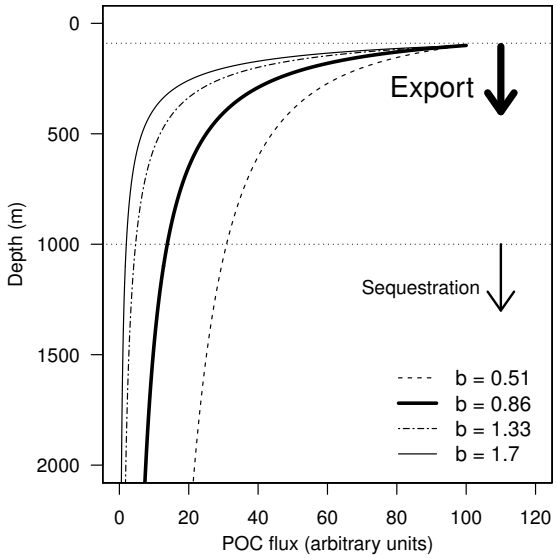

Figure 1.1 – Example of the decrease in POC flux with depth using Equation 1.1 after *Martin et al.* (1987), with four different values for the exponent b taken from the literature (from lowest to highest b: *Buesseler et al.* 2007b; *Martin et al.* 1987; *Buesseler et al.* 2007b; *Lampitt et al.* 2008b). The depth horizons at 100 m and 1000 m indicate the difference between export flux and sequestration flux (depths as appropriate for the temperate and sub-polar North Atlantic).

1.1.2 Attenuation of flux with depth

Particle flux decreases rapidly with depth. One of the most commonly used descriptions is the power-law introduced by *Martin et al.* (1987), based on sediment trap data from the sub-tropical Pacific:

$$F_z = F_{z_0} \left(\frac{z}{z_0} \right)^{-b}, \tag{1.1}$$

where F_z is the POC flux at depth z, F_{z_0} is the flux at an arbitrary reference depth z_0 (often export flux at 100 m), and b is a unitless parameter whose magnitude describes how heavily the flux is attenuated with depth (*Martin et al.* (1987) found $b = 0.858$). While other formulations have since been proposed to fit deep ocean POC fluxes better (*e.g. Armstrong et al.* 2002; *Lutz et al.* 2002), and it has long been known that no single b-value accurately describes the attenuation of flux with depth (*Berelson* 2001), it is still a useful approximation to illustrate how flux changes with depth. An example is shown in Figure 1.1, which also indicates the distinction between export and sequestration flux (with depths chosen as appropriate for the temperate and sub-polar North Atlantic). Clearly, export and sequestration flux can differ strongly, depending on how heavily flux is attenuated with depth — and the range of b-values reported in the literature for different regions at different times varies substantially, from around 0.5 (*Buesseler et al.* 2007b; *Martin et al.* 2011) to 1.7 (*Lampitt et al.* 2008b), which would correspond to a fifteen-fold difference in flux at 1000 m starting from an equal export flux.

Estimates from a range of models agree that global export via the BCP is around $10\,\mathrm{Pg\,C\,y^{-1}}$ (*Dunne et al.* 2007), although *Henson et al.* (2011) estimated just $5\,\mathrm{Pg\,y^{-1}}$. $<1\,\mathrm{Pg\,C\,y^{-1}}$ ultimately sinks below 1000–2000 m (*Lampitt and Antia* 1997; *Dunne et al.* 2007; *Honjo et al.* 2008). While the BCP does not currently contribute to net sequestration of atmospheric CO_2, any change in its strength could impact atmospheric CO_2 concentration significantly by changing the amount of dissolved inorganic C (DIC) stored in the deep ocean. For instance, *Kwon et al.* (2009) showed with a model that if the depth at which particle flux is reduced to $\frac{1}{e}$ of the initial export flux were to deepen by a global average of 24 m, the atmospheric CO_2 concentration could drop by 10–27 ppmv (this would correspond to a change in b in Equation 1.1 from 1.0 to 0.9). On the other hand, when primary productivity and export flux completely ceased in a global model (in this case by removing all aeolian iron supply), atmospheric CO_2 increased by 170 ppmv (*Parekh et al.* 2006). Although neither case is necessarily a realistic future scenario, these studies highlight the importance of understanding the functioning of the BCP for understanding and predicting atmospheric CO_2 concentrations under future climate change. The two key questions that need to be investigated are hence:

1. What controls the magnitude of export flux in different regions / at different times?
2. What controls the degree of flux attenuation with depth, and thus the sequestration flux, in different regions / at different times?

The attenuation with depth is caused by microbial consumption and solubilisation, zooplankton feeding, and dissolution. Microbial degradation of particles takes place particularly via ectohydrolase activity, solubilising POM and releasing it to the surrounding water (*e.g. Smith et al.* 1992). While this in itself is obviously not remineralization, dissolved organic matter can then be respired by free-living microbes (*Cho and Azam* 1988), and in any case is registered as a decrease in particulate flux. Dissolution of diatom opal is in fact also mediated by bacteria, as they remove the organic coatings that surround the frustules (*Bidle and Azam* 1999, 2001). Zooplankton are also known to feed off detritus in the mesopelagic (*Lampitt et al.* 1993; *Steinberg* 1995), but the relative role of zooplankton *versus* microbial remineralization is still unclear. Disconcertingly, *Steinberg et al.* (2008) found that the carbon demand in the mesopelagic by both bacteria and zooplankton exceeded carbon supply to the mesopelagic by sinking particles several-fold. The authors attributed this discrepancy to a combination of vertically-migrating zooplankton and zooplankton carnivory, though temporal offsets in carbon supply and consumption might also be involved. While all these processes are already known to be potentially important, it is clearly very challenging to determine their relative magnitude even in just one region.

The discussion so far has focussed exclusively on particles, although dissolved organic matter (DOM) may play an important role as well. Some tens of percent of phytoplankton production can be excreted by cells as dissolved organic carbon, DOC (*Lancelot* 1979; *Biddanda and Benner* 1997), and viral lysis of phytoplankton (and of other cells) can additionally be an important source of DOC and a significant pathway of mortality (*Bratbak et al.* 1993; *Baudoux et al.* 2007; *Suttle* 2007). Much of the DOC is labile and is taken up and respired by microbes (*e.g. Amon et al.* 2001), but some is less readily metabolised, and labile carbon can also eventually be

channelled into the pool of refractory DOC by microbial metabolism. This has been termed the "microbial carbon pump" (*Jiao et al.* 2010), and the flux through it into the long-lived, recalcitrant DOC pool needs to be studied further. Moreover, labile DOC can also be exported to deeper waters by vertical mixing and deep water formation; this fraction of carbon export is obviously not captured by sediment traps or particle-reactive radionuclide-based methods. However, while DOC is certainly an important part of C export, the present work focuses specifically on the flux of particulate C.

1.2 Controls on the BCP

1.2.1 Supply of nutrients

The supply of macro- and micronutrients exerts a primary control on phytoplankton production throughout the oceans, and thus impacts the magnitude of export production. Phytoplankton production in much of the oceans is limited by nutrient availability, usually by N or Fe (*Falkowski et al.* 1998; *Tyrrell* 1999), and overall, regions of low primary production are also regions of low particle export. However, while early models of the BCP expressed particle flux as a function of net primary productivity (NPP; *Suess* 1980; *Pace et al.* 1987), this is no longer considered to be a reliable global predictor of particle flux (*Lampitt and Antia* 1997; *Boyd and Trull* 2007). For instance, a recent modelling study found that future warming might increase NPP, with direct temperature effects on phytoplankton physiology and microbial nutrient recycling outweighing the reduction in new nutrient supply due to stronger stratification, but that export production decreased, being tied strongly to the supply of new nutrients (*Taucher and Oschlies* 2011).

Since export of biogenic particles removes not just carbon but also nutrients from the surface, the amount of particle export is limited to the amount of production sustained by the annual supply of N to the euphotic zone. P is rarely a limiting nutrient (*Tyrrell* 1999): while P limitation was reported for the North Pacific sub-tropical gyre by *Karl et al.* (1995), this appears to have been a temporary condition (*Van Mooy and Devol* 2008). The production sustained by annual N supply is termed "new production" (*Dugdale and Goering* 1967), and is based on supply of NO_3^- from below the seasonal thermocline and biological fixation of N_2. Recycling of newly-produced biomass by microbial and zooplankton activity in the surface layer can remineralize a substantial amount of nutrients, which are then available again to fuel more primary production. However, such a recycling system cannot sustain a high rate of export relative to total NPP, as the necessary N would be removed from the surface. Moreover, the relative role of regenerated *versus* new production (described by the f-ratio, where $f = \frac{\text{new production}}{\text{total production}}$, *Eppley and Peterson* 1979) is highly variable regionally, with high-latitude, seasonal environments having several-fold higher f-ratios than the sub-tropical gyres (*Laws et al.* 2000). Even within a region the f-ratio can vary seasonally: in the Irminger Basin, and presumably in much of the sub-polar North Atlantic, the majority of annual new production takes place during the diatom-dominated spring bloom, with production during the summer more heavily reliant on regenerated nitrogen (*Henson et al.* 2006; *Sanders et al.* 2005).

If nutrients and C were always taken up at a fixed ratio by primary producers, and remineralized at the same ratio, then the BCP could not be a large longer-term net sink for C, as nutrients would be depleted very soon and prevent further export. While it was originally proposed that the C:N:P stoichiometry of planktonic production and remineralization was approximately constant at a molar ratio of 106:16:1 (*Redfield et al.* (1963); now termed the "Redfield ratio"), it has since become apparent that the stoichiometry of production can deviate significantly from this ratio (*e.g. Weber and Deutsch* 2010). And importantly for the BCP, the nutrients N and P are usually preferentially remineralized over C, so the C:N ratio of POM increases with depth (*Copin-Montegut and Copin-Montegut* 1983; *Loh and Bauer* 2000; *Schneider et al.* 2003), and the re-supply of nutrients to the surface layer by vertical mixing is not offset entirely by re-supply of DIC (*Christian et al.* 1997). Preferential sequestration of C relative to nutrients is thus possible, with nutrients that are sequestered long-term being replaced by biological N_2 fixation and chemical weathering / riverine input.

The availability of Si exerts additional control on export production, though not necessarily on overall NPP, as it is required by diatoms to construct their opaline frustules. In temperate and sub-polar regions, ample Si is available at the start of the growing season following winter convective mixing, and spring phytoplankton blooms in these regions tend to be dominated by diatoms. Diatoms are often thought to contribute disproportionately to export production (*Dugdale et al.* 1995; *Buesseler* 1998; *Boyd and Newton* 1999; *Salter et al.* 2007), with substantial export occurring during the late phase of a bloom (*Buesseler et al.* 1992, 2001). The availability of Si relative to other nutrients may thus contribute to controlling the magnitude of export flux; moreover, it appears as though the presence of biominerals in particles might enhance POC export (see Section 1.2.4).

There is thus no global relationship between particle export and nutrient supply / NPP. However, nutrient supply certainly does matter for export: for instance, additional supply of nutrients by mesoscale eddies and fronts can enhance phytoplankton production and enhance the export flux of at least some biogenic phases (enhancement of opal, though not POC, flux was recorded by *Buesseler et al.* (2008) and *Maiti et al.* (2008) inside eddies, while *Peinert and Miquel* (1994) found enhanced POC flux due to a front).

It is now also recognised that large areas of the ocean are limited by the micronutrient Fe, especially the Southern Ocean (*de Baar et al.* 2005; *Boyd et al.* 2007). These areas have been termed "High Nutrient – Low Chlorophyll", or HNLC, regions, because of their perennially high concentrations of the macronutrients N and P, and in many cases also Si. Fe thus appears to limit new production in these areas, and one might hence expect that supplying more Fe to these regions would enhance export (this is in fact being discussed as a possible geoengineering method, see *Lampitt et al.* 2008a; *Lenton and Vaughan* 2009). On balance, it appears as though export would indeed be enhanced by alleviating Fe limitation in some Fe-limited regions (*de Baar et al.* 2005; *Blain et al.* 2007; *Boyd et al.* 2007; *Pollard et al.* 2009). However, many complicating factors appear to act on the BCP, such as the composition of the phytoplankton and zooplankton community (*Boyd and Trull* 2007; *Lam and Bishop* 2007; *Buesseler and Boyd* 2009), interactions between Fe and organic ligands that mediate Fe bioavailability (*Parekh et al.*

2006), and the potential at high latitudes for photosynthesis to become light limited (*de Baar et al.* 2005; *Dutkiewicz et al.* 2006; *Parekh et al.* 2006).

Overall then, the availability and stoichiometric ratios of nutrients set important boundary conditions on the level of export that can be sustained in a given region, and influence the community composition of the phytoplankton.

1.2.2 Phytoplankton community composition and the role of zooplankton

The taxonomic composition of the phytoplankton community exerts a major control on the BCP by governing the structure of the pelagic food web and thus influencing the type of particles that form. Zooplankton were originally thought to be responsible for virtually all downward particle flux by packaging small, slowly-sinking particles into fast-sinking faecal pellets — individual phytoplankton cells, for instance, mostly sink $<$1–10 m d^{-1} (*Smayda* 1970; see review by *Turner* 2002). However, it is now clear that rapid sinking of ungrazed phytoplankton aggregates can also occur, and play a large role in the BCP (*Billett et al.* 1983; *Beaulieu* 2002; *Thornton* 2002; *Turner* 2002). Overall, the BCP is strongly influenced by complex interactions between phytoplankton and zooplankton, with nutrient concentrations influencing the phytoplankton community, which in turn influences the zooplankton community — but the zooplankton community composition can then feed back on the phytoplankton, and substantially modulate the amount of export (*Wassmann* 1998; *Smetacek et al.* 2004).

Photosynthesis in nutrient-poor regions such as the sub-tropical gyres or the Fe-limited Southern Ocean is dominated by pico- and nanophytoplankton ($<$20 µm diameter), as their high $\frac{\text{surface area}}{\text{volume}}$ ratios enable faster nutrient uptake per unit biovolume. Much of their production is thought to be processed by the microbial food web, passing through 1–3 additional trophic levels (bacteria and microzooplankton) before being accessible to crustacean (primarily copepod) grazing, and these microbial levels are likely to remineralize the majority of the NPP (*Azam et al.* 1983; *Fenchel* 2008). Such low-nutrient, picophytoplankton-dominated systems with high microzooplankton grazing pressure do not build up high levels of biomass; hence no substantial export via phytodetrital aggregates occurs, and export overall is low (*Passow and Peinert* 1993).

In contrast, nutrient-replete conditions allow for high biomass accumulation, and larger microphytoplankton cells ($\geq$20 µm diameter), such as diatoms, can form large blooms — presumably because cells of this size are under less grazing pressure, at least temporarily, than the smaller size-classes (*Smetacek et al.* 2004). In the temperate and sub-polar North Atlantic, large diatom blooms occur in spring that collapse upon Si-limitation (*Sieracki et al.* 1993; *Leblanc et al.* 2005), and can lead to phytodetrital aggregates with intact diatom cells sinking several kilometres to the seafloor (*Billett et al.* 1983). Accumulation of phytodetrital "fluff" on the seafloor has now been documented from a range of locations — although invariably in regions where the magnitude of particle flux is highly seasonal — with diatoms and coccolithophores contributing substantially in many instances (*Beaulieu* 2002). Bloom-forming diatoms in particular are noted for their ability to adhere to each other and form aggregates, which can have sinking rates of $\geq$100 m d^{-1} (*Kranck and Milligan* 1988; *Alldredge and Gotschalk* 1989; *Thorn-*

ton 2002); this is also reported for coccolithophores (*Cadée* 1985). Such ungrazed aggregates probably contribute significantly to annual POC export (*Thornton* 2002; *Smetacek et al.* 2004). In the Fe-replete Southern Ocean, however, diatom blooms can also be heavily grazed by krill, leading to high POC export in form of faecal strings — although such heavy grazing might reduce the export of ungrazed diatom aggregates (*von Bodungen* 1986; *Le Fèvre et al.* 1998; *Smetacek et al.* 2004).

Zooplankton are thus not responsible for all global POC export, although they invariably contribute some proportion of export, and sometimes all or the majority. Besides faecal material, discarded pteropod feeding nets and larvacean houses can also make significant contributions to flux (*Davoll and Youngbluth* 1990; *Bathmann et al.* 1991; *Kiørboe et al.* 1996), potentially during specific flux events that are readily missed by ship-board sampling, and the overall significance of which is thus particularly difficult to quantify. Salps are very efficient at filtering particles as small as $<1\,\mu m$ diameter (*Sutherland et al.* 2010), and their compact faecal pellets, which can sink kilometres per day (*Caron et al.* 1989), can cause large POC fluxes during mass salp occurrences. *Ramaswamy et al.* (2005) attributed fluxes of $100 s\,mg\,m^{-2}\,d^{-1}$ to salps in the Arabian Sea, and *Phillips et al.* (2009) report fluxes of $10 s\,mg\,m^{-2}\,d^{-1}$ due to salps in the Southern Ocean. By thus packaging large quantities of very small particles, they probably genuinely enhance POC export, and reduce mesopelagic remineralization.

However, zooplankton can also retard particle flux. Copepods have been shown to break apart copepod faecal pellets very effectively, but to ingest only a small portion of each pellet, yielding fragments with lower sinking speed that would be much more vulnerable to microbial degradation (*Lampitt et al.* 1990; *Noji et al.* 1991; *Iversen and Poulsen* 2007). Copepod faecal pellets are hence usually thought not to contribute much downward particle flux (*Le Fèvre et al.* 1998; *Turner* 2002), even when faeces of other zooplankton are contributing the bulk of sinking particles (*González et al.* 2000, 2004). Some zooplankton taxa also engage in "flux feeding" below the surface mixed layer, for instance some copepods and pteropods (*e.g. Jackson* 1993; *Gowing and Wishner* 1998). The effect of such a re-processing community on particle flux is complex: re-packaging of slowly sinking or non-sinking particles into faster-sinking faecal pellets could enhance fluxes (*Gowing and Wishner* 1998). Conversely, if the re-processing community is feeding off already fast-sinking faecal material such as krill faecal strings, the net effect would be a reduction in flux (*Lam and Bishop* 2007).

Additionally, zooplankton can contribute to export by diel and seasonal / ontogenetic vertical migrations; this is termed "active" flux to distinguish it from the flux of passively sinking particles. Respiration, excretion, and mortality at depth by diel vertically-migrating zooplankton can amount to 30–50% of the passive flux in oligotrophic conditions (*Al-Mutairi and Landry* 2001; *Yebra et al.* 2005). In high-latitude settings with higher passive flux, the active contribution would probably be less (*Al-Mutairi and Landry* 2001), and indeed, flux due to faecal production at depth was estimated at <5% of sediment trap-derived POC flux in the north-east Atlantic, although respiratory flux was not considered (*Lampitt et al.* 1993). Ontogenetic vertical migrations by certain copepod species (adults of which migrate downward to over-winter and reproduce at depth, and then die there) were found to nearly double the passive POC flux at 1000 m in the sub-arctic Pacific (*Kobari et al.* 2003, 2008). This might hence be a very im-

portant phenomenon in some regions, but is not captured by thorium-based export estimates, and is very difficult, if not impossible, to distinguish from "swimmer" contamination in sediment traps (see Appendix A.1).

1.2.3 The importance of TEP

While some zooplankton faecal material is relatively compact, *e.g.* covered by a membrane, physically-driven aggregation of particles requires a sticky substance. Transparent exopolymer particles, TEP, provide this stickiness and marine snow particles without a TEP matrix have not yet been found (*Passow* 2002). TEP are acidic polysaccharides that bind the stain Alcian Blue, and are excreted by diverse groups of phytoplankton and even bacteria (*Passow* 2002). They are found particularly during phytoplankton (especially diatom) blooms, and their stickiness appears to be the factor that allows aggregation to occur (*Passow and Alldredge* 1994; *Passow et al.* 1994; *Mari and Kiørboe* 1996). Interestingly, TEP themselves were found in one study to be positively buoyant, so a TEP-rich aggregate would need to contain enough particles denser than seawater to sink (*Azetsu-Scott and Passow* 2004).

There is overall relatively good evidence that TEP are necessary for mass aggregation and hence for mass sinking of ungrazed diatom detritus (*Passow et al.* 1994; *Alldredge et al.* 1995; *Logan et al.* 1995; *Kiørboe et al.* 1996), but TEP are not required at some fixed ratio to total mass for the BCP to operate (*Passow et al.* 2001). Clearly, the importance of TEP will depend on the types of sinking particles, and will thus show large regional and temporal variation. The greatest difference is likely to be between fluxes that are heavily dominated by zooplankton faecal material (probably little TEP) and fluxes that consist primarily of ungrazed phytodetritus / marine snow that has physically aggregated by particles colliding (probably rich in TEP). There appear to be only three studies of downward TEP flux at present (one of which is the work presented in Chapter 2), and more such measurements are needed from a range of different planktonic communities to really understand the role that TEP play in the BCP.

It is also still unclear why phytoplankton produce TEP. Mass sinking of diatoms has been interpreted as an adaptive response to escape from a nutrient-depleted euphotic zone (*Smetacek* 1985), and the data in Chapter 2 are consistent with this view. However, TEP are produced by such a great taxonomic and functional diversity of organisms that TEP might have diverse ecological roles (*e.g.* protection from grazing, *Malej and Harris* 1993). Evidence is also emerging that TEP production may depend on interactions between phytoplankton and bacteria (*Gärdes et al.* 2011).

1.2.4 The ballast hypothesis

Armstrong et al. (2002) advanced a model of downward POC flux in which one fraction of sinking POC was physically protected from degradation by association with minerals, and the remaining unprotected pool decayed exponentially; the model fit observed POC fluxes in several regions very well. There is chemical evidence for strong protection of marine organic compounds by minerals (*Hedges et al.* 2001; *Hedges and Keil* 1995; *Rothman and Forney* 2007), and *Boyd*

and Trull (2007) point out the advantage that this "ballast model" is simple by assuming first-order decay, rather than power-law behaviour.

Klaas and Archer (2002) then investigated the link between POC and mineral flux in a global bathypelagic sediment trap data set using multiple regression analysis. They concluded that 80% of annual POC flux was carried by $CaCO_3$, and calculated that ballasting by $CaCO_3$, because of its higher density, could result in 50% greater sinking speed compared to ballasting by opal.

François et al. (2002) combined a global dataset of annual sediment trap fluxes at >2000 m with satellite-derived estimates of annual export flux above each trap to calculate the transfer efficiency, T_{eff} ($T_{\text{eff}} = \frac{\text{export flux}}{\text{sediment trap flux}}$). Using multiple regression analysis to test the effect of $CaCO_3$, opal, and lithogenic flux on T_{eff} they found that T_{eff} was most closely related to the $CaCO_3$ flux, with opal and lithogenic flux exerting only a small, and in fact negative, effect. They concluded that T_{eff} was low in high-latitude diatom-dominated systems and high in low-latitude $CaCO_3$-dominated regions, for which they proposed three, potentially interacting, reasons:

1. Particles might sink faster if ballasted by $CaCO_3$
2. Particles at low latitudes might be packaged more tightly into fast-sinking faecal pellets (indeed, *Fischer and Karakaş* (2009) present observational evidence that particles in a carbonate-dominated region do sink faster)
3. Organic matter in phytodetrital aggregates sinking out of diatom blooms might be more labile

François et al. (2002) did openly acknowledge that if they had systematically under-estimated export at low latitudes (or over-estimated at high latitudes), their conclusions could be wrong. The export algorithm they used was taken from *Laws et al.* (2000), which probably does over-estimate export at high latitudes (*Henson et al.* 2011). However, using a more realistic export algorithm and a larger sediment trap database, *S. Henson et al.* (in prep.) obtained comparable results.

Based on the factors by which Si:POC ratios increase between production by diatoms at the surface and catches in sediment traps at 1000 m across different regions (data from *Ragueneau et al.* 2002), *Ragueneau et al.* (2006) also concluded that a large proportion of the POC produced by diatoms is remineralized either in the surface before being exported, or otherwise in the mesopelagic. They suggested that the greater activity of meso- and macrozooplankton in the mesopelagic at higher latitudes, and greater lability of fresh diatom detritus exported in these areas, might account for the high remineralization.

Ragueneau et al. (2006) also showed that the globally weak relationship between POC flux and opal flux in sediment traps is due to the greater variation between ocean basins in this relationship, yielding a solid, but different, relationship for each basin — whereas the relationship between POC flux and $CaCO_3$ flux is mostly identical across all the regions. Ultimately, they concluded that what is needed is not a search for a global descriptor of POC flux, but that future studies should examine what controls the regional and temporal variability in the

importance of different ballast phases or particle types, and how that affects the magnitude and efficiency of the BCP.

Nevertheless, the question of the relative global role of opal and $CaCO_3$ in ballasting POC has important implications for the BCP on geological time-scales: production and sinking of $CaCO_3$ produce CO_2 and remove alkalinity from the surface ocean (where $\frac{\text{released } CO_2}{\text{precipitated } CaCO_3} = 0.67\,\text{mol}\,\text{mol}^{-1}$, *Frankignoulle and Canon* 1994). Whether the $CaCO_3$:POC ratio in the BCP is relatively fixed or variable hence has implications for the possible role of the BCP in influencing atmospheric CO_2 concentration (*Archer and Maier-Reimer* 1994; *Klaas and Archer* 2002), besides having implications for the possible effects of ocean acidification on the BCP (*Barker et al.* 2003).

However, the association between POC flux and mineral fluxes can also be interpreted in reverse, *i.e.* that the magnitude of POC flux determines the magnitude of mineral flux (*Passow* 2004). Laboratory roller-tank experiments showed that POM can incorporate suspended minerals, and that increasing the mineral concentration in tanks reduced particle volume and increased particle density, with POC:mineral ratios reaching an asymptote at $\sim$5% w/w, as found in deep-sea particles (*Hamm* 2002; *Passow and De La Rocha* 2006; *De La Rocha et al.* 2008). These results were observed with all mineral types used (illite, kaolinite, smectite, quartz, $CaCO_3$ as coccoliths and as laboratory reagent, and diatom frustules), and are hence most probably due to the stickiness of POM (TEP would undoubtedly play a role when present). It even appears as though minerals are able to scavenge DOM (*De La Rocha et al.* 2008). The asymptotic value of 5% POC for aggregates would thus simply reflect the carrying capacity of POM for minerals (*Passow* 2004), and indeed aggregates were seen to fragment into tiny particles at the highest mineral concentrations tested (*Passow and De La Rocha* 2006). The potential for sinking particles to scavenge suspended minerals certainly exists *in situ*, and in fact more so for $CaCO_3$ than for opal, as discussed by *De La Rocha and Passow* (2007): coccoliths can detach from coccolithophore cells relatively easily to form a suspended stock of coccoliths (*Honjo* 1976), but diatom frustules tend to be more intimately associated with diatom organic matter.

While particle sinking rates can increase with mineral concentration in such experiments, the reduction in particle volume complicates the relationship (*Hamm* 2002; *Passow and De La Rocha* 2006). Despite the decrease in aggregate size upon mineral scavenging, *De La Rocha and Passow* (2007) calculate that over a water column of about 3000 m an aggregate might accumulate enough minerals to sink 1–2 orders of magnitude faster than initially (based on data from the *Passow and De La Rocha* (2006) experiments). Average particle sinking speeds apparently do increase with depth (*Berelson* 2002), although it is unclear whether mineral scavenging would be substantial enough to affect the attenuation of POC flux in the upper mesopelagic, where remineralization is greatest (*De La Rocha and Passow* 2007). However, while mineral scavenging by organic particles is probably part of the ballast story, recent evidence suggests that an association between POC flux and mineral flux is also found for shallow export out of the surface ocean, both in sediment trap and ^{234}Th studies (*Thomalla et al.* 2008; *Lee et al.* 2009; *Sanders et al.* 2010).

Overall, it is clear that POC and minerals interact in very complex ways into which more research is needed; certainly it would be mistaken to conclude that any one mineral is responsible

for most POC flux, or that a change in the magnitude of the BCP therefore automatically implies a corresponding change in the mineral flux. An outstanding question that is examined in the present study (Chapter 2) is whether export out of a high-latitude diatom bloom really is transferred to depth relatively inefficiently. While numerous studies on the ballast hypothesis suggest that the T_{eff} in such a setting may indeed be low (*François et al.* 2002; *Ragueneau et al.* 2006; *S. Henson et al.* in prep.), this stands in contrast to observational evidence of bloom sedimentation leading to thick phytodetrital fluff layers with sinking rates of 100–150 $\mathrm{m\,d^{-1}}$ (*Billett et al.* 1983; *Lampitt* 1985), and a regional comparison of process studies that concluded that a diatom bloom in the North Atlantic actually had high efficiencies for both export and transfer (*Buesseler and Boyd* 2009).

1.2.5 Inter-annual variability

Multi-year time-series studies with bottom-tethered sediment traps have revealed substantial inter-annual variability in particle flux (*Conte et al.* 2001; *Waniek et al.* 2005; *Lampitt et al.* 2010), and at one north-east Atlantic site part of this variability has been attributed to occasional sinking of major pulses of Radiolaria, which could contribute up to 60% of annual POC flux (*Lampitt et al.* 2009). Such stochastic sedimentation pulses are likely to be of significance for the overall magnitude of the BCP; *Ragueneau et al.* (2006) speculate that mesopelagic food-webs might not be able to respond instantly to a sudden dramatic increase in food supply, thus allowing relatively more efficient transfer to depth. Sudden pulses may occur relatively predictably as part of the annual cycle of phytoplankton production (sedimentation of a spring bloom, or a "fall dump" when stratification breaks down in autumn, *Kemp et al.* 2000). But irregular mass occurrences of particular organisms are also likely to play a role (*e.g.* Radiolaria or salps as discussed above; also jellyfish, *Billett et al.* 2006). Such events might be at least part of the reason why a multi-year bathypelagic particle flux data set in the north-east Atlantic showed no clear links to mixed layer characteristics or chlorophyll concentration / NPP (*Lampitt et al.* 2010).

1.3 Measuring POC flux

Broadly speaking, three main approaches can be used to measure the strength of the BCP. The first and most direct method is to use sediment traps; these are funnel-shaped or conical devices deployed at a particular depth that intercept sinking particles. Upon recovery, particle samples are then available for chemical or biological analysis, allowing a detailed characterisation of the sinking particles to be made. Moreover, by normalising laboratory measurements on the samples to the deployment duration and the collection area of the trap, an exact flux can be calculated for any measured quantity. However, sediment traps suffer from numerous biases, for instance caused by horizontal currents and by zooplankton actively entering the trap; these are discussed in detail in Appendix A.1. Two types of traps were used for the present work: bottom-tethered traps, which were deployed for eight months in the bathypelagic and collected a time-series of particle flux (Appendix A.1.2), and neutrally buoyant drifting sediment traps,

which were deployed for up to six days in the mesopelagic (Appendix A.1.1). Sediment traps can be used throughout the water column.

The second approach makes use of particle-reactive radionuclides that are produced naturally in seawater, principally the isotope ^{234}Th. Briefly, ^{234}Th is produced from natural ^{238}U, which is dissolved and conservative in seawater. Th, however, readily adsorbs to all types of particles and is thus exported from the surface when particles sink. The resulting radioactive disequilibrium between parent and daughter nuclide can be measured, and because the rates of production and decay of ^{234}Th are known, the downward flux necessary to sustain the measured disequilibrium can be calculated. It is then possible to convert the calculated daily ^{234}Th export to export of element X if one has measurements of the X:^{234}Th ratio in sinking particles. The ^{234}Th method was used for the present work as well, and full details of the method are given in Appendix B.5. ^{234}Th can only be used to measure shallow export flux, as equilibrium with ^{238}U is typically reached between 100–200 m; the method has an integration time-scale of several days to weeks. Almost inevitably, there are also significant uncertainties associated with the ^{234}Th method: the greatest challenges are constraining the POC:^{234}Th ratio in sinking particles well, and testing whether the ^{234}Th concentration is changing over time-scales of a few days to weeks by repeatedly sampling the same water mass.

A third possibility is to measure the fraction of primary production that is available for export. This can be done by measuring the seasonal uptake of NO_3^-, assuming that all NO_3^- is supplied as "new nutrient" during winter mixing (*e.g. Sanders et al.* 2005); this should then equal the seasonal new production. Alternatively, it is possible to take instantaneous measurements of the uptake rate of NO_3^- by phytoplankton compared to NH_4^+ uptake using incubations with isotopically-labeled NO_3^- (*e.g. Dugdale and Goering* 1967). However, both of these methods suffer from the drawback of either a very long integration time-scale (in the case of seasonal nutrient budgets), or a very short integration time-scale (^{15}N incubations). Moreover, the ratio of C:N needs to be known / assumed. Consequently, new production methods usually yield different export estimates to ^{234}Th or sediment trap estimates. However, it is also possible to measure net community production, NCP, using the ratio of O_2:Ar in surface waters (NCP = Net primary production − heterotrophic respiration). While the O_2 concentration is affected by photosynthesis, respiration, and physical gas exchange (*e.g.* bubbles from white-caps), the Ar concentration is only affected by physical processes, but the two gases have similar solubilities. Over- or under-saturation of O_2 relative to Ar is then a measure of NCP, and has an integration time-scale of one to two weeks. O_2:Ar-based NCP was estimated during LohaFEX (Chapter 3), and a more comprehensive explanation of the method is given in Appendix B.7.

Some additional methods to study the BCP exist, but are not in routine use yet. For instance, particle cameras can be lowered through the water column, and image analysis software then allows particle characteristics such as equivalent spherical diameter to be extracted; flux can then be calculated using a set of conversion equations, although detailed information about particle size-spectra and concentration profiles are inherently interesting as well (*Gorsky et al.* 2000). Autonomous profiling floats have also been equipped with optical sensors able to count and size particles (*Checkley et al.* 2008), and even to measure an index of particle flux based on the accumulation of sinking particles on an upward-looking transmissometer (*Bishop et al.*

2004). Such autonomous instruments could deliver a large increase in our understanding of the BCP if deployed in large numbers; while there are of course significant uncertainties in converting optical measurements into a value of particle flux, such platforms allow much greater synoptic spatial coverage, and are not necessarily limited to the duration of single cruises. However, these technologies are still under active development and not yet widely available.

1.4 Structure of the present work

Three distinct studies were conducted. The first (Chapter 2) was a Lagrangian study of POC export and its attenuation in the mesopelagic during a spring diatom bloom in the sub-polar North Atlantic. A large pulse of TEP- and diatom-rich phytodetritus sank and was tracked with both ^{234}Th and neutrally buoyant PELAGRA traps, allowing the transfer efficiency, as well as the chemical and biological composition of the material, to be investigated.

The second study (Chapter 3) focussed on export during the artificial iron-fertilisation experiment LohaFEX, conducted in low-Si waters of the Antarctic Polar Frontal Zone. The long duration of the experiment (39 d) allowed a comparison of ^{234}Th-based export estimates to the O_2:Ar ratio method for measuring new production, while PELAGRA traps were deployed in the mesopelagic to monitor the sequestration flux. Fe-fertilisation enhanced neither export nor sequestration flux, which is attributed to heavy copepod grazing pressure and the inability of a diatom bloom to develop.

The third study was an analysis of a mesoscale array of four bottom-tethered sediment traps deployed for eight months at 2000 m in the sub-polar North Atlantic, which is reported in two chapters. Chapter 4 describes the surprising discovery of large numbers of acantharian cysts in the traps during spring, demonstrating that the celestite shells of these protists do not necessarily dissolve in the upper mesopelagic as has previously been thought. Some speculative thoughts are presented for why Acantharia might benefit from sinking so deep in the sub-polar North Atlantic.

Finally, Chapter 5 investigates the mesoscale variability in particle flux between the four deep sediment traps over the full eight-month deployment period. A mass spectrometric method to measure ^{230}Th was set up at NOCS to control for any differences in cumulative particle flux due to differences in collection efficiency between the traps. Cumulative flux showed ∼30% mesoscale variability that could not be explained by differences in trapping efficiency. One trap under-caught ^{230}Th flux by half, suggesting considerably lower efficiency, but there was no clear link between efficiency and horizontal current speed, which is usually thought to be the main factor leading to under-trapping.

Chapter 2

Export and Mesopelagic Particle Flux During a North Atlantic Spring Diatom Bloom

The following chapter has been reproduced with some textual modifications and additions from *Deep-Sea Research I* with permission from Elsevier. Publication: Martin P., Lampitt R. S., Perry M. J., Sanders R., Lee C., D'Asaro E. (2011). Export and mesopelagic particle flux during a North Atlantic spring diatom bloom. *Deep-Sea Research I*, *58*, 338-349, doi:10.1016/j.dsr.2011.01.006.

Data contribution

All chemical measurements were taken by the author, except for dissolved nutrients (Emily Kallin, U. of Maine), chlorophyll (Andrea Drzewianowski, U. of Maine), and POC/PON (samples prepared by the author, then measured by Bob Head, PML). PELAGRA samples were processed by the author (swimmer picking, splitting, filtering). Darryl Green and Mark Stinchcombe helped with ICP-OES and BSi measurements, respectively (both NOCS). Sebastian Steigenberger (NOCS) provided advice while setting up the TEP method, and Paul Morris (WHOI) helped with ^{234}Th data analysis. Phytoplankton cell counts were taken by Alex Poulton (NOCS), and Tatiana Rynearson (U. of Rhode Island) incubated resting spores at sea. PELAGRA deployments were conducted by Richard Lampitt and Kevin Saw (both NOCS), and on-board sample processing was undertaken jointly by Richard Lampitt and the author. Chlorophyll data from fluorescence were collected and analysed by Eric D'Asaro (U. of Washington). Brandon Sackman (U. of Maine) obtained and processed the satellite data from the NASA OceanColour Web and the ESA MERCI Website. Tatiana Rynearson, Kirk Cochran (Stony Brook U.), and two anonymous referees provided helpful comments on the original submission to DSR I.

Abstract

Spring diatom blooms are important for sequestering atmospheric CO_2 below the permanent thermocline in the form of POC. We measured downward POC flux during a sub-polar North Atlantic spring bloom at 100 m using ^{234}Th disequilibria, and below 100 m using neutrally buoyant drifting sediment traps. The cruise followed a Lagrangian float, and a pronounced diatom bloom occurred in a 600 km^2 area around the float. Particle flux was low during the

first three weeks of the bloom, between 10 and 30 mg POC m^{-2} d^{-1}. Then, nearly twenty days after the bloom had started, export as diagnosed from ^{234}Th rose to 360–620 mg POC m^{-2} d^{-1}, co-incident with silicic acid depletion in the surface mixed layer. Sediment traps at 600 and 750 m depth collected 160 and 150 mg POC m^{-2} d^{-1}, with a settled volume of particles of 1000–1500 mL m^{-2} d^{-1}. This implies that 25–43% of the 100 m POC export sank below 750 m. The sinking particles were ungrazed diatom aggregates that contained transparent exopolymer particles (TEP) and large numbers of *Chaetoceros* spp. resting spores. It is concluded that diatom blooms can lead to substantial particle export that is transferred efficiently through the mesopelagic.

2.1 Introduction

Pronounced spring phytoplankton blooms with chlorophyll-*a* concentration $\geq$1.5 mg m^{-3} and primary productivity of 500–1500 mg C m^{-2} d^{-1} occur in the North Atlantic in response to spring stratification (*Savidge et al.* 1995; *Bury et al.* 2001; *Henson et al.* 2009). These blooms are initially dominated by diatoms, with a community-shift to smaller flagellates once diatoms have depleted surface silicic acid (*Lochte et al.* 1993; *Sieracki et al.* 1993; *Leblanc et al.* 2009). Such diatom blooms are known to trigger substantial export of fast-sinking phytodetrital aggregates that can carpet abyssal plains (*Lampitt* 1985; *Honjo and Manganini* 1993), and they are hence considered to be an important part of the biological carbon pump (*Turner* 2002).

Although this broad outline (spring stratification $\rightarrow$ diatom bloom $\rightarrow$ silicic acid depletion + substantial particle export $\rightarrow$ community-shift) is well established, we still lack a more detailed understanding of what triggers particle export, why such high particle export should occur, what the chemical and biological composition of the exported particles is, and how strongly the particle flux is attenuated in the mesopelagic.

Aggregation of phytoplankton blooms appears to be driven by transparent exopolymer particles (TEP) (*Passow et al.* 1994; *Alldredge and Jackson* 1995; *Logan et al.* 1995). These are a class of acidic polysaccharides excreted by diverse groups of phytoplankton, and even bacteria (*Passow* 2002). They promote particle aggregation via their stickiness and form the matrix of all marine snow particles studied to date (*Alldredge et al.* 1993; *Dam and Drapeau* 1995; *Passow and Alldredge* 1995a; *Engel* 2000). TEP can thus be separate particles, or by aggregating other particles such as phytoplankton cells, become a constituent of larger particles. Consequently, one might expect particle flux, or at least the flux of phytodetritus, to be strongly associated with TEP flux. For instance, a diatom bloom in a Norwegian fjord that failed to produce TEP did not aggregate (*Kiørboe et al.* 1996). However, high stickiness and aggregate formation did not lead to sedimentation of a diatom bloom in the Benguela upwelling (*Kiørboe et al.* 1998).

TEP have very rarely been measured in sediment traps. *Reigstad and Wassmann* (2007) found that TEP can be associated with peaks of *Phaeocystis* sp. export, but not always. A two-year record of 500 m particle flux in the Santa Barbara Channel indicated that the sedimentation of diatoms was always associated with the presence of TEP in the sediment trap samples, but that only 67% of peaks in POC flux were associated with the peaks in TEP flux (*Passow et al.* 2001). While TEP therefore undoubtedly play a role in particle flux, sinking of some particle

classes, perhaps faecal pellets, clearly does not depend upon TEP. In the case of a diatom bloom, however, one might expect that sedimentation should be driven by TEP-mediated aggregation.

The presence of biominerals has also been posited as an important factor in regulating particle flux, either by ballasting particles with excess density or by physically protecting organic matter from degradation (*Armstrong et al.* 2002; *François et al.* 2002; *Klaas and Archer* 2002; *Ingalls et al.* 2003). *Klaas and Archer* (2002) concluded that $CaCO_3$ is a much more important ballast than opal, based on global relationships between mineral and organic carbon fluxes. *François et al.* (2002) concluded that particle export is also transferred more efficiently through the mesopelagic to depths >2000 m in $CaCO_3$-dominated regions than in opal- (*i.e.* diatom-) dominated regions. Based on changes in Si:C ratios with depth across different ocean basins, *Ragueneau et al.* (2006) concluded that diatom-dominated, more seasonal, regions remineralize a greater proportion of export flux in the mesopelagic, and suggested that organic matter in these areas might be more labile. These conclusions are perhaps somewhat surprising, given that diatom blooms are thought to export a substantial fraction (up to 79%) of primary production (*Buesseler* 1998), and result in aggregates that can sink apparently intact for thousands of metres (*Lampitt* 1985). A recent re-analysis by *Buesseler and Boyd* (2009) concluded that a North Atlantic spring bloom was actually very efficient at exporting POC and transferring it through the mesopelagic.

Consequently, it is still unclear how efficiently POC flux is transferred to depth during a spring diatom bloom. However, there may be a question of time-scale underlying these contradictory conclusions, as *François et al.* (2002) and *Ragueneau et al.* (2006) used annually averaged particle flux data, while *Buesseler and Boyd* (2009) used data gathered specifically during a bloom. Hence it is possible that particle flux during a spring bloom is transferred to depth more efficiently than at other times.

Particle flux was therefore estimated during a sub-polar North Atlantic spring bloom using neutrally buoyant sediment traps and ^{234}Th measurements.

2.2 Methods

A multi-disciplinary research cruise was undertaken in the Iceland Basin from 1 to 21 May 2008 aboard R/V *Knorr*. The cruise track followed a Lagrangian bio-optical float deployed in the surface mixed layer (but profiling to 250 m once daily). Four seagliders measured physical and bio-optical parameters in the area before, during and after the cruise. Figure 2.1 shows the study site, the trap and the ^{234}Th sampling locations, and indicates on a time-line the trap deployment periods and times of ^{234}Th sampling.

2.2.1 Neutrally buoyant sediment traps

Four deployments of 1–3 d each were undertaken with PELAGRA traps (described in Appendix A.1.1) at depths between 150 and 750 m. Deployments are referred to as D1–D4 below. Collection cups opened 24 h after deployment, and closed again minutes before the trap ascended to the surface. During D1–D3, all cups on each trap collected simultaneously; during

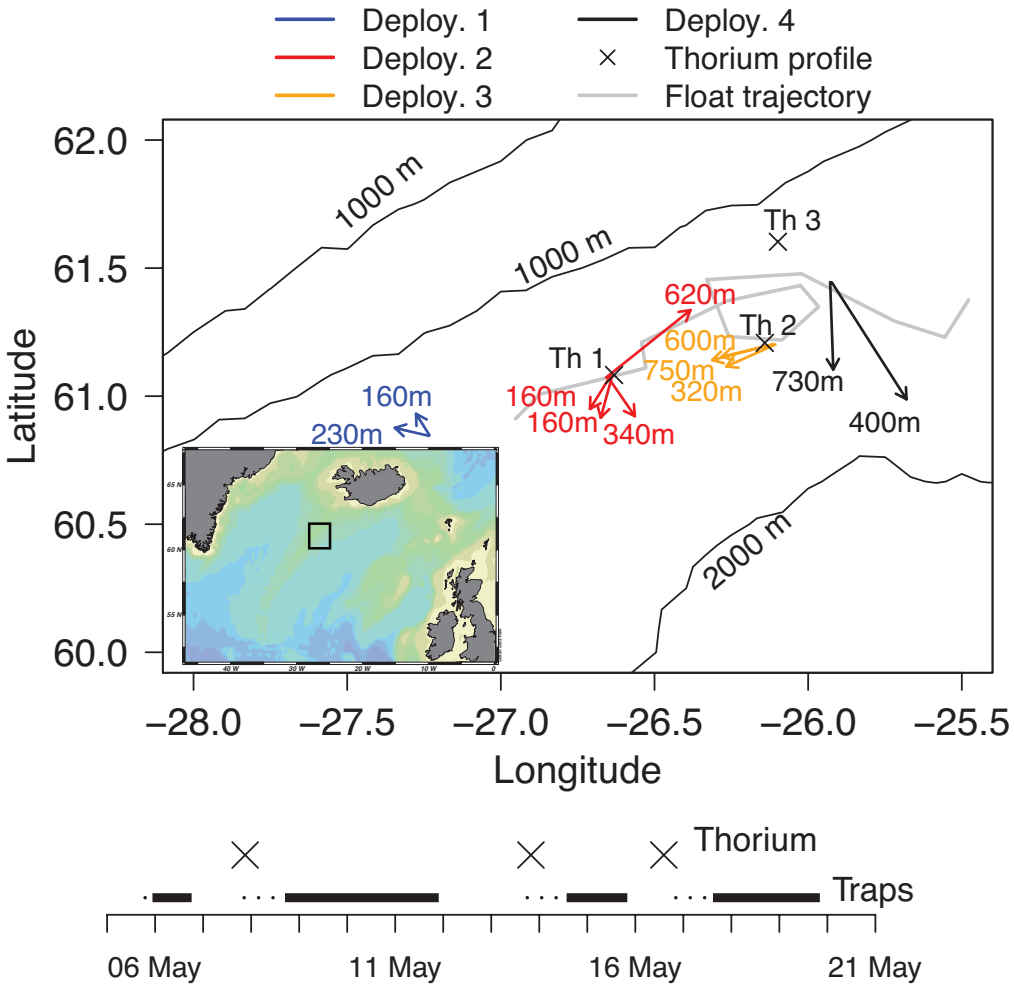

Figure 2.1 – Map of the study area. The inset shows the Iceland Basin, with the black box marking the region shown in the main map. The grey line shows the trajectory of the Lagrangian float from the day of the first sediment trap deployment until the end of the cruise. The trajectories of all sediment traps and the locations of the three ^{234}Th profiles are shown. The time-line at the bottom shows the deployment periods of the sediment traps (black bars) in relation to the times of ^{234}Th sampling (crosses). The solid part of each line shows the collection period for the traps (when collection cups were open), the dotted part shows the trap stabilisation period (when cups were still closed).

D4, the traps collected with two cups for the first 24 h, closed these, and collected with the remaining two cups for the next 24 h. Three cups on each trap were filled with formalin solution (Appendix A.2), and one cup on each trap was filled with unpoisoned seawater. $SrCl_2$ was added to all poisoned cups on D2 prior to deployment to prevent dissolution of Acantharia, single-celled organisms with a shell of celestite (final Sr concentration of 88 mg L^{-1}; *Beers and Stewart* 1970), but not on other deployments.

On recovery, 1 mL of 40% buffered formaldehyde was added to each poisoned cup, and the settled height of sediment in each sample was measured after 24 h. Samples from each trap were divided at sea with a Folsom splitter, and further on land with a rotary splitter. Different cups on the same trap sometimes contained visibly different quantities of material, despite collecting simultaneously. In these cases, all poisoned samples of a trap were pooled before splitting. Owing to the difficulties of splitting the resulting large volumes with a Folsom splitter, cups were treated individually whenever material was evenly distributed between cups. Swimmers were removed under a Wild dissecting microscope (60×–120× magnification) from all samples except from the sub-samples for ^{234}Th.

2.2.2 Analyses of trap samples

Sub-samples of 2–15 mg dry weight were used to measure dry weight + POC + PON, PIC + celestite, BSi, and ^{234}Th.

Sub-samples for dry weight + POC + PON were filtered onto pre-combusted GF/F filters, rinsed with MilliQ, and analysed as described in Appendix B.1. Analyses were conducted in triplicate using three separate splits for D2 and D3 traps, with relative standard deviations (RSD) of <9.5% for dry weight (mean RSD 5%), <8% for POC (mean RSD 5%), and <12% for PON (mean RSD 7%). For D1 and D4, the mean RSDs from D2 and D3 were applied. These errors are a combination of uncertainties from sample splitting and processing, and the analytical uncertainty.

Sub-samples for PIC + celestite and BSi were filtered onto 0.4 µm Millipore polycarbonate filters, rinsed with MilliQ, and analysed as described in Appendices B.2 and B.3, respectively. Analyses were duplicated for the D2 and D3 samples, and percentage differences between duplicates were <30% (and mostly <10%) for BSi, and <23% for PIC and celestite (except for D2#160, which had low Sr flux with a percentage difference of 89%).

Blanks for POC/PON, PIC/celestite and BSi were prepared by filtering MilliQ through the appropriate filter type and treating them exactly as samples.

^{234}Th in sinking particles was measured in PELAGRA sub-samples from D1–D3 as described in Appendix B.5.2 (^{234}Th in D4 could not be measured due to time-constraints at the end of the cruise).

TEP were measured using a modified version of the dye-binding assay of *Passow and Alldredge* (1995b) as described in Appendix B.4. TEP were measured (by determining the absorbance of the quantity of dye bound to the sample) in aliquots between $\frac{1}{1600}$ and $\frac{1}{370}$ of the original sample. For each sample, two dilutions were prepared with a NaCl solution (35 g NaCl in 1 L MilliQ), and 1 mL was filtered in triplicate at each dilution. For D1 samples, aliquots of

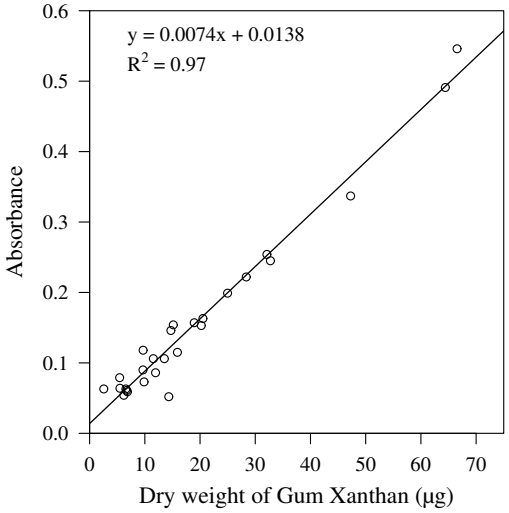

Figure 2.2 – Calibration curve for TEP to convert sample absorbances to units of µg Gum Xanthan equivalents.

the concentrated sample solution were filtered as well. For each dilution, the mean absorbance of the triplicate measurements was used to calculate the TEP concentration per mL of the analysed solution, and the sample TEP content was calculated from the mean of the two dilutions. Percentage differences in TEP content between the two dilutions were 10–22%, except for D3#750, where the difference as 34%. The calibration curve used to convert measured absorbance to units of g Gum Xanthan eq. is shown in Figure 2.2.

Phytoplankton cell counts were taken by allowing 1 mL suspensions of trap samples to settle in a Sedgwick Rafter Cell, and counting 5–50 fields of view under an inverted light microscope depending on the amount of material present and the abundance of each taxon. For very rare taxa the full area of the Sedgwick Rafter Cell was counted.

2.2.3 Water column ^{234}Th

Total ^{234}Th was measured in 10 L water samples taken at 5–400 m depth as described in Appendix B.5.2. Three vertical profiles of ^{234}Th were taken, allowing a non-steady-state flux model according to *Buesseler et al.* (1992) (Appendix B.5.4) to be applied.

2.2.4 Chlorophyll and silicic acid

Chlorophyll-*a* was measured by a fluorometer on the Lagrangian float (WetLabs FLNTU, excitation wavelength 470 nm). This sensor was calibrated against a similar fluorometer on the CTD rosette. Chlorophyll-*a* was analysed from water samples concurrently collected by the CTD rosette; samples were filtered onto GF/F filters, extracted with 90% acetone for 24 h in the dark at −20 °C, and measured on a Turner Designs AU-10 fluorometer. The relationship between measured chlorophyll-*a* concentration from the bottle samples and the fluorescence measured *in situ* by the rosette-mounted fluorometer was then applied to the fluorescence

measured by the float. The relative standard deviation of the chlorophyll concentration thus calculated from the float was 30–40% (*E. D'Asaro*, pers. comm.). Samples for $Si(OH)_4$ were taken throughout the cruise, and frozen at sea (−20 °C). $Si(OH)_4$ was then measured after transporting back to land on a Lachat Quickchem 8000 Flow Injection Analysis System using standard absorptiometric techniques. Samples were slowly thawed in the dark at room temperature for 24 h and vigorously vortexed before analysis (*Gordon et al.* 1994). The data presented here are the mean concentration in the upper 20 m (n = 2–3 samples), and stations thought to have been outside of the bloom patch are omitted here.

2.2.5 Satellite imagery

Daily composite images were created by averaging individual MODIS and MERIS images on a pixel-wide basis and gridding them on a 1 km resolution grid.

2.3 Results

2.3.1 Surface biogeochemical and hydrographical setting

The bloom did not occur homogeneously over a large area. The Lagrangian float followed a distinct patch of enhanced chlorophyll-*a* concentration that was dominated by diatoms. This patch was clearly visible in MODIS/MERIS sea-surface colour images (Figure 2.3), and could be distinguished from the surrounding waters with the bio-optical measurements taken by the gliders and from the ship (*A. Gray*, pers. comm.). The patch was 600 km^2 on 6 May (Figure 2.3a), but had shrunk to 250 km^2 by 11 May (Figure 2.3b). This patch was intensively studied during the cruise, and constituted the bloom discussed here.

Chlorophyll-*a* fluorescence and dissolved O_2 as measured by the seagliders increased from 19 April, indicating that the bloom started approximately ten days prior to the cruise. Nutrient concentrations in the surface mixed layer decreased due to phytoplankton production: NO_3^- declined from 11 to 8.5 $\mu mol\,L^{-1}$ over the course of the cruise, while $Si(OH)_4$ decreased from 4 to $<1\,\mu mol\,L^{-1}$ over the same period, and was $<2\,\mu mol\,L^{-1}$ by 7 May. Consequently, there was a phytoplankton community-shift from diatom dominance to pico-eukaryotes, with shipboard observations suggesting a peak in diatom abundance between 8 and 11 May (*M. Sieracki*, pers. comm.). Chlorophyll-*a* as measured by the float rose from close to 1 $mg\,m^{-3}$ to a peak of nearly 4 $mg\,m^{-3}$ between 1 and 12 May, and declined thereafter to around 1 $mg\,m^{-3}$ again. By the time of the final trap deployment (17 May), chlorophyll-*a* and diatom numbers in the patch had decreased substantially, making it harder to track the patch.

2.3.2 Trap deployments

Traps were successfully deployed eleven times during four separate deployments, which are referred to as Deployment Number#Depth (*e.g.* D3#750 refers to the 750 m trap on the third deployment). Deployment depths and durations are listed in Table 2.1, and profiles of trap

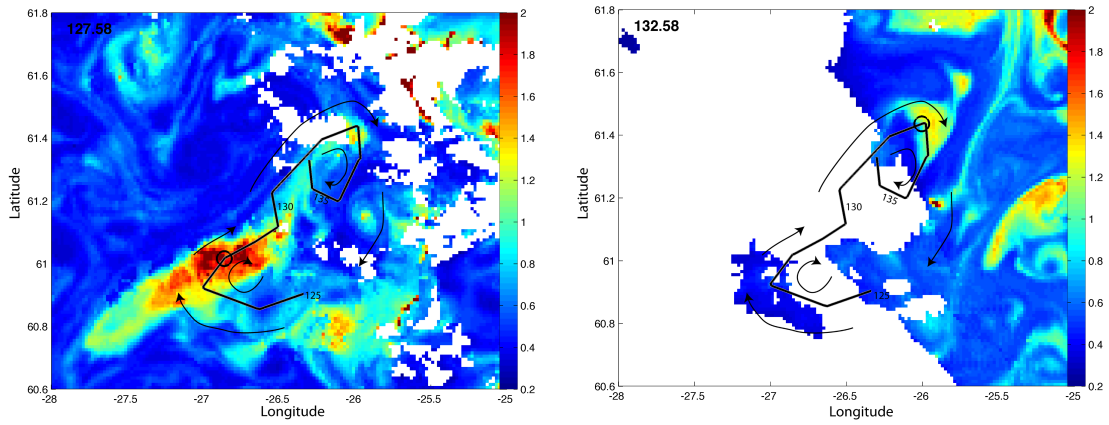

(a) **(b)**

Figure 2.3 – MODIS/MERIS daily composite chlorophyll-*a* images of the extent of the float patch on (a) 6 May and (b) 11 May. Scale bars show chlorophyll concentration in mg m^{-3}. The track of the Lagrangian float between 4 May and 19 May is marked with the black line. The circle in each image indicates the float position at the time of the image, and numbers along the float trajectory mark the float position on the corresponding year–day number (125 = 44 May, 130 = 9 May, 135 = 14 May). The arrows show the approximate direction of the surface currents (*A. Gray*, pers. comm.).

depth against time for each trap are shown in Figure 2.4. Trap trajectories are shown in Figure 2.1.

2.3.3 Trap-derived particle flux

Fluxes of total dry weight, POC, PON, PIC, BSi, celestite, ^{234}Th, and TEP for each trap are summarised in Table 2.2.

2.3.3.1 POC flux and POC:PON ratios

Figure 2.5a–d shows POC fluxes and POC:PON ratios for each deployment. POC flux was very low during the first two deployments (10–30 mg POC m^{-2} d^{-1}), but then increased to 75–165 mg POC m^{-2} d^{-1} during the final two deployments, peaking during D3. During D2 and D3, fluxes caught by the shallowest traps were two- to three-fold lower than those caught by the deeper traps, which is attributed to temporal and spatial variability in particle flux. Molar POC:PON ratios ranged from 4.4 to 6.7, with higher values in the D3 and D4 traps, and a mean weighted by POC flux of 6.1. The correlation between POC:PON and depth was not significant (Spearman's rank correlation, rho = 0.452, $p = 0.121$, $n = 13$).

POC contributed 8–13% of total mass flux in all cups (Table 2.2), with the highest percentages during D1 and D2, and in D4#400. The D3 traps contained substantial quantities of diatom-opal, and these samples contained the lowest percentage POC contribution.

Figure 2.6 shows photographs of the D3 samples (24 h collection). The collection cups are 500 mL Nalgene jars, and the settled volume flux was 1000–1500 mL m^{-2} d^{-1}. The photos

Trap ID (Deployment number#Depth)	Date/time of cup opening	Date/time of cup closing
D1#140	5 May 08 23:10	6 May 08 15:10
D1#230	6 May 08 00:55	6 May 08 15:55
D2#160*	8 May 08 19:25	11 May 08 19:25
D2#340	9 May 08 18:55	11 May 08 18:55
D2#160*	8 May 08 19:10	11 May 08 19:10
D2#620	9 May 08 06:40	11 May 08 18:40
D3#320	14 May 08 17:40	15 May 08 17:40
D3#600	14 May 08 15:55	15 May 08 15:55
D3#750	14 May 08 16:10	15 May 08 16:10
D4#400†	17 May 08 17:50	18 May 08 17:50
D4#400‡	18 May 08 17:55	19 May 08 17:55
D4#730†	17 May 08 17:05	18 May 08 17:05
D4#730‡	18 May 08 17:10	19 May 08 17:10

* Two traps were deployed at this depth

† First 24 h of deployment

‡ Second 24 h of deployment

Table 2.1 – Summary of trap deployments. Note that all traps were deployed 18–24 h before cups opened. In the case of D4, only one trap was deployed at each depth, but they collected in time-series mode; two collection cups were open for the first 24 h, closed, and then the next two cups opened.

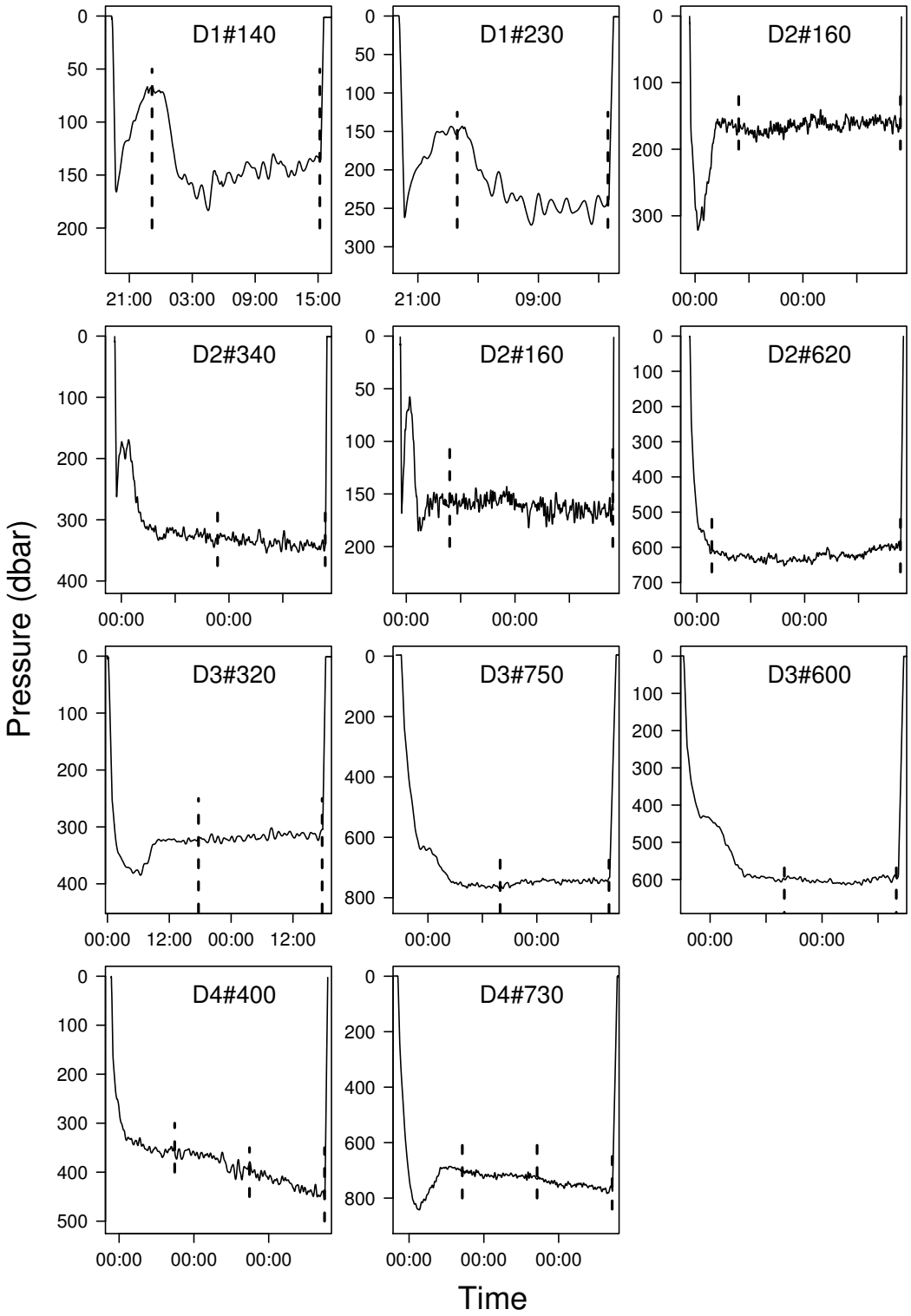

Figure 2.4 – Profiles of depth against time for each of the PELAGRA traps. Vertical dashed lines indicate the time of cup opening and closing. Note that the axes differ between plots.

Trap	Mass flux	POC flux	PON flux	Molar POC:PON	Opal flux	Molar Si:POC	PIC flux	Celestite flux	TEP flux	TEP:POC	^{234}Th flux
D1#140	121	15.4 ± 0.8	3.1 ± 0.49	5.80 ± 0.96	28 ± 0.8	0.33 ± 0.02	0.14 ± 0.02	ND	ND	NA	141
D1#230	138	14.4 ± 0.7	3.1 ± 0.52	5.42 ± 0.95	34 ± 3.7	0.43 ± 0.05	1.8 ± 0.27	ND	ND	NA	183
D2#160	94.3	10.3 ± 0.3	2.7 ± 0.25	4.41 ± 0.43	24 ± 5.0	0.43 ± 0.09	1.2 ± 0.14	1.4 ± 1.2	ND	NA	244
D2#340	240	30.6 ± 1.7	6.7 ± 0.32	5.33 ± 0.39	63 ± 3.8	0.37 ± 0.03	3.3 ± 0.50	26.2 ± 2.9	ND	NA	606
D2#160	119	13.3 ± 0.7	3.0 ± 0.34	5.17 ± 0.65	31 ± 1.9	0.43 ± 0.03	1.0 ± 0.22	11.1 ± 2.4	ND	NA	249
D2#620	235	27.2 ± 1.8	6.3 ± 0.68	5.04 ± 0.64	32 ± 1.3	0.21 ± 0.02	1.9 ± 0.36	18.2 ± 1.3	ND	NA	311
D3#320	878	76.2 ± 6.1	17.4 ± 2.2	5.11 ± 0.76	398 ± 40	0.95 ± 0.12	6.2 ± 0.81	ND	30	0.39	2200
D3#600	1875	164 ± 4.1	29.1 ± 2.5	6.59 ± 0.58	1040 ± 83	1.15 ± 0.10	17.8 ± 2.5	ND	122	0.74	5477
D3#750	1933	154 ± 4.8	30.4 ± 3.9	5.91 ± 0.78	1098 ± 316	1.28 ± 0.37	15.3 ± 1.8	ND	118	0.77	6015
D4#400†	1048	120 ± 5.8	21.5 ± 1.5	6.54 ± 0.55	432 ± 48	0.65 ± 0.08	13.0 ± 2.0	102 ± 13	42	0.35	NM
D4#400‡	929	112 ± 5.4	19.5 ± 1.4	6.69 ± 0.57	498 ± 55	0.81 ± 0.10	13.3 ± 2.0	80.7 ± 10.5	37	0.33	NM
D4#730†	995	95.2 ± 4.6	$17.6 \pm 1{,}2$	6.31 ± 0.54	605 ± 67	1.15 ± 0.14	9.3 ± 1.4	46.3 ± 6.0	35	0.37	NM
D4#730‡	779	75.1 ± 3.7	13.7 ± 1.0	6.40 ± 0.57	436 ± 48	1.05 ± 0.13	9.0 ± 1.4	58.0 ± 7.5	47	0.63	NM

ND = not detected; NA = not applicable; NM = not measured

† First 24 h of collection

‡ Second 24 h of collection

Table 2.2 – Summary of fluxes of chemical phases into the PELAGRA sediment traps, and elemental ratios. Note that for biominerals, the fluxes are as mass of mineral, not element, *e.g.* "opal flux" is the flux of hydrated SiO_2, not of Si. All fluxes are in $mg\,m^{-2}\,d^{-1}$, apart from TEP ($mg\,GX\,eq.\,m^{-2}\,d^{-1}$) and ^{234}Th ($dpm\,m^{-2}\,d^{-1}$); TEP:POC ratios are hence in $mg\,GX\,eq.\,mg^{-1}$.

clearly show that the settling material was predominantly phytodetrital, although some faecal pellets were also present.

2.3.3.2 Opal flux and Si:POC ratios

Opal flux (as hydrated SiO_2) ranged from about 25 to 1000 $mg\,m^{-2}\,d^{-1}$. Traps during D1 and D2 caught the lowest, and D3#600 and D3#750 the highest opal fluxes. During D4, opal fluxes were around half those during D3. The percentage contribution by opal to total dry weight was 15–25% during D1 and D2, and 40–60% in D3 and D4 (Figure 2.5e–h). The molar Si:POC ratios ranged from 0.2 to 1.3, and showed a significant increase with depth (Figure 2.5e–h, Spearman's rank correlation, rho = 0.651, $p = 0.016$, $n = 13$). However, this trend is also a function of time, as the deeper traps with high Si:POC were deployed during D3 and D4.

2.3.3.3 PIC and celestite flux

PIC flux was very low throughout the cruise (0.14–18 $mg\,m^{-2}\,d^{-2}$), and hence the rain ratio (PIC:POC) never rose above 0.13. As for most components, PIC flux also increased from D1/D2 to D3/D4. The percentage of total mass flux contributed by $CaCO_3$ (as calculated from Ca flux) was notably variable; the two D1 traps differed by a factor of ten in this measure, and the D2 traps differed by a factor of 1.5, even between the two 160 m traps.

PIC variability was similar to that of celestite, which was detected in all traps on D2 and D4: the percentage contribution of celestite to total mass flux varied by a factor of ten on D2, and by a factor of two on D4. Celestite contributed up to 10% of total mass flux during D2 and D4 (up to 100 $mg\,celestite\,m^{-2}\,d^{-1}$). Celestite is precipitated exclusively by Acantharia, single-celled organisms related to the Radiolaria. Although surface-dwelling as adults, Acantharia can form rapidly sinking reproductive cysts. Cysts of the type reported by *Martin et al.* (2010) (see Chapter 4) were found in samples from all traps upon recovery; hence the lack of measurable particulate celestite in D1 and D3 must be due to dissolution of this very soluble biomineral (*Beers and Stewart* 1970). Dissolution was prevented in D2 with $SrCl_2$ addition, and in D4 the flux of acantharian cysts was probably so high that the preservative solution saturated from just a proportion of the cysts dissolving (*Martin et al.* 2010). Therefore, except for D2, the estimates of celestite flux are significant under-estimates, and some celestite was certainly present in D1 and D3.

2.3.3.4 TEP flux

TEP were barely detectable in D1 and D2, but reached 30–120 $mg\,GX\,eq.\,m^{-2}\,d^{-1}$ during D3 and D4. Although absorbances of stained filters from D1 and D2 were always slightly higher than blanks, the small positive y-intercept of the calibration line (Figure 2.2) brought the calibrated TEP concentration in these samples to zero. This indicates that a small quantity of TEP was present, but not enough to be quantified using our calibration. TEP fluxes were highest in D3#600 and D3#750, which also had the highest TEP:POC ratios (0.8 and 0.7 $mg\,GX\,eq.\,mg^{-1}$). TEP flux in D3#320 and in the D4 traps was $<50\,mg\,GX\,eq.\,m^{-2}\,d^{-1}$,

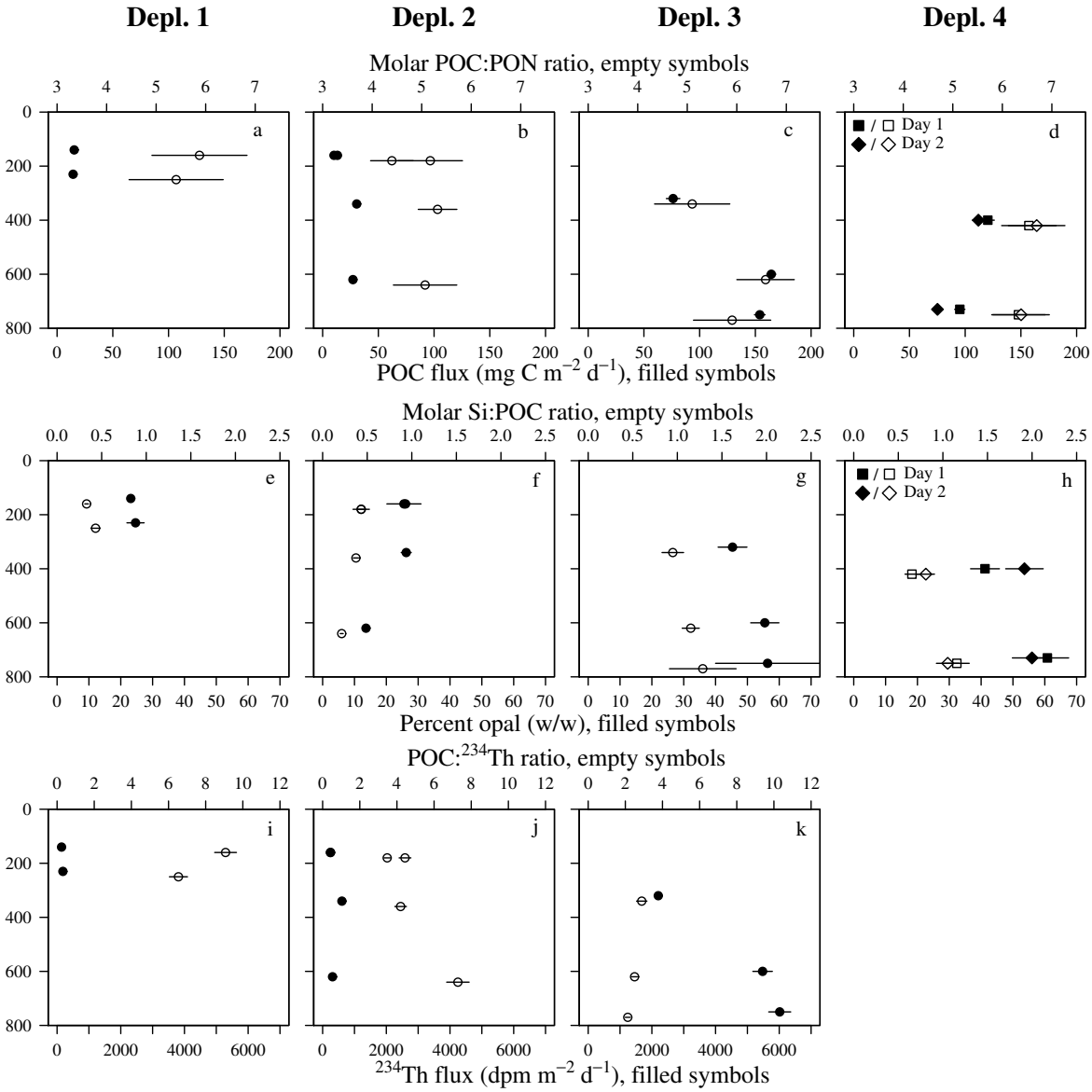

Figure 2.5 – (a–d) POC fluxes and molar POC:PON ratios for each sediment trap. Symbols for POC:PON ratios have been offset by 20 m from symbols for POC flux to prevent error bars from overlapping. (e–h) Percentage contribution by opal to total dry weight, and molar Si:POC ratios, for each sediment trap. Symbols for Si:POC ratios have been offset by 20 m from symbols for percentage opal content to prevent error bars from overlapping. (i–k) ^{234}Th fluxes and POC:^{234}Th ratios for each sediment trap (note that no ^{234}Th measurements were taken from D4 traps due to time constraints). All error bars are one standard deviation, showing the analytical error of the measurement based on propagated uncertainties.

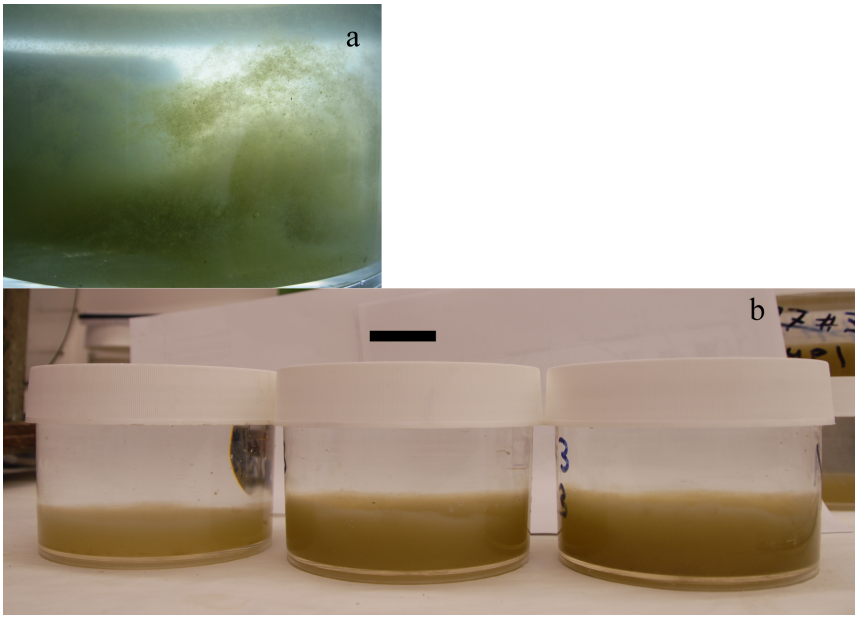

Figure 2.6 – Photographs of sediment trap samples from the third deployment. (a) Close-up photo of a sample from D3#750, showing the loose, fragile, nature of the trapped particles; (b) one sample each from (left to right) D3#320, D3#600, and D3#750, as photographed on board. Scale bar = 2.5 cm.

and TEP:POC in these samples was $<0.4\,\mathrm{mg\,mg^{-1}}$ (apart from D4#730 on Day 2, in which TEP:POC was $0.6\,\mathrm{mg\,mg^{-1}}$).

These results should be treated with some caution, given the scatter around the calibration curve at the low absorbances measured in our samples. However, initial trial measurements while developing the method gave very similar absorbances, although a good calibration had not yet been established. Moreover, this assay actually measures not the absolute amount of TEP, but the amount of binding sites available for the dye. The present data are only quantitatively comparable to other studies if the number of binding sites per amount of TEP is constant, but this could vary depending on factors such as the species producing the TEP and the extent of degradation (*U. Passow*, pers. comm.). Consequently, the TEP data should be considered semi-quantitative, clearly demonstrating the presence of TEP in the D3 and D4 samples, and indicating the presence of a small amount of TEP in the D1 and D2 samples.

2.3.3.5 Diatom cell fluxes

The PELAGRA catches were particularly notable for the very large numbers of *Chaetoceros* spp. resting spores they contained. They always equalled or outnumbered *Chaetoceros* spp. vegetative cells, and often outnumbered the combined number of vegetative cells of all diatom species (Table 2.3). Spore and cell fluxes increased sharply between D1/D2 and D3/D4, and it is also notable that the flux of total vegetative cells was 3–10-fold lower in the D2 samples than in the D1 samples. Particularly intriguing was the fact that the resting spores were healthy

Trap	Spore/cell fluxes (individuals $* 10^6\,m^{-2}\,d^{-1}$)			
	Chaetoceros spp. spores	*Chaetoceros* spp. vegetative cells	Total diatom vegetative cells	$\frac{\text{Spores}}{\text{Total diatom veg. cells}}$ ratio
D1#140	30.8	12.0	22.4	1.4
D1#230	20.5	20.8	31.5	0.65
D2#160	25.2	2.7	7.5	3.4
D2#340	80.0	2.2	7.2	11
D2#160	37.2	0.82	5.8	6.4
D2#620	26.2	1.5	3.7	7.1
D3#320	411	33.1	58	7.1
D3#600	471	188	318	1.5
D3#750	531	333	443	1.2
D4#400	96.3	41.0	101	0.95
D4#400	83.3	42.2	75.3	1.1
D4#730	113	46.2	159	0.71
D4#730	132	59.7	244	0.54

Table 2.3 – Fluxes of intact diatom vegetative cells and of *Chaetoceros* spp. resting spores (in millions of individuals).

and viable, and when incubated in nutrient-replete medium under a light:dark cycle on board, they excysted and started dividing approximately once per day (*T. Rynearson*, in prep.).

2.3.3.6 ^{234}Th flux from traps and POC:^{234}Th ratios

^{234}Th fluxes ranged from 140 to 600 dpm $m^{-2}\,d^{-1}$ during D1 and D2, with POC:^{234}Th ratios of 3.5–9.1 μmol dpm^{-1} (Figure 2.5i–k). There was no clear trend with depth, although the highest ^{234}Th fluxes were found in the deeper traps. ^{234}Th flux was substantially higher in the D3 traps, with 2200, 5500, and 6000 dpm $m^{-2}\,d^{-1}$ in D3#320, D3#600, and D3#750, respectively. POC:^{234}Th ratios in these traps were 2.9, 2.5, and 2.1, respectively. Overall, there was no clear trend in POC:^{234}Th ratios with depth, but it appears as though the ratio was decreasing over time (Figure 2.5i–k).

2.3.4 Water column ^{234}Th deficits and diagnosed ^{234}Th fluxes

The three profiles of total ^{234}Th activity are shown in Figure 2.7, with the integrated (to 100 m) deficit of ^{234}Th for each profile, calculated by trapezoid integration, in Figure 2.8. Locations of the profiles are marked in Figure 2.1. The small deficit in Profile 1 (9400 ± 4700 dpm m^{-2}, Figure 2.8) shows that export was low in the weeks before 7 May. The deficit of Profile 2 was much greater ($47{,}000 \pm 5200$ dpm m^{-2}, Figure 2.8), indicating that substantial export occurred

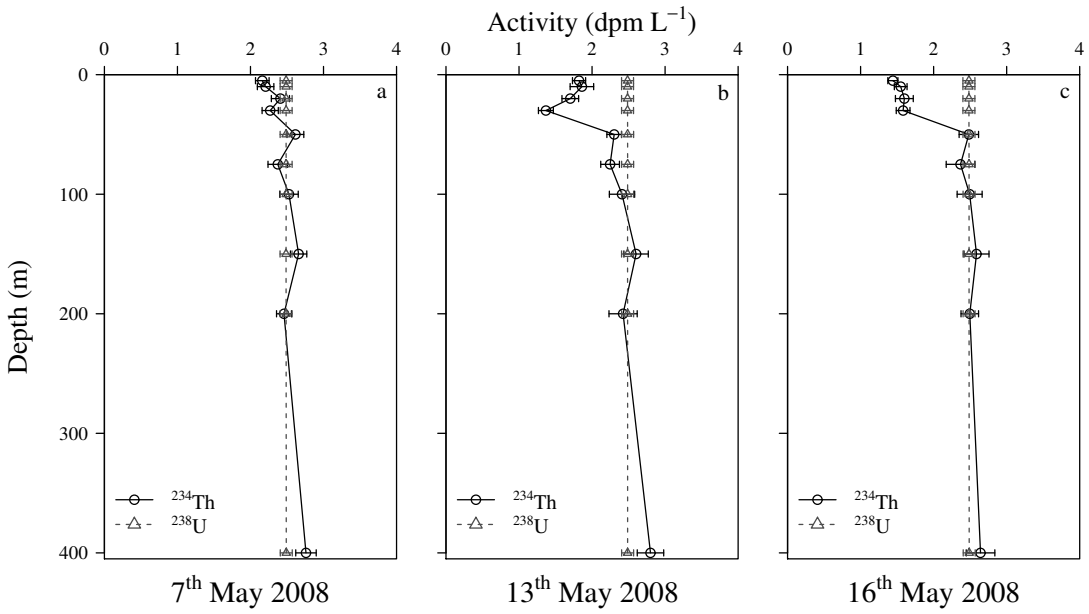

Figure 2.7 – Vertical profiles of ^{234}Th and ^{238}U activity concentration. Error bars are one standard deviation, showing the analytical uncertainty based on propagated errors. The first two profiles were taken directly adjacent to the Lagrangian float, *i.e.* within the float patch, but the third profile was taken outside of the patch.

between 7 and 12 May. Profile 3 shows a smaller deficit, owing to the shallower ^{234}Th depletion (Figure 2.7). However, Profile 3 was taken approximately 10 km north of the Lagrangian float and outside of the bloom patch. Consequently, only Profiles 1 and 2 were used to calculate ^{234}Th fluxes.

An SS model applied to the first profile yielded a flux at 100 m of $240 \pm 430\,\mathrm{dpm\,m^{-2}\,d^{-1}}$, which we take as a level of flux representative of the previous weeks. An NSS calculation between the first and second profile (6 d apart) yields a ^{234}Th flux of $7400 \pm 2400\,\mathrm{dpm\,m^{-2}\,d^{-1}}$ during this period. The importance of using an NSS model in this case is illustrated by the fact that an SS model applied to the second profile would yield a flux of only $1350 \pm 400\,\mathrm{dpm\,m^{-2}\,d^{-1}}$, or 20% of the NSS flux.

2.4 Discussion

The ^{234}Th- and trap-derived particle flux estimates, and the time-series of chlorophyll-*a* and $\mathrm{Si(OH)_4}$, are summarised and plotted on a common x-axis in Figure 2.9. This plot also shows the local chlorophyll-*a* and $\mathrm{Si(OH)_4}$ concentrations (mean of upper 20 m) measured from the CTD cast closest to each trap deployment and ^{234}Th profile. These measurements matched the overall trends in chlorophyll-*a* and $\mathrm{Si(OH)_4}$ at each time-point well, suggesting that spatial variability within the patch was much smaller than temporal variability.

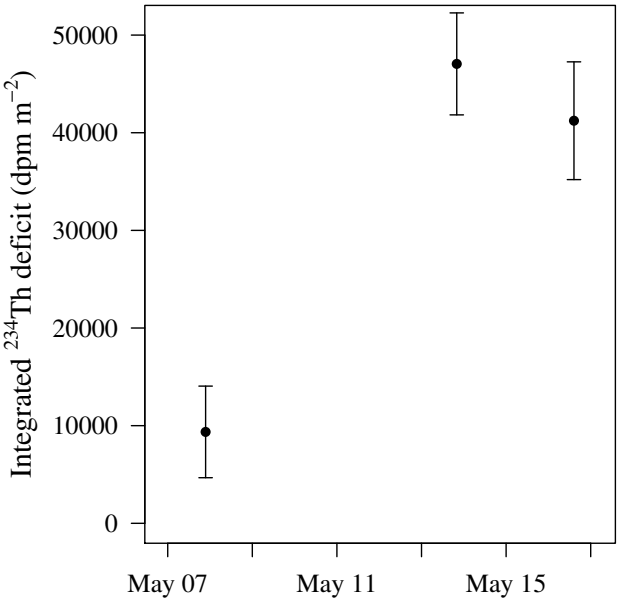

Figure 2.8 – Calculated deficit of ^{234}Th against time from each of the three profiles. The deficits were calculated by trapezoidal integration to 100 m. The strong increase in the deficit between the first two profiles indicates that substantial particle export occurred in the intervening period.

2.4.1 Timing of bloom sedimentation

The ^{234}Th profiles clearly show that a large export event occurred between 7 and 12 May, around 20 d after the bloom had started. This is supported by spikes appearing below the mixed layer in the chlorophyll-*a* and backscatter sensors on the gliders and the CTD rosette between 5 and 8 May, indicating that aggregates were sinking (*N. Briggs et al.* submitted). By this time, $Si(OH)_4$ concentrations were low ($<1\,\mu mol\,L^{-1}$) and did not decrease very much further (Figure 2.9). Diatom growth during North Atlantic spring blooms is thought to be terminated by silicate limitation (*Sieracki et al.* 1993; *Savidge et al.* 1995; *Henson et al.* 2006; *Leblanc et al.* 2009), and that clearly occurred during the present study as well.

Surprisingly, the D2 traps, which collected between 8 and 11 May, did not catch this export pulse. However, all but the deepest trap on D2 drifted southward and perpendicular to the float. Given the sharply delimited southern boundary of the patch, which drifted north-eastwards (Figure 2.3a), it is possible that the D2 traps collected particles mostly from outside of the patch — with the exception of the 620 m trap that was probably too deep to catch the export event yet.

The D3 traps, however, caught a large pulse of opal- and TEP-rich particles that very probably were derived from this export event, suggesting that the exported material reached 750 m depth between 14 and 15 May. If export below 100 m started on 8 May, that would imply a minimum sinking rate of $110\,m\,d^{-1}$, which is within the range of sinking speeds reported for phytodetritus and marine snow (50–$200\,m\,d^{-1}$; *Turner* 2002), and slightly higher than the

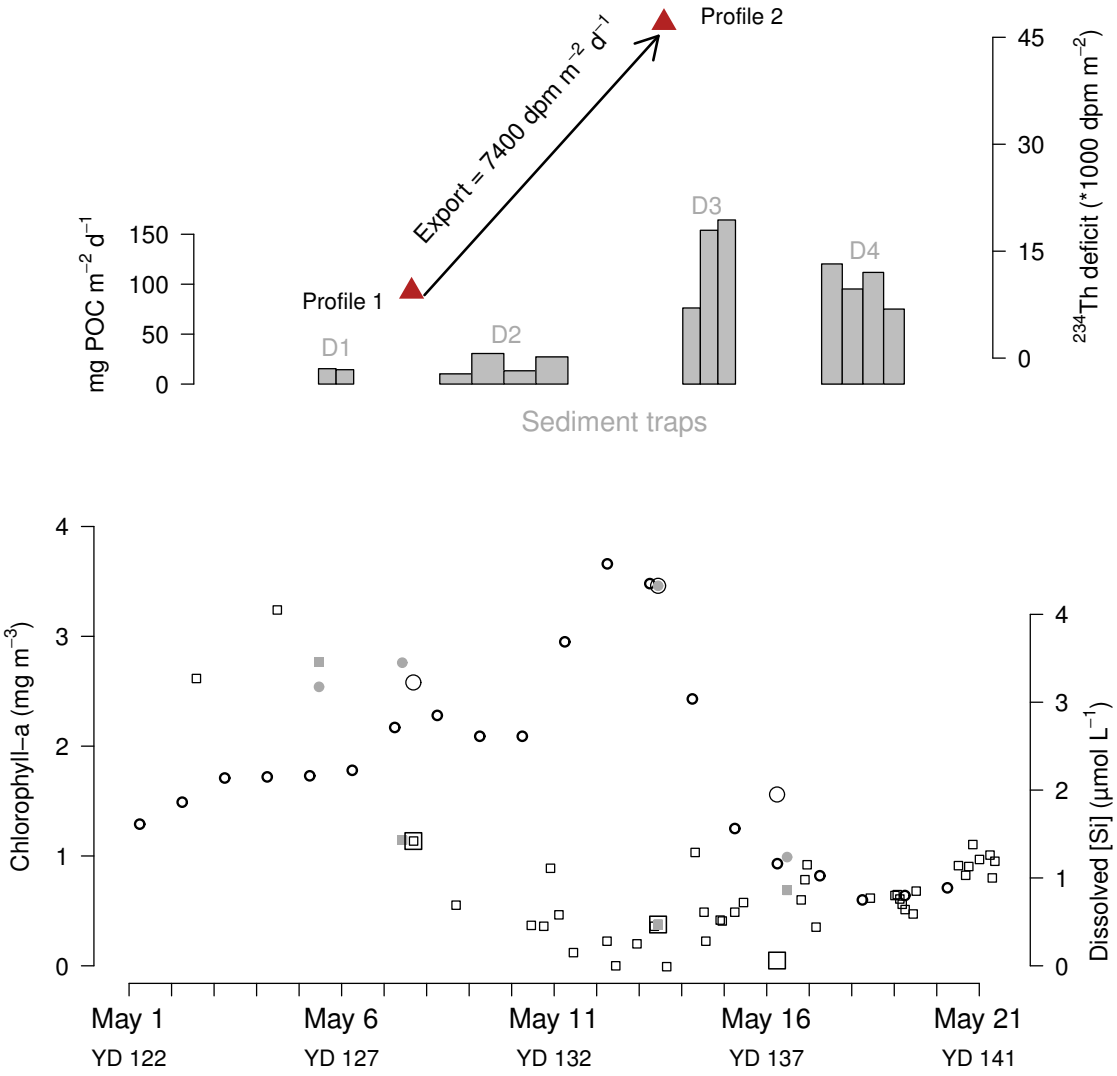

Figure 2.9 – Overview plot of the sediment trap and ^{234}Th results, together with daily mean chlorophyll-*a* concentration measured by the float (from fluorescence, small open circles) and mean $Si(OH)_4$ concentration in the upper 20 m inside the patch measured from bottle samples (small open squares). The local mean chlorophyll-*a* concentration in the upper 20 m where each trap deployment was made and each ^{234}Th profile taken is shown with closed grey circles (traps) and large open circles (^{234}Th). Similarly, the local mean $Si(OH)_4$ concentration in the upper 20 m for each trap deployment and ^{234}Th profile is shown with closed grey squares (traps) and large open squares (^{234}Th). For the trap POC fluxes, the total width of each group of bars indicates the collection period of that set of traps (*i.e.* 1 d for D1, 3 d for D2, etc.). The arrow between the ^{234}Th measurements indicates the growing depletion between Profile 1 and Profile 2, from which a flux of 7400 dpm m^{-2} d^{-1} was diagnosed.

range of 65–90 m d^{-1} calculated by *N. Briggs et al.* (submitted) during the cruise from the spikes in seaglider optical backscattering.

Why the shallower trap, D3#320, caught less material than the two deep D3 traps is unclear. It is possible that the traps lagged behind the patch, which drifted north-westward, and thus collected partly below adjacent, low-chlorophyll water. In such a case, deeper traps might still collect particles derived only from within the patch for several more days, while shallower traps will start to catch more recent particles from the overlying water, and thus contain less material (and sediment traps do not necessarily collect particles from directly above; see *Siegel et al.* 2008). Alternatively, particle export might have decreased suddenly after 12 May. Seeing how rapidly the chlorophyll-*a* concentration dropped after 12 May (Figure 2.9), a rapid decrease in export may well have occurred. The shallower trap would then also have caught less material than the deeper traps. This question cannot be resolved here, but it seems likely that the flux caught in D3#320 was less representative of flux during the height of the export event than the flux caught in the two deep D3 traps.

2.4.2 Magnitude of 100 m POC export

Converting the daily ^{234}Th export at 100 m into POC export is complicated in this case by the uncertainty in the most appropriate POC:^{234}Th ratio to use: we were unable to sample material from the large flux event as it left the surface, and POC:^{234}Th ratios invariably decrease with depth (*Buesseler et al.* 2006; *Maiti et al.* 2010). Therefore, the POC:^{234}Th ratios measured in D3#600 and D3#750 are almost certainly lower than the ratio at 100 m. However, it appears as though the POC:^{234}Th ratio was decreasing over the course of the cruise (Figure 2.5i–k), suggesting that the POC:^{234}Th ratio at 100 m for the high flux event was lower than in D1 (9.1 mmol POC dpm^{-1}). This is consistent with the greater TEP-richness of the D3 and D4 material, as Th has a high affinity for acidic polysaccharides and TEP-rich material should hence have lower POC:^{234}Th ratios (*Passow et al.* 2006). Given this substantial uncertainty, we present the 100 m POC export between 7 and 13 May as a function of the POC:^{234}Th ratio (Figure 2.10). Realistically, the appropriate POC:^{234}Th ratio was probably between 4 and 7 µmol dpm^{-1} (globally, POC:^{234}Th ratios tend to fall within this range as well; *Buesseler et al.* 2006), which translates to a POC export between 360 ± 120 and 620 ± 200 mg POC m^{-1} d^{-1} at 100 m. This export estimate spans the range of values reported by *Buesseler et al.* (1992) for a North Atlantic bloom at 48°N. It also agrees both with a model of the 2008 sub-polar spring bloom, which yields POC export of 480–570 mg m^{-2} d^{-1} (*Bagniewski et al.* 2011), and with an export estimate of 550 mg m^{-2} d^{-1} based on glider optical backscatter (*N. Briggs et al.* submitted).

2.4.3 Transfer efficiency

We can then estimate the transfer efficiency (defined as the percentage of the export flux that is collected at a particular depth) of the export event by comparing POC export at 100 m to the flux in the sediment traps. For this we use the mean POC flux of D3#600 and D3#750 (154 mg POC m^{-2} d^{-1}), which we believe to be most representative of the export event. Transfer

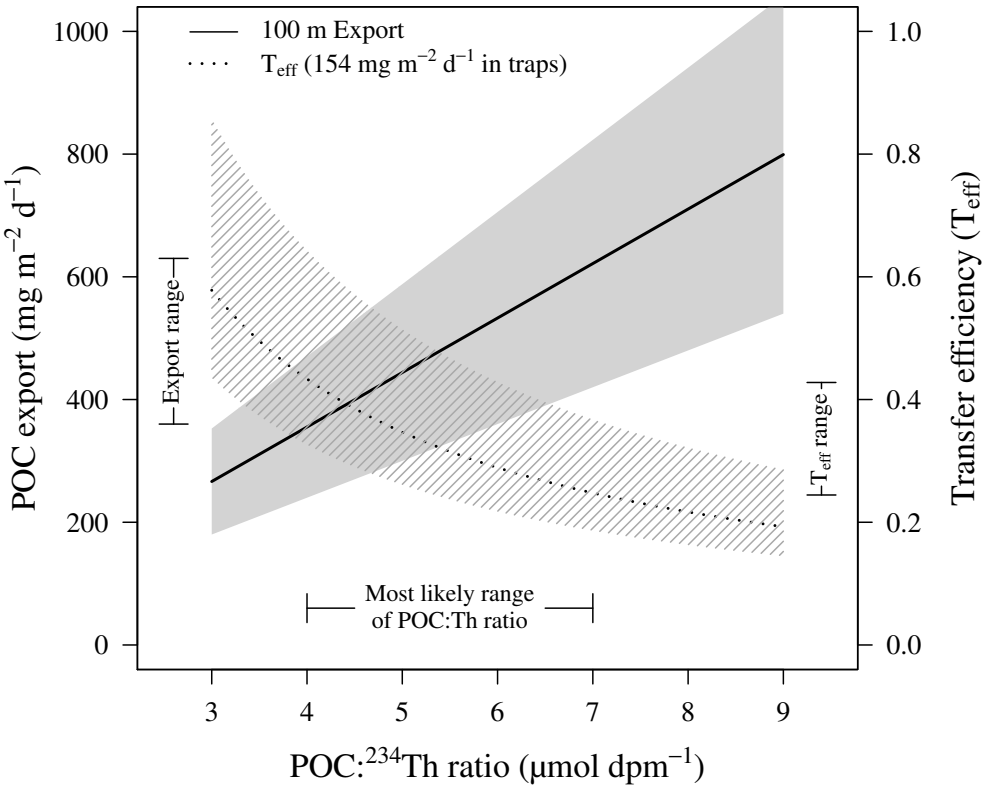

Figure 2.10 – Diagram showing the POC export at 100 m, calculated from ^{234}Th depletion, as a function of the POC:^{234}Th ratio. Also shown is the resulting transfer efficiency, T_{eff}, of the export at 100 m to the two deep traps on Deployment 3 (600 and 750 m), which caught nearly identical POC flux. T_{eff} is defined as the ratio of deep flux to shallow flux. We consider a likely range of POC:^{234}Th to be between 4 and 7 µmol POC dpm^{-1} (indicated on the x-axis), but as the large particle export event was not sampled at shallow depth, we are unable to constrain this ratio well. The resulting bounds on export and T_{eff} of a range in POC:^{234}Th ratio from 4 to 7 are marked on the corresponding y-axes.

efficiency is also plotted in Figure 2.10, using the range of export values based on ^{234}Th. Given a POC:^{234}Th ratio between 4 and 7 μmol dpm^{-1}, the POC transfer efficiency ranges from $43 \pm 11\%$ to $25 \pm 6\%$.

This transfer efficiency through the mesopelagic is high. In comparison, a Martin-type flux attenuation from 100 to 700 m, using Equation 1.1 following *Martin et al.* (1987) would give a transfer efficiency between 100 and 700 m of 19%. The transfer efficiencies we obtained (25–43%) would correspond to a Martin-curve b-exponent between -0.71 and -0.43. This calculation would be compromised if the traps had collected material derived partly from surface waters adjacent to the bloom patch. However, as those waters were mostly low in chlorophyll-a throughout this study (the region of high-chlorophyll water northeast of the patch was 40–60 km away), one would then expect the traps to collect less material than if they collected only particles from inside the patch, thus under-estimating the true flux. In that case, the true transfer efficiency would be even higher than the above estimate.

The calculation of transfer efficiency further assumes that the traps collected with 100% efficiency. Although trapping efficiency can be calculated from the collected flux of natural radionuclides such as ^{234}Th (*Buesseler et al.* 2007a), the depth difference between traps and calculated ^{234}Th export is too great in the present case to do so reliably. However, there was no major discrepancy between the ^{234}Th fluxes caught by the traps and the fluxes calculated from the ^{234}Th profiles. Hence there is no particular reason to question the trap results.

The data presented here are consistent with the comparison of regional studies by *Buesseler and Boyd* (2009), who found that a diatom bloom at 48°N in the Atlantic (*Buesseler et al.* 1992) had the highest transfer efficiency of the nine studies they examined (based on the data between 50 and 150 m, and a model down to 500 m). The present data thus confirm that diatom blooms can lead to large export and efficient transfer of POC through the mesopelagic.

2.4.4 Chemical composition of trap samples

The POC:PON ratios were notably low, mostly below the Redfield ratio of 6.6, and showed no clear increase with depth. This suggests that the particles were relatively undegraded, as carbon has a longer remineralization length-scale than nitrogen, and the POC:PON ratio is often above the Redfield ratio in sediment trap samples (*Schneider et al.* 2003).

The Si:POC ratios overall show a clear increase with depth, which could indicate POC remineralization (*Nelson et al.* 1996; *Ragueneau et al.* 2002). However, the low shallow values were all from D1 and D2, which caught a different particle pulse to the later traps. For instance, the D3 and D4 samples contained large numbers of broken diatom frustules, contributing mostly opal but little POC, but these were much less common in D1 and D2.

The high celestite fluxes, up to 100 mg m^{-2} d^{-1}, are not unexpected in this region. Acantharian cysts rarely sink below the first few 100 m, as their mineral shell dissolves (*Bernstein et al.* 1987; *Antia et al.* 1993; *Michaels et al.* 1995). In the Iceland Basin, however, *Martin et al.* (2010) found a particularly large and fast-sinking type of acantharian cyst (up to 1 mm long; sinking speed 500 m d^{-1}) in sediment traps at 2000 m during spring. The present study confirms that these cysts sink out annually during spring. Celestite is the densest oceanic biomineral

($3.96\,\mathrm{g\,cm^{-3}}$), hence one might speculate whether it ballasts a disproportionate amount of POC. However, the large, smooth-walled cysts in the present samples were generally not entangled with aggregates. While celestite certainly increased the density of the cysts themselves (presumably leading to their high sinking speed), it seems unlikely that celestite played a significant role in ballasting other particles. This could be investigated more thoroughly in future using sampling methods that preserve intact particles, such as polyacrylamide gels (*Ebersbach and Trull* 2008).

2.4.5 Biological composition of trap samples

The material caught during D3 and D4 was rich in TEP, and consisted primarily of phytodetritus. This is consistent with *Passow et al.* (2001), who found that diatom sedimentation was always associated with increased TEP sedimentation. It is also consistent with the hypothesis that TEP are required for particle aggregation during blooms (*Passow et al.* 1994; *Alldredge and Jackson* 1995; *Logan et al.* 1995), as a large flux of phytodetritus should then be TEP-rich. Production of TEP may actually be an ''overflow'' mechanism for excess photosynthate produced by cells that are photosynthesising but unable to divide (*Engel* 2000; *Kahl et al.* 2008), as would happen under Si-limitation. TEP production is hence observed during bloom senescence when cells are physiologically stressed (*Kahl et al.* 2008).

It is still unclear why phytoplankton should produce such sticky exudates, given that they cause mass sinking (see review by *Thornton* 2002). *Smetacek* (1985) hypothesised that mass sinking occurs in response to nutrient stress, and enables cells to rapidly leave nutrient-depleted, warm surface waters (in which survival and formation of resting stages are significantly compromised) and form resting stages in cold, dark waters below. *Logan and Alldredge* (1989) also calculated that cells inside sinking, porous aggregates can take up nutrients twice as fast as non-aggregated cells. Spores are usually heavily-silicified, and their production can more than double cellular $Si(OH)_4$ demand (*Kuwata et al.* 1993; *Oku and Kamatani* 1995) — however, at least some cells in the samples were apparently still in the process of spore formation (*T. Rynearson* pers. comm.), so it is possible that cells only started upon reaching high-Si waters below the mixed layer. *Alldredge et al.* (1995) also found that *Chaetoceros* resting spores were present mostly within aggregates at the end of a diatom bloom in a mesocosm.

The co-incidence of export with Si-depletion, and the large numbers of viable resting spores recovered by the traps, are consistent with the hypothesis of *Smetacek* (1985). Yet if sinking and spore formation are to have any survival value, spores must be able to return to the surface again. In coastal areas where the full water column can be mixed, spores can reach from the sediment back to the surface. In open ocean settings such as the Iceland Basin, spores would need to remain in the mesopelagic to be mixed back to surface waters, but this appears to be possible: *D'Asaro* (2008) showed with a model that winter-time convection in the North Atlantic can entrain slowly-sinking phytoplankton back to the surface. Moreover, living phytoplankton cells have been found throughout the winter mixed layer to depths of 800 m in the North Atlantic, with integrated chlorophyll-*a* over this layer around $2\,\mathrm{mg\,m^{-3}}$ (*Backhaus et al.* 2003). *McQuoid and Hobson* (1996) also speculate that diatom resting stages might be

able to remain suspended within the water column throughout the winter, and *Smetacek* (1985) suggested that active buoyancy control might play a role.

The particles caught in the sediment traps were apparently sinking very rapidly, and would probably have sunk below the permanent thermocline within a few more days. However, while the transfer efficiency of this export pulse was comparatively high, at least 55% of the exported POC was either remineralized or its sinking rate substantially slowed before reaching the deep sediment traps. This leaves open the possibility that significant numbers of spores dissociated from sinking aggregates in the mesopelagic, so rapid sinking and comparatively high transfer efficiency do not necessarily counter-indicate the possible survival value of sinking.

2.5 Conclusions

A sub-polar North Atlantic diatom bloom led to substantial export of particulate organic carbon in the form of phytoplankton aggregates during a sudden export event. These particles were rich in TEP, and had a high transfer efficiency through the mesopelagic. Sedimentation of the bloom probably occurred because Si stress of diatoms led to TEP production, which promoted aggregation and sinking. It is possible that particle flux changed very rapidly over time, with a very sudden and large decrease in flux causing a shallower trap to catch lower flux than deeper traps. Large numbers of resting cysts were found, consistent with the hypothesis that rapid sinking can be of survival value to diatoms.

Chapter 3

Particle Flux During LohaFEX

Data contribution

PELAGRA traps were deployed by the author and Kevin Saw (NOCS), and samples were processed by the author (swimmer picking, splitting, filtering). Samples for POC/PON were prepared by the author, and measured by Bob Head (PML). Darryl Green and Mark Stinchcombe helped with ICP-OES and BSi measurements, respectively (both NOCS). Nutrients were measured by Anil Pratihary (NIO, India). $\frac{F_V}{F_M}$ was measured by Maurizio Ribera d'Alcalà (SZN, Italy). ^{234}Th was measured by Michiel Rutgers van der Loeff (AWI), Melena Soares (NIO, India), and R. Rengarajan (PRL, India). Faecal pellet carbon, and unicellular plankton cell counts and calculation of unicellular plankton cell carbon were undertaken by Humberto González (UAC, Chile), and Friederike Ebersbach (AWI), respectively. Friederike Ebersbach additionally prepared and analysed the polyacrylamide gels. O_2:Ar data processing and NCP calculation were performed by Nicolas Cassar (Duke U.); Hema Naik (NIO, India) took care of the mass spectrometer on board. Maureen Pagnani (NOCS) processed the ARGO data to obtain mixed layer depths. The model of patch movement was developed and calculated by Francesco d'Ovidio (Institute of Complex Systems, Paris), who also analysed the suitability of candidate eddies from altimeter data.

Abstract

Downward particle flux was measured during a 39 d artificial iron fertilisation experiment in the Polar Frontal Zone of the Atlantic sector of the Southern Ocean. Two tonnes of iron (as $FeSO_4$) were applied to a $\sim$300 km^2 area inside the closed core of a cyclonic eddy, with a second application of another two tonnes of iron after 18 d. NO_3^- and PO_4^{3-} concentrations were high, but $Si(OH)_4$ was $<2\,\mu mol\,L^{-1}$. A modest response by phytoplankton was observed (doubling of chlorophyll-a and primary productivity, increase in $\frac{F_V}{F_M}$ from 0.25 to 0.35–0.45); diatoms contributed $<$10% of carbon biomass and the phytoplankton was dominated by cells $<$10 µm in size. Grazing pressure by zooplankton, especially copepods, was very high. Export as diagnosed from ^{234}Th profiles remained unchanged inside the patch ($\sim$75 mg POC m^{-2} d^{-1} at 100 m) and did not differ from adjacent unfertilised waters. Neutrally buoyant sediment traps deployed at 200 m and 450 m inside and outside the patch recorded low fluxes and no increase upon fertilisation (mostly $<$15, and not exceeding 23 mg POC m^{-2} d^{-1} at 450 m). Samples contained mostly faecal material. Net community production inside the patch as measured continuously from O_2:Ar ratios was on average 98–115 mg POC m^{-2} d^{-1}, but was largely balanced by down-

ward export, suggesting that total organic carbon accumulation was probably $<1\,\mu mol\,L^{-1}$. That particle flux did not increase upon fertilisation is attributed to strong grazing pressure on the phytoplankton, which limited biomass build-up, and to substantial re-processing of sinking particles by detritus feeders. Fe fertilisation of low-$Si(OH)_4$ areas may not lead to substantial enhancement of downward POC flux because diatoms do not build up enough biomass, although the outcome probably depends strongly on the zooplankton community. Combining O_2:Ar and ^{234}Th measurements over $\sim$1 month appears to be a way of obtaining estimates of net community production and POC export that can be sensibly compared over this time-scale.

3.1 Introduction

Anthropogenic CO_2 emissions are currently around $8.5\,Pg\,C\,y^{-1}$, and account for the majority of radiative forcing from total anthropogenic greenhouse gas emissions (*IPCC* 2007 [pp. 137–140]; *Friedlingstein et al.* 2010). Because large-scale cuts to emissions are proving politically very difficult to implement, the scientific community has started to consider ways of artificially altering the climate or removing CO_2 from the atmosphere, so-called geoengineering (*Lenton and Vaughan* 2009). One such scheme is the artificial fertilisation of large areas of the open ocean with iron (Fe), with the intention of sequestering organic carbon in the deep ocean below the permanent thermocline.

Fe is required in several essential enzyme systems, such as for chlorophyll synthesis and electron transport chains. However, Fe concentrations in the open ocean are very low, both because of limited supply (chiefly by aeolian dust and upward mixing from deeper water), and because dissolved Fe is rapidly oxidised to the relatively insoluble Fe(III) in seawater (*Millero et al.* 1987). Early shipboard incubation studies showed that growth of natural phytoplankton populations can be Fe-limited (*Martin and Fitzwater* 1988), and led to the suggestion that glacial-interglacial changes in atmospheric CO_2 concentration may have been caused by changes in atmospheric dust (*i.e.* Fe) supply to the oceans (*Martin* 1990). While it is now thought that changes in Fe supply cannot account for the majority of glacial–interglacial CO_2 changes (*Röthlisberger et al.* 2004), it has become clear that primary productivity in much of the Southern Ocean and the sub-arctic and equatorial Pacific is limited by Fe availability (*de Baar et al.* 2005; *Boyd et al.* 2007). These areas have perennially high NO_3^- and PO_4^{3-} concentrations, but relatively low chlorophyll-*a*, and are hence known as High Nutrient Low Chlorophyll (HNLC) areas.

The twelve mesoscale artificial Fe fertilisation experiments (FeAXs) conducted to date demonstrated that Fe addition leads to blooms of large-celled diatoms, draw-down of macronutrients and fCO_2 in the surface mixed layer, and in a few cases enhanced particle export flux out of the surface mixed layer (*de Baar et al.* 2005; *Boyd et al.* 2007). However, none of these experiments were designed to test the effectiveness of Fe fertilisation as a geoengineering tool — thus the POC flux below the permanent thermocline was not measured in any FeAX. However, POC flux decreases sharply between the depth of shallow export (typically 100 m) and the permanent thermocline, and the magnitude of this decrease is highly dependent on biological community structure in the surface and mesopelagic (*Boyd and Trull* 2007; *Lam and Bishop*

2007; *Buesseler and Boyd* 2009). Therefore, an enhancement of export flux upon Fe addition cannot be taken as evidence that sequestration below the permanent thermocline has also been enhanced, as heterotrophic activity in the mesopelagic might also be stimulated. Hence FeAXs must be conducted in which the sequestration flux over the full bloom period is also measured.

Two studies have investigated the effect of natural iron fertilisation from the Crozet and the Kerguelen islands, both in the Southern Ocean. Export flux was enhanced several-fold in the Kerguelen bloom (*Blain et al.* 2007), and both export and sequestration flux were enhanced in the Crozet bloom (*Pollard et al.* 2009). These cases are especially significant, since these naturally fertilised blooms recur annually, and thus mimic sustained fertilisation for geoengineering purposes better than one-off FeAXs. Modelling studies also suggest that large-scale Fe fertilisation (*e.g.* fertilising the whole Southern Ocean) might cause a modest decrease in atmospheric CO_2 concentration (sequestering $\leq 1\,\mathrm{Pg\,C\,y^{-1}}$) (*Zeebe and Archer* 2005; *Aumont and Bopp* 2006; *Lenton and Vaughan* 2009). Fe fertilisation alone is thus clearly not capable of solving the anthropogenic CO_2 problem, but could be included in a portfolio of strategies to stabilise, and ultimately reduce, atmospheric CO_2 (see *Pacala and Socolow* 2004). Fe fertilisation might also have negative consequences (see *Lampitt et al.* 2008a), and more research is undoubtedly needed to determine (a) how much carbon really can be sequestered this way, and (b) whether negative side-effects might outweigh the benefits of reducing atmospheric CO_2.

A recurrent problem in biogeochemical flux studies, not only FeAXs, is that particle flux can in principle be quantified using different observational techniques — and when several are applied during the same cruise, their results can often differ several-fold. This holds particularly for comparisons between sediment trap or ^{234}Th measurements and techniques that measure new production (NP), net community production (NCP), or f-ratios, with discrepancies usually attributed to POC or DOC accumulation, or to the different integration time-scales of the methods (*Smith and Dunbar* 1998; *Morris et al.* 2007; *Lampitt et al.* 2008b; *Savoye et al.* 2008). Recently, mass spectrometric methods have been developed for continuous high-frequency NCP measurements based on the O_2:Ar ratio in seawater, which has an integration time-scale of 1–2 weeks (*Kaiser et al.* 2005; *Cassar et al.* 2009), *i.e.* more similar to the integration time-scale of the ^{234}Th method than either seasonal nutrient budgets (*Sanders et al.* 2005, 2007) or ^{15}N uptake methods (*Dugdale and Goering* 1967). Using both ^{234}Th and O_2:Ar-based NCP over approximately one month (the integration time of ^{234}Th) in the same water mass should therefore give results either comparable in magnitude, or differing due to POC/DOC storage, without the confounding differences in integration time-scale.

This study therefore aimed to measure export and sequestration flux during LohaFEX (*loha* is the Hindi word for iron), a mesoscale FeAX of >1 month duration, and to compare the export flux estimated from ^{234}Th to NCP estimated from O_2:Ar.

3.2 Methods

3.2.1 Site selection

A ten-week research-cruise was undertaken aboard R/V *Polarstern* from January to March 2009 to test whether artificial iron-fertilisation enhances particle export in the Atlantic sector of the Southern Ocean. The intention was to fertilise the closed core of a stable mesoscale eddy formed from meandering frontal jets in the Antarctic Polar Frontal Zone (*Smetacek and Naqvi* 2008). These eddies can extend to the sea floor and are relatively stationary, with low current speeds in the centre. If a patch is fertilised in the very centre of such an eddy, its horizontal movement, dilution with adjacent unfertilised waters, and distortion of the initial shape will be low. Moreover, the surface and sub-surface circulation are relatively contiguous, and thus neutrally buoyant sediment traps deployed in the mesopelagic (as used in this study) are likely to remain below the patch, and to collect particles derived from surface waters directly above.

Potentially suitable eddies for fertilisation were identified from satellite altimeter images during transit to the study site. Their stability was assessed by modelling the rate at which trajectories starting from adjacent points within the eddy diverged, and by studying the evolution of the altimeter images over time. Several eddies were then investigated more closely from the ship to assess their suitability based on physical (current speeds and trajectories), chemical (nutrient concentrations), and biological (phytoplankton community structure) properties. The goal had been to fertilise a water-mass high in $Si(OH)_4$ to promote a diatom bloom. However, low $Si(OH)_4$ concentrations ($\leq 2\,\mu mol\,L^{-1}$) were found throughout the cruise-track during site selection, and thus the experiment had to be conducted under low-Si conditions (although NO_3^- and PO_4^{3-} were both high). A cold-core eddy at 48°S 15°W was selected, fertilised, and studied for 39 d post-fertilisation. Measurements taken inside the patch were compared to control observations taken in unfertilised waters of the eddy. The study area and two altimeter images of the eddy are shown in Figure 3.1.

3.2.2 Fertilisation and patch tracking

Fertilisation started on 27 January 2009. Two drifting buoys with sub-surface drogues at 30 m were deployed to mark the presumed centre of the eddy, and transmitted their positions via satellite every ten minutes. Ten tonnes of $FeSO_4 * 7\,H_2O$ (containing two tonnes of Fe) were then dissolved in seawater acidified with HCl, and pumped out into the ship's propeller wash as the ship steamed outwards in a spiral around the drifting buoys. A circular area of approximately $300\,km^2$ was thus fertilised. The inert tracer SF_6 was injected along with the iron to label the patch. After 18 d the patch was re-fertilised with a further ten tonnes of $FeSO_4 * 7\,H_2O$, although an instrument fault prevented injection of further SF_6.

Unfortunately, the patch started drifting, completing two revolutions inside the eddy and finally being expelled from the eddy core during the final days of the experiment. The location of the patch was tracked using the positions of the drifting buoys, and measurements of SF_6 (via gas chromatography), of the fluorescence ratio $\frac{F_V}{F_M}$ of phytoplankton, and of the concentration of chlorophyll-*a* as measured in discrete water samples. The first two drifting buoys eventually

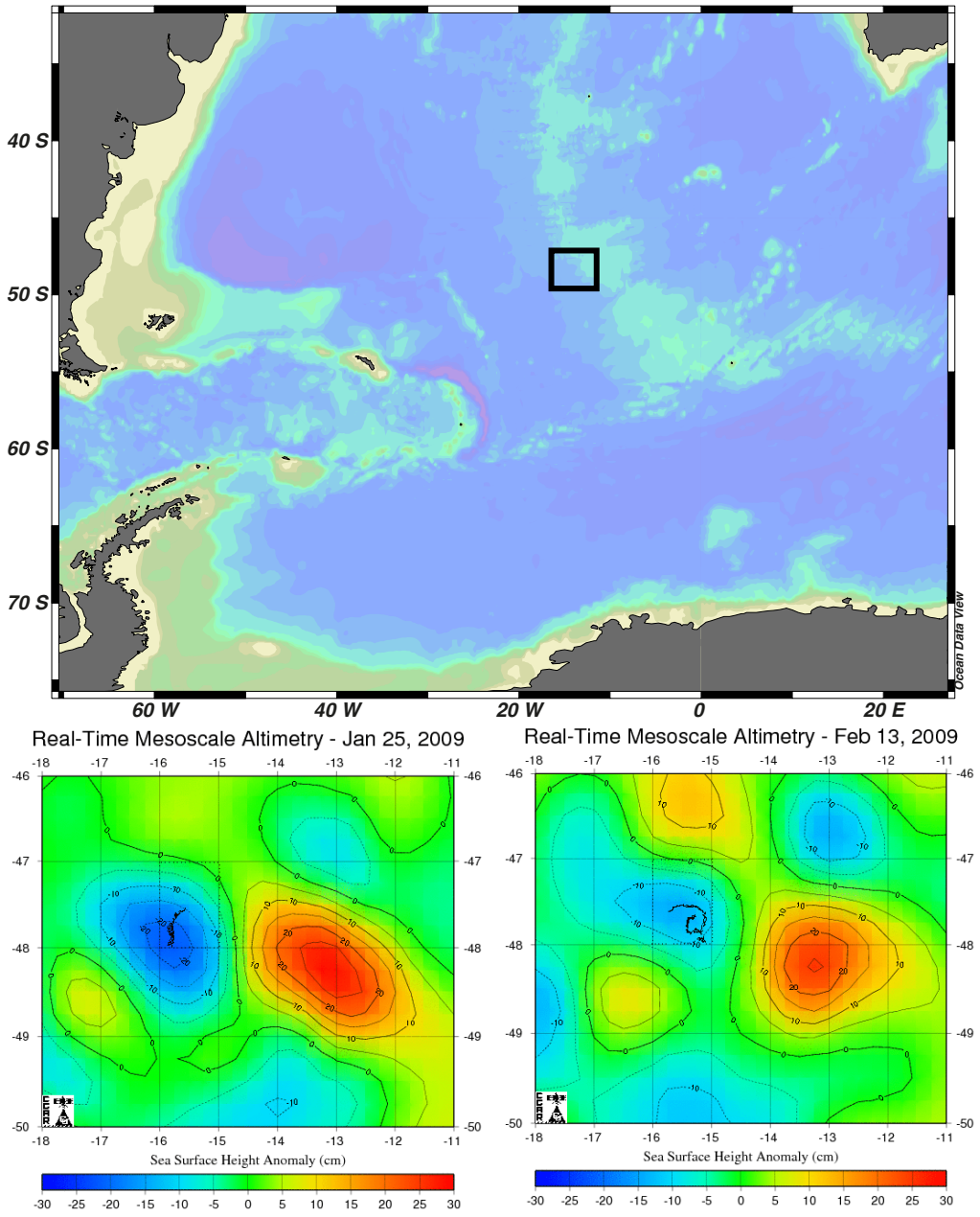

Figure 3.1 – Bathymetric chart of the South Atlantic, with the LohaFEX study area marked by the black box. Two altimeter images of the cold-core eddy chosen for fertilisation are also shown, with the scale bars indicating the sea surface height anomaly (from −30 cm to +30 cm). The drift of the buoys is shown until Day 5 in the 25 Jan image, and between Day 5 and Day 17 in the 13 Feb image. Altimeter images were downloaded from `http://argo.colorado.edu/~realtime/gsfc_globalrealtime_ssh/`

became detached from the main area of the patch, probably due to wind forcing, so a third buoy was deployed after 13 d. After 24 d, the first buoy was recovered and re-deployed in the centre of the main area of the patch, and a fourth buoy was deployed after 31 d. The first three buoys are referred to as Buoys 1–3. After being re-deployed, Buoy 1 was designated Buoy 4, and the fourth buoy (deployed after 31 d) is therefore referred to as Buoy 5.

To obtain an estimate of the location and extent of the patch throughout the cruise, the movement of the patch was modelled as described in Section 3.2.8.

3.2.3 Macronutrients and $\frac{F_V}{F_M}$

The macronutrients $NO_3^- + NO_2^-$, NH_4^+, PO_4^{3-}, and $Si(OH)_4$ were measured at sea in discrete water samples on a Skalar segmented-flow autoanalyser using standard procedures.

$\frac{F_V}{F_M}$ was measured continuously from the underway supply using a Chelsea Technology Group Fast Repetition Rate Fluorometer (FRRF), and averaged over 2 min intervals. Due to strong fluorescence quenching during the day, only night-time $\frac{F_V}{F_M}$ values were used (19:00 to 06:00).

3.2.4 ^{234}Th measurements

Vertical profiles of total ^{234}Th were measured using a 4 L technique with ^{230}Th added as a recovery standard (*Pike et al.* 2005; Appendix B.5.3). Sinking particles (>53 µm) for POC:^{234}Th ratio measurements were collected with *in situ* pumps (ISPs) at ten stations at 100 m depth (Appendix B.5.3). Smaller size-fractions were also sampled, and samples were also taken from 200 m depth — but as ^{234}Th export was calculated at 100 m, only the >53 µm data from 100 m were used here. POC:^{234}Th ratios were also measured in six sediment trap samples, as described in Section 3.2.6.

3.2.4.1 Underway surface sampling

^{234}Th was additionally measured every 4 h from the underway supply using an automated sampler (*Rutgers van der Loeff et al.* 2004, 2006). This device first filters 5 L of water from the underway supply onto a QMA filter to measure particulate ^{234}Th, and then co-precipitates dissolved ^{234}Th in the filtrate with MnO_2 (Appendix B.5.2). The activity on both filters was counted as for water-column samples (Appendix B.5.3). The precipitation efficiency was measured using water from 400–3000 m depth, and found to be 1.00 ± 0.07.

Measurements were designated as In- or Out-patch measurements based on the model of patch movement described in Section 3.2.8 (between Days 0 and 31), and based on the distance between the sampling location and Buoy 5 thereafter (measurements were designated "In" if they were within ten nautical miles of the buoy). Results from the underway samples are presented as the activity ratio of ^{234}Th:^{238}U, which is 1 under secular equilibrium, and <1 if ^{234}Th is depleted relative to ^{238}U. This was calculated from the concentration of ^{234}Th and of ^{238}U in each sample (^{238}U calculated from salinity; *Chen et al.* 1986). For the particulate samples, the activity ratio was calculated as the ratio of the activity of particulate ^{234}Th to total ^{238}U in the sample; particulate ^{238}U was not measured.

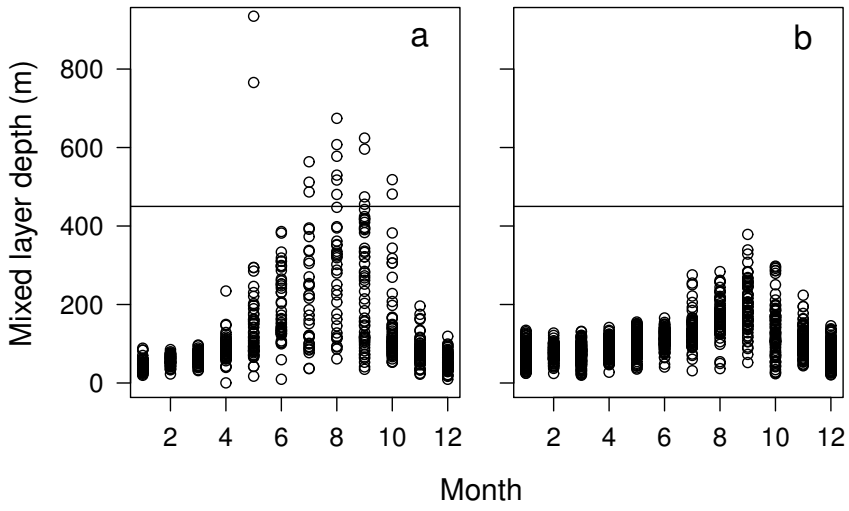

Figure 3.2 – Estimated mixed layer depth for each month in (a) the original target study area from 55°S 60°W to 50°S 30°W during 2003–2008; and (b) in the actual study area from 55°S 25°W to 45°S 5°W during 2005–2010. Mixed layer depths were estimated as the depth at which temperature changed by 0.5 °C from the surface value. The horizontal lines are drawn at 450 m, the depth of trap deployment.

3.2.5 Sediment trap deployments

Neutrally buoyant PELAGRA sediment traps (*Lampitt et al.* 2008b; Appendix A.1.1) were deployed inside and outside of the patch, nominally at 200 m and 450 m. Only one or two traps were deployed on each deployment out of a total of five traps on board; thus a new trap could be deployed 24 h before any currently-collecting trap was due to surface (collection cups were only opened 18–24 h after deployment). This strategy yielded greater temporal coverage at the expense of higher depth and/or spatial resolution. As the onset of particle export during phytoplankton blooms can be very sudden (*Martin et al.* 2011; Chapter 2), greater temporal coverage was prioritised. Deployment durations were therefore typically 5–6 d. 450 m was chosen as a conservative estimate of the maximum depth of convective mixing during austral winter, *i.e.* the depth below which particles need to sink to be sequestered. This was based on isothermal layer depth estimates from ARGO data (depth at which temperature changes by 0.5 °C relative to the surface value), obtained before the cruise for the period 2003–2008 in the area 55°S 60°W to 50°S 30°W (the original target study area). These data are shown in Figure 3.2a. Mixed layer depths around the actual study area were slightly shallower, as shown in Figure 3.2b for 55°S 25°W to 45°S 5°W during 2005–2010.

Cups were filled with formalin preservative (Appendix A.2) to measure fluxes of total mass, POC, PON, PIC, BSi, intact faecal pellets, intact phytoplankton cells, and on some traps ^{234}Th. A 0.5% v/v solution of chloroform in seawater was used in some cups to preserve particles for trace metal flux measurements. Finally, some cups were equipped with polyacrylamide gels, which preserve sinking particles intact without disruption (*Ebersbach and Trull* 2008).

3.2.6 Sediment trap sample analyses

3.2.6.1 Sample processing on board

All cups on a trap that contained formaldehyde preservative (usually three cups per trap) were recombined in a 4 L LDPE bottle, shaken, and split into sub-samples using a rotary splitter identical to that described by *Lamborg et al.* (2008). Split sizes were between $\frac{1}{8}$ and $\frac{3}{64}$. Swimmers were removed at sea from splits for mass+POC+PON, PIC, BSi, and ^{234}Th measurements under a Wild dissecting microscope (magnification 60–120×). Swimmer-free splits were then filtered onto pre-combusted (4 h at 550 °C), pre-weighed 25 mm Whatman GF/F filters (mass+POC+PON), 25 mm polycarbonate filters (0.4 µm mesh, for PIC and BSi), or 25 mm QMA filters (POC:^{234}Th ratios). All filters were then rinsed once with MilliQ. Filters for ^{234}Th were processed as for ISP samples (Appendix B.5.3); the other filters were stored at −20 °C until analysis on land. Splits for phytoplankton cell counts and for faecal pellet analysis were stored at +4 °C until analysis on land.

Polyacrylamide gels were photographed on board following *Ebersbach and Trull* (2008).

3.2.6.2 Chemical analyses

Fluxes of dry weight, POC, PON, and BSi were measured as described in Appendices B.1 and B.3. POC:^{234}Th samples were measured as described in Appendix B.5.3.

PIC samples were size-fractionated to determine coccolith and foraminiferan/pteropod carbonate separately as described in Appendix B.2.

Blanks for POC/PON, PIC, and BSi were prepared by filtering ∼200 mL of blank formalin preservative through the appropriate filter type and then treating the filters exactly as for samples.

The contribution by intact faecal pellets to POC flux was quantified in one split by removing faecal pellets onto a pre-combusted Whatman GF/F filter (450 °C, 6 h). Filters were acid-fumed with concentrated HCl, oven-dried at 55 °C, and POC analysed on a Europa Hydra 20-20 continuous-flow isotope ratio mass spectrometer after combustion at 1000 °C at the University of California Davies Stable Isotope Facility Laboratory; acetanilide was used as the standard.

Unfortunately, not enough material was available for the various measurements to be replicated; measurement errors can therefore not be directly quantified. However, judging by the results especially from Chapter 2, it would be reasonable to assume around 10% error for the chemical analyses conducted on the trap samples.

3.2.6.3 Cell counts

Unicellular organisms in the sediment trap material were counted under inverted light and epifluorescence microscopy (Axiovert 135 and 200 inverted microscopes, Zeiss, Germany) following *Utermöhl* (1958). 10 or 50 mL aliquots of each sample were settled in sedimentation chambers (Hydrobios, Germany) for 48 h, and cells counted at 100, 200, or 400× magnification, depending on cell size. For each taxon, the average biovolume was measured from 10–20 specimens (*Hille-*

brand et al. 1999), which was then converted to organic carbon according to *Menden-Deuer and Lessard* (2000). The combined POC flux from all unicellular plankton taxa was then calculated.

3.2.7 Net community production

The ratio of O_2:Ar was measured continuously in surface seawater by equilibrator inlet mass spectrometry following *Cassar et al.* (2009). Water from the underway supply was pumped into a gas equilibrator cartridge with a 2 mL headspace. The O_2:Ar ratio of the equilibrated gas in the headspace was measured continuously by a quadrupole mass spectrometer (Pfeiffer Prisma QMS 200 M1), which was calibrated by sampling outside air every 2–4 h. Measurements were averaged over 2 min intervals. NCP, in mmol O_2 m^{-2} d^{-1}, was calculated from each O_2:Ar ratio as described in *Reuer et al.* (2007). Further details regarding the method and calculation are given in Appendix B.7.

This yielded a dataset with >10,000 observations, derived from fertilised and un-fertilised waters within the eddy, as well as from waters outside of the eddy. To use this dataset to help analyse the biogeochemical developments after fertilisation, it needed to be separated into In-patch and Out-patch measurements. This was first done crudely by just averaging the NCP values collected during each station occupation — as it was clear during the stations whether the ship, and thus the NCP measurements, were inside or outside of the patch. A more refined approach was also employed, in which the extent and trajectory of the patch were modelled at hourly intervals, and the position of each NCP measurement compared to the modelled patch location at the corresponding time-point. The model and the subsequent analysis of the NCP data are described in Section 3.2.8. Short gaps in the dataset ($\leq$1 h) occurred due to routine calibration, but instrument problems caused gaps of up to several days. In particular, no measurements are available from the final week of the experiment, and thus the NCP data were only analysed up until 30 d post-fertilisation (NCP values at the very end of the experiment were approximately equal to values around Day 30).

3.2.8 Model of patch movement and NCP calculations

The shape of the patch was modelled as an ellipse, described by a centre-point and two axis lengths, and an angle of rotation of the major axis. The model was calculated at hourly resolution, with the centre chosen as the position of the buoy closest to the centroid of $\frac{F_V}{F_M}$ of that day's $\frac{F_V}{F_M}$ measurements (using only $\frac{F_V}{F_M}$ values $\geq$0.35 as recommended by *M. Ribera d'Alcalà*, pers. comm.). The axis lengths for each centre were chosen based on a Lagrangian model applied to the initial patch that consisted of the surface geostrophic velocities (derived from daily satellite altimeter data) and accounted for horizontal diffusion of 20 m^2 s^{-1}. In other words, the initial fertilised area was assumed to be homogeneous and was then advected using the Lagrangian model, which accounted for lateral stirring and diffusion. For each hourly time-step, the axis lengths were calculated and combined with the corresponding centre-point. The orientation of the patch was chosen to be tangential to the modelled trajectory of the patch centroid, and calculated as an angle of rotation of the major axis. The reason why the centre-point was not taken from the Lagrangian model was that small errors in the altimetry-derived

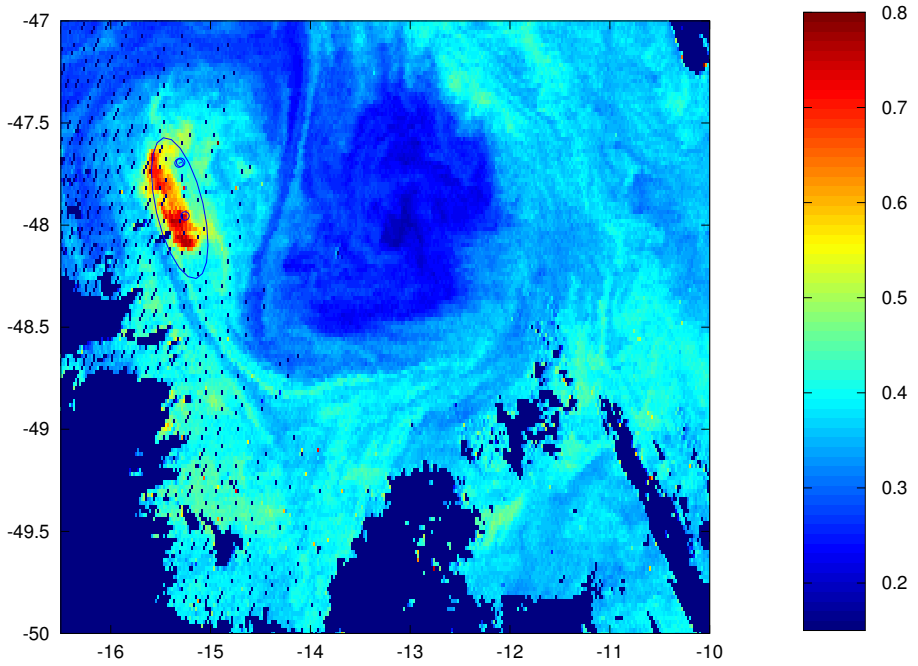

Figure 3.3 – Daily composite MODIS map of chlorophyll concentration from 14 Feb with the modelled extent of the patch for that day shown by the ellipse. The scale bar indicates chlorophyll-*a* in $\mathrm{mg\,m^{-3}}$.

velocities could lead to a systematic lead or lag of the modelled patch relative to the real patch. When the centre-point was shifted from one buoy to another, smoothing was applied to the shift to prevent sudden jumps. For each day, the first and last patch model is shown together with the daily drift of the buoys, the night-time $\frac{F_V}{F_M}$ measurements, and station locations in Figures 3.4–3.6. The ellipses inevitably include some unfertilised areas, and exclude some fertilised areas. However, there was close agreement between the modelled extent of the patch and the only good-quality satellite image of surface chlorophyll concentration, taken on 14 Feb (Figure 3.3) — this image was used to correct the centre point of the patch, so it is not an independent estimate of the patch centre, but it was not used in calculating the axis lengths of the patch, thus providing an independent control on the modelled dispersion and shape of the patch.

NCP data were further analysed in R version 2.12.1 to calculate the overall mean NCP for the first 30 d of the study. At each hourly step of the patch model, the NCP measurements taken during that hour were designated as In or Out measurements depending on whether they were inside or outside of the model ellipse. This yielded a dataset with a clear temporal trend, but extensive gaps — the mean of the observations would therefore not reflect the true mean NCP over the period.

To interpolate between the gaps, and thus calculate a less biased mean, a loess function was fit to the In patch data. This is a non-parametric smoothing method in which a polynomial function is fit at each point to a subset of the data using a weighted least squares method (data points are weighted according to their distance from the point of calculation, with more distant data points given lower weights) (*Cleveland and Devlin* 1988). Five loess models were tested,

using subsets of 5–35% of all data points. From each loess model, interpolated NCP data were calculated at 2 min frequency across all gaps in the NCP measurements and then combined with the measured values. The mean NCP was then calculated as the overall mean of the measured and interpolated NCP values up until Day 30.

The uncertainty around these mean NCP values was then estimated by de-trending the time-series with each loess fit (*i.e.* the modelled NCP value at each time-point was subtracted from the measured NCP value), and then calculating the standard error of the de-trended time-series. Each standard error was then multiplied by the correction factor proposed by *Bence* (1995) for autocorrelated time-series

$$k = \sqrt{\frac{1+\rho}{1-\rho}}, \tag{3.1}$$

where ρ is the autocorrelation function at lag = 1.

To test how strongly the calculation of mean NCP was affected by changes in the patch model, it was repeated using only NCP measurements from within an ellipse with axis lengths half those of the original patch model. Both results are presented here.

3.3 Results

3.3.1 Surface biological and biogeochemical response to fertilisation

$\frac{F_V}{F_M}$ was low (∼0.25) prior to fertilisation, and increased to around 0.35–0.45 post-fertilisation. The chlorophyll-*a* concentration approximately doubled inside the patch after fertilisation, with concentrations around 1–1.5 mg m^{-3} (but >80% of total chlorophyll-*a* was always found in the <20 µm size-fraction). Primary productivity as measured in ^{14}C bottle incubations also increased, with values outside of the patch remaining <1000 mg C m^{-2} d^{-1} but increasing to up to 1600 mg C m^{-2} d^{-1} inside (*M. Gauns*, pers. comm.). The NO_3^- concentration inside the patch was initially 20 µmol L^{-1}, and decreased by ∼2.5 µmol L^{-1} during the 39 d. The $Si(OH)_4$ concentration inside the patch was very low, between 0.6–1.6 µmol L^{-1}, and did not show a steady decrease over time. While diatoms were present and even growing at high rates (especially *Fragilariopsis kerguelensis* and *Corethron pennatum*) they were at the small end of their species' size ranges, and 70–80% of phytoplankton biomass was contributed by small flagellates (<10 µm; *P. Assmy*, pers. comm.). The coccolithophore *Emiliania huxleyi* was present initially, but declined after fertilisation. Copepods exerted very high grazing pressure on the phytoplankton community: grazing by *Calanus simillimus* could usually account for >30% of NPP (range: 0.7–240%, *H. González*, pers. comm.). Copepods of the genus *Oithona* (mostly *Oithona similis*) were particularly abundant, with numbers on the order of 200,000 m^{-2} (*M. G. Mazzocchi*, pers. comm.).

3.3.2 Movement of the patch and trap trajectories

Figures 3.4–3.6 show daily images of the modelled patch position together with the drift of the buoys and the night-time $\frac{F_V}{F_M}$ values. The patch completed two rotations within the eddy, of

approximately 100 km diameter, and was then expelled from the eddy around 28 Feb. However, it remained relatively intact throughout this period and although it became elongated, it was not drawn out into a narrow filament. Moreover, dilution with non-fertilised waters was modest (*F. d'Ovidio* pers. comm.).

Trajectories of the sediment traps are shown in Figure 3.7, with the modelled patch positions, night-time $\frac{F_V}{F_M}$ values, and trajectories of the drifting buoys. Clearly, the trajectories of the traps are consistent with the surface circulation indicated by the drifting buoys; moreover, traps deployed at the same location but different depths during the first deployment surfaced very close to each other (see Figure 3.7a), suggesting relatively homogeneous circulation down to 450 m depth. Based on these maps, traps were designated as In- or Out-patch traps as listed in Table 3.1.

Traps D2#440 and D3#200 are ambiguous: they were deployed close to Buoys 1 and 2, and followed the buoys closely, but the main part of the patch seemed to lag behind Buoys 1 and 2 (hence Buoy 3 was deployed at this time). Buoys 1 and 2 were probably not completely expelled from the patch, but may have moved with only a narrow tongue of fertilised water, thus these traps might have collected particles from outside of the patch.

Traps D7#430 and D8#230 were both deemed Out traps as they were deployed quite far behind the patch, and both appeared to surface outside the patch. Although the surfacing position of D7#430 is inside the patch model, the real patch was squeezed up against the eastern edge of the eddy at this time, resulting in a very sharp boundary with unfertilised waters (Figure 3.7g), and D7#430 did surface outside of the patch.

While all but two traps are referred to here as simply In or Out, no traps should be considered entirely unambiguous. Although the fertilised patch was large, tracking its movement and shape over the substantial distance it drifted was very challenging, and it is hence impossible to be sure that the In traps only collected particles from undiluted waters inside the patch. Conversely, constraints on ship-time limited how far outside of the patch the Out traps could be deployed, and it is thus possible that their collections were partly influenced by the patch.

3.3.3 Export based on ^{234}Th

Figure 3.8a shows the export flux of ^{234}Th calculated with a steady-state model at 100 m. The flux varied from 1020 to 1740 $\mathrm{dpm\,m^{-2}\,d^{-1}}$, with stations inside the patch ranging from 1120 to 1690 $\mathrm{dpm\,m^{-2}\,d^{-1}}$. Total analytical uncertainties were $\leq$13%, typically between 6% and 9%. There was no clear trend over time inside the patch indicative of a fertilisation-induced export event: the range in flux during the first six days was nearly as large as the range over the entire experiment. Increases in particle export tend to occur mostly upon collapse of a bloom (*Buesseler et al.* 1992; *Cochran et al.* 2000; *Buesseler et al.* 2001; *Martin et al.* 2011), hence the range in ^{234}Th-based export estimates over the first 6 d probably reflects existing spatial variability in the patch, rather than an increase upon fertilisation. Because subsequent measurements mostly fell within the same range, and no clear trend over time was apparent, a steady-state model of ^{234}Th flux was applied (Appendix B.5.4).

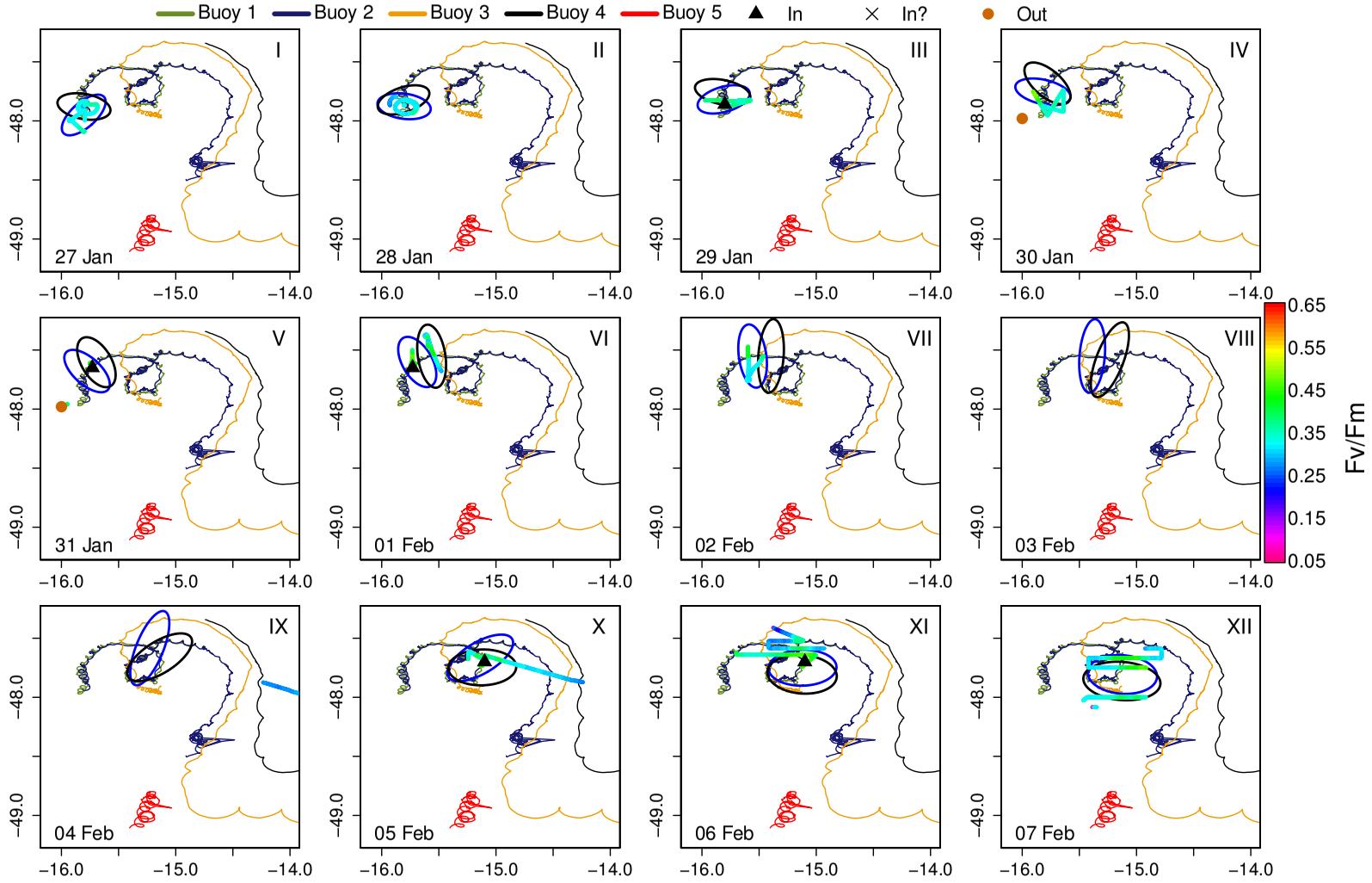

Figure 3.4 – Daily maps of patch position and night-time $\frac{F_V}{F_M}$ from 27 Jan to 07 Feb superimposed on the trajectories of the drifting buoys. The position of each CTD station is also shown, with the plotting symbol indicating whether that station was In, probably In, or Out of the patch.

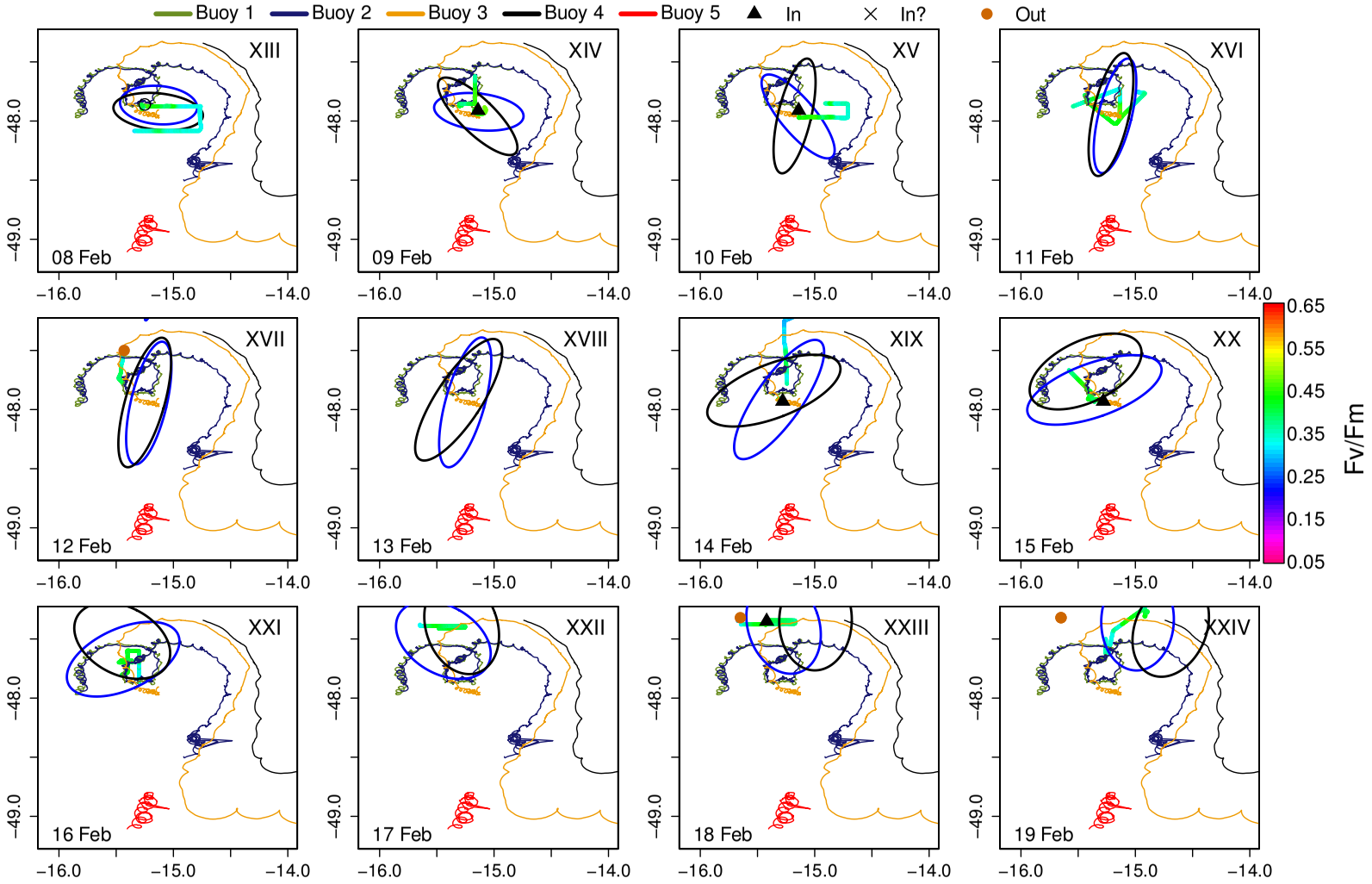

Figure 3.5 – Daily maps of patch position and night-time $\frac{F_V}{F_M}$ from 08 Feb to 19 Feb superimposed on the trajectories of the drifting buoys. The position of each CTD station is also shown, with the plotting symbol indicating whether that station was In, probably In, or Out of the patch.

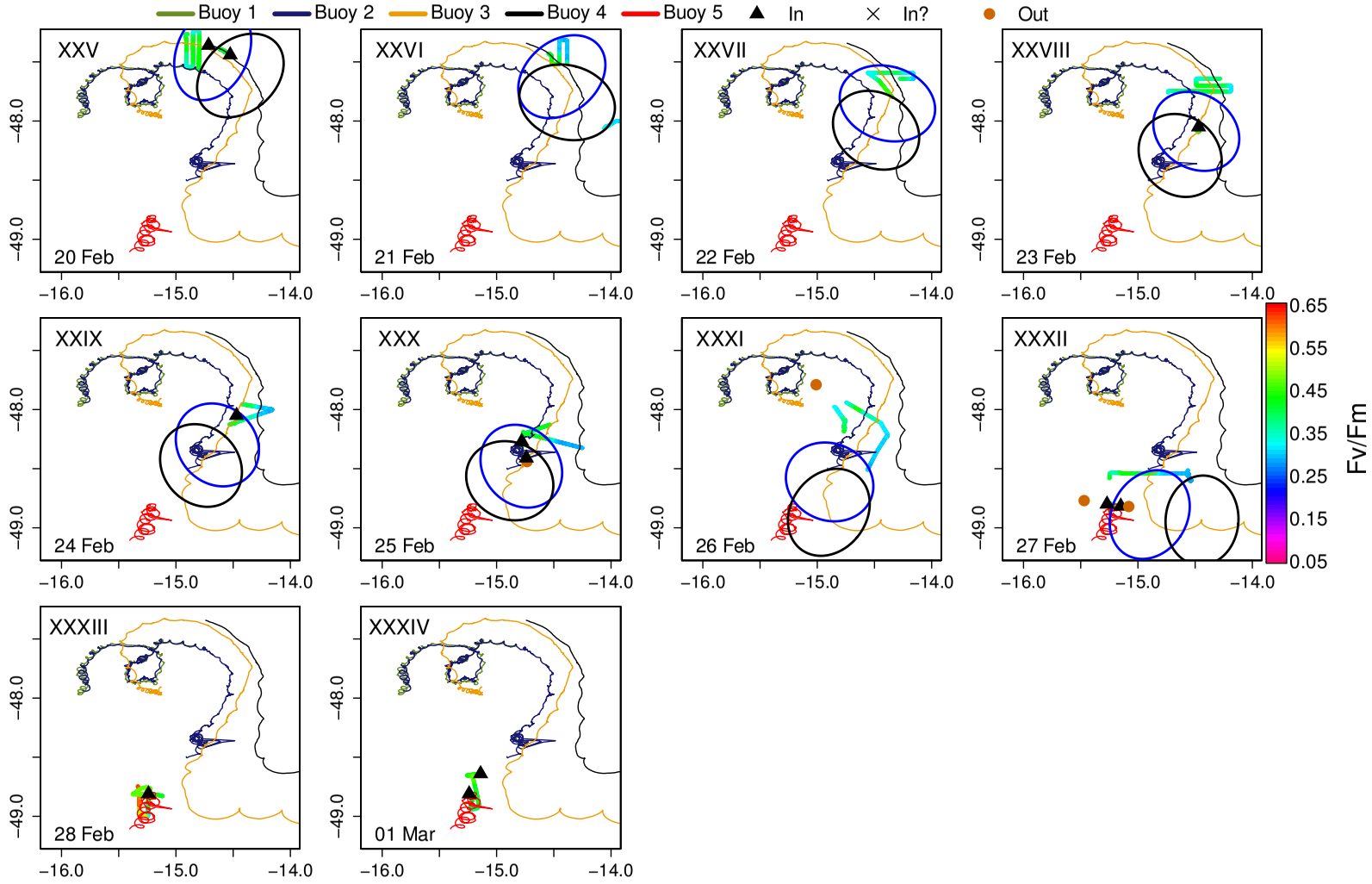

Figure 3.6 – Daily maps of patch position and night-time $\frac{F_V}{F_M}$ from 20 Feb to 01 Mar superimposed on the trajectories of the drifting buoys. The position of each CTD station is also shown, with the plotting symbol indicating whether that station was In, probably In, or Out of the patch.

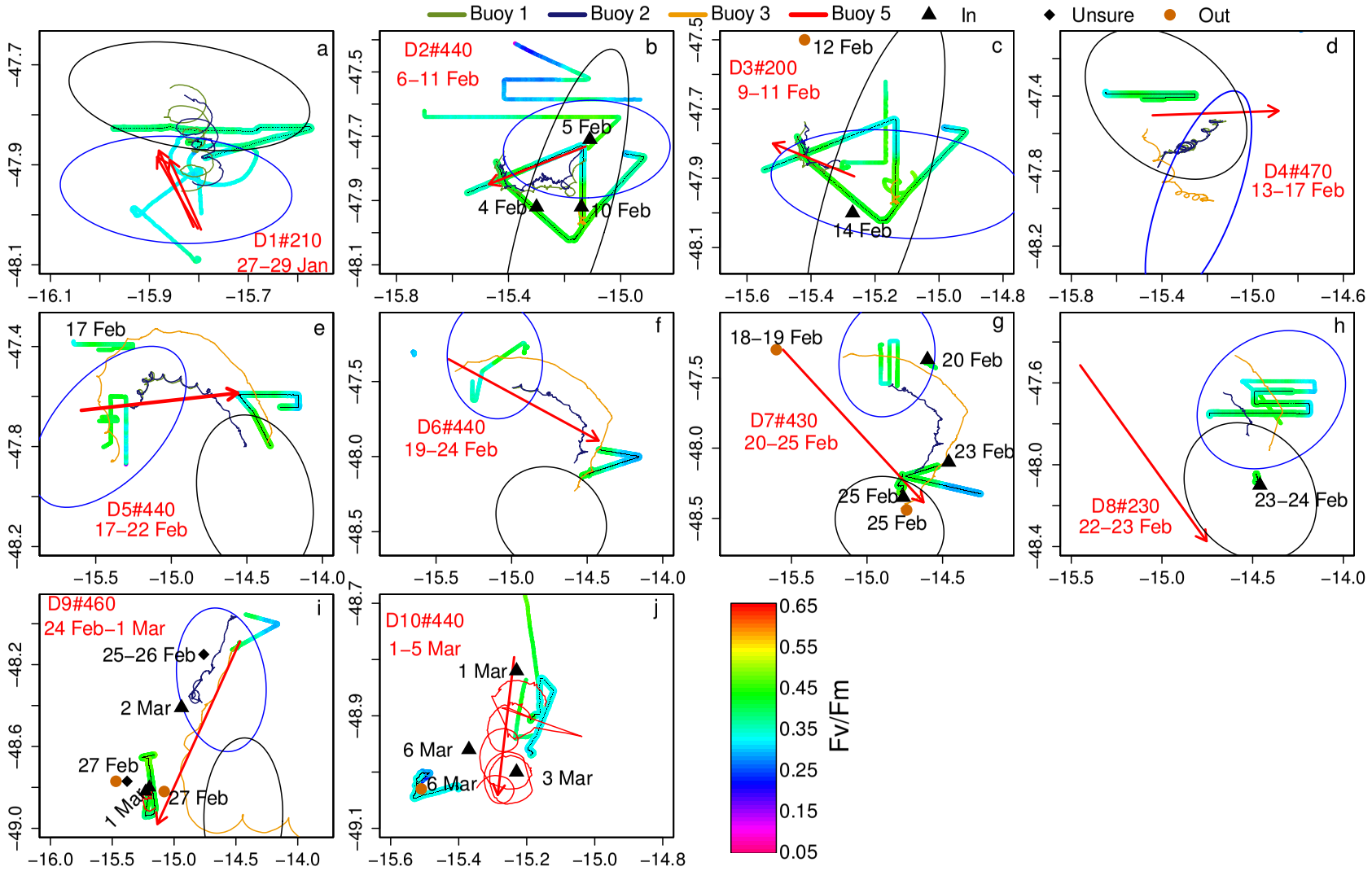

Figure 3.7 – Maps of trap trajectories, with modelled patch positions, night-time $\frac{F_V}{F_M}$ values, and trajectories of drifting buoys. Blue ellipses show the patch positions when traps started collecting, black ellipses show the patch positions when traps stopped collecting. Only $\frac{F_V}{F_M}$ values taken on the start and end days of collection are shown, measurements taken on the end day are marked with a small black dot at the centre (this appears as a thin black line due to the high measurement frequency).

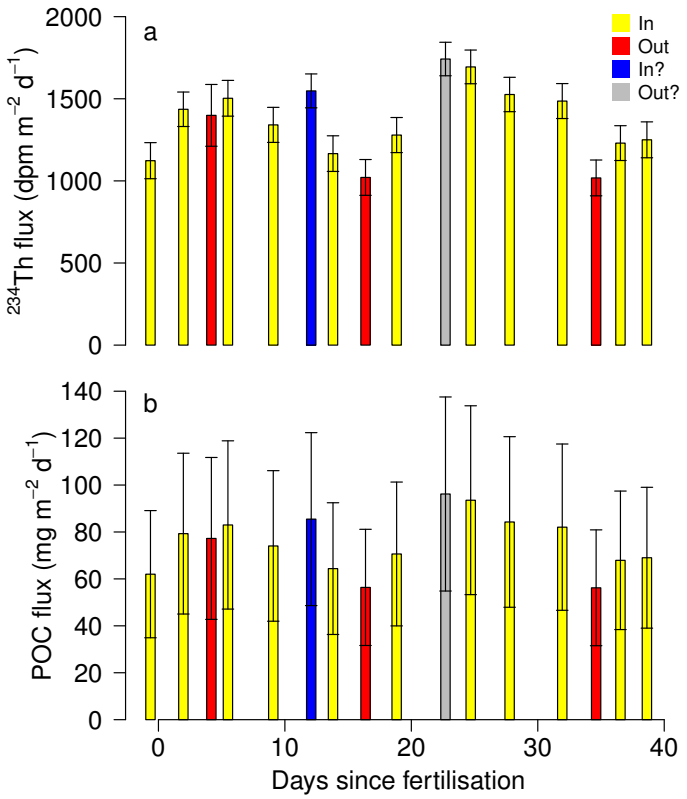

Figure 3.8 – (a) Export flux of ^{234}Th calculated with a steady-state model at 100 m; (b) export of POC based on ^{234}Th fluxes and a POC:^{234}Th ratio of 4.6 ± 2.0 µmol dpm^{-1}.

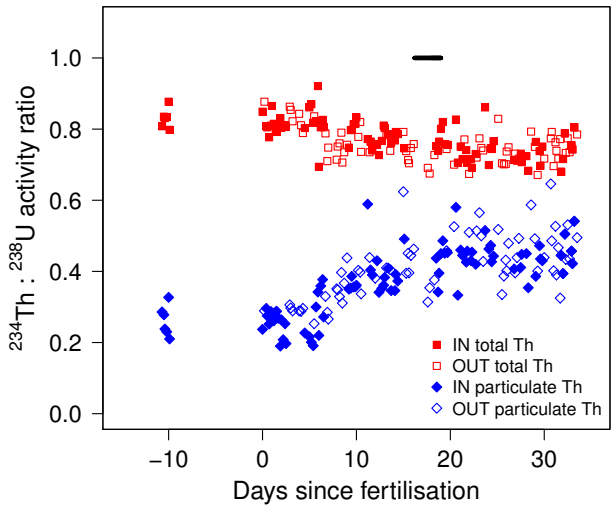

Figure 3.9 – Activity ratios of ^{234}Th:^{238}U as measured by the automated sampler from the underway supply. An activity ratio of 1 means that the two nuclides are in secular equilibrium, *i.e.* that there is no depletion of ^{234}Th. Ratios of <1 indicate depletion of ^{234}Th relative to ^{238}U. Activity ratios are shown both for particulate ^{234}Th and for total ^{234}Th (dissolved + particulate). The horizontal black bar at 18 d indicates the time of second fertilisation.

Trap	Cup opening	Cup closing	In / Out
D1#210	27 Jan 21:30	29 Jan 21:25	In
D2#440	06 Feb 15:00	11 Feb 14:00	Probably In
D3#200	09 Feb 15:30	11 Feb 15:30	Probably In
D4#470	13 Feb 10:00	17 Feb 13:00	Out
D5#440	17 Feb 13:00	22 Feb 16:00	In
D6#440	19 Feb 10:15	24 Feb 16:15	In
D7#430	20 Feb 04:00	25 Feb 16:00	Out
D8#230	22 Feb 06:15	23 Feb 06:15	Out
D9#460	24 Feb 16:15	01 Mar 16:15	In
D10#440	01 Mar 17:00	05 Mar 07:05	In

Table 3.1 – Summary of PELAGRA trap deployments. Traps are referred to as Deployment Number#Depth.

^{234}Th flux was converted to POC flux using the mean of the POC:^{234}Th ratios measured in the >53 µm ISP samples at 100 m and in the three traps that collected at around 200 m; this mean value was 4.6 ± 2.0 µmol dpm^{-1}. POC:^{234}Th in the ISP samples ranged from 2.9 to 6.9 µmol dpm^{-1}, with the lowest and highest value both measured inside the patch. In the traps, POC:^{234}Th ranged from 2.1 to 8.2 µmol dpm^{-1}, with the lowest value measured outside of the patch in trap D8#230. As there was no clear difference in POC:^{234}Th between ISP samples inside or outside of the patch, the mean of all ratios (4.6 ± 2.0 µmol dpm^{-1}) was applied to all the profiles, whether inside or outside of the patch, and the standard deviation of this mean was propagated through the calculation. The resulting estimates of POC export are shown in Figure 3.8b, and range from 62 ± 27 to 94 ± 40 mg POC m^{-2} d^{-1} inside the patch. Outside of the patch, POC export ranged from 56 ± 25 to 77 ± 35 mg POC m^{-2} d^{-1}.

The automated underway ^{234}Th measurements also suggest that no large export event occurred, and that there was no difference in ^{234}Th depletion inside the patch compared to outside (Figure 3.9). The total activity ratio of ^{234}Th:^{238}U declined slightly from around 0.8 on Day 0 to around 0.75 at the end of the experiment, with a range at any time of around ± 0.1 (note that this decrease in surface activity ratio does not necessarily indicate that the ^{234}Th depletion increased throughout the upper 100 m). More striking are the changes in the particulate fraction, in which the activity ratio increased from around 0.25 initially to around 0.45, with most of the change between Days 5–10. This increase in the particulate ^{234}Th fraction could reflect either a build-up of particles, or fragmentation of existing particles.

3.3.4 Trap samples

Depth profiles of the sediment traps are shown in Figure 3.10; results from the traps are summarised in Figure 3.11 and Table 3.2. POC flux at 450 m ranged from 9.2–23 mg m^{-2} d^{-1}

inside the patch, and from 2.8–8.4 mg m^{-2} d^{-1} outside of the patch. At 200 m, POC flux was 5.6 mg m^{-2} d^{-1} inside the patch (Days 0–2), but 28 mg m^{-2} d^{-1} outside of the patch. Molar POC:PON ratios were relatively high, ranging from 8.4–9.6, and did not differ between In- and Out-patch traps. Intact faecal pellets contributed 24–92% of total POC flux (even 200% in D4#470, suggesting an error in either the total POC or the faecal pellet C measurements. As this trap was found to have the lowest total POC flux, it is likely that an error occurred in the total POC measurement, but no further sub-samples were available from this trap to repeat the POC measurement). Although only two traps successfully sampled with polyacrylamide gels, these samples confirmed that faecal pellets dominated the particle flux. However, particles in the gel traps had evidently been altered by rolling down the collection funnels, confounding a more detailed analysis of particle types (*F. Ebersbach*, pers. comm.).

Both opal and $CaCO_3$ were found in the samples, but $CaCO_3$ flux exceeded opal flux by a factor of 2–7. Opal contributed 3.8–14% of total mass flux, while $CaCO_3$ contributed 16–49% (concentrations of Na and Sr in the Ca digests were negligible). The contribution of neither opal nor $CaCO_3$ differed clearly between sampling depth or between In- and Out-patch traps. The molar Si:POC ratios were consequently low (0.04–0.25) and showed no trend with depth or sampling location. Molar PIC:POC ratios ranged from 0.20–0.59, with the 200 m traps containing the lowest ratios. Finally, the ratio of large- to small-fraction $CaCO_3$ varied from 0.5–4.9, with a mean (weighted by magnitude of total $CaCO_3$ flux) of 1.2. However, microscopic examination of aliquots of the small size-fractions revealed that they contained almost exclusively fragmented Foraminifera (*A. Poulton*, pers. comm.). This would suggest that the $CaCO_3$ flux from coccoliths was negligible, although cells of the coccolithophore *Emiliania huxleyi* were found in all sub-samples for unicellular plankton analysis. Some degree of coccolith dissolution may therefore have occurred during sample storage and processing.

Unicellular plankton contributed only 0.3–9% of total POC flux, with the exception of 14% in trap D2#440. The majority ($\geq$75%) of unicellular plankton carbon was contributed by dinoflagellates and flagellates, with only 5–25% from diatoms. Broken and empty diatom frustules far out-numbered intact diatom cells, and these fragments contributed the majority of the opal flux.

^{234}Th was measured in six traps: D1#210, D3#200, D6#440, D7#430, D8#230, and D9#460. Strangely, flux into the first two traps was only 60 dpm m^{-2} d^{-1}, far lower than the fluxes of $>$1000 dpm m^{-2} d^{-1} predicted from the ^{234}Th profiles at 100 m. Fluxes in the other traps were 510–775 dpm m^{-2} d^{-1}.

3.3.5 Net community production

Time-series of NCP up until Day 30 are shown in Figure 3.12. NCP ranged from -45 to 56 mmol O_2 m^{-2} d^{-1} in the full dataset, but only from -32 to 56 and -28 to 56 mmol O_2 m^{-2} d^{-1} inside the patch using the full and reduced patch models, respectively. The full time-series (Figure 3.12a) contained 13,559 observations, while the In-patch dataset based on the full patch model contained 6972, and the dataset based on the reduced patch model 3552, observations.

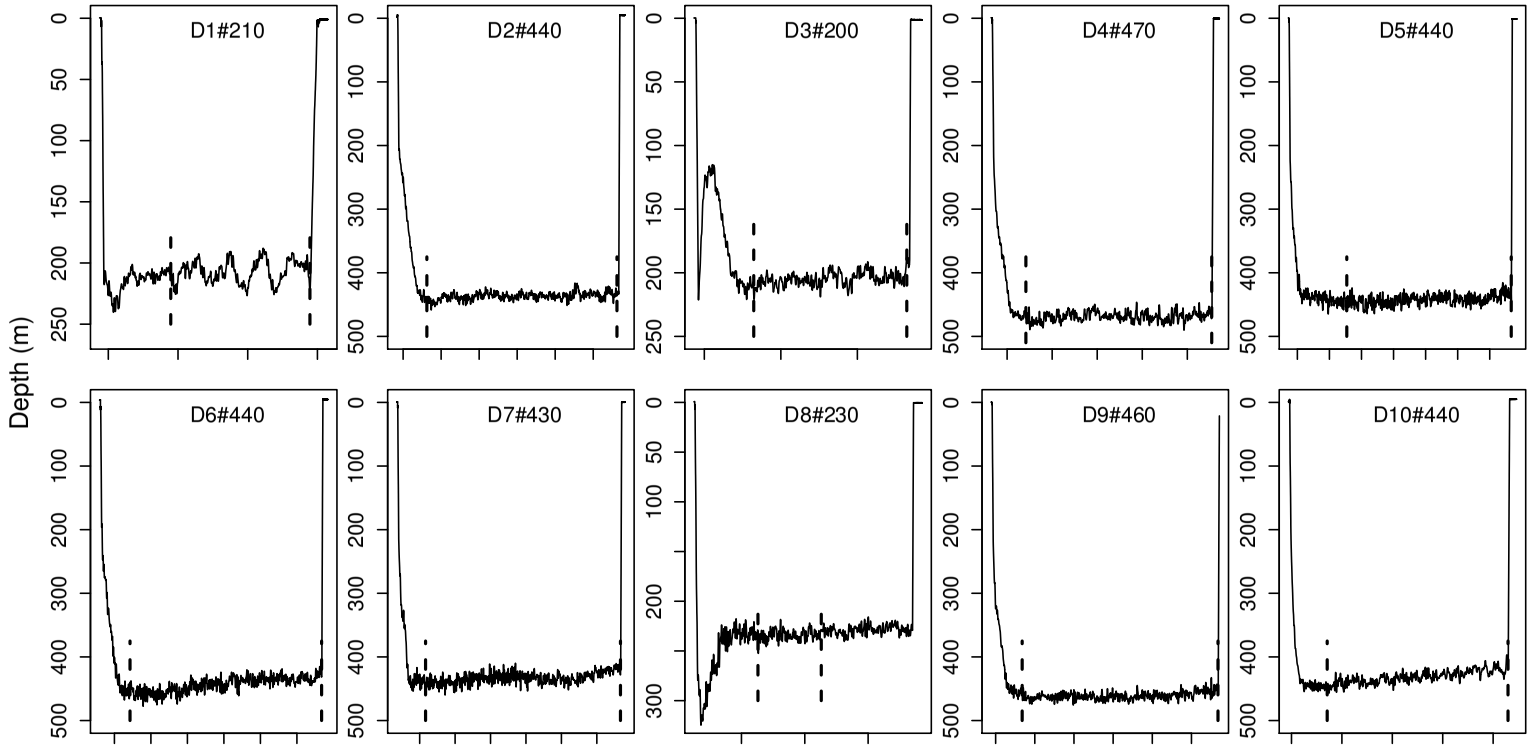

Figure 3.10 – Profiles of depth against time for each PELAGRA trap. Vertical dashed lines indicate the time of cup opening and closing. x-axis tick marks are spaced at 24 h intervals in all plots; note that the y-axis scales differ.

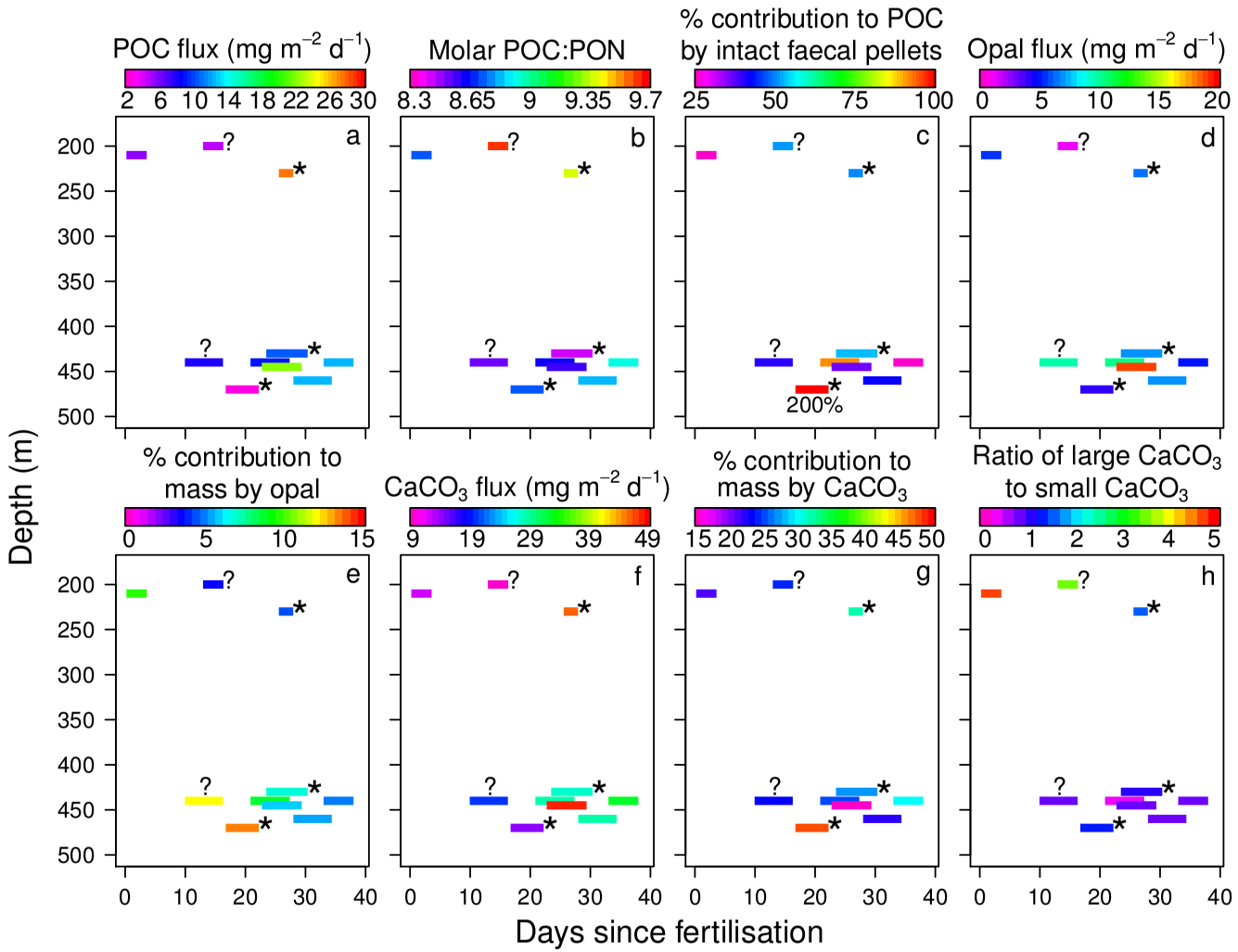

Figure 3.11 – Results from PELAGRA sediment traps. Each horizontal line represents one trap, with line length indicating the collection period and colour indicating the magnitude of the measured property (but note the different colour scale-bars). Out-patch traps are marked with an asterisk, and the two traps that were ambiguous are identified with question marks (see Section 3.3.2). (a) POC flux; (b) molar POC:PON ratio; (c) percentage contribution by intact faecal pellets to the total POC flux (note that measured faecal pellet POC was D4#470); (d) opal flux; (e) percentage contribution by opal to total mass flux; (f) $CaCO_3$ flux; (g) percentage contribution by $CaCO_3$ to total mass flux; (h) ratio of $>30\,\mu m$ $CaCO_3$ to $<30\,\mu m$ $CaCO_3$.

Trap	In/Out	Mass flux	POC flux	PON flux	POC:PON	Opal flux	Si:POC	PIC flux >30 µm	PIC flux <30 µm	PIC:POC	^{234}Th flux
D1#210	In	54.9	5.56	0.75	8.7	5.61	0.18	9.66	1.96	0.25	62.8
D2#440	Prob. In	80.5	8.44	1.15	8.5	10.4	0.22	8.22	10.7	0.27	NM
D3#200	Prob. In	35.3	4.78	0.58	9.6	1.33	0.05	6.70	1.91	0.22	60.8
D4#470	Out	28.4	2.83 *	0.38	8.7	3.95	0.25	8.09	5.81	0.59	NM
D5#440	In	112	9.18	1.24	8.6	10.6	0.21	9.19	19.5	0.38	NM
D6#440	In	311	23.0	3.12	8.6	19.9	0.16	22.7	26.2	0.26	692
D7#430	Out	98.7	11.0	1.52	8.4	7.45	0.12	13.9	13.4	0.30	513
D8#230	Out	143	28.4	3.53	9.4	6.82	0.04	28.8	17.7	0.20	776
D9#460	In	125	12.8	1.69	8.9	7.07	0.10	12.3	16.3	0.27	521
D10#440	In	105	12.9	1.68	8.9	5.44	0.08	14.7	17.7	0.30	NM

* Note that this value is questionable, see Section 3.3.4

Table 3.2 – Fluxes recorded in the sediment traps. Traps are referred to as Deployment Number#Depth. All fluxes are in units of mg m^{-2} d^{-1} except for ^{234}Th flux (dpm m^{-2} d^{-1}). All ratios are in units of mol mol^{-1}. "NM"=not measured.

Loess model	Full patch model		Reduced patch model	
	Mean NCP ($\mathrm{mmol\,O_2\,m^{-2}\,d^{-1}}$)	St. err.	Mean NCP ($\mathrm{mmol\,O_2\,m^{-2}\,d^{-1}}$)	St. err.
5% of points	13.1	0.5	17.9	0.3
10% of points	9.6	0.8	12.3	0.4
15% of points	11.5	1.0	13.5	0.7
25% of points	12.9	1.4	15.3	0.9
35% of points	12.8	1.5	16.7	1.0

Table 3.3 – Estimated mean NCP inside the patch over the first 30 d post-fertilisation. Estimates are presented for all five loess models, and for both the full patch model and the reduced patch model (in which the axis lengths of the ellipses were halved).

There was a trend in NCP over time, rising from around −5 to $\sim$30 $\mathrm{mmol\,O_2\,m^{-2}\,d^{-1}}$ during the first 10 d, and declining to negative values at the end. The time-series inside the patch (Figure 3.12b,c) showed a clearer trend without dropping to low or negative values as frequently as in the complete dataset. Moreover, the time-series based on the full patch model (Figure 3.12b) did not differ strongly from that based on the reduced patch model (Figure 3.12c), although the latter time-series contained far fewer data points. All three time-series showed substantial but irregular high-frequency variability.

In modelling the In-patch time-series, the loess model based on 15% of points was considered best: models based of fewer points tended to over-fit the data locally, leading to unlikely interpolations across the gaps (grey line in Figure 3.12b,c). Conversely, models based on a greater percentage of points smoothed out the measured variability very strongly, and tended to interpolate higher values across the gaps (green line in Figure 3.12b,c).

The estimates of mean In-patch NCP with each loess model are shown in Table 3.3. Estimates based on the full patch model are lower by 2–5 $\mathrm{mmol\,O_2\,m^{-2}\,d^{-1}}$ than estimates based on the reduced patch model. Mean In-patch NCP calculated from the 15% loess model was 11.5 ± 1.0 $\mathrm{mmol\,O_2\,m^{-2}\,d^{-1}}$ with the full patch model, and 13.5 ± 0.7 $\mathrm{mmol\,O_2\,m^{-2}\,d^{-1}}$ with the reduced patch model.

NCP was also averaged over a 1 h period during water column ^{234}Th sampling to compare directly to the ^{234}Th observations. However, no relationship between the two was observed (Figure 3.13).

3.4 Discussion

3.4.1 Effect of fertilisation on downward particle flux

Neither the ^{234}Th measurements nor the sediment trap collections indicated an enhancement of particle flux in response to iron fertilisation. The phytoplankton response during LohaFEX was modest compared to iron fertilisation experiments in waters with high $Si(OH)_4$ concentration

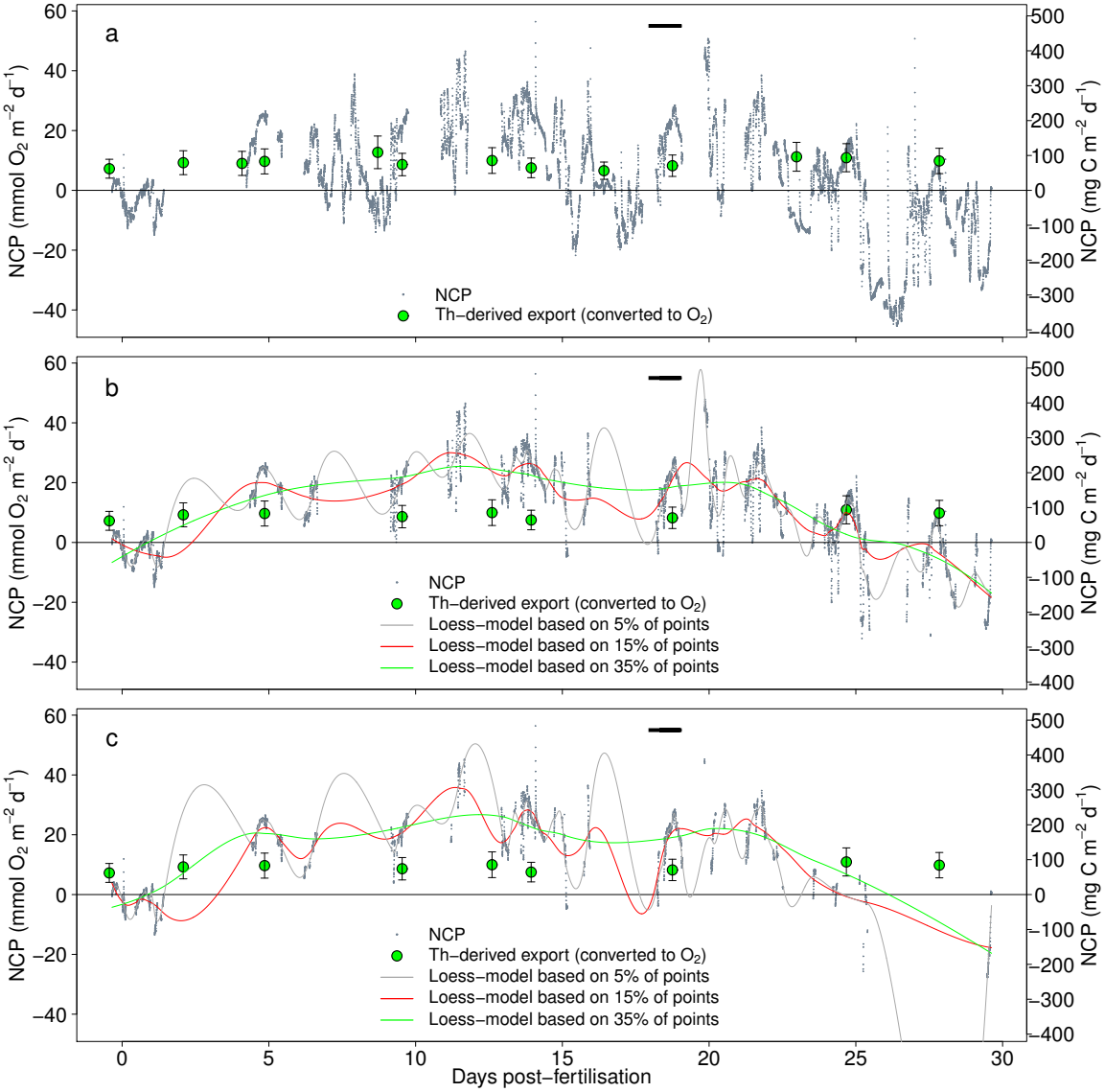

Figure 3.12 – NCP time-series with ^{234}Th-derived export fluxes for comparison. (a) Time-series of all NCP measurements from 26 Jan to 28 Feb, with all ^{234}Th-derived export estimates (*i.e.* In- and Out-patch measurements); (b) time-series of all NCP measurements inside the modelled patch ellipses, with all ^{234}Th-derived export estimates inside the patch; (c) time-series of all NCP measurements within the reduced patch model (ellipses with axis lengths half those of the original patch model). In (b) and (c) the coloured lines show three of the loess models that were fit to the data. The solid black bar at the top of each plot shows when the second fertilisation was applied.

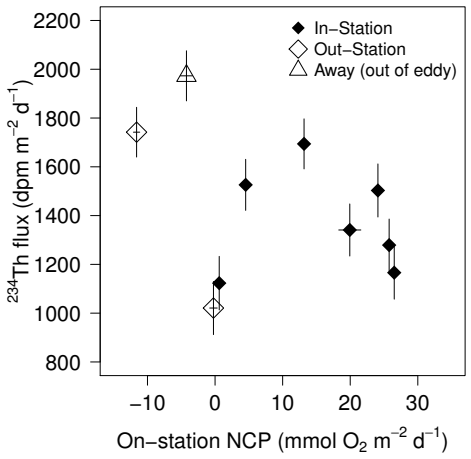

Figure 3.13 – Scatter-plot of ^{234}Th-derived export against NCP averaged over 1 h period during water column ^{234}Th sampling.

(*Boyd et al.* 2007), with chlorophyll and primary productivity only doubling. Some previous iron fertilisation experiments found no increased particle flux, even in high-Si waters, but probably because they did not continue for long enough to study the collapse of the blooms (*de Baar et al.* 2005). Enhanced export was reported during SOFeX (*Bishop et al.* 2004; *Buesseler et al.* 2004), during SEEDS II (*Aramaki et al.* 2009), during SERIES (*Boyd et al.* 2005), and during IronEx-II (*Bidigare et al.* 1999), with daily POC fluxes at around 100 m exceeding those reported here for LohaFEX two- or more-fold. During LohaFEX, most of the exported material was remineralized above 450 m (sediment trap POC fluxes were mostly $<15\,\mathrm{mg\,m^{-2}\,d^{-1}}$, while export at 100 m was about $75\,\mathrm{mg\,m^{-2}\,d^{-1}}$); thus little POC actually sank below the permanent thermocline.

This presents an interesting contrast to the SOFeX North case, in which iron-fertilisation of low-Si sub-Antarctic waters did lead to enhanced export after about 30 d (*Bishop et al.* 2004). NO_3^- decreased by $\sim 2\,\mu\mathrm{mol\,L^{-1}}$ in SOFeX North (*Coale et al.* 2004), very similar to LohaFEX. However, the initial $Si(OH)_4$ concentration in SOFeX North was $3\,\mu\mathrm{mol\,L^{-1}}$, approximately double that during LohaFEX, and diatoms contributed 44% to total phytoplankton carbon in SOFeX North (*Coale et al.* 2004). Moreover, these diatoms were relatively weakly silicified and eventually aggregated, suggesting that grazing pressure on them was probably moderate (*Coale et al.* 2004). During LohaFEX, diatoms contributed <10% of total phytoplankton carbon. The initial conditions during LohaFEX were thus more similar to those during the recent iron fertilisation experiment SAGE in the sub-Antarctic, in which the $Si(OH)_4$ concentration was $<1\,\mu\mathrm{mol\,L^{-1}}$ (*Harvey et al.* 2010), and diatoms contributed <1% of phytoplankton biomass (*Peloquin et al.* 2010). Unfortunately, downward POC flux was not quantified during SAGE, but the modest phytoplankton response (chlorophyll-*a* doubled from about 0.5 to $1\,\mathrm{mg\,m^{-3}}$ and was mostly in the $<20\,\mu\mathrm{m}$ size-fraction; *Peloquin et al.* 2010) was similar to observations during LohaFEX. During SOFeX, however, chlorophyll exceeded $2\,\mathrm{mg\,m^{-3}}$ after about 25 d and then decreased to about $1.5\,\mathrm{mg\,m^{-3}}$ within a few days (*Coale et al.* 2004).

Export flux during SOFeX North was measured using a different method than during LohaFEX: *Bishop et al.* (2004) used the accumulation of sinking particles on an upward-looking transmissometer to derive an index of particle flux. While it cannot be ruled out that such methodological differences contributed to the different results, the method of *Bishop et al.* (2004) directly measured the quantity of sinking particles, and should yield reasonably robust estimates; thus it seems very unlikely that the large increase they recorded could have been primarily due to biases in the method. Conversely, the conclusion that export was not enhanced during LohaFEX is supported by multiple independent methods. It is therefore very likely that the difference in export during SOFeX and LohaFEX was genuine, and not a result of methodological differences.

Whether the LohaFEX phytoplankton community was actually Si-limited is debateable, as the growth-rates of diatom cells were close to maximal values. Certainly the $Si(OH)_4$ concentration would have been too low to allow the same degree of diatom biomass accumulation seen in high-Si FeAXs; however, diatom accumulation may have been controlled more by zooplankton grazing than by Si availability during LohaFEX (indeed, growth of many diatom species only becomes restricted at $Si(OH)_4$ well below $1\,\mu mol\,L^{-1}$, see review by *Martin-Jézéquel et al.* 2000). Thus most of the opal in the sediment traps was in form of broken or empty frustules. The high growth-rates imply that some diatom biomass might have accumulated if grazing had been less intense. It is also very likely that there was substantial re-processing of particles by detritus feeders during LohaFEX, especially given the high abundances of copepods of the genus *Oithona*. These are known to feed off detritus and to engage in coprophagy, and are hence highly likely to reduce POC flux (*González and Smetacek* 1994). While recognisable faecal material contributed typically 50% to the sediment trap catches, the remainder consisted largely of unrecognisable material, which could well have been faecal material falling apart due to coprochaly, suggestive of substantial re-processing of faecal material. If this were the case, then the high grazing pressure on the phytoplankton would just be part of the reason for low particle flux during LohaFEX; the presence of a detritus re-processing copepod community would have been a further important aspect.

The contrast to SOFeX North is hence particularly interesting, since both sites would be characterised as "low-Si" waters, yet SOFeX North apparently allowed weakly silicified diatoms to accumulate and be exported as diatom aggregates, but LohaFEX did not. The chief difference between the two experiments was possibly in the zooplankton community rather than in the $Si(OH)_4$ concentration. In particular, there was probably a combined onslaught from high grazing pressure on phytoplankton and high levels of detritus feeders during LohaFEX. The contrasting outcomes between LohaFEX and SOFeX North thus suggest that the zooplankton community was probably more important in setting the magnitude of the BCP in these two cases. Whether this difference in the zooplankton communities between LohaFEX and SOFeX North was linked to the small difference in $Si(OH)_4$ concentration is unclear, but the contrasting outcomes suggest that future iron fertilisation experiments should invest more effort in studying the zooplankton community. It is possible that simply dividing Fe-limited regions of the Southern Ocean into high-Si and low-Si waters, and attributing, respectively, high and low potential for export enhancement, is too simple.

Lam and Bishop (2007) concluded that the SOFeX North patch became a "high biomass low export" (HBLE) area upon fertilisation owing to responses by the grazing communities to fertilisation: thus, although fertilisation caused biomass accumulation, fluxes through the upper mesopelagic were initially reduced (note that this conclusion did not account for the export event reported by *Bishop et al.* 2004). There was no evidence that fertilisation led to HBLE conditions during LohaFEX, although particle flux was already being attenuated heavily with depth at the start of the experiment.

3.4.2 Performance of the sediment traps

While the sediment traps appeared to follow the surface circulation relatively well, it is very difficult to be fully confident of their collection source areas. Other iron fertilisation experiments have made use of surface-tethered sediment traps (*e.g. Nodder and Waite* 2001; *Boyd et al.* 2005; *Aramaki et al.* 2009), the exact positions of which can be tracked throughout the deployment period — but the accuracy of tethered traps is very questionable (Appendix A.1). Nevertheless, if a large increase in flux had occurred inside the patch, it would probably have been caught by the traps.

The sediment trap deployment strategy during LohaFEX was designed to provide a near-continuous record of trap samples over the experiment by maximising the collection period of each trap. This obviously increased the distance of trap movement, and thus the scope for loosing the patch, and also led to longer gaps in the record whenever a trap deployment failed. In hindsight, it might have been better to allow for some short gaps in the trap record and reduce the collection period. As it is very difficult to locate and fertilise just the stationary core of an eddy, any future iron fertilisation experiment will probably have to contend with a moving patch, too. Additional techniques for measuring downward particle flux (*e.g.* ^{234}Th) should hence always be employed.

3.4.3 Comparison between NCP and ^{234}Th

The most reasonable estimates of mean NCP up until Day 30 were 11.5–13.5 mmol O_2 m^{-2} d^{-1}, which equates to 98–115 mg C m^{-2} d^{-1} using 1.4 as the photosynthetic quotient to convert moles of O_2 to moles of C (*Laws* 1991). In comparison, the mean export inside the patch at 100 m diagnosed from ^{234}Th was 75 mg POC m^{-2} d^{-1} for the whole experimental period, and 76 mg POC m^{-2} d^{-1} up until Day 30, with a propagated standard deviation of 34 mg m^{-2} d^{-1}. NCP thus exceeded export at 100 m by only 23–41 mg POC m^{-2} d^{-1}. However, there is also a depth-difference here: export based on ^{234}Th was calculated at 100 m depth, while the surface mixed layer depth inside the patch was mostly between 45 m and 75 m (measured from CTD profiles at each station, and based on a density change of 0.02 kg m^{-3} relative to the surface). NCP only tracks developments inside the mixed layer, and any particles exported below the base of the mixed layer still needed to sink several tens of metres before becoming part of the export tracked by the ^{234}Th. Some fraction would certainly have become remineralized between the two depth horizons, so one would expect NCP to be higher than ^{234}Th-derived export in this case.

Net accumulation of organic carbon in the mixed layer (either dissolved or particulate) must therefore have been small at most: even if all the difference between NCP and ^{234}Th-derived export (23–41 mg POC m^{-2} d^{-1}) were ascribed to accumulation, with a mixed layer depth of around 60 m and over 30 d that would allow for accumulation of 0.96–1.7 µmol C L^{-1}. However, this calculation would over-estimate POC accumulation, as it does not account for remineralization between the base of the mixed layer and 100 m.

A key assumption of the O_2:Ar method is that upward transport across the thermocline is negligible. Such transport would carry O_2-under-saturated waters into the mixed layer, lowering the biological O_2 saturation (BOS, see Appendix B.7), and would cause NCP to be under-estimated. In practice, this would certainly be significant in upwelling regions, but was probably not a major problem during LohaFEX. No drastic deepening of the surface mixed layer was observed between Days 22 and 30 (when NCP declined). Upward transport would also bias ^{234}Th measurements, for instance, but is considered negligible in ^{234}Th studies outside of upwelling areas.

A more significant error can stem from O_2 consumption by biofilms in the tubing of underway seawater supplies (*Juranek et al.* 2010). Unfortunately, this error is very difficult to quantify: it varies between ships, but also appears to be temperature-dependent, with respiration in cold water considerably lower (*Juranek et al.* 2010). Seeing as LohaFEX took place in surface waters consistently colder than 10 °C, the problem was hopefully not a major one. *Juranek et al.* (2010) state that a 1% bias in BOS in a sub-tropical region would equate to an error in NCP of 10 mmol O_2 m^{-2} d^{-1}, and they report errors of this magnitude from sub-tropical waters. However, the temperature-dependence of their data suggests that at water temperatures below 10 °C the error in BOS might be several-fold lower. To mitigate the problem, the water flow rate through the underway supply was kept as high as possible (*M. Rutgers van der Loeff*, pers. comm.). Given also the acknowledged uncertainty in the mean NCP calculated for LohaFEX, the additional uncertainty regarding respiration is perhaps not a major problem — but it cannot be ruled out that NCP was significantly under-estimated.

The NCP thus appears to have been more or less balanced by particle export as diagnosed from ^{234}Th profiles, with little biomass accumulation. The increase in particulate ^{234}Th seen in the automated underway measurements was hence probably caused more by fragmentation of existing particles than accumulation of new ones; perhaps via coprorhexy and coprochaly by copepods (*Lampitt et al.* 1990; *Noji et al.* 1991). This conclusion might seem to contradict the increase in chlorophyll-*a* upon fertilisation, but carbon:chlorophyll-*a* ratios invariably decrease upon alleviation of iron stress (*Coale* 1991; *Landry et al.* 2000; *Peloquin et al.* 2010), so the chlorophyll-*a* increase does not necessarily indicate carbon accumulation.

Over an annual cycle, NCP, new production, and export flux should be equal. The discrepancies often observed between these parameters (*Smith and Dunbar* 1998; *Morris et al.* 2007; *Lampitt et al.* 2008b; *Savoye et al.* 2008) are clearly due to a combination of temporal decoupling between production and export, and the different integration time-scales of the methods used to estimate them. That the present estimates of NCP and ^{234}Th-derived export flux approximately match is presumably because measurements were taken for longer than the integration time-scale of either method. This suggests that NCP based on O_2:Ar ratios and

^{234}Th can be usefully compared over shorter time-scales (∼1 month) to assess what fraction of net production is exported *versus* being stored as POM or DOM. However, it is also evident that NCP and ^{234}Th-derived export did not correlate on a station-by-station basis, probably because the integration time-scales of the two methods are not actually equal.

3.5 Conclusions

Particle export out of the fertilised patch was tracked successfully for almost 40 d, and the location of the experiment inside a closed eddy core allowed neutrally buoyant sediment traps to follow the drift of the patch reasonably well and thus measure the sequestration flux. Neither export nor sequestration flux changed upon iron addition, and neither differed clearly inside compared to outside of the patch. Particle flux was reduced ∼5-fold between 100 m and 450 m. Net community production was positive for much of the experiment, but over a period of 30 d it was largely balanced by particle export, implying little or no accumulation of organic matter. This is primarily attributed to high zooplankton grazing pressure and to substantial re-processing of particle flux by zooplankton, with copepods playing a major role in both processes. It is likely that zooplankton grazing played a greater role than Si availability in controlling diatom biomass, so the LohaFEX results might not necessarily apply to all low-Si iron-limited regions in the Southern Ocean.

Chapter 4

Sedimentation of Acantharian Cysts in the Iceland Basin

The following chapter has been reproduced with minor textual modifications and additions from *Limnology & Oceanography* with permission from the American Society for Limnology and Oceanography. Publication: Martin P., Allen J. T., Cooper M. J., Johns D. G., Lampitt R. S., Sanders R., Teagle D. A. H. (2010). Sedimentation of acantharian cysts in the Iceland Basin: Strontium as a ballast for deep ocean particle flux, and implications for acantharian reproductive strategies. *Limnology & Oceanography, 55*(2), 604–614.

Data contribution

Sediment traps were deployed and recovered during RRS *Discovery* cruises D312 and D321, respectively. Corinne Pebody (NOCS) removed swimmers from the sediment trap samples, and subsequent sample processing (splitting, filtering, drying) was undertaken by the author. Samples for POC and PON were prepared by the author, and measured by Bob Head (PML). Samples and standards for Sr analysis were prepared by the author, and measured by Matthew Cooper (NOCS). Scanning electron microscopy was undertaken with the help of Richard Pearce and Dave Spanner (both NOCS), and light microscopy was undertaken with the help of Anton Page at the Biomedical Imaging Unit (U. of Southampton). Advanced Microwave Scanning Radiometer (AMSR-E) data were produced by Remote Sensing Systems and sponsored by the National Aeronautics and Space Administration, and processed by Graham Quartly (NOCS). Continuous Plankton Recorder data were produced by the Sir Alister Hardy Foundation for Ocean Science and provided by David Johns (SAHFOS).

Abstract

Acantharian cysts were discovered in sediment trap samples from spring 2007 at 2000 m in the Iceland Basin. Although these single-celled organisms contribute to particulate organic matter flux in the upper mesopelagic, their contribution to bathypelagic particle flux has previously been found negligible. Four time-series sediment traps were deployed and all collected acantharian cysts, which are reproductive structures. Across all traps, cysts contributed on average 3–22%, and 4–24% of POC and PON flux, respectively, during three separate collection intervals (the maximum contribution in any one trap was 48% for POC and 59% for PON).

Strontium (Sr) flux during these six weeks reached $3\,\mathrm{mg\,m^{-2}\,d^{-1}}$. The acantharian celestite ($SrSO_4$) skeleton clearly does not always dissolve in the mesopelagic as often thought, and their cysts can contribute significantly to particle flux at bathypelagic depths during specific flux events. Their large size ($\sim$1 mm) and mineral ballast result in a sinking rate of $\sim$500 m d^{-1}, and thus they reached the bathypelagic before dissolving. Our findings are consistent with a vertical profile of salinity-normalized Sr concentration in the Iceland Basin, which shows a maximum at 1700 m. Profiles of salinity-normalized Sr concentration in the sub-arctic Pacific reach maxima at $\leq$1500 m, suggesting that Acantharia might contribute to the bathypelagic particle flux there as well. We hypothesize that Acantharia at high latitudes use rapid, deep sedimentation of reproductive cysts during phytoplankton blooms so that juveniles can exploit the large quantity of organic matter that sinks rapidly to the deep-sea following a bloom.

4.1 Introduction

Sedimentation of organic matter in the oceans is both an important control on atmospheric CO_2 levels, and the main source of energy and nutrients for deep-sea organisms. Studies using sediment traps to capture the sinking flux have shown that episodic mass sedimentation caused by specific groups of organisms can play an important role in the biological carbon pump (*von Bodungen* 1986; *Bathmann et al.* 1991; *Lampitt et al.* 2009).

Global correlations between fluxes of POC and the biominerals opal and calcite led to the hypothesis that biominerals enhance POC flux, either by increasing particle density and sinking rate or by protecting particles from degradation (*Armstrong et al.* 2002; *François et al.* 2002; *Klaas and Archer* 2002). This is discussed in detail in the Introduction (Section 1.2.4), but while biominerals almost certainly do affect POC flux, a straightforward, globally applicable ballasting mechanism does not appear to exist.

The densest known oceanic biomineral is celestite ($SrSO_4$, density = $3.96\,\mathrm{g\,cm^{-3}}$), which is precipitated by Acantharia to construct their skeletons and cyst shells. Acantharia are unicellular organisms related to the Radiolaria, and have been found to contribute significantly to the flux of material above 500 m, in particular during the cyst stage of their life cycle (*Bernstein et al.* 1987; *Antia et al.* 1993; *Michaels et al.* 1995). Ballasted with celestite, one might expect Acantharia to sink rapidly to the seafloor; yet, research to date suggests that they contribute negligibly to sediment trap catches below the mesopelagic (100–1000 m) because celestite is highly soluble in seawater, and their skeletons and shells dissolve by about 500 m depth. It is, therefore, thought that Acantharia do not contribute to the particle flux into the bathypelagic, *i.e.* below 1000 m (*Honjo et al.* 2008).

However, if for some reason the celestite did not dissolve completely within the mesopelagic, its density would make it an effective ballast for POC flux to greater depth. This could be the case for unusually large species: larger particles sink faster, and larger cysts should therefore sink deeper than smaller cysts before becoming fully dissolved. Moreover, shells of larger, more robust cysts may also have an inherently lower dissolution rate. Several studies have found occasional Acantharia at or close to bathypelagic depths: *Schewiakoff* (1926) occasionally caught some individuals in net hauls at 1000 m in the Mediterranean, acantharian gene sequences have

been found at 900 m off the Californian coast (*Gilg et al.* 2010), and two sediment trap studies caught a few individuals below 1000 m (*Bernstein et al.* 1987; *Antia et al.* 1993).

Acantharia occur throughout the world's oceans at abundances equal to or exceeding those of Foraminifera and Radiolaria (*Beers and Stewart* 1970; *Michaels et al.* 1995; *Henjes et al.* 2007). The contribution to primary productivity by their algal symbionts is especially significant in oligotrophic waters (*Michaels* 1991; *Caron et al.* 1995). Adults occur mostly above 300 m (*Bottazzi and Andreoli* 1982; *Michaels* 1988, 1991), and many species eventually encyst to form a reproductive stage. These cysts sink to depth to release flagellated gametes and then die (*Schewiakoff* 1926; *Hollande et al.* 1965), with zygotes possibly sinking further to the seafloor before ascending to the surface at a later developmental stage (*Schewiakoff* 1926). However, it is not known at what depth the gametes are released, how and at which depths juvenile development proceeds, or why reproduction and early development should take place below the euphotic zone at all.

By precipitating celestite, Acantharia can reduce surface seawater strontium (Sr) concentrations by up to 5% (*Bernstein et al.* 1987; *de Villiers* 1999; *De Deckker* 2004). Consequently, they cause regional variation in the seawater Sr:Ca ratio by several percent, complicating the use of the Sr:Ca proxy for palaeotemperature reconstruction (*de Villiers* 1999; *De Deckker* 2004). Moreover, Acantharia have been shown to affect Ba concentrations: the high Ba:Sr distribution coefficient (ratio of solid-phase Ba:Sr to dissolved Ba:Sr, mean of 2.6 across North Pacific, North Atlantic, and South Atlantic) in acantharian celestite indicates that preferential co-precipitation of Ba takes place (*Bernstein et al.* 1998). Further laboratory work revealed that dissolution of Acantharia can lead to formation of barite ($BaSO_4$) particles, implicating Acantharia as a possible source of the barite particles found throughout the oceans (*Bernstein and Byrne* 2004). Vertical excess barite distribution is used as a proxy for organic carbon remineralization in the mesopelagic, termed the Ba_{xs} proxy (*Cardinal et al.* 2005), and it is therefore of relevance to quantify the role that Acantharia may have in barite formation. *Jacquet et al.* (2007) showed that during an iron fertilisation experiment in the Southern Ocean, Acantharia contributed a significant, but small fraction of total biogenic barite in the mesopelagic, supporting the validity of the Ba_{xs} proxy in this case. The degree to which they influence the distribution of Sr and Ba means that further research into acantharian biology and biogeochemistry is warranted.

Here we quantify the contribution from acantharian cysts to fluxes of particulate Sr, organic carbon, and nitrogen at 2000 m in the Iceland Basin (60°N, 20°W), measure the sinking rate of the cysts, and compare our results to data on the vertical distribution of Sr in different ocean basins.

4.2 Methods

4.2.1 Sediment traps and sample handling

Four Parflux sediment traps (see Section A.1.2), spaced 70–100 km apart, were deployed at 2000 m (Figure 4.1). Traps are referred to by their relative position to each other (NW = north-western trap, NE = north-eastern trap, S = southern trap, C = central trap). An Aanderaa

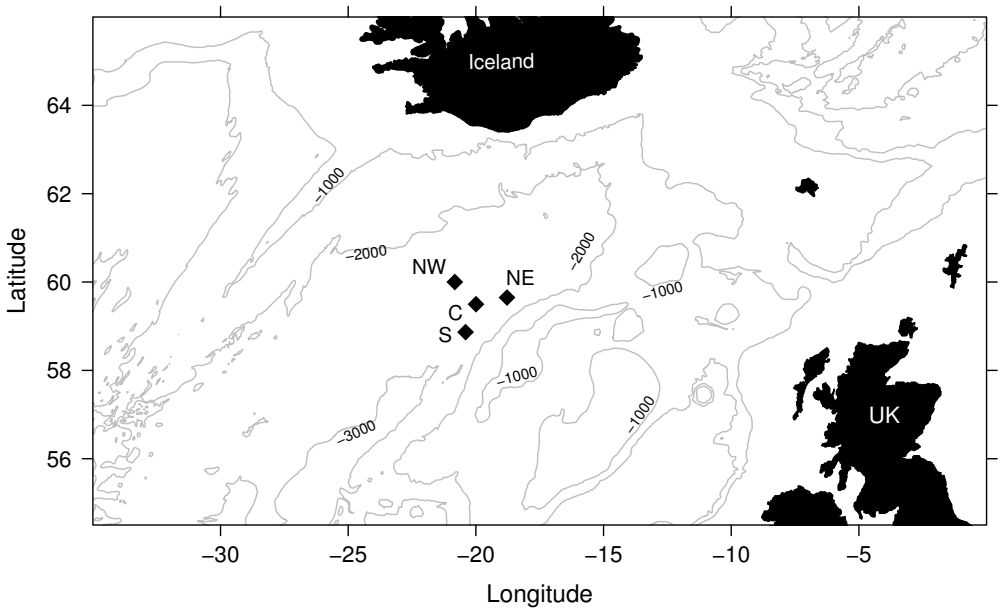

Figure 4.1 – Chart of the Iceland Basin showing locations of the sediment traps (filled diamonds).

RCM 8 current meter was attached to the mooring line 15 m below each trap. Samples were collected continuously from 22 November 2006 to 15 August 2007, with each cup (250 mL) collecting for two weeks, and using formaldehyde preservative (Appendix A.2). Upon recovery, an additional 1 mL of buffered 37% formaldehyde was added to each sample cup. Samples were capped, sealed with Parafilm, and stored at 4 °C. Each sample was then split into $\frac{1}{8}$ using a rotary-splitter, five splits were filtered together onto a 47 mm 0.45 µm cellulose nitrate filter, the material scraped off the filter with a PTFE-coated spatula, freeze-dried in clean glass vials and weighed on a Sartorius microbalance. The material was then crushed with a small stainless steel spatula, and chemical analyses were conducted on aliquots of the powder, which were weighed on a microbalance. The rationale for re-combining five splits is explained in Appendix A.3.

Owing to the high solubility of celestite in seawater, Acantharia readily dissolve in sediment trap samples. Adding $SrCl_2$ to the preservative prevents dissolution (*Beers and Stewart* 1970), but because traps in the present study were not deployed in order to study Acantharia, $SrCl_2$ was not added.

4.2.2 Light and electron microscopy

Light microscopy revealed acantharian cysts in the sample cups from mid-April (collecting from 11 April 2007 to 25 April 2007), early May (25 April 2007 to 09 May 2007), and mid-May (09 May 2007 to 23 May 2007). All cysts were removed from the mid-April and early May sample cups using Pasteur pipettes under a Wild dissecting microscope at magnifications between 60× and 120×, split into eight sub-samples, and stored in polypropylene centrifuge tubes. The mid-May sample cups contained a large volume of phytodetritus due to sedimentation of the spring

diatom bloom (samples contained large numbers of *Chaetoceros* and *Rhizosolenia* frustules), making reliable removal of cysts impossible. Therefore, the acantharian contribution to these cups was determined by measuring Sr (see below).

Cyst shells of all cysts in the mid-April sample cups, and of some cysts in the early May cups, had dissolved, leaving only the organic cyst bodies. These were identified by their elongate shape, size, green-brown coloration and the presence of dark pigment inclusions running along the central axis inside the cysts (Figure 4.2). Numerous individuals were found in which part of the shell had broken off, revealing the cyst body, and some fully shelled individuals were accidentally broken during picking. All shell-less cyst bodies that were removed were identical in the above features to the cyst bodies of the broken individuals, and were distinct from all other particle types found in the samples. Light micrographs of cysts and cyst bodies found in our samples were taken with a Nikon Coolpix 4500 digital camera on an Olympus SZX9 dissecting microscope at magnifications up to 200×.

That the cysts were Acantharia was confirmed by scanning electron microscopy (SEM; Leo 1450VP, Carl Zeiss SMT) after rinsing in MilliQ water and sputter-coating with carbon. Cyst elemental compositions were measured using an energy-dispersive X-ray probe to test for peaks in Sr and S (EDX; Princeton Gamma-Tech Energy Dispersive Spectrometer fitted with a light-element detector).

4.2.3 Sr measurements

To calculate Sr flux, the evident dissolution of celestite needed to be taken into account. Dissolved Sr was therefore measured in the preservative solution from all sample cups of each trap, and from a blank sample of the original preservative solution that had not been deployed on the traps. Sub-samples of the preservative solution were taken before microscopic inspection and other sample handling, and because all sample cups were still full to the brim with preservative at this stage, serious evaporation had not occurred. Therefore, and due to the NaCl addition, measured Sr concentration in the preservative was not normalized to salinity to account for possible evaporation during sample storage.

Particulate Sr was measured in a sub-sample of cysts from each of the mid-April and early May cups. Particulate Sr in the mid-May cups was measured in 5–7 mg aliquots of the bulk material after freeze-drying, because cysts could not be reliably removed due to the large volume of phytodetritus. Cysts were rinsed with isotonic ammonium formate as per Joint Global Ocean Flux Study (JGOFS) protocol for sediment trap samples (early May cup of traps NW and NE; *Newton et al.* 1994) or with MilliQ water (all other cysts), and dissolved in MilliQ water acidified with HNO_3 purified by sub-boiling distillation. Freeze-dried material was dissolved directly in MilliQ water acidified with sub-boiled HNO_3. Sr was measured at NOC Southampton on a Thermo X Series inductively coupled plasma mass spectrometer in 2% HNO_3 containing $10\,\mu g\,g^{-1}$ In and Re as internal standards. The instrument was calibrated with single-element Sr standards containing $10\,\mu g\,g^{-1}$ In and Re. Samples of MilliQ water and ammonium formate solution were used as blanks. The precision of all Sr measurements was taken to be ±1%, based on prior experience with the method, although triplicate analysis of two seawater samples

analyzed in parallel during one of the runs yielded relative standard deviations (RSD) of 0.2% and 0.5%. The method for calculating fluxes is described below.

4.2.4 POC and PON

Acantharian POC and PON were determined from a sub-sample of cysts from each sample cup. Cysts were rinsed in MilliQ water and analysed in silver cups (Appendix B.1). Non-acantharian POC and PON from the same sample cups was determined after removing swimmers as described in Chapter 5.2.2.

The Acantharian POC and PON fraction in the mid-May cups could not be measured directly, because cysts were not removed. These values were hence calculated by multiplying the Sr fluxes measured in the mid-May cups by the mean POC:Sr and PON:Sr ratios measured in the mid-April and early May cups. The uncertainty on the values thus calculated was estimated from the standard deviation of the ratios, and yielded an overall uncertainty of ∼20% for cyst POC and ∼30% for cyst PON in these cups.

4.2.5 Calculation of Sr, POC, and PON fluxes

Total particulate Sr flux was calculated from the sum of dissolved Sr in the preservative (corrected for the blank) and particulate Sr in cysts (mid-Apr and early May cups) or in bulk sediment (mid-May cups). POC and PON fluxes were calculated from the sum of acantharian and non-acantharian POC and PON (see Appendices A.4 and A.5). Uncertainty on dissolved Sr measurements was estimated as 1% (Section 4.2.3), while errors for all particulate Sr measurements were assumed to be 10% (both for cysts and for bulk sediment, derived from measurement error, the sample-splitting procedures, and from weighing errors). Errors were propagated through the flux calculations to yield the final overall uncertainty (<5% in all cases for Sr).

Errors on acantharian POC and PON fluxes were assumed to be 10%, to account for splitting and analytical error. Unfortunately, replication of these measurements was not possible, and we therefore lack a direct estimate of the uncertainty. As for Sr, these errors were fully propagated through the flux calculations to yield an overall uncertainty (∼10% wherever cyst POC and PON were directly measured).

4.2.6 Continuous Plankton Recorder data

Monthly mean abundances of Acantharia from 2004 to 2009 in the area 57°N to 62°N and 17°W to 30°W were obtained from the Continuous Plankton Recorder Survey (*Richardson et al.* 2006; data freely available from `http://www.sahfos.ac.uk/data-archive/database.aspx`). CPR samples integrate over approximately 3 m^3, hence the numbers were divided by three, and values quoted here give the mean number of adult Acantharia per m^3 at approximately 10 m depth for each month. These data are interpreted as relative abundance of Acantharia, as an unknown number may have dissolved prior to sample counting.

4.2.7 Sinking rates

Cyst sinking rates were determined in a 6 cm-diameter measuring cylinder filled with Iceland Basin seawater at 5 °C. 29 cysts were sized, transferred to the cylinder in a pipette, and their descent timed over a distance of 10 cm after having sunk 6 cm below the water level. Only cysts with intact shells were used, but it is possible that some of their celestite had dissolved. The measured sinking rates might hence be under-estimates.

4.3 Results

4.3.1 Microscopy and sinking rates

A SEM image of a representative specimen (from the mid-May cup of trap NW) is shown in Figure 4.2a, with its EDX spectrum in Figure 4.2b. Cyst dimensions ranged from 600 µm to 1000 µm in length, and 100 µm to 300 µm in width. The mean sinking rate ± standard deviation was $490 \pm 150\,\mathrm{m\,d^{-1}}$ ($n = 29$) ranging from $250\,\mathrm{m\,d^{-1}}$ to $770\,\mathrm{m\,d^{-1}}$. The cysts found by us most closely resemble those pictured in figures 6.153 and 6.158 in *Bernstein et al.* (1999) as ''Acantharian cysts — family unknown,'' and the cyst Type IX found by *Spindler and Beyer* (1990) in the Weddell Sea. *Hollande et al.* (1965) picture a light micrograph of a very similar cyst in their plate VIII-6, which they list as ''*Fusellina magna* nov. gen. nov. sp.'' under the heading ''Acanthaires *incertae sedis*,'' emphasizing its uncertain taxonomy.

Figure 4.2c shows several cysts from the late April cup of Trap NE, the shells of all of which had dissolved prior to removal from the sample. Figure 4.2d shows several cysts at different stages of dissolution from the mid-May cup of Trap C. In Figure 4.2e and f, respectively, two cysts are pictured first with intact shells, and then the same two cysts after deliberately breaking open their shells (Trap C, mid-May). The images clearly show that the cyst bodies are distinctive in size, shape, and pigmentation, allowing cysts to be readily identified even after dissolution of the shell.

4.3.2 Sr flux

Figure 4.3a shows the concentration of dissolved Sr in each sample cup of the four traps, and Figure 4.3b shows the time-series of Sr flux into each trap. The presence of acantharian cysts always coincided with strongly elevated levels of dissolved Sr in the preservative solution. High Sr flux was only found in the early and mid-May cups of Traps NW, NE, and C (cup opening dates 25 April and 09 May, respectively), with small fluxes also during mid-April and late May into Traps NW and NE. In all cups, the majority (≥60%) of the Sr was dissolved (Table 4.1). Although a very small Sr flux ($0.1\,\mathrm{mg\,m^{-2}\,d^{-1}}$) was also detected in Trap C during mid-April, no cysts were found in this sample and cyst flux was assumed to be zero. Sr flux collected by Trap S was comparatively low throughout the entire collection period. Flux of Acantharia was thus restricted to April and May, and most cysts were collected in just three of the traps. The mean flux for each collection interval was 0.15 ± 0.10, 2.0 ± 1.4, 1.3 ± 0.9, and $0.14 \pm 0.11\,\mathrm{mg\,Sr\,m^{-2}\,d^{-1}}$ for mid-April, early May, mid-May, and late May, respectively (mean

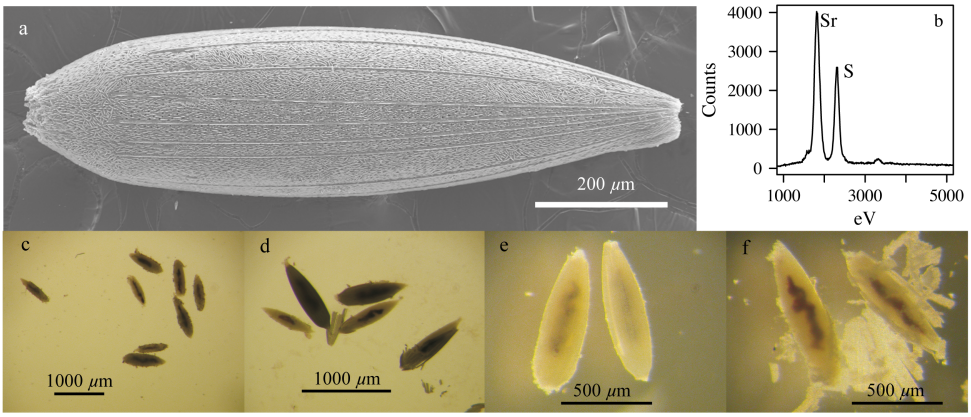

Figure 4.2 – (a) Scanning electron micrograph of an acantharian cyst from the mid-May sample of Trap NW, and (b) its energy-dispersive X-ray spectrum showing strontium and sulphur peaks (eV = electron Volt). Light-micrographs show cysts from (c) late April in Trap NE, the shells of which had dissolved prior to being removed, (d) cysts from mid-May in Trap C showing (left to right) a cyst whose shell has dissolved, two cysts still with a complete shell, one cyst with only an apical portion of the shell remaining (left part of the cyst), and a cyst with a partially broken shell revealing the cyst body. Two cysts from mid-May in Trap C are pictured first (e) with their shells and then (f) with the shells purposely broken to show the cyst bodies. (c,d) were taken under transmitted light, (e,f) with reflected light. Note in all cases the distinctive size, shape, and coloration of the cyst bodies, and the pigment inclusions; these features allowed cysts to be identified even after dissolution of the shell, as in (c).

± SD, all $n = 4$). The mean cumulative flux amounted to 50 ± 35 mg Sr m^{-2} over the course of these eight weeks (mean ± SD, all $n = 4$).

4.3.3 POC and PON flux and elemental ratios

The contribution of acantharian cysts to POC and PON flux in each trap during mid-April to mid-May is shown in Table 4.1. The greatest cyst flux was found in the early May cup of Trap NW, where they contributed 0.45 mg POC m^{-2} d^{-1} and 0.10 mg PON m^{-2} d^{-1}. This corresponds to 48% of total POC flux and 59% of total PON flux over the two weeks. Averaging the percentage contribution of acantharian cysts across the four traps suggests that they were responsible for $3.1\% \pm 5.3\%$, $22\% \pm 19\%$, and $3.5\% \pm 3.3\%$ of total POC flux during mid-April, early May, and mid-May, and contributed $3.6\% \pm 6.3\%$, $29\% \pm 24\%$, and $4.8\% \pm 4.5\%$ of PON flux during these periods (mean ± SD, all $n = 4$). The high standard deviations result from the very low cyst flux into Trap S. Although Sr flux during late May equalled the mid-April flux in Traps NW and NE (Figure 4.3), the acantharian contribution to the total particle flux during late May was likely negligible because the late May cups contained a 5- to 10-fold higher volume of particles than even the early May cups.

The mean ± standard deviation POC and PON content per cyst was 0.99 ± 0.24 mg POC and 0.18 ± 0.04 mg PON, as calculated from the six samples from which these properties were directly measured (as opposed to calculated from the Sr flux, see Table 4.1). The POC:Sr and PON:Sr ratios were 0.120 ± 0.022 mg mg^{-1} and 0.023 ± 0.007 mg mg^{-1}, respectively. Furthermore, the cyst POC:PON ratios were relatively low, ranging from 5.0 to 8.8, with higher values in cups

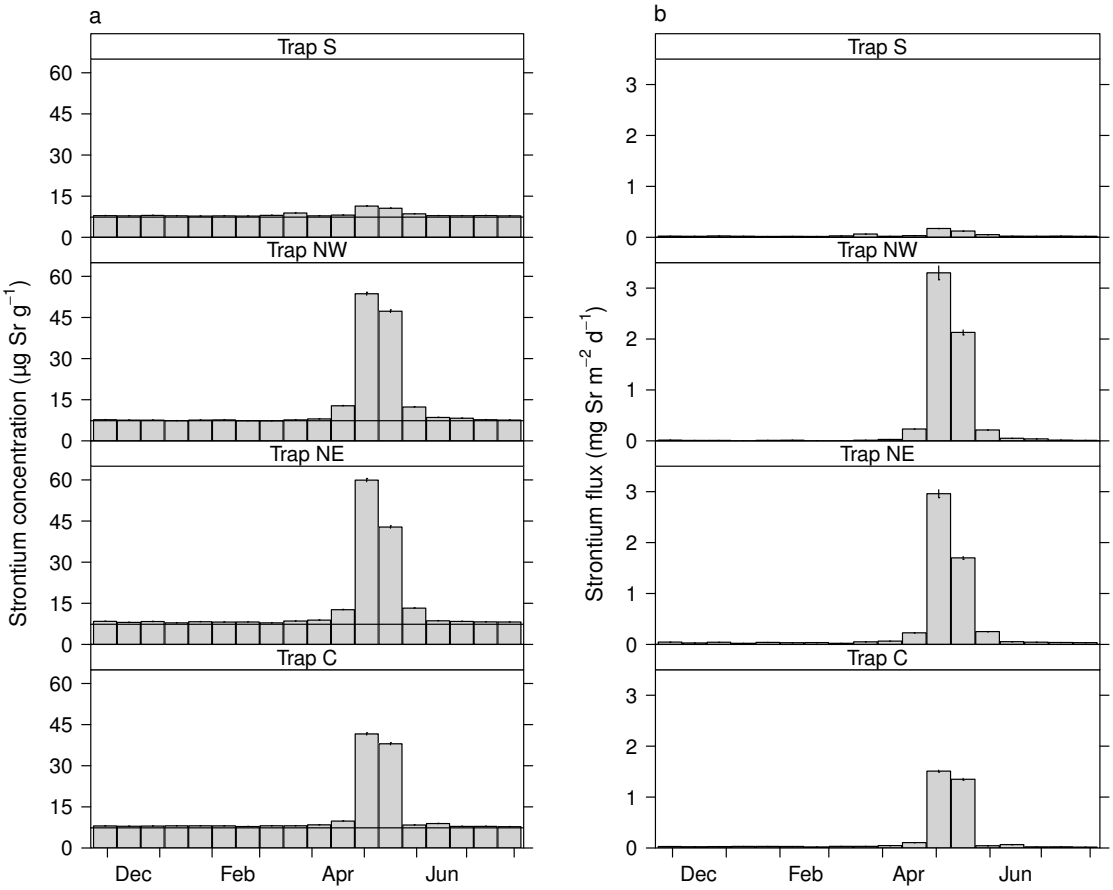

Figure 4.3 – (a) Concentration of dissolved Sr in all sample cups of each trap. The horizontal line shows the concentration in the preservative blank, a sample of the original preservative used for these traps ($7.35\,\mathrm{mg\,Sr\,g^{-1}}$). Error bars are $\pm 1\%$ of measured values, the estimated standard deviation of the preservative concentration measurements. (b) A time-series of Sr flux into each of the four sediment traps. The cups opening on 09 May and 23 May 2007 contained a large volume of phytodetritus due to sedimentation of the spring bloom; the contribution from Acantharia to the 23 May cups was, therefore, deemed negligible compared to the quantity of non-acantharian organic matter. Error bars are ± 1 standard deviation, based on propagation of errors from dissolved and particulate Sr measurements (<5% in all cases).

with fewer (*i.e.* more dissolved) cysts. The best estimates of the ratio are hence probably from the three mid-May samples with most cysts, which are 5.3 (Trap NW), 5.0 (Trap C), and 5.3 (Trap NE). Together with the high sinking rates, this demonstrates that the cysts are rapidly sinking particles that experience very little degradation until their shell dissolves.

4.3.4 Continuous Plankton Recorder survey

Table 4.2 shows the mean number of Acantharia recorded by the CPR survey for each month between 2004 and 2009. Acantharia were recorded between spring and summer in five of the six years, but the timing and magnitude of their occurrence is highly variable. During 2004, Acantharia were only found in May and in low abundance (6 individuals m^{-3}), while in 2005 they were recorded in May, August and September at densities up to 63 individuals m^{-3}. In 2006, abundances of 27 and 3 individuals m^{-3} were found in July and October, respectively, but no earlier. From 2007–2009 sample coverage was quite poor. In 2007, only 2 individuals m^{-3} were found, but as early as March — four months earlier than in 2006 — but no more samples were taken until June 2008, and we are hence without data for the period of highest cyst flux in our traps. In August and September 2008 there was a very high peak, 100 and 1250 individuals m^{-3}, but no more Acantharia were found after that.

It should be noted that some Acantharia might have been present in samples in which none were recorded, as many individuals would probably have dissolved in the CPR's formaldehyde preservative between collection and microscopic examination. All abundances of Acantharia in the CPR are thus probably under-estimates, and there is probably a threshold abundance below which they are not recorded.

4.4 Discussion

4.4.1 POC, PON, and Sr fluxes

The Sr fluxes we report are too high to be attributed to non-acantharian sources. All cups with acantharian cysts contained between 1 mg Sr and 21 mg Sr; although dissolution of $CaCO_3$ may release some Sr, $CaCO_3$ typically contains no more than $\sim$1 mg Sr g^{-1} $CaCO_3$. Although we did not measure Ca in the preservative, even complete dissolution of 1 g $CaCO_3$ would only have contributed 5–10% of the Sr in those cups with fluxes greater than 1 mg Sr m^{-2} d^{-1}. $CaCO_3$ dissolution may have made a greater relative Sr contribution to cups with low Sr fluxes, although these cups also contained low total particle quantities ($\leq$330 mg total sample dry weight). Hence substantial $CaCO_3$ flux into these cups seems unlikely. Lithogenic sources of Sr can be ruled out, because the Sr we measured was labile enough to dissolve in the trap preservative and in weakly acidified MilliQ water. Moreover, the acantharian celestite was most probably derived from the direct sinking of intact cysts, given their abundance in the collection cups. The size and relative robustness of the cysts would probably render them unavailable to many grazers, suggesting that celestite flux in faecal pellets is probably not important — in particular because celestite that was ingested by a grazer would be fragmented during ingestion, and thus probably dissolve more rapidly.

Trap	Sample	Collection period	Cyst flux	Cyst POC	Cyst PON	total Sr flux	Dissolved Sr flux	Non-cyst POC	Non-cyst PON
NW	mid-April	11 Apr–25 Apr	18	0.026 ± 0.003	<0.005	0.233 ± 0.004	0.233 ± 0.004	0.21 ± 0.02	0.027 ± 0.003
60.00°N,	early May	25 Apr–09 May	577	0.45 ± 0.05	0.099 ± 0.010	3.30 ± 0.14	1.96 ± 0.02	0.49 ± 0.04	0.069 ± 0.007
20.83°W	mid-May	09 May–23 May	235*	$0.26^* \pm 0.05$	$0.049^* \pm 0.016$	2.13 ± 0.05	1.69 ± 0.02	2.9 ± 0.3	0.40 ± 0.04
C	mid-April	11 Apr–25 Apr	0	0	0	0	0	0.24 ± 0.02	0.029 ± 0.003
59.50°N,	early May	25 Apr–09 May	210	0.17 ± 0.02	0.04 ± 0.004	1.51 ± 0.02	1.44 ± 0.02	0.91 ± 0.07	0.14 ± 0.01
20.00°W	mid-May	09 May–23 May	149*	$0.16^* \pm 0.03$	$0.03^* \pm 0.01$	1.35 ± 0.02	1.29 ± 0.02	4.3 ± 0.38	0.53 ± 0.11
NE	mid-April	11 Apr–25 Apr	20	0.019 ± 0.002	<0.005	0.228 ± 0.004	0.228 ± 0.004	1.3 ± 0.1	0.17 ± 0.02
59.65°N,	early May	25 Apr–09 May	401	0.39 ± 0.04	0.087 ± 0.009	2.96 ± 0.08	2.23 ± 0.03	1.3 ± 0.1	0.18 ± 0.02
18.78°W	mid-May	09 May–23 May	188*	$0.20^* \pm 0.04$	$0.04^* \pm 0.01$	1.70 ± 0.03	1.5 ± 0.02	11 ± 0.6	1.7 ± 0.1
S	mid-April	11 Apr–25 Apr	<2	0	0	0	0	0.53 ± 0.04	0.09 ± 0.01
58.87°N,	early May	25 Apr–09 May	25	0.025 ± 0.002	<0.005	0.173 ± 0.004	0.173 ± 0.004	1.3 ± 0.1	0.21 ± 0.02
20.04°W	mid-May	09 May–23 May	14*	$0.015^* \pm 0.003$	<0.005	0.123 ± 0.006	0.12 ± 0.005	3.4 ± 0.3	0.45 ± 0.04

* Values calculated from the Sr flux and mean cyst:Sr, POC:Sr, and PON:Sr ratios measured in early May samples of Traps NW, NE, and S.

Table 4.1 – Summary of trap locations and collection intervals for each sample cup found to contain acantharian cysts. For each sample cup the flux of cysts (individuals $m^{-2}\,d^{-1}$), the cyst and non-cyst flux of POC and PON, as well as Sr flux, are listed (all fluxes in $mg\,m^{-2}\,d^{-1}$). Although the mid-April cup of Trap C did contain a very small amount of Sr above the background, no cysts were found upon microscopic examination of the sample and cyst fluxes are hence given as zero. 'Dissolved Sr flux' is the Sr flux calculated only from the excess dissolved Sr concentration in the preservative solution (in $mg\,Sr\,m^{-2}\,d^{-1}$); when no particulate Sr was detected, this is equal to the total Sr flux. All errors are one standard deviation based on propagated uncertainties.

	Month											
Year	Jan	Feb	Mar	Apr	May	Jun	Jul	Aug	Sept	Oct	Nov	Dec
2004	NA	0 (14)	0 (6)	NA	6 (3)	NA	0 (2)	NA	0 (6)	0 (6)	0 (6)	0 (6)
2005	0 (15)	0 (5)	0 (7)	0 (7)	50 (1)	0 (3)	0 (6)	3 (6)	63 (5)	NA	NA	0 (2)
2006	0 (5)	NA	0 (11)	0 (6)	0 (6)	0 (6)	27 (5)	0 (6)	0 (3)	3 (5)	0 (2)	0 (6)
2007	0 (6)	0 (6)	2 (7)	0 (7)	NA	NA	NA	NA	NA	NA	NA	NA
2008	NA	NA	NA	NA	NA	0 (1)	0 (1)	100 (1)	1250 (1)	0 (1)	0 (1)	0 (1)
2009	0 (9)	0 (5)	NA	0 (8)	0 (8)	NA	0 (1)	NA	0 (1)	0 (5)	0 (3)	NA

NA = no samples taken

Table 4.2 – Monthly mean numbers of Acantharia per m^3 in the Iceland Basin as recorded by the Continuous Plankton Recorder survey between 2004 and 2007. Values are monthly means, followed in parentheses by the number of samples from which the mean was calculated. Zeroes indicate that samples were taken, but no Acantharia were found.

The flux of Acantharia we measured is the highest ever recorded in the bathypelagic. In Figure 4.4 we compare our fluxes to those reported by other authors. The acantharian-associated POC fluxes recorded by us fall into the range measured by *Michaels et al.* (1995) at 150 m off Bermuda (up to $0.74\,mg\,C\,m^{-2}\,d^{-1}$) and by *Michaels* (1991) at 150 m in the Northeastern Pacific ($0.39–1.08\,mg\,C\,m^{-2}\,d^{-1}$). In half of our sample cups, they are higher than the $0.13\,mg\,C\,m^{-2}\,d^{-1}$ found by *Antia et al.* (1993) at 1000 m in the East Greenland Sea, while at 2200 m, *Antia et al.* (1993) measured an Acantharian contribution of only $0.005\,mg\,C\,m^{-2}\,d^{-1}$. Moreover, *Antia et al.* (1993) recorded no Acantharia in a sediment trap deployed for a full year at 2200 m in the East Greenland Sea. Similarly, *Bernstein et al.* (1987) found lower Sr flux at 900 m ($\leq 0.095\,mg\,Sr\,m^{-2}\,d^{-1}$) and 400 m ($0.01–1.48\,mg\,m^{-2}\,d^{-1}$) and, with one exception, no flux at all at 2200 m in the Pacific, and *Bernstein et al.* (1992) report negligible flux of Acantharia at 1500 m in the Sargasso Sea. *Lamborg et al.* (2008) collected up to $0.35\,mg\,Sr\,m^{-2}\,d^{-1}$ at Station ALOHA (150 m, Central Pacific) using neutrally buoyant sediment traps, but only $0.02–0.09\,mg\,m^{-2}\,d^{-1}$ at 300 m and 500 m. During the same cruise, *Bishop and Wood* (2008) sampled unusually high levels of particulate Sr in the surface mixed layer using a large-volume in situ pump, which they attributed to Acantharia, but noted a decrease in particulate Sr by three orders of magnitude down to 800 m. While *Lamborg et al.* (2008) collected Sr fluxes of $0.34–0.1\,mg\,m^{-2}\,d^{-1}$ in the sub-arctic Pacific (station K2), *Bishop and Wood* (2008) concluded that most particulate Sr at this station was present in carbonates and adsorbed onto Mn and Fe oxides — the fact that particulate Sr in the K2 trap samples did not decrease over time in a particle ageing experiment (*Lamborg et al.* 2008) also implies that it was not acantharian celestite.

The discrepancy between our results and other studies are probably not due to differences in trap preservative choice. *Michaels* (1991) and *Michaels et al.* (1995) added $SrCl_2$ to their sediment traps, preventing dissolution. *Antia et al.* (1993) added $SrCl_2$ to their sediment trap samples 6–8 weeks after collection, but noted signs of dissolution in the adult Acantharia;

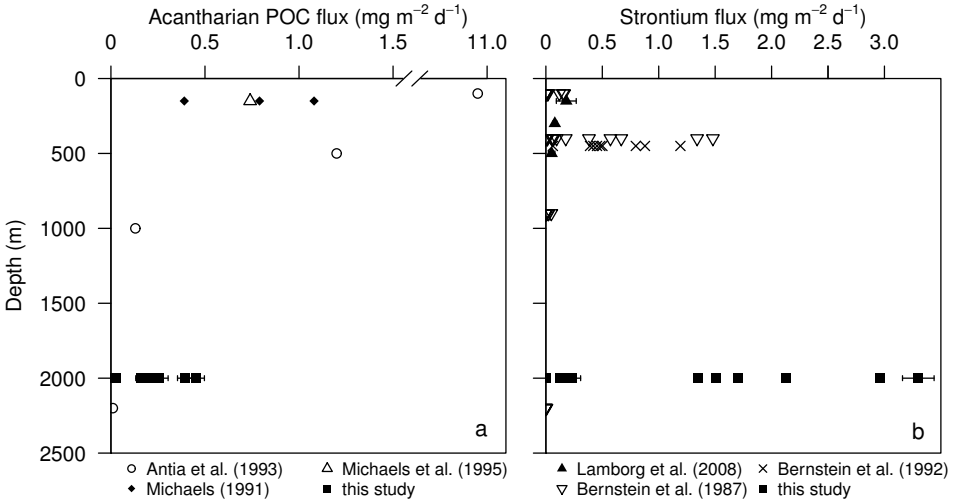

Figure 4.4 – Comparison of the magnitude of acantharian (a) POC and (b) Sr fluxes found in our traps to values reported in the literature. Both plots show all twelve data points from the present study, with error bars denoting one standard deviation. All data points from *Antia et al.* (1993) and *Michaels* (1991) are shown, but only the maximum value from *Michaels et al.* (1995) is shown (as flux data therein are presented only in figures, and separately for adult Acantharia and cysts). In (b), all values reported by *Bernstein et al.* (1987, 1992) are shown (because only few measurements were in triplicate), while data points for *Lamborg et al.* (2008) are mean ± standard deviation of all trap deployments at each depth at Station ALOHA (no distinction made between trap type and deployment number; data from Station K2 are omitted).

it is, therefore, possible that their fluxes are under-estimates. Their long-term mooring would almost certainly have suffered significantly from celestite dissolution if Acantharia were present, as discussed in their paper. *Lamborg et al.* (2008) added no $SrCl_2$, but their traps were deployed for only 3–5 d and samples were processed on board upon recovery. Nevertheless, they observed significant dissolution of particulate Sr in their samples from station ALOHA during a particle ageing experiment, which suggested that their particulate Sr fluxes may need to be revised upwards by between 17% and 48%. Yet even if this correction were applied, the Sr fluxes would not exceed $0.5\,\mathrm{mg\,m^{-2}\,d^{-1}}$. *Bernstein et al.* (1987) and *Bernstein et al.* (1992) did not add $SrCl_2$ either, but their sediment trap deployments lasted only 24 h and samples were processed on board upon recovery, precluding substantial dissolution.

In the present samples, acantharian cysts contributed significantly to the total POC and PON flux during the period in question, particularly during the two weeks prior to the sedimentation of the spring bloom. Even during sedimentation of the bloom, we found that acantharian cysts contributed on the order of 3% of the total POC and 4.5% of PON flux. In comparison, *Antia et al.* (1993) found that Acantharia contributed only 0.9% and <0.1% of total POC flux at 1000 m and 2200 m, respectively, despite accounting for 32% at 100 m. However, the cumulative cyst POC and PON fluxes into our traps did not exceed 10 mg POC and 2.1 mg PON $\mathrm{m^{-2}}$ even in Trap NW; as annual cumulative POC flux in the traps was around 700–800 $\mathrm{mg\,m^{-2}\,d^{-1}}$ (Chapter 5.3.2), Acantharia did not contribute more than 2% of annual POC flux at 2000 m.

4.4.2 Regional variability in cyst flux

Throughout the three collection periods the acantharian flux in the southern trap was one order of magnitude lower than in the other traps. Weekly composite images of sea-surface temperature in the region (from the Advanced Microwave Scanning Radiometer [AMSR-E]; data available at `http://www.remss.com/amsr/amsr_data_description.html#amsre_data`) show a sharp temperature gradient within the trap deployment area during April and May (Figure 4.5). The southern trap was below an area with sea-surface temperature around 0.5 °C higher than above the other traps. This is particularly pronounced from 02 May to 09 May 2007 (Figure 4.5d,e), when the temperature was >0.5 °C warmer above the southern trap than above the others — which is during the period when acantharian flux was highest in the region. The cyst sinking speed was so high that they would only have taken around 4 d to sink from the surface to the traps. Even a current as fast as $20\,\mathrm{cm\,s^{-1}}$ from one direction throughout the entire upper 2000 m could not have moved the cysts >70 km horizontally before reaching the trap depth. During the three collection periods, the mean current speed at trap depth on the southern mooring was $8\,\mathrm{cm\,s^{-1}}$, $6\,\mathrm{cm\,s^{-1}}$, and $15\,\mathrm{cm\,s^{-1}}$, respectively, suggesting that the cysts left the upper ocean close to the trap location and, hence, from within the area of higher temperature. We therefore suggest that Acantharia of the species in our samples occur mostly within colder waters north of the southern trap, and that the southern trap was consistently collecting particles derived from the area of warmer surface temperature. If this was indeed the case, it would imply that our estimate of average acantharian flux in the basin, which was calculated as the mean of all four traps, is probably an under-estimate. Physical conditions, especially ocean circulation, are known to affect the distribution of the related Radiolaria — which also seem to show intraspecific variation in morphology with latitude (*Casey* 1971; *Welling et al.* 1996).

4.4.3 Reasons for deep sedimentation

The present cysts probably sank deeper than previously recorded due to their high sinking rate; resulting from their size and their mineral shell. We recorded a mean sinking rate two-fold greater than *Antia et al.* (1993), probably because their cysts were much smaller ($234 \pm 80\,\mu\mathrm{m}$ diameter). *Bernstein et al.* (1987) do not quote mean sizes or sinking rates, but the cysts in their figure 2 are all smaller than 200 µm, suggesting slower sinking. A higher sinking rate due to greater size would allow a cyst to sink deeper before its ballast dissolves. It is also possible that the celestite of some species of Acantharia take longer to dissolve, for instance due to greater mineralization or organic coating of the mineral.

The ultimate question is how Acantharia might benefit from sinking so deep. Because Acantharia can ascend and descend in the water column by controlling their buoyancy (*Schewiakoff* 1926) they should be able to resurface from any depth. Indeed, *Schewiakoff* (1926) observed that zygotes loose the flagellae that the gametes possessed, and concludes that they continue to sink during early development (even to the seafloor, which he explicitly suggests they reach, although his observations were made in the comparatively shallow Gulf of Naples). It is pos-

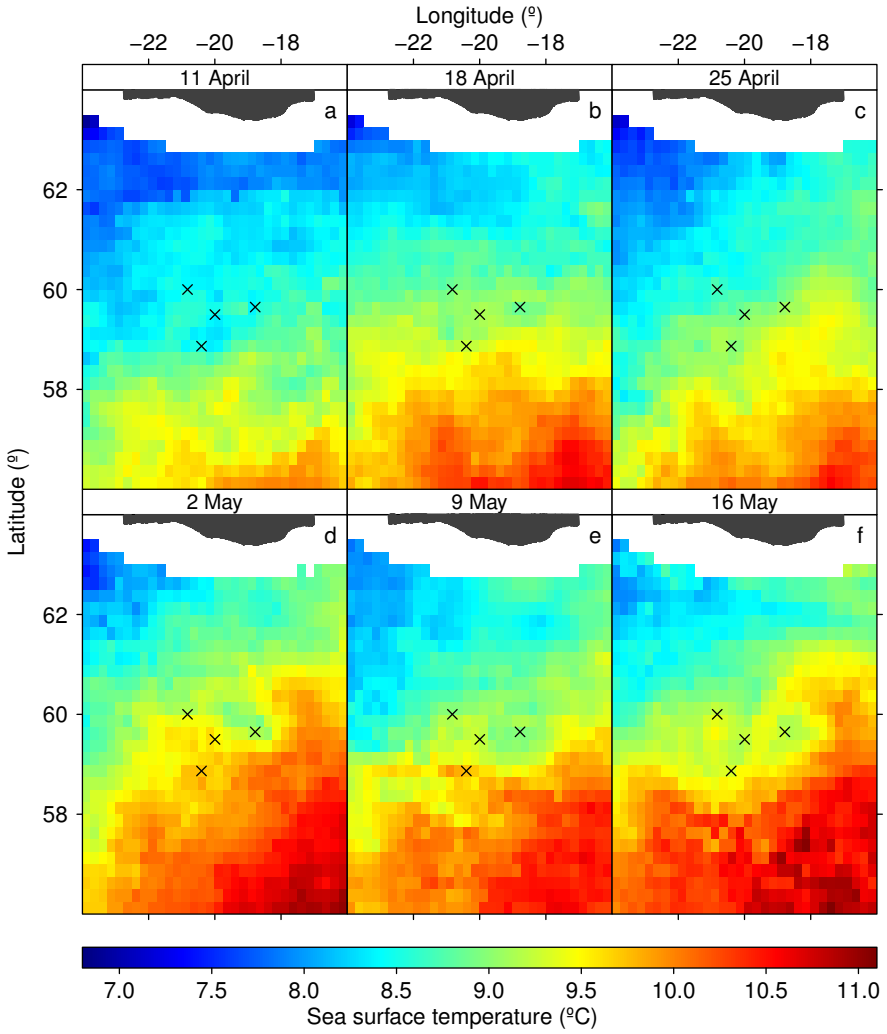

Figure 4.5 – Weekly composite images of satellite-derived sea-surface temperature for the Iceland Basin starting on 11 April 2007. Sediment trap locations are marked with black crosses. Note that the southern trap, which consistently caught one order of magnitude lower acantharian flux, is located below an area of higher sea-surface temperature than the other traps. This is most pronounced between 02 May and 09 May 2007 (d,e), which was during the period of highest acantharian flux in all traps.

sible that Acantharia in the Iceland Basin are under pressure to sink particularly deep (or particularly quickly, or both — the two are evidently linked) before releasing gametes.

While our observations cannot resolve this question, we note that the main pulse of cysts was caught in the cup preceding the spring bloom phytodetritus. It is possible that Acantharia in this region have adapted to grow during the spring bloom, and then to sink very rapidly and release gametes at considerable depth (possibly at the seafloor), which are shortly thereafter met by a large pulse of relatively fresh organic matter on which to feed, before ascending to the surface. Phytodetrital aggregates usually sink 100–200 $\mathrm{m\,d^{-1}}$, slower than the cysts, and diatom blooms tend to sink in brief, large pulses of aggregates that can carpet the seafloor (*Billett et al.* 1983; *Alldredge and Gotschalk* 1989). If detritus and cysts left the surface at the same time, the cysts should arrive at depth several days in advance. If this is, indeed, the strategy pursued by the Acantharia under consideration here, they would need to sink very rapidly and also quite deep into the water column to ensure that the bloom detritus has not already passed by the time their gametes are released and have formed zygotes. The result would then be a rapidly sinking cyst that does not dissolve until it is at bathypelagic depths.

This hypothesis could also explain the far shallower dissolution of cysts observed at lower latitudes, where particle flux is lower and shows less extreme seasonality — in such settings it may not be advantageous to sink rapidly and release gametes at great depth, but rather to form zygotes in the upper mesopelagic where the organic matter supply is greater and fresher, but the density of possible predators would be lower. It is, thus, possible that the depth of gamete release and juvenile development in Acantharia might be controlled by different factors in different regions: food supply in high latitudes, but maybe predation at low latitudes.

4.4.4 Deep cyst sedimentation during other years

The above hypothesis predicts that deep sedimentation of Acantharia should occur annually in the Iceland Basin. To investigate whether this is the case, we draw on the Continuous Plankton Recorder (CPR) survey and on published vertical profiles of salinity-normalized Sr concentration. Adult Acantharia were recorded by the CPR in the Iceland Basin in five of six years for which Acantharia were counted separately, at mean monthly abundances up to 1250 individuals $\mathrm{m^{-3}}$. Given the presence of adults, sedimentation of cysts probably recurs annually, although the CPR data suggest that the timing of acantharian occurrence is variable. However, peaks in different months might be due to different species, and while Acantharia were not always recorded during spring, it is possible that Acantharia were also present in some months for which none were recorded, due to dissolution between sampling and analysis. However, it is evident that the cyst flux in 2007 was not due to a freak bloom never found in other years.

Moreover, identical cysts, and high Sr fluxes, were found in PELAGRA sediment traps in the mesopelagic during the 2008 spring bloom, conclusively demonstrating a large export event of acantharian cysts during the spring bloom in a second year (see Chapter 2).

Vertical profiles of Sr concentration can be indicative of the dissolution depth of Acantharia; thus, *Bernstein et al.* (1992) conclude that the shallow dissolution of Acantharia implied by their sediment trap samples is supported by the observation of *Mackenzie* (1964) of maximum

Sr concentration at 600 m in the Sargasso Sea. *de Villiers* (1999) report a vertical Sr profile at 60°N, 20°W that shows a 1% depletion in surface Sr concentration relative to waters below 1000 m. Although her data show more pronounced vertical concentration gradients in the mesopelagic of the South Atlantic and South Pacific, the Sr profile from 60°N, 20°W reaches its maximum value only at 1700 m, compared with the 800 m maxima at the other two stations. The deep Sr maximum in the Iceland Basin supports the hypothesis that Acantharia routinely sink to the depths we report, instead of dissolving in the mesopelagic.

4.4.5 Possible deep sedimentation of Acantharia in other regions

Bernstein et al. (1987) report both mesopelagic celestite dissolution and mesopelagic Sr maxima (all normalized to salinity) across the North Pacific, noting that the lowest surface Sr values and highest 400 m Sr flux were both measured at 45°N 167°E. The vertical Sr profile at this station increases approximately linearly to 3000 m depth, instead of having a maximum at or above 1000 m. *de Villiers* (1999) also presents a Sr profile from 45°N 179°E that shows more pronounced surface depletion than the Iceland Basin profile and a deep maximum at 1600 m. It is, therefore, possible that the sub-arctic Pacific is a region in which Acantharia sink to similar depths to those we report for the Iceland Basin.

Although *Bernstein et al.* (1987) detected no Sr flux at 2200 m at 45°N 179°E, they recorded by far the highest 900 m fluxes of their study at the other two stations in the sub-arctic Pacific (∼50°N, 175°E and 50°N, 150°W). Unfortunately, they had no 900 m traps at the 45°N station. The deep Sr fluxes found by *Bernstein et al.* (1987) in the sub-arctic Pacific are very modest compared to those we present here. Yet because their traps were deployed for just several days it is possible that mass sinking of Acantharia below the mesopelagic occurs at a different time of year — a point also made by *Antia et al.* (1993) for their own results. Our data show that acantharian sedimentation can take place over a very short time, and if deep sedimentation of cysts is indeed linked to the sedimentation of phytoplankton blooms as suggested above, one would expect this to take place before late spring and summer, the periods studied by *Bernstein et al.* (1987) and *Antia et al.* (1993).

Vertical fluxes of Acantharia should, therefore, also be studied using sediment traps on long-term moorings, provided that celestite dissolution is corrected for by measuring the preservative Sr concentration, or prevented by adding $SrCl_2$. With trap collection cups of a few hundred mL volume collecting for around two weeks or more, celestite fluxes of 0.1–0.2 mg m^{-2} d^{-1} or more should lead to a significant increase in preservative Sr concentration (by several mg g^{-1} above blank values; Figure 4.3a). Other sources of Sr are likely to be negligible, unless large amounts (upwards of 0.5 g) of Sr-rich $CaCO_3$ are caught, which would be evident from the nature of the samples. While short-term trap deployments have the distinct advantage of largely avoiding preservation artefacts (and thus recording even small fluxes of Acantharia quite accurately), long-term traps stand a far greater chance of catching short sedimentation events. Short-term deployments may also fail to catch a pulse of particles in a deep trap that was caught in a shallower trap, simply because the particles take longer to sink than the deployment period.

4.4.6 Celestite as a ballast mineral

Our data show that celestite can ballast POC flux to the bathypelagic in the Iceland Basin, and this may also occur in the sub-arctic Pacific. However, the cyst sedimentation we recorded was confined to a short period of time, and although Acantharia thus contributed significantly to the particle flux in that period, they probably did not contribute a very significant proportion of the annual bathypelagic flux. We tentatively suggest that their deep sedimentation is a suitable reproductive strategy in regions with high seasonality, in which case one would expect to find acantharian cysts in the bathypelagic flux in other high-latitude regions during phytoplankton blooms. In lower latitudes, or outside of bloom periods, the rapid dissolution of celestite with depth might contribute to the rapid attenuation in POC flux with depth in the mesopelagic. In certain settings it may, therefore, be warranted to consider the effect of celestite as a ballast mineral, because Acantharia are globally distributed and often very abundant.

Chapter 5

Mesoscale Variability in Bathypelagic Particle Fluxes

Data contribution

Sediment traps were deployed and recovered during RRS *Discovery* cruises D312 and D321, respectively. Corinne Pebody (NOCS) removed swimmers from the sediment trap samples, and subsequent sample processing (splitting, filtering, drying) was undertaken by the author. Samples for POC and PON were prepared by the author, and measured by Bob Head (PML). Mark Stinchcombe (NOCS) helped with BSi analyses. Samples and standards for PIC measurements were prepared by the author, and measured by Darryl Green (NOCS). The method for analysing ^{230}Th and ^{231}Pa was established at NOCS jointly with Alfred Aquilina and with the help of Andy Milton (both NOCS), both of whom invested substantial time and effort into this project. The author was taught the technique by Alex Thomas and Ben Hickey while working in Gideon Henderson's laboratory (U. of Oxford), without the help and advice of whom this project would have been impossible. Rachel Mills supervised the method's establishment at NOCS, and Matthew Cooper and Phil Warwick provided a lot of assistance with laboratory logistics and radiological safety, respectively (all at NOCS).

Abstract

Four bottom-tethered sediment traps were deployed in the Iceland Basin at 2000 m depth within a 125×125 km grid, and collected in synchrony over 14 d intervals from November 2006 to August 2007. The seasonal cycle of flux was nearly identical between traps, with spring and summer peaks in particle flux arriving in each trap during the same collection intervals. However, for each individual collection interval there was a difference of at least a factor of two between lowest and highest mass flux measurement, and at least a factor of 1.5 for POC flux. Over the entire collection interval, three traps caught indistinguishable quantities of ^{230}Th ($\sim$310 pg m^{-2}), despite differing by up to 30% in cumulative mass flux (9.4–13 mg m^{-2}). Mass flux in the fourth trap was only 7.5 mg m^{-2}, but with ^{230}Th flux of only 160 pg m^{-2}. This implies that cumulative bathypelagic particle flux can show genuine mesoscale variability of around 30%, and that the fourth trap under-collected significantly relative to the other traps. There was an overall significant inverse association between current speed (at trap depth) over each 14 d sample collection and the relative rank of mass flux between the four traps for each

collection period. However, the trap that did under-collect particle flux relative to the other traps experienced neither higher average current speeds, nor more or higher peaks in current speed. Overall, it appears as though the traps probably under-collected ^{230}Th in absolute terms by at least 50%, although this estimate is subject to large uncertainties.

5.1 Introduction

Sediment trap deployments in the bathypelagic are very rarely replicated spatially. Owing to the substantial logistical and financial investments required for such deployments, it is more common to deploy any additional traps at different depths on the same mooring, studying the attenuation of flux with depth rather than mesoscale variability in flux at any one depth. While mesoscale spatial variability in particle export out of the surface ocean has received increasing attention and is often found to be several-fold over spatial scales of 100 km or less (*Buesseler et al.* 2008; *Maiti et al.* 2008; *Buesseler et al.* 2009; *Cai et al.* 2010, see also supplementary data in *Sanders et al.* 2010), comparable estimates of variability in bathypelagic flux are rare. This probably reflects primarily the relative ease with which shallow export can be measured (especially using ^{234}Th) and linked to surface ocean processes over typical cruise durations, compared to the greater efforts that would be required to obtain similarly large numbers of bathypelagic flux measurements. However, the current interest in multi-year time-series of bathypelagic particle flux, and the discovery of significant intra-annual variability in flux as recorded at individual time-series stations (*Neuer et al.* 1997; *Conte et al.* 2001; *Waniek et al.* 2005; *Lampitt et al.* 2010), mean that assessments of the spatial variability in bathypelagic particle flux are warranted, too.

It has been established that sediment traps below 1000 m can collect particles that were formed in surface waters >100 km away, *i.e.* at spatial scales far exceeding those typical of mesoscale physical features, because currents transport particles at far greater horizontal speeds than the particles' sinking speeds due to gravitational settling (*Siegel and Deuser* 1997; *Siegel and Armstrong* 2002; *Waniek et al.* 2000). Over an annual deployment, a trap may hence collect particles derived from within a circle with radius of several hundred kilometres approximately centred on the trap — but this does not mean that bathypelagic particle flux is homogenised over such spatial scales (*Waniek et al.* 2000). Rather, the horizontal movement of sinking particles would occur primarily via mesoscale turbulent flow, which can stretch particular patches of water into thin filaments, but without substantially eroding horizontal gradients over time-scales of several weeks (as shown recently for surface phytoplankton communities by *d'Ovidio et al.* 2010). Homogenisation of flux would occur via small-scale turbulence (*e.g.* breaking of internal waves) over spatial scales of ∼1 km. The effects of small-scale turbulence would of course depend on the sinking speed of particles, with slowly-sinking particles affected more than fast-sinking ones.

Overall, one would expect some reduction in the mesoscale variability of particle flux with depth, but it might still be significant. *Newton et al.* (1994) reported that a major autumn peak in POC flux in the north-east Atlantic was recorded by one trap at 3000 m, but not by a second trap 100 km away. Using a camera system, *Guidi et al.* (2007) showed sharp horizontal gradients

in particle concentration down to at least 500 m depth in the north-east Atlantic, although a concomitant sediment trap study by *Guieu et al.* (2005) revealed only ∼20% variability in cumulative annual flux between traps 400 km apart.

A significant problem in trying to assess spatial or temporal variability in bathypelagic particle flux is that sediment traps can suffer from several biases (discussed in Appendix A.1), and we currently lack other readily available techniques for measuring bathypelagic fluxes (unlike shallow export fluxes, which can additionally be tracked by ^{234}Th profiles, nutrient budgets, or dissolved O_2 measurements). The most important problem in this case is that high horizontal currents relative to a trap are linked to reduced "efficiency" of trapping (*Gardner* 1980a,b, 1985; *Butman et al.* 1986; *Gardner and Zhang* 1997). However, despite targeted laboratory and field work, no clear relationship has emerged between current speed and the degree to which collections are compromised (*Buesseler et al.* 2007a; see Appendix A.1), so measured fluxes cannot be corrected based on a time-series of current speed at the trap depth. Measuring the annual flux of ^{230}Th into the trap does allow some assessment of trapping efficiency to be made (*Bacon et al.* 1985; *Scholten et al.* 2001; *Yu et al.* 2001), but it remains unclear whether the trapping efficiency for ^{230}Th really does apply equally to all phases (*Buesseler et al.* 2007a). Such trap "calibration" studies have concluded that sediment traps below 1000–1500 m tend to perform reasonably well (*Scholten et al.* 2001; *Yu et al.* 2001). But trapping efficiency even at these depths can be as low as 20% (*Scholten et al.* 2001), so traps below 1000 m are by no means guaranteed to yield accurate samples.

This study aimed to assess the mesoscale variability in bathypelagic flux in the Iceland Basin, an area with substantial mesoscale physical activity, by analysing particle flux and ^{230}Th flux intercepted by an array of four sediment traps. Given different amounts of particle flux between the traps, the ^{230}Th flux might either be equal between the traps (implying genuine variability in particle flux), or the ^{230}Th flux might also differ between the traps (implying differences in trapping efficiency). It is assumed here that ^{230}Th is a constant flux tracer, and that there is no genuine mesoscale variability in ^{230}Th flux.

5.2 Methods

5.2.1 Sediment trap deployments and sample handling

The sediment traps are the same ones discussed in Chapter 4, and the deployment and sample handling methods are given in Section 4.2.1. Figure 5.1 shows the deployment locations; all traps collected in synchrony from 22 November 2006 until 01 August 2007, thus covering 70% of an annual cycle. Each mooring was equipped with an Aanderaa RCM 8 current meter 15 m below the trap taking spot measurements at hourly intervals. Traps were located 580–840 m above the seafloor.

Long-lived mesoscale eddies of ∼100 km diameter are a regular feature in the Iceland Basin (*Martin et al.* 1998; *Read and Pollard* 2001), and the geometry of the mooring array was chosen to prevent any one such mesoscale feature from affecting all four sediment traps simultaneously.

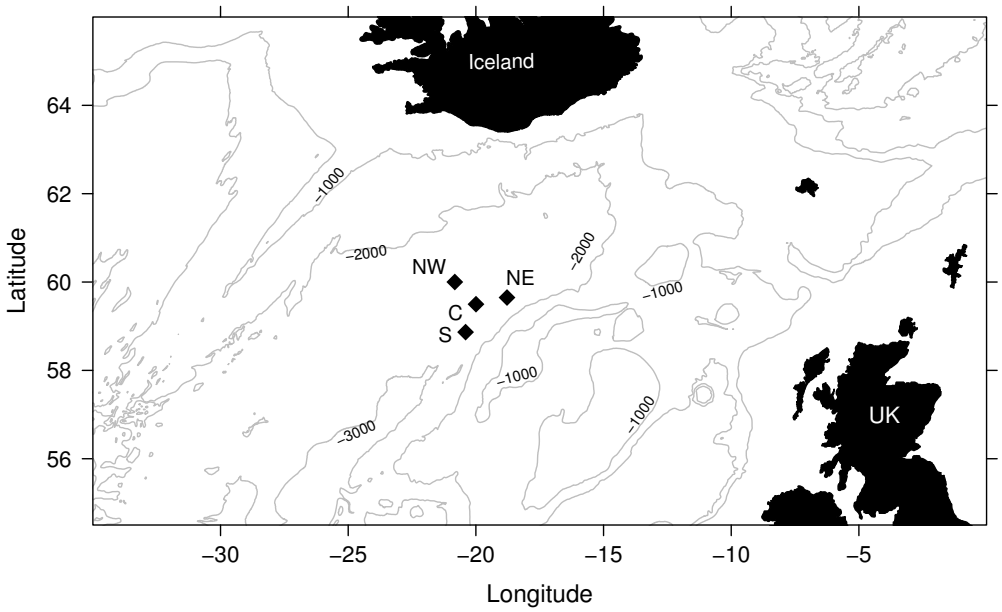

Figure 5.1 – Bathymetric chart of the Iceland Basin showing the location of the four sediment traps (filled diamonds).

5.2.2 POC/PON, PIC, and BSi

POC/PON, PIC, and BSi were measured in aliquots of freeze-dried sediment weighed on a Sartorius microbalance (typically 1–5 mg). POC and PON were measured in silver capsules after removing carbonate by *in situ* acidification with 2 mol L^{-1} HCl (Appendix B.1). PIC was measured as Ca by ICP-OES after leaching aliquots in 1 mol L^{-1} acetic acid for 24 h (Appendix B.2). BSi was measured on an autoanalyser after dissolving silica in 0.2 mol L^{-1} NaOH at 90 °C (Appendix B.3). Samples for BSi were run in two separate batches of two traps each.

All measurements were conducted in triplicate if enough material was available, and standard deviations of triplicates propagated through the calculations to yield a final error for each flux. Relative standard deviations of triplicates were mostly <10% for POC and PON (mean = 7.5% for C; 8.6% for N), <7% for Ca (mean = 1.7%), and <12% for BSi (mean = 3.2% and 3.8% for the two batches). For samples that were only analysed singly, the mean RSD of each measurement was applied as the measurement uncertainty.

5.2.3 ^{230}Th

The principles of the ^{230}Th method for sediment trap "calibration" are explained in Appendix B.6.1. Owing both to the large sample weights needed (∼100 mg) and the substantial time required for the full analytical procedure, ^{230}Th was measured after pooling aliquots from each sample into three combined samples for each trap, covering "winter" (22 November to 09 May), "spring" (09 May to 20 June), and "summer" (20 June to 01 August) (see Appendix B.6.5; these dates were chosen based on the time-series of particle flux). The measurement method is described

in detail in Appendix B.6, and is based on procedures developed by *Thomas* (2006) at the University of Oxford. Briefly, samples were subjected to total dissolution using HNO_3, aqua regia, $HClO_4$, and HF, spiked with a ^{229}Th+^{236}U double-spike, and Th was then purified by anion exchange chromatography. The content of ^{230}Th and ^{232}Th in each pooled sample was then calculated from the 229:230 and 229:232 ratios measured by mass spectrometry, and converted to a flux of $^{230}Th_{xs}$ for each of the three periods ($^{230}Th_{xs}$ is total ^{230}Th corrected for lithogenic ^{230}Th, see Appendix B.6.2). The cumulative $^{230}Th_{xs}$ flux (in $pg\,m^{-2}$) into each trap for the full deployment period was calculated as well. All ^{230}Th values presented below are $^{230}Th_{xs}$.

To test the accuracy of the ^{230}Th measurements, three Southern Ocean sediment samples that had already been analysed for ^{230}Th and ^{231}Pa at the University of Oxford were measured alongside the sediment trap samples.

Although ^{231}Pa measurements were also attempted in the sediment trap samples (the samples were hence also amended with a ^{233}Pa spike "milked" from a ^{237}Np "cow" and a Pa fraction was purified during chromatography), the final ^{231}Pa values in the Southern Ocean sediment samples differed 1.8–3.3-fold from the values obtained in Oxford. The analyses at NOCS were hence deemed unreliable, and ^{231}Pa results are not presented here. Possible reasons for the discrepancy include the unfortunately long period for which the purified Pa fractions were stored before analysis (∼3 months, due to a string of technical problems with the mass spectrometer), errors in the calibration of the ^{233}Pa spike (calibrated against CRM-145 natural U standard; with hindsight, calibration against the artificial ^{236}U in the ^{229}Th+^{236}U double-spike might have been wiser, although this is unlikely to have caused such a large and inconsistent error), or errors in the quantification of ^{232}Th hydride formation and abundance sensitivity (which may be matrix-dependent, *A. Thomas*, pers. comm.). ^{231}Pa is a much more complicated measurement than the comparatively easy ^{230}Th, so it is not entirely surprising that this first attempt did not work.

5.2.4 Satellite data

Weekly composite satellite data products were obtained for sea surface temperature (SST), sea surface height anomaly (SSH), and chlorophyll-*a*. SST data were from the same sensor as in Section 4.4.2. SSH data were combined products from multiple altimeters, provided by CLS/Aviso as the DUACS 7-d "update" product (`http://www.aviso.oceanobs.com/es/data/product-information/duacs/ssaltoduacs-products/index.html`). Chlorophyll-*a* data were from the ocean colour sensor SeaWiFS on the Sea Star platform; daily files of $\frac{1}{12}^\circ$ resolution were obtained fromthe NASA/GSFC server, composited to weekly files and interpolated to the same 0.25° grid as the SST data (`http://oceancolor.gsfc.nasa.gov/`).

5.3 Results

Time-series of fluxes in the following sections are presented as step-plots, in which the flux (or chemical composition of the samples) during each 14 d collection period is shown by the stepped

blue line. Each step corresponds to 14 d on the x-axis, and the vertical black bars at the centre of each step indicate one standard deviation of the measured value.

5.3.1 Time-series of particle flux

The fluxes during each collection interval are listed in Table 5.1. Figure 5.2 shows the time-series of POC flux into the sediment traps. As is typical in temperate to sub-polar settings, there is a clear peak in POC flux during spring, and again later in the summer, with flux decreasing steadily from late autumn to spring (*Lampitt and Antia* 1997; *Waniek et al.* 2005; *Lampitt et al.* 2010). However, during the individual collection periods the mass flux differed 2–16-fold between traps (1.5–8-fold for POC flux), and the spring and late summer peaks in flux were not equally pronounced in all traps. Moreover, the relative magnitude of the spring and summer peaks to each other differed somewhat between traps. Nevertheless, the seasonal cycle in particle flux is effectively identical between traps, with the spring and summer peaks arriving at the same time in each trap. POC flux ranged from near-zero up to $\sim$13 mg m^{-2} d^{-1}, but was mostly $<$6 mg m^{-2} d^{-1}. Given that POC fluxes were relatively high both at the beginning and end of the deployment (November and August, respectively), it is likely that a significant portion of the total annual flux was missed. While the percentage content of POC was mostly $<$10%, values up to 22% were found as well (range: 3.9–22%; Figure 5.3). However, these very high values were rarely in samples with high POC flux: of the twelve samples with POC flux $>$5 mg m^{-2} d^{-1}, only three samples had a POC content $>$10%, and there was an overall inverse correlation between POC flux and percentage POC content (Figure 5.4; Spearman's $\rho = -0.495$, $p < 0.001$). There was no clear annual trend in the percentage POC content, but values tended to reach a minimum between spring and early summer, rising again thereafter. Molar POC:PON ratios were mostly between 6.6 and 8.8, *i.e.* above the Redfield Ratio, and showed no annual trend (Figure 5.5).

Time-series of opal and $CaCO_3$ flux are shown in Figures 5.6 and 5.7, and both showed a very similar trend, and similar variability between traps, to POC flux. POC flux thus correlated clearly with both opal and $CaCO_3$ flux, although most samples with POC fluxes $<$2 mg m^{-2} d^{-1} had near-zero opal flux (Figure 5.8). $CaCO_3$ flux was invariably greater than opal flux, and only eight samples had a molar Si:POC ratio $>$0.6 (opal contributed $<$20% of total mass flux in most samples, while $CaCO_3$ contributed $>$50% in most samples) Over the entire study period, the cumulative PIC:POC ratios for the four traps were 1.01 ± 0.06 (NW), 1.05 ± 0.12 (C), 1.01 ± 0.05 (NE), and 0.84 ± 0.05 (S).

POC flux was clearly related to total mass flux (Figure 5.2), and a linear regression $y = 0.677 + 0.054x$ yielded $R^2 = 0.898$ ($p < 0.001$) — although a quadratic model ($y = 0.334 + 0.0712x - 0.0000869x^2$, $R^2 = 0.913$, $p < 0.001$) actually fit the data significantly better (ANOVA, $F = 11.858$; d.f. $= 1, 69$; $p = 0.00098$), and had a slightly higher adjusted R^2 value (0.917 for the quadratic model compared to 0.897 for the linear model).

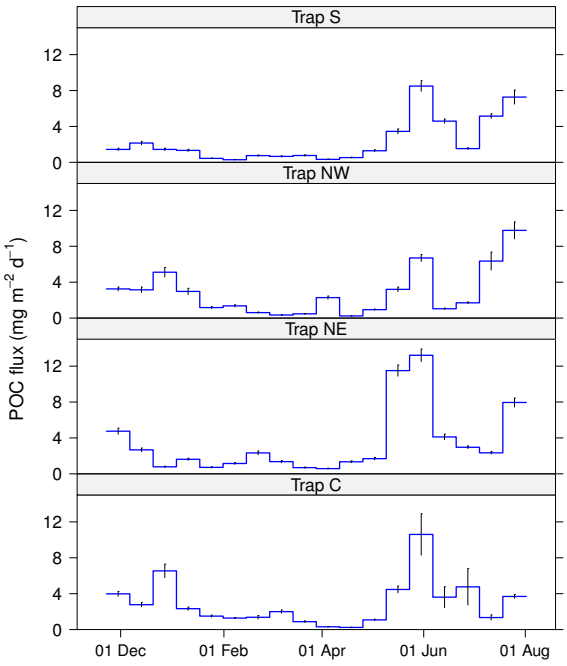

Figure 5.2 – Time-series of POC flux into each sample.

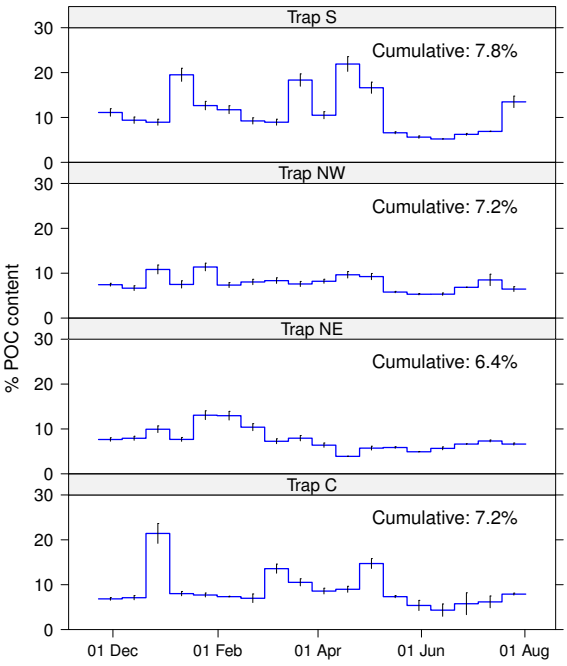

Figure 5.3 – Percentage content of POC in each sample.

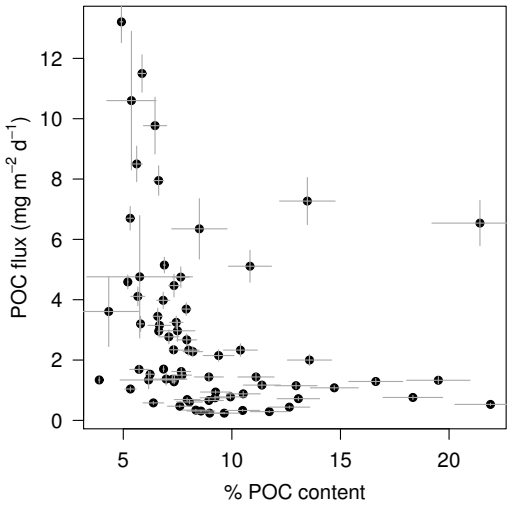

Figure 5.4 – Scatter-plot of POC flux against percentage POC content for each trap sample. Grey lines indicate one standard deviation.

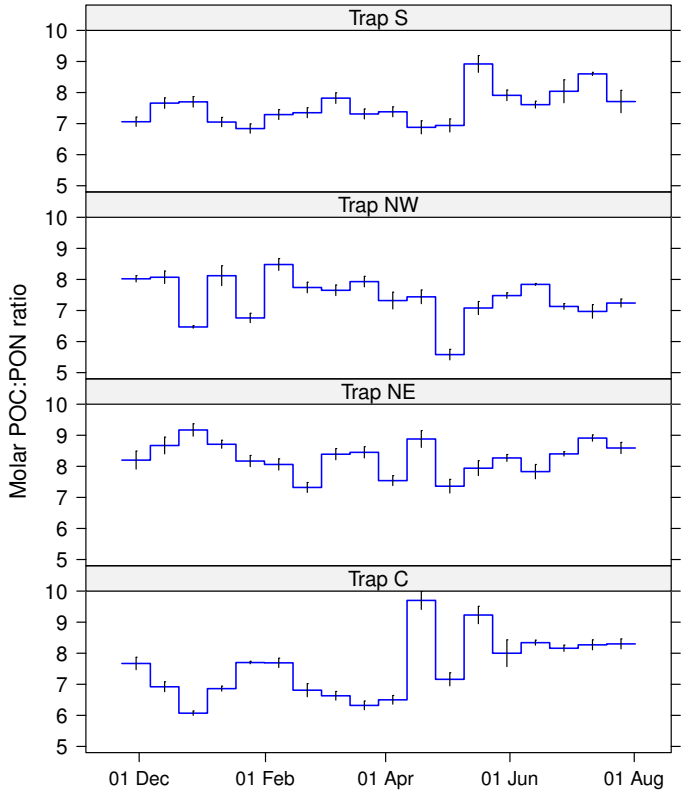

Figure 5.5 – Molar POC:PON ratio of each sample.

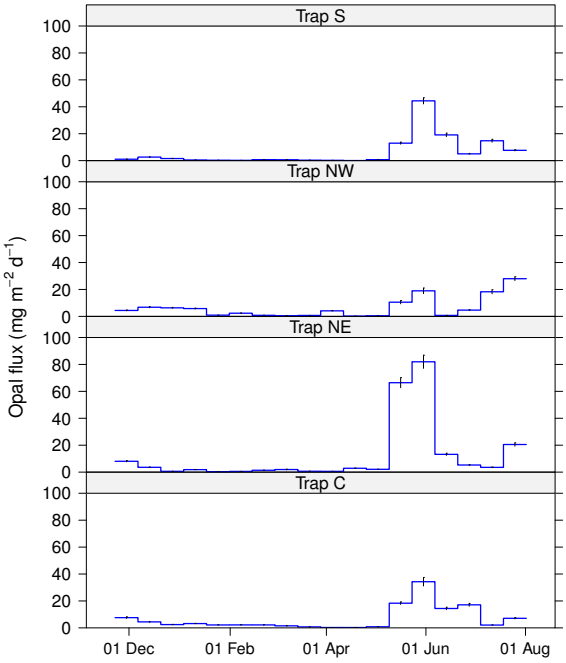

Figure 5.6 – Time-series of opal flux into the four traps.

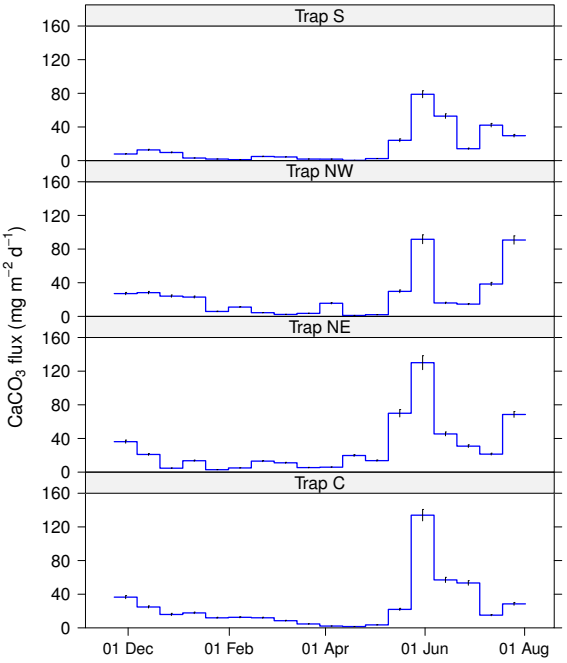

Figure 5.7 – Time-series of $CaCO_3$ flux into the four traps.

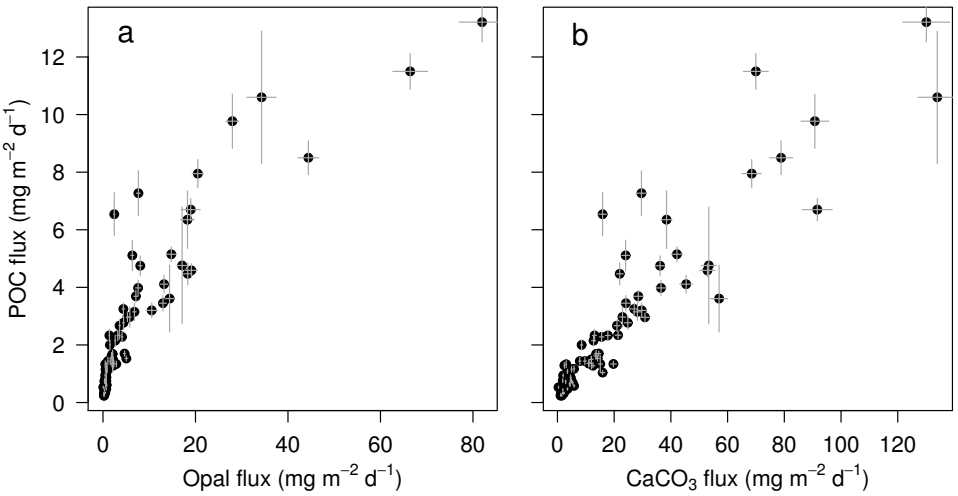

Figure 5.8 – Scatter plots of POC flux *versus* (a) opal flux; and (b) $CaCO_3$ flux. Grey lines indicate one standard deviation.

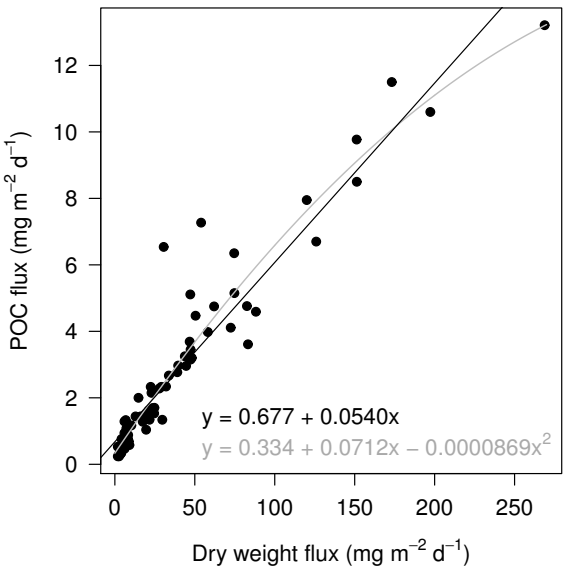

Figure 5.9 – Plot of POC flux against total mass flux. The straight black line shows the linear regression model (equation in black text), the grey line shows the quadratic regression model (equation in grey text), which fit the data significantly better (see Section 5.3.1).

Table 5.1 – Chemical fluxes in the bottom-tethered traps, in $\mathrm{mg\,m^{-2}\,d^{-1}}$ of the corresponding element. All ratios are molar ratios.

Trap-cup	Open date	Mass flux	POC flux	PON flux	POC:PON	$CaCO_3$ flux	PIC flux	PIC:POC	Opal flux	Si:POC
NW-1	22 Nov 06	43.8 ± 2.2	3.25 ± 0.21	0.474 ± 0.035	8.02 ± 0.10	27.1 ± 1.40	3.25 ± 0.17	1.00 ± 0.08	4.40 ± 0.29	0.246 ± 0.023
NW-2	06 Dec 06	47.4 ± 2.4	3.15 ± 0.30	0.457 ± 0.046	8.07 ± 0.20	28.2 ± 1.48	3.38 ± 0.18	1.07 ± 0.12	6.79 ± 0.39	0.390 ± 0.043
NW-3	20 Dec 06	47.2 ± 2.4	5.11 ± 0.53	0.922 ± 0.094	6.47 ± 0.04	24.1 ± 1.36	2.88 ± 0.16	0.56 ± 0.07	6.34 ± 0.33	0.225 ± 0.026
NW-4	03 Jan 07	39.6 ± 2.0	2.97 ± 0.35	0.428 ± 0.067	8.12 ± 0.32	22.9 ± 1.17	2.75 ± 0.14	0.93 ± 0.12	5.80 ± 0.31	0.355 ± 0.046
NW-5	17 Jan 07	10.3 ± 0.5	1.17 ± 0.11	0.202 ± 0.020	6.76 ± 0.15	5.84 ± 0.31	0.700 ± 0.037	0.60 ± 0.06	0.901 ± 0.051	0.139 ± 0.015
NW-6	31 Jan 07	18.6 ± 0.9	1.36 ± 0.12	0.188 ± 0.019	8.48 ± 0.19	11.1 ± 0.58	1.33 ± 0.07	0.97 ± 0.10	2.35 ± 0.17	0.312 ± 0.036
NW-7	14 Feb 07	7.60 ± 0.4	0.61 ± 0.06	0.092 ± 0.009	7.74 ± 0.17	4.38 ± 0.23	0.526 ± 0.028	0.86 ± 0.09	0.786 ± 0.049	0.234 ± 0.026
NW-8	28 Feb 07	4.04 ± 0.20	0.34 ± 0.03	0.051 ± 0.005	7.65 ± 0.17	2.31 ± 0.12	0.277 ± 0.015	0.82 ± 0.09	0.493 ± 0.031	0.266 ± 0.029
NW-9	14 Mar 07	6.13 ± 0.31	0.47 ± 0.04	0.069 ± 0.007	7.93 ± 0.17	3.55 ± 0.19	0.425 ± 0.022	0.91 ± 0.10	0.699 ± 0.044	0.273 ± 0.030
NW-10	28 Mar 07	27.8 ± 1.4	2.28 ± 0.17	0.364 ± 0.038	7.32 ± 0.27	15.6 ± 0.82	1.87 ± 0.10	0.82 ± 0.07	4.11 ± 0.24	0.327 ± 0.031
NW-11	11 Apr 07	1.85 ± 0.09	0.24 ± 0.02	0.032 ± 0.003	7.44 ± 0.22	1.09 ± 0.06	0.131 ± 0.007	0.56 ± 0.05	0.202 ± 0.013	0.156 ± 0.015
NW-12	25 Apr 07	5.97 ± 0.30	0.94 ± 0.06	0.168 ± 0.012	5.58 ± 0.17	2.01 ± 0.11	0.241 ± 0.013	0.26 ± 0.02	0.465 ± 0.029	0.090 ± 0.008
NW-13	09 May 07	48.1 ± 2.4	3.20 ± 0.25	0.452 ± 0.035	7.08 ± 0.21	29.7 ± 1.65	3.56 ± 0.20	1.11 ± 0.11	10.5 ± 1.2	0.598 ± 0.083
NW-14	23 May 07	126 ± 6	6.70 ± 0.39	1.05 ± 0.063	7.48 ± 0.09	91.6 ± 5.27	11.0 ± 0.6	1.64 ± 0.13	19.0 ± 2.1	0.515 ± 0.063
NW-15	06 Jun 07	19.6 ± 1.0	1.04 ± 0.07	0.155 ± 0.011	7.84 ± 0.03	15.9 ± 0.84	1.91 ± 0.10	1.83 ± 0.16	0.723 ± 0.055	0.126 ± 0.013
NW-16	20 Jun 07	24.7 ± 1.2	1.70 ± 0.09	0.277 ± 0.014	7.13 ± 0.09	14.6 ± 0.73	1.75 ± 0.09	1.03 ± 0.07	4.66 ± 0.24	0.499 ± 0.036
NW-17	04 Jul 07	74.6 ± 3.7	6.35 ± 1.00	1.06 ± 0.176	6.97 ± 0.22	38.5 ± 1.95	4.61 ± 0.23	0.73 ± 0.12	18.3 ± 1.5	0.523 ± 0.093
NW-18	18 Jul 07	151 ± 7.6	9.77 ± 0.94	1.57 ± 0.157	7.24 ± 0.13	90.8 ± 4.92	10.9 ± 0.6	1.11 ± 0.12	28.0 ± 1.4	0.520 ± 0.057
C-1	22 Nov 06	58.1 ± 2.9	3.98 ± 0.27	0.606 ± 0.052	7.67 ± 0.20	36.5 ± 1.83	4.38 ± 0.22	1.10 ± 0.09	7.59 ± 0.60	0.346 ± 0.036

Trap-cup	Open date	Mass flux	POC flux	PON flux	POC:PON	$CaCO_3$ flux	PIC flux	PIC:POC	Opal flux	Si:POC
C-2	06 Dec 06	39.1 ± 2	2.77 ± 0.23	0.468 ± 0.046	6.92 ± 0.16	24.8 ± 1.25	2.98 ± 0.15	1.07 ± 0.10	4.44 ± 0.22	0.291 ± 0.028
C-3	20 Dec 06	30.5 ± 1.5	6.54 ± 0.75	1.26 ± 0.151	6.07 ± 0.07	15.9 ± 1.34	1.91 ± 0.16	0.29 ± 0.04	2.44 ± 0.15	0.068 ± 0.009
C-4	03 Jan 07	29.1 ± 1.5	2.33 ± 0.18	0.396 ± 0.028	6.86 ± 0.08	17.8 ± 0.89	2.13 ± 0.11	0.92 ± 0.09	3.19 ± 0.16	0.249 ± 0.023
C-5	17 Jan 07	19.5 ± 1.0	1.50 ± 0.11	0.227 ± 0.017	7.70 ± 0.04	11.9 ± 0.63	1.43 ± 0.08	0.96 ± 0.09	2.16 ± 0.11	0.261 ± 0.024
C-6	31 Jan 07	17.4 ± 0.9	1.28 ± 0.07	0.194 ± 0.011	7.69 ± 0.15	12.5 ± 0.66	1.50 ± 0.08	1.18 ± 0.09	2.20 ± 0.13	0.312 ± 0.025
C-7	14 Feb 07	19.7 ± 1.0	1.37 ± 0.20	0.235 ± 0.034	6.81 ± 0.21	12.0 ± 0.63	1.44 ± 0.08	1.05 ± 0.16	2.19 ± 0.16	0.290 ± 0.048
C-8	28 Feb 07	14.8 ± 0.7	2.00 ± 0.18	0.353 ± 0.035	6.63 ± 0.14	8.52 ± 0.45	1.02 ± 0.05	0.51 ± 0.05	1.50 ± 0.08	0.136 ± 0.014
C-9	14 Mar 07	8.33 ± 0.42	0.88 ± 0.08	0.162 ± 0.016	6.32 ± 0.14	4.65 ± 0.25	0.557 ± 0.029	0.64 ± 0.07	0.729 ± 0.046	0.151 ± 0.017
C-10	28 Mar 07	3.59 ± 0.18	0.31 ± 0.03	0.055 ± 0.006	6.50 ± 0.14	2.16 ± 0.11	0.259 ± 0.014	0.84 ± 0.09	0.275 ± 0.017	0.162 ± 0.018
C-11	11 Apr 07	2.63 ± 0.13	0.24 ± 0.02	0.029 ± 0.003	9.70 ± 0.29	1.55 ± 0.08	0.186 ± 0.010	0.79 ± 0.07	0.260 ± 0.016	0.199 ± 0.020
C-12	25 Apr 07	7.18 ± 0.36	1.08 ± 0.07	0.176 ± 0.015	7.16 ± 0.21	3.54 ± 0.19	0.424 ± 0.022	0.39 ± 0.03	0.817 ± 0.051	0.137 ± 0.013
C-13	09 May 07	50.5 ± 2.5	4.47 ± 0.38	0.565 ± 0.115	9.23 ± 0.28	22.0 ± 1.25	2.63 ± 0.15	0.59 ± 0.06	18.3 ± 0.9	0.744 ± 0.074
C-14	23 May 07	197 ± 10	10.6 ± 2.3	1.56 ± 0.410	8.00 ± 0.43	134 ± 6.81	16.1 ± 0.8	1.51 ± 0.34	34.3 ± 3.2	0.587 ± 0.138
C-15	06 Jun 07	83.3 ± 4.2	3.61 ± 1.16	0.505 ± 0.165	8.34 ± 0.08	57.0 ± 3.07	6.83 ± 0.37	1.90 ± 0.62	14.4 ± 0.9	0.725 ± 0.237
C-16	20 Jun 07	82.6 ± 4.1	4.76 ± 2.03	0.678 ± 0.280	8.16 ± 0.10	53.4 ± 2.70	6.40 ± 0.32	1.35 ± 0.58	17.1 ± 1.1	0.653 ± 0.281
C-17	04 Jul 07	21.7 ± 1.1	1.34 ± 0.29	0.189 ± 0.042	8.27 ± 0.16	15.1 ± 0.76	1.81 ± 0.09	1.36 ± 0.30	2.08 ± 0.11	0.282 ± 0.063
C-18	18 Jul 07	46.8 ± 2.3	3.69 ± 0.21	0.519 ± 0.030	8.30 ± 0.16	28.5 ± 1.69	3.42 ± 0.20	0.93 ± 0.08	7.11 ± 0.46	0.350 ± 0.030
NE-1	22 Nov 06	62.1 ± 3.1	4.75 ± 0.34	0.676 ± 0.057	8.20 ± 0.29	36.2 ± 1.85	4.34 ± 0.22	0.91 ± 0.08	8.06 ± 0.42	0.308 ± 0.027
NE-2	06 Dec 06	33.8 ± 1.7	2.67 ± 0.20	0.361 ± 0.037	8.67 ± 0.27	21.0 ± 1.05	2.52 ± 0.13	0.94 ± 0.09	3.58 ± 0.18	0.243 ± 0.022
NE-3	20 Dec 06	7.89 ± 0.39	0.78 ± 0.07	0.100 ± 0.010	9.17 ± 0.20	4.67 ± 0.25	0.560 ± 0.030	0.71 ± 0.07	0.602 ± 0.036	0.139 ± 0.015
NE-4	03 Jan 07	21.1 ± 1.1	1.62 ± 0.12	0.217 ± 0.019	8.71 ± 0.13	13.5 ± 0.71	1.62 ± 0.09	1.00 ± 0.09	1.85 ± 0.10	0.207 ± 0.019
NE-5	17 Jan 07	5.51 ± 0.28	0.72 ± 0.06	0.103 ± 0.010	8.17 ± 0.18	2.89 ± 0.15	0.347 ± 0.018	0.48 ± 0.05	0.326 ± 0.019	0.082 ± 0.009

Trap-cup	Open date	Mass flux	POC flux	PON flux	POC:PON	$CaCO_3$ flux	PIC flux	PIC:POC	Opal flux	Si:POC
NE-6	31 Jan 07	8.87 ± 0.44	1.15 ± 0.10	0.166 ± 0.017	8.06 ± 0.18	4.97 ± 0.26	0.596 ± 0.031	0.52 ± 0.05	0.540 ± 0.032	0.085 ± 0.009
NE-7	14 Feb 07	22.4 ± 1.1	2.33 ± 0.21	0.372 ± 0.037	7.32 ± 0.16	13.1 ± 0.69	1.57 ± 0.08	0.67 ± 0.07	1.38 ± 0.08	0.108 ± 0.012
NE-8	28 Feb 07	18.7 ± 0.9	1.36 ± 0.12	0.189 ± 0.019	8.39 ± 0.18	11.1 ± 0.58	1.33 ± 0.07	0.98 ± 0.10	1.92 ± 0.25	0.257 ± 0.040
NE-9	14 Mar 07	8.71 ± 0.44	0.69 ± 0.06	0.095 ± 0.010	8.45 ± 0.18	5.38 ± 0.28	0.645 ± 0.034	0.93 ± 0.10	0.646 ± 0.038	0.170 ± 0.018
NE-10	28 Mar 07	9.10 ± 0.45	0.58 ± 0.05	0.090 ± 0.009	7.54 ± 0.16	5.87 ± 0.31	0.703 ± 0.037	1.21 ± 0.13	0.578 ± 0.034	0.181 ± 0.019
NE-11	11 Apr 07	29.7 ± 1.5	1.34 ± 0.10	0.176 ± 0.018	8.88 ± 0.27	19.7 ± 1.04	2.37 ± 0.12	1.77 ± 0.17	2.87 ± 0.15	0.389 ± 0.036
NE-12	25 Apr 07	23.5 ± 1.2	1.69 ± 0.13	0.268 ± 0.021	7.36 ± 0.22	13.7 ± 0.72	1.64 ± 0.09	0.97 ± 0.09	2.09 ± 0.11	0.224 ± 0.021
NE-13	09 May 07	173 ± 9	11.5 ± 0.6	1.69 ± 0.089	7.94 ± 0.24	70.0 ± 4.38	8.39 ± 0.52	0.73 ± 0.06	66.4 ± 3.8	1.05 ± 0.08
NE-14	23 May 07	269 ± 13	13.2 ± 0.7	1.86 ± 0.094	8.27 ± 0.11	130 ± 8.30	15.6 ± 1.0	1.18 ± 0.10	82.0 ± 4.9	1.13 ± 0.09
NE-15	06 Jun 07	72.5 ± 3.6	4.11 ± 0.31	0.613 ± 0.061	7.83 ± 0.23	45.4 ± 2.29	5.44 ± 0.27	1.32 ± 0.12	13.2 ± 0.8	0.583 ± 0.057
NE-16	20 Jun 07	44.6 ± 2.2	2.96 ± 0.15	0.410 ± 0.021	8.40 ± 0.07	30.9 ± 1.57	3.70 ± 0.19	1.25 ± 0.09	5.28 ± 0.27	0.324 ± 0.023
NE-17	04 Jul 07	32.0 ± 1.6	2.34 ± 0.14	0.307 ± 0.017	8.91 ± 0.10	21.4 ± 1.07	2.56 ± 0.13	1.09 ± 0.08	3.53 ± 0.22	0.273 ± 0.023
NE-18	18 Jul 07	120 ± 6	7.95 ± 0.49	1.08 ± 0.078	8.59 ± 0.18	68.5 ± 3.43	8.21 ± 0.41	1.03 ± 0.08	20.5 ± 1.2	0.468 ± 0.040
S-1	22 Nov 06	12.9 ± 0.7	1.44 ± 0.13	0.237 ± 0.024	7.06 ± 0.15	7.89 ± 0.42	0.946 ± 0.050	0.66 ± 0.07	1.05 ± 0.06	0.133 ± 0.014
S-2	06 Dec 06	22.9 ± 1.2	2.15 ± 0.19	0.328 ± 0.033	7.66 ± 0.17	12.7 ± 0.73	1.53 ± 0.09	0.71 ± 0.08	2.64 ± 0.14	0.223 ± 0.023
S-3	20 Dec 06	16.1 ± 0.8	1.44 ± 0.13	0.218 ± 0.022	7.70 ± 0.17	9.68 ± 0.51	1.16 ± 0.06	0.81 ± 0.08	1.56 ± 0.09	0.196 ± 0.021
S-4	03 Jan 07	6.81 ± 0.34	1.33 ± 0.12	0.220 ± 0.022	7.05 ± 0.15	3.10 ± 0.16	0.371 ± 0.020	0.28 ± 0.03	0.483 ± 0.029	0.066 ± 0.007
S-5	17 Jan 07	3.50 ± 0.17	0.44 ± 0.04	0.075 ± 0.008	6.84 ± 0.15	1.89 ± 0.10	0.226 ± 0.012	0.51 ± 0.05	0.304 ± 0.018	0.125 ± 0.013
S-6	31 Jan 07	2.51 ± 0.13	0.29 ± 0.03	0.047 ± 0.005	7.29 ± 0.16	1.19 ± 0.06	0.143 ± 0.008	0.49 ± 0.05	0.221 ± 0.013	0.136 ± 0.015
S-7	14 Feb 07	8.16 ± 0.41	0.75 ± 0.07	0.119 ± 0.012	7.35 ± 0.16	4.93 ± 0.26	0.591 ± 0.031	0.78 ± 0.08	0.719 ± 0.042	0.173 ± 0.019
S-8	28 Feb 07	7.34 ± 0.37	0.66 ± 0.06	0.098 ± 0.010	7.82 ± 0.17	4.37 ± 0.23	0.524 ± 0.028	0.80 ± 0.08	0.660 ± 0.039	0.183 ± 0.020
S-9	14 Mar 07	4.16 ± 0.21	0.76 ± 0.07	0.122 ± 0.012	7.31 ± 0.16	1.88 ± 0.10	0.225 ± 0.012	0.29 ± 0.03	0.335 ± 0.020	0.080 ± 0.009

Trap-cup	Open date	Mass flux	POC flux	PON flux	POC:PON	$CaCO_3$ flux	PIC flux	PIC:POC	Opal flux	Si:POC
S-10	28 Mar 07	3.15 ± 0.16	0.33 ± 0.03	0.052 ± 0.005	7.38 ± 0.16	1.79 ± 0.09	0.215 ± 0.011	0.65 ± 0.07	0.234 ± 0.014	0.128 ± 0.014
S-11	11 Apr 07	1.85 ± 0.09	0.53 ± 0.04	0.090 ± 0.009	6.88 ± 0.21	0.37 ± 0.02	0.044 ± 0.002	0.08 ± 0.01	0.064 ± 0.004	0.022 ± 0.002
S-12	25 Apr 07	5.99 ± 0.30	1.29 ± 0.10	0.217 ± 0.022	6.94 ± 0.21	2.43 ± 0.13	0.292 ± 0.015	0.23 ± 0.02	0.729 ± 0.043	0.103 ± 0.010
S-13	09 May 07	47.4 ± 2.4	3.45 ± 0.27	0.451 ± 0.036	8.92 ± 0.27	24.1 ± 1.71	2.89 ± 0.21	0.84 ± 0.09	13.0 ± 0.8	0.683 ± 0.067
S-14	23 May 07	151 ± 8	8.50 ± 0.59	1.26 ± 0.105	7.91 ± 0.17	78.9 ± 4.15	9.46 ± 0.50	1.11 ± 0.10	44.4 ± 2.3	0.949 ± 0.082
S-15	06 Jun 07	88.2 ± 4.4	4.59 ± 0.23	0.704 ± 0.038	7.61 ± 0.11	52.9 ± 2.69	6.34 ± 0.32	1.38 ± 0.10	19.1 ± 1.3	0.755 ± 0.064
S-16	20 Jun 07	24.6 ± 1.2	1.53 ± 0.09	0.223 ± 0.020	8.04 ± 0.37	14.2 ± 0.71	1.70 ± 0.09	1.11 ± 0.09	5.04 ± 0.32	0.598 ± 0.052
S-17	04 Jul 07	74.7 ± 3.7	5.15 ± 0.26	0.699 ± 0.035	8.60 ± 0.05	42.1 ± 2.12	5.05 ± 0.25	0.98 ± 0.07	14.8 ± 1.1	0.521 ± 0.047
S-18	18 Jul 07	53.9 ± 2.7	7.27 ± 0.78	1.11 ± 0.167	7.71 ± 0.36	29.6 ± 1.54	3.55 ± 0.18	0.49 ± 0.06	7.65 ± 0.41	0.191 ± 0.023

5.3.2 Flux of ^{230}Th

The time-series of ^{230}Th flux into each trap is shown in Figure 5.10; note that samples were combined into three composite samples for each trap, so the temporal resolution in Figure 5.10 differs from the preceding figures. During the first period (December to May), the flux into Traps NW, NE, and C was indistinguishable (1.4–1.5 $\mathrm{pg\,m^{-2}\,d^{-1}}$), but flux into Trap S was much lower at 0.5 $\mathrm{pg\,m^{-2}\,d^{-1}}$. During May to July, each trap caught a different flux, ranging from 0.47–1.35 $\mathrm{pg\,m^{-2}\,d^{-1}}$, with values either lower than in the preceding period (NW and C), ∼unchanged (NE), or higher (S). Fluxes during the final period were less variable, with similar values in Traps S, NE, and C (0.64–0.75 $\mathrm{pg\,m^{-2}\,d^{-1}}$), but a higher flux in Trap NW (1.1 $\mathrm{pg\,m^{-2}\,d^{-1}}$).

However, the content of ^{230}Th per unit dry weight varied much less between traps (Figure 5.11). During the first period, Traps NW, NE, and C had indistinguishable ^{230}Th contents (67.4–68.7 $\mathrm{fg\,mg^{-1}}$), though Trap S had slightly less (60.8 $\mathrm{fg\,mg^{-1}}$). ^{230}Th content then dropped sharply in all traps (7.26–7.96 $\mathrm{fg\,mg^{-1}}$ in NW, NE, and C, but 12.5 $\mathrm{fg\,mg^{-1}}$ in S), and rose again slightly in the final period (12.6–14.0 $\mathrm{fg\,mg^{-1}}$).

The ^{230}Th fluxes are shown in Table 5.2 together with the average fluxes of total mass, POC, $CaCO_3$, and opal for each of the three periods covered by the combined samples. Also shown are the total cumulative fluxes over the entire eight months for each trap.

There were significant Spearman's rank correlations between the specific content of ^{230}Th and the specific content of opal (inverse correlation, $\rho = -0.629$, $p = 0.033$, with $n = 12$), and the specific content of POC ($\rho = 0.839$, $p = 0.0012$, with $n = 12$). There was no significant correlation with $CaCO_3$ content ($\rho = -0.189$, $p = 0.558$, $n = 12$). However, the correlation with POC content could be spurious, and caused by the mineral-rich (especially opal-rich) samples in late spring having low ^{230}Th and low POC contents while the ^{230}Th-rich winter samples contained several spikes in POC content that raised the POC content of the pooled winter samples as a whole — rather than because of a genuine link between POC content and ^{230}Th content.

Overall, the relationship between ^{230}Th flux and dry weight flux was not very good due to the high ^{230}Th fluxes in Traps NW, NE, and C during the winter period (Figure 5.12). Disregarding these three points, a linear regression model was significant with ^{230}Th flux = $0.00573 * \text{mass flux} + 0.396$, $R^2 = 0.696\, p = 0.0052$ (^{230}Th and mass fluxes in units of pg and $\mathrm{mg\,m^{-2}\,d^{-1}}$, respectively).

5.3.3 Cumulative particle and ^{230}Th fluxes

Cumulative fluxes of ^{230}Th and of total dry weight were calculated over the entire deployment period of the traps (November to August) by summing the individual daily fluxes in each sample multiplied by the 14 d of collection (Figure 5.13; Table 5.2). Cumulative mass flux differed between all traps, with differences exceeding two times the standard deviation estimated for each flux, and ranged from 7.5–13 $\mathrm{g\,m^{-2}}$ (Figure 5.13a). In contrast, the cumulative ^{230}Th flux was indistinguishable for NW, C, and NE (range: 299–324 $\mathrm{pg\,m^{-2}}$), but significantly lower for Trap S (159 $\mathrm{pg\,m^{-2}}$; Figure 5.13b). Thus, while the cumulative dry weight flux into Traps C

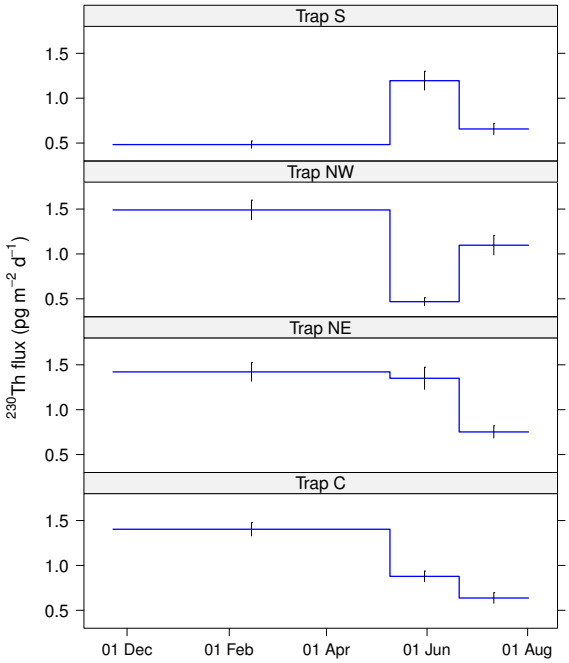

Figure 5.10 – Time-series of ^{230}Th into the four traps. Note that samples were pooled into three composite samples for each trap.

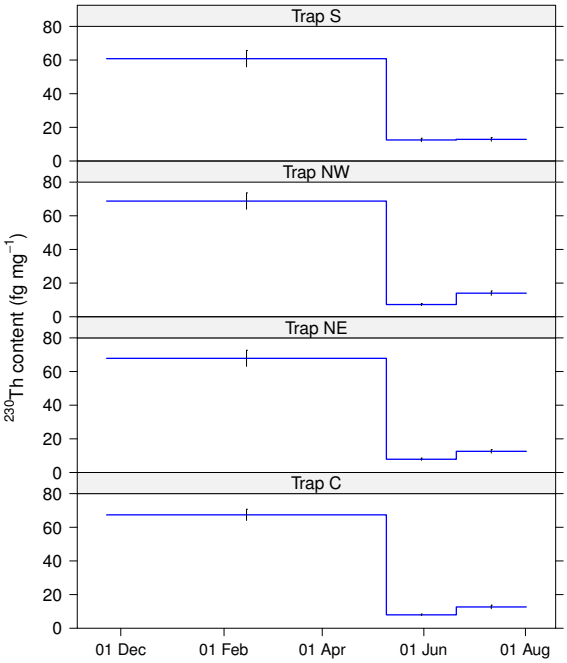

Figure 5.11 – Time-series of specific ^{230}Th content in the four traps.

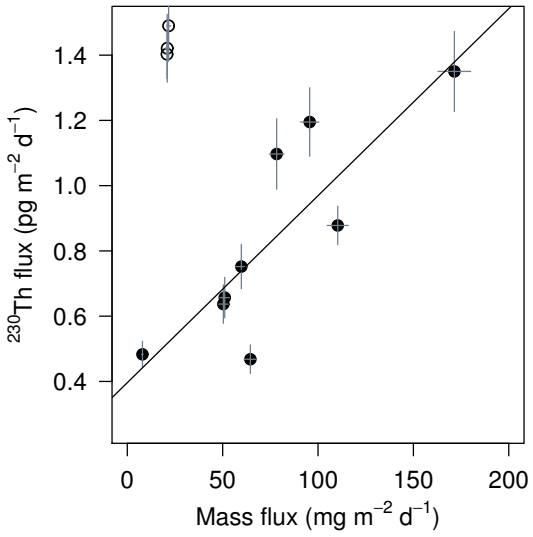

Figure 5.12 – Plot of daily ^{230}Th flux against daily mass flux for all four traps. The solid black line is the regression line calculated without the three outlying points shown with unfilled circles, which are data from the winter period in Traps NW, NE, and C (^{230}Th flux = 0.00573∗mass flux+ 0.396, $R^2 = 0.696\, p = 0.0052$).

Trap / Period	Dates	^{230}Th flux	Mass flux	POC flux	$CaCO_3$ flux	Opal flux
42 / Winter	22 Nov – 09 May	1.49 ± 0.11	21.7 ± 1.1	1.82 ± 0.06	12.3 ± 0.2	2.76 ± 0.06
42 / Spring	09 May – 20 Jun	0.47 ± 0.04	64.5 ± 3.2	3.65 ± 0.15	45.8 ± 1.9	8.76 ± 0.74
42 / Summer	20 Jun – 29 Jul *	1.10 ± 0.11	78.3 ± 3.9	5.64 ± 0.45	44.6 ± 1.6	16.1 ± 0.7
42	total cumulative	313 ± 19	9406 ± 212	680 ± 35	5736 ± 181	1460 ± 68
43 / Winter	22 Nov – 09 May	1.40 ± 0.07	20.8 ± 1.0	2.02 ± 0.08	12.7 ± 0.3	2.28 ± 0.06
43 / Spring	09 May – 20 Jun	0.88 ± 0.06	110 ± 5.5	6.23 ± 0.87	71.0 ± 2.5	20.0 ± 1.1
43 / Summer	20 Jun – 01 Aug	0.64 ± 0.06	50.4 ± 2.5	3.26 ± 0.69	32.3 ± 1.1	8.77 ± 0.39
43	total cumulative	299 ± 13	10246 ± 180	738 ± 78	6465 ± 194	1593 ± 73
44 / Winter	22 Nov – 09 May	1.42 ± 0.10	20.9 ± 1.0	1.64 ± 0.04	12.7 ± 0.2	2.04 ± 0.05
44 / Spring	09 May – 20 Jun	1.35 ± 0.12	172 ± 9	9.61 ± 0.33	81.8 ± 3.2	53.9 ± 2.1
44 / Summer	20 Jun – 28 Jul *	0.75 ± 0.07	59.8 ± 3.0	4.05 ± 0.15	37.3 ± 1.1	8.64 ± 0.35
44	total cumulative	324 ± 18	12994 ± 301	833 ± 27	6981 ± 218	2933 ± 109
45 / Winter	22 Nov – 09 May	0.48 ± 0.04	7.95 ± 0.40	0.951 ± 0.028	4.35 ± 0.09	0.750 ± 0.016
45 / Spring	09 May – 20 Jun	1.20 ± 0.10	95.6 ± 4.8	5.51 ± 0.23	52.0 ± 1.7	25.5 ± 0.9
45 / Summer	20 Jun – 01 Aug	0.657 ± 0.062	51.1 ± 2.6	4.65 ± 0.28	28.6 ± 0.9	9.16 ± 0.40
45	total cumulative	159 ± 8	7498 ± 146	587 ± 26	4117 ± 126	1581 ± 58

* These traps were recovered a few days early

Table 5.2 – Fluxes of ^{230}Th into each trap, and average fluxes of mass, POC, $CaCO_3$, and opal for the period covered by each combined sample. Total cumulative fluxes over the eight months are given as well. Units are $\mathrm{mg\,m^{-2}\,d^{-1}}$ for the combined samples (pg for ^{230}Th), and $\mathrm{mg\,(pg)^{-2}}$ for the total cumulative fluxes.

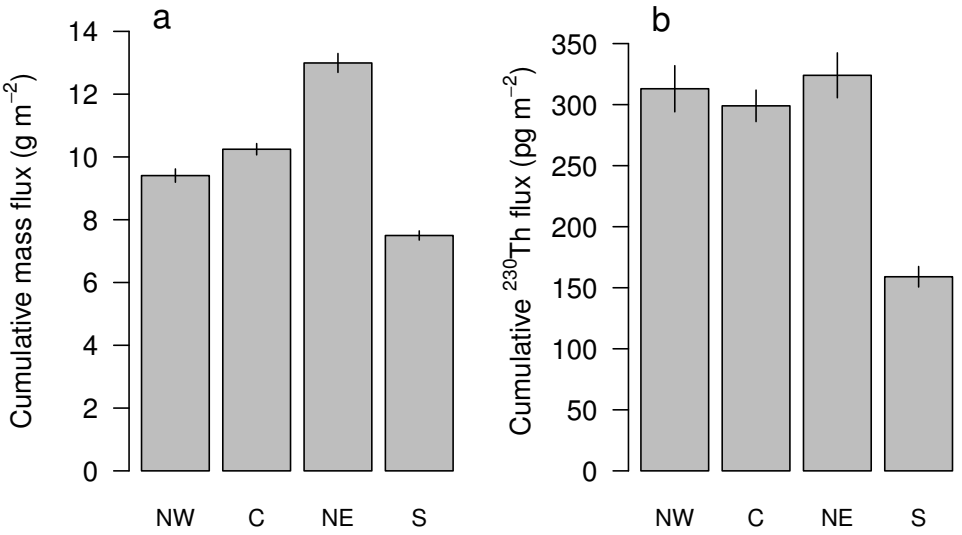

Figure 5.13 – Cumulative fluxes of (a) total dry weight, and (b) ^{230}Th, over the entire deployment period (November–August) into each of the traps. Error bars indicate one standard deviation.

and NW was only 79% and 72%, respectively, of that into Trap NE, there was no difference in cumulative ^{230}Th flux between these three traps.

5.3.4 Current speeds at trap depth

The time-series of current speed are shown in Figure 5.14, which also has time-series of total dry weight flux superimposed. Current speeds were relatively high: maximum speeds reached 35–37 cm s^{-1}, and both mean and median speeds on all moorings fell between 8–11 cm s^{-1}. There was a clear 12 h periodicity in the autocorrelation functions, indicating a tidal cycle. For each of the individual 14 d periods of sample collection, often more than 40% of current speed measurements were $\geq$12 cm s^{-1} (Figure 5.15). However, while the time-series in both figures clearly differ between traps (and current speed at each time-point was very poorly related between traps), there was little evident overall difference in the current regime experienced by the traps: overall mean, median, and maximum speeds were similar, and histograms of the distribution of current speeds were similar (Figure 5.16). In particular, there was little to distinguish Trap S from Trap NE, the two traps that differed most in particle flux, although Trap NE did have somewhat fewer current speeds exceeding 20 cm s^{-1} than the other traps.

5.4 Discussion

5.4.1 Were differences in flux due to variable trapping efficiency?

The ^{230}Th data indicate that Trap S under-collected by a factor of around two relative to the other traps, evidently owing to the much lower ^{230}Th flux during winter. If that was indeed the case, then applying an overall correction for trapping efficiency would suggest that particle flux should have been $\sim$15 g m^{-2} in Trap S, higher than for any of the other traps. In

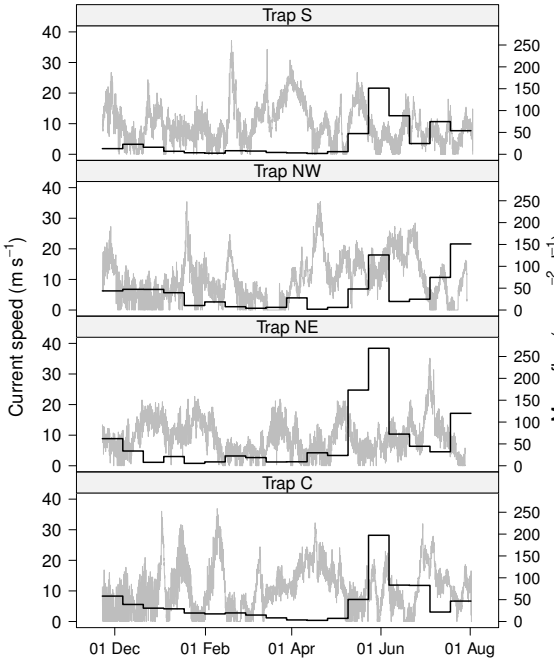

Figure 5.14 – Time-series of current speeds (grey lines) and total dry weight flux (black stepped lines) for each trap. The error on total dry weight fluxes was assumed to be 5% (see Appendix A.3), but error bars have been omitted for clarity.

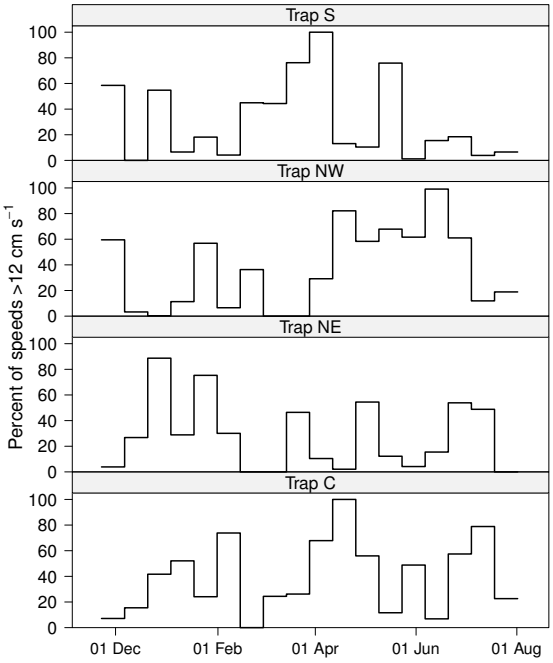

Figure 5.15 – Percentage of current speed measurements $\geq$12 cm s^{-1} for each 14 d sample collection period.

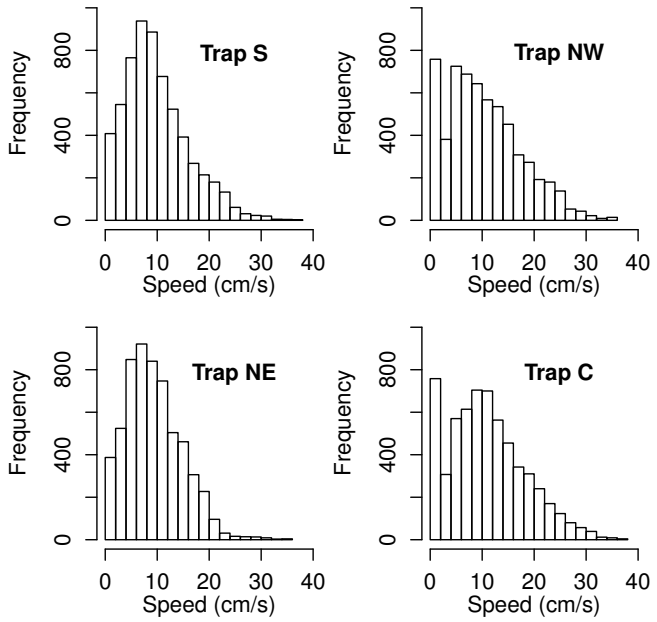

Figure 5.16 – Histograms of current speed for each of the four traps.

contrast, the differences in cumulative flux between Traps NW, C, and NE cannot be explained by differences in trapping efficiency, as they all caught equal ^{230}Th fluxes. It thus appears as though cumulative bathypelagic particle flux in the Iceland Basin shows genuine spatial variability by ∼30%. The variability between traps in cumulative POC flux is somewhat lower than for cumulative dry weight flux (Table 5.2), but Traps NW and C still caught only 89% and 82% of the POC flux in Trap NE, suggesting genuine spatial variability in POC flux by ∼20%.

It is important to note that this conclusion would not hold if the flux of ^{230}Th also shows genuine mesoscale variability. It is assumed here that this is not the case, *i.e.* that it is a constant flux tracer (as is done in other sediment trap "calibration" studies). Unfortunately, this assumption cannot be tested properly, and in principle, the fact that ^{230}Th flux shows a relationship to particle flux would suggest that mesoscale differences in particle flux should lead to mesoscale differences in ^{230}Th flux. However, there is appreciable scatter around the ^{230}Th *versus* mass flux relationship, and the fact that annual ^{230}Th flux to the sediment is close to annual ^{230}Th production in most areas of the oceans (*Henderson et al.* 1999) implies that ^{230}Th flux can be independent of total mass flux.

While spatial variability in particle flux in the upper mesopelagic has received increasing attention of late, especially regarding the effect of mesoscale physical structures on shallow particle export (*McGillicuddy et al.* 1998; *Buesseler et al.* 2008; *Maiti et al.* 2008; *Verdeny et al.* 2008), less is known about the spatial variability in bathypelagic flux. Mesoscale eddies in the subtropical Atlantic and Pacific have been shown to enhance export of opal several-fold locally, though not necessarily of POC, based on profiles of ^{234}Th, and of ^{210}Pb and ^{210}Po (*Buesseler et al.* 2008; *Maiti et al.* 2008; *Verdeny et al.* 2008), and work with sediment traps has shown that fronts can substantially enhance particle export (*Peinert and Miquel* 1994). *Sanders et al.* (2010) presented ^{234}Th data from a 125×125 km grid directly above the sediment traps analysed here, which indicate around five-fold spatial variability in POC, $CaCO_3$, and opal export during August 2007 (although these measurements are too late in the year to directly compare the magnitude of particle export to flux in the deep traps). *Guidi et al.* (2007) found that the concentration of large particles (>110 µm) can vary several-fold down to 500 m across distances of ∼100 km in the north-east Atlantic (between 39 and 45°N), implying differences in flux. However, sediment traps at 1000 m during the same study found that ^{230}Th-normalised annual dry weight flux varied by no more than 20% between sediment traps 440 km apart (*Guieu et al.* 2005; disregarding their north-western trap, for which no summer data were available). In contrast, *Newton et al.* (1994) concluded that significant mesoscale variability in bathypelagic flux exists, since a major peak in flux in their sediment trap at 48°N 19.5°W was not recorded by *Honjo and Manganini* (1993) in a trap ∼100 km away.

The studies showing high mesoscale variability in shallow export were all conducted over time-scales of around one month. Over individual 14 d collection periods, the traps analysed here also showed several-fold variability, and it is only because this short-term variability is, unsurprisingly, not consistent between traps throughout the entire deployment period that the variability in overall cumulative flux is only ∼30%. It is unclear how much of this short-term

variability is genuine, but to yield a genuine difference in cumulative flux, some portion of it must be real.

Particles caught in bathypelagic sediment traps are known to potentially originate from across a large area of the surface waters surrounding the trap (termed the statistical funnel, *Siegel et al.* 1990; *Siegel and Deuser* 1997), which is likely to be a radius of several hundred kilometres for a trap at 2000 m (*Siegel and Armstrong* 2002). The statistical funnels of the four traps here would almost certainly have overlapped substantially — but overlapping statistical funnels do not mean that traps are sampling from a homogenised particle pool. Rather, particles of any one sinking speed at any one collection time will have originated from a very specific, small, area of the surface (*Waniek et al.* 2000). Although this source area may be distant from the trap, it is unlikely to overlap with the source area for similar particles at the same time-point in a second trap 100 km away. The large statistical funnel comes about by averaging the descent trajectories of thousands of particles over time-scales of thousands of days, exposing them to a variable current regime over that period (*Siegel and Deuser* 1997), but mesoscale variability in flux should at least partly be maintained, at least for relatively fast-sinking particles (the concentration of suspended particles would probably be more homogenous due to their longer residence time, and depending on the re-aggregation mechanisms at work, downward flux out of this pool at bathypelagic depths might be more uniform).

5.4.2 Flux *versus* annual production of ^{230}Th

Interestingly, the ^{230}Th flux in all traps was much lower than the annual production of ^{230}Th in the overlying 2000 m of water column, which is 1100 $\mathrm{pg\,m^{-2}\,y^{-1}}$ (based on production of 0.0252 $\mathrm{dpm\,m^{-3}\,y^{-1}}$; *Henderson and Anderson* 2003; *Yu et al.* 2001). Partly, this is because the traps did not collect for the full annual cycle, and a significant portion of the annual flux may have been missed (August–November). Moreover, although much of the ^{230}Th that is produced in the north-east Atlantic appears to sink to the seafloor locally (*Henderson et al.* 1999), the water column ^{230}Th profiles in the North Atlantic demonstrate that some ^{230}Th is advected southward, instead of scavenged locally (*Moran et al.* 1997; *Vogler et al.* 1998). The flux to sediment traps would thus probably be a little lower than the annual production.

The traps collected for a total of 250 d, and over this period collected ∼28% of the annual ^{230}Th production (15% for Trap S). If they had collected a daily flux of equal magnitude to the flux during the winter period, *i.e.* around 1.45 $\mathrm{pg\,m^{-2}\,d^{-1}}$, for the remaining 115 d, the total annual flux for Traps NW, C, and NE would have been around 477 $\mathrm{pg\,m^{-2}}$, or 43% of the annual ^{230}Th production. This is likely to be a generous estimate, as the summer fluxes were considerably lower than 1.4 $\mathrm{pg\,m^{-2}\,d^{-1}}$, and may have remained lower than the winter fluxes for at least part of the remaining 115 d. Unfortunately, it is not possible to constrain the advection, although the results of *Henderson et al.* (1999) suggest that it is unlikely to be more than 10% of the annual production (see their figure 6). This would suggest that Traps NW, C, and NE had a trapping efficiency of only ∼50%, and only ∼30% for Trap S. This would imply an annual cumulative mass flux of closer to 30 $\mathrm{mg\,m^{-2}\,d^{-1}}$. However, it must be stressed

that this is a very rough estimate indeed, with large uncertainties on the ^{230}Th flux for the remaining 115 d and the ^{230}Th content of that material.

The cumulative dry weight flux in the present traps ($\sim$10 g m^{-2}) is similar to, or lower than, reported annual fluxes at sites further south or north. *Waniek et al.* (2005) reported annual dry weight flux at 2000 m of $\sim$10 g m^{-2} y^{-1} at Station L3 (54°N 20°W), and $\sim$22 g m^{-2} y^{-2} further south at Station L2 (47°N 20°W) (estimated from their figures 6 and 7). At the long-term PAP Observatory (49°N 16.5°W), mean annual dry weight flux over eight years was 24.6 g m^{-2} y^{-1} (range: 15.7–47 g m^{-2} y^{-1}; *Lampitt et al.* 2010). Based on a compilation of sediment trap studies, *Jickells et al.* (1996) reported a gradient of increasing particle flux with latitude between 25°N and 48°N in the north-east Atlantic, and *Waniek et al.* (2005) concluded that this gradient extends to 70°N based on sediment trap data by *Peinert et al.* (2001) and *von Bodungen et al.* (1990). One might therefore expect the annual flux in the region studied here to be higher than the 7–13 g m^{-2} found here, so the conclusion of under-trapping of the present traps is consistent with other sediment trap results in the north-east Atlantic. Moreover, a recent compilation and global model of sediment trap results by *Honjo et al.* (2008) even yielded annual POC flux at 2000 m in the North Atlantic Drift region of 6–12 g m^{-2} (shown in their figure 9), much greater than the $<$1 g m^{-2} found here.

5.4.3 Particle flux and current speeds

Laboratory and theoretical analyses have shown that trapping efficiency can be reduced by current speeds, and is also heavily affected by trap geometry (*Gardner* 1980a; *Butman et al.* 1986; *Gardner and Zhang* 1997). Field studies have confirmed these conclusions (*Gardner* 1980b; *Baker et al.* 1988), and the results of *Baker et al.* (1988) suggested that current speeds up to 12 cm s^{-1} did not bias the collection of a moored, cylindrical trap relative to drifting traps. High current speeds are hence considered to compromise samples, but there are clearly very complex interactions between trap geometry, current speed, and the nature (*e.g.* size, sinking rate, fragility) of the particles that together determine the trapping efficiency, and thus no clear relationships between current speed and trapping efficiency have emerged (*Buesseler et al.* 2007a). What appears to be important is not necessarily current speed *per se*, but rather the ratio of particle sinking speed to horizontal current speed, and the interaction of current speed with trap geometry (as trap Reynolds number; *Butman et al.* 1986; *Baker et al.* 1988; *Gustafsson et al.* 2004). While funnel-shaped traps may tend to under-collect (*Gardner* 1980a; *Butman et al.* 1986), the four traps used here had identical geometries and thus geometry should not have influenced the relative trapping efficiencies in the present case.

Guieu et al. (2005) found some evidence for a link between the current speed experienced by a trap and the trapping efficiency as measured by ^{230}Th. In the present case, no association was found between either the cumulative ^{230}Th or dry weight flux and either mean current speed or the percentage of current speed measurements that exceeded 12 cm s^{-1}, for each trap (Figure 5.17). Further, Spearman's rank correlations between dry weight flux in each sample and mean current speed or percentage of measurements exceeding 12 cm s^{-1} over the period

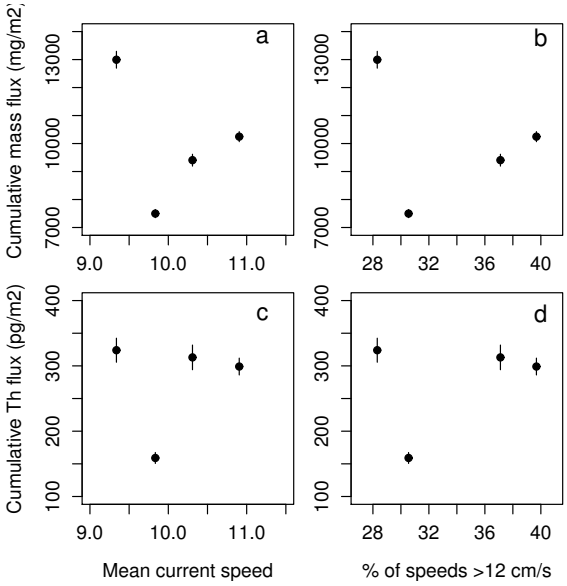

Figure 5.17 – Cumulative fluxes of dry weight (a,b) and of ^{230}Th (c,d) plotted against overall mean current speed for entire deployment period (a,c), and against the percentage of current speed measurements exceeding $12\,\mathrm{cm\,s^{-1}}$ (b,d).

of sample collection were significant, but weak (Figure 5.18, see figure caption for correlation parameters).

Such sample-by-sample comparisons of particle flux and current speed over an annual cycle suffer from the obvious bias that particle flux shows a pronounced annual cycle with many genuinely low values, while current speed (in this case) shows no such cycle. In Figure 5.18, there are hence many points with very low particle flux at both high and low currents. To overcome this problem, the total dry weight fluxes into each trap were ranked separately for each 14 d sample collection period from 1 (lowest flux) to 4 (highest flux). The differences in flux between the four traps were thus expressed on a common scale throughout the annual cycle, allowing a test of whether lower particle flux relative to the other traps during each period was associated with higher current speeds. This was indeed the case, both for mean current speed over each sample collection period and for percentage of current speed measurements above $12\,\mathrm{cm\,s^{-1}}$ (Figure 5.19, Spearman's rank correlations: $\rho = -0.376$, $p = 0.0011$ for mean speed; and $\rho = -0.365$, $p = 0.0016$ for percent of measurements exceeding $12\,\mathrm{cm\,s^{-1}}$; all $n = 72$). Figure 5.19 does not indicate a threshold speed above which samples might have been compromised, but a threshold would probably be difficult to detect using an approach such as this. Interestingly, the data from Trap S, which under-collected relative to the other traps based on the ^{230}Th data, indicate relatively modest current speeds compared to the other traps in Figure 5.19. Thus, while there was an overall significant inverse correlation between current speed and particle flux, the one trap which overall significantly under-collected did not appear to have suffered much from high current speeds.

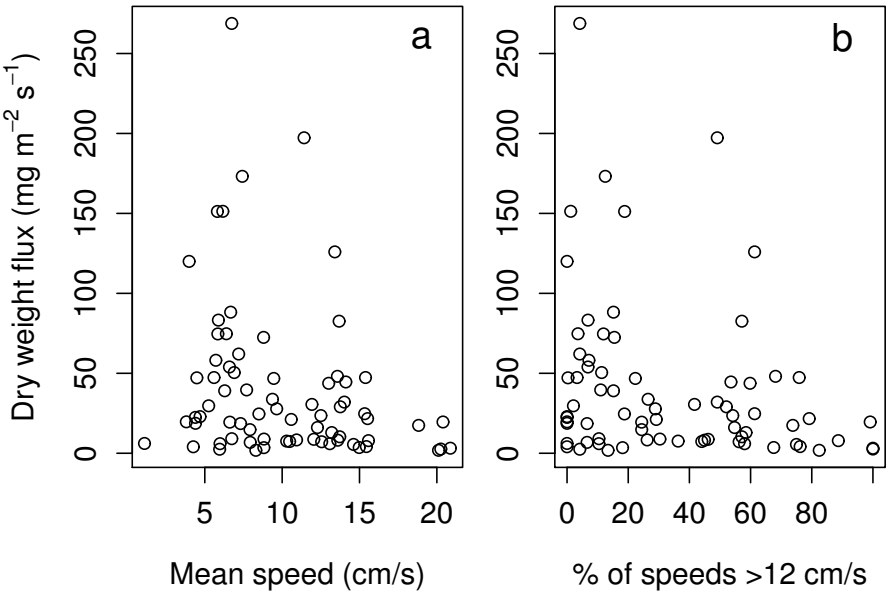

Figure 5.18 – Mass flux in each sample for all four traps plotted against (a) mean current speed over each 14 d sample collection period, and (b) percentage of current speed measurements over each collection period that exceeded 12 cm s^{-1}. Spearman's rank correlations were significant, but weak: for (a), $\rho = -0.300$, $p = 0.010$; for (b) $\rho = -0.278$, $p = 0.018$; all $n = 72$.

Overall then, the present data support a link between current speed and trapping efficiency, but suggest that current speed alone is not enough to explain the variable trapping efficiency diagnosed from the ^{230}Th fluxes.

5.4.4 Possible link to surface ocean properties

It was hypothesised in Chapter 4 that the low flux of Acantharia into Trap S might be linked to the higher spring-time SST over Trap S, and the overall north-south gradient in SST across the basin. It is certainly notable that Trap S also systematically under-collected in general relative to the other traps, which obviously need not be linked to surface ocean properties. However, since the only other obvious factor, current speed, appeared to play no major role in under-trapping, surface properties were investigated as well.

Figure 5.20 shows weekly composite maps of SST throughout the deployment period. The overall north-south gradient in SST was apparent throughout the year, and Trap S was usually below slightly warmer water than the other traps. Figure 5.21 makes this clearer, showing a time-series of mean SST in a $1^\circ \times 0.8^\circ$area above each trap ($\sim 100 \times 60$km). However, the differences are modest, and the gradient across the area is relatively smooth. While it is still possible that this gradient influences the distribution of Acantharia, the SST data do not indicate any particular features that might explain the differences between traps.

Next, SSH data were investigated. Mesoscale eddies show up as SSH anomalies, and weekly composite maps of SSH are shown in Figure 5.22. A possibility might have been that Trap S was persistently below eddies that did not influence the other traps, and thus experiencing

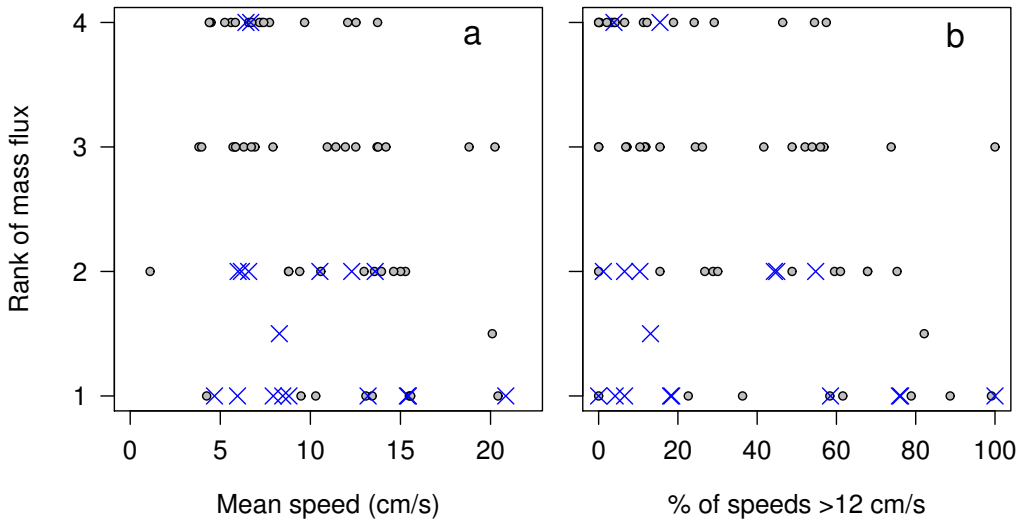

Figure 5.19 – Ranks of dry weight flux for each 14 d sample collection period plotted against (a) mean current speed over each 14 d sample collection period, and (b) percentage of current speed measurements over each collection period that exceeded 12 cm s^{-1}. Data from Trap S, which under-collected ^{230}Th by a factor of two relative to the other traps, are shown as blue crosses. Spearman's rank correlations were significant for both cases (see text Page 108).

a biologically and physically very different water mass. However, this was probably not the case: while there were numerous mesoscale eddies moving through the region, Trap S was not particularly strongly affected compared to the other traps; indeed, none of the traps were often below the centre of a strong eddy. Since eddies can have a small degree of lateral displacement with depth, it cannot be ruled out that eddies were involved. However, the SSH maps show no compelling reason to assume that this was the case. It should also be noted that the SSH data clearly show that the spatial arrangement of the trap array was successful: at no time were all traps simultaneously affected by any one physical feature.

Finally, Figure 5.23 shows weekly composite maps of surface chlorophyll-*a* concentration. Two localised blooms are clearly visible in the 01 May image, one directly above the trap array. Chlorophyll then decreased and remained $<$1 mg m^{-3} until 12 June, when a summer bloom took place. This bi-modal chlorophyll time-series is very probably the reason for the bi-modal particle flux time-series seen clearly in all four traps. The patchiness in the chlorophyll concentration might be the reason for the ∼two-fold variability in particle flux between traps during the spring and summer flux peaks, but without an estimate of the source region for each trap it is impossible to conclude more.

5.4.5 Chemical composition of the particle flux

A big surprise was the high Sr content of the spring samples, as discussed in Chapter 4. The POC:PON ratios were mostly 7–9, fully in the range of other sediment trap studies at this depth (*Schneider et al.* 2003), and the greater fluxes of $CaCO_3$ compared to opal (and the high percentage contribution by $CaCO_3$ to mass flux, and hence the overall PIC:POC ratios) are in

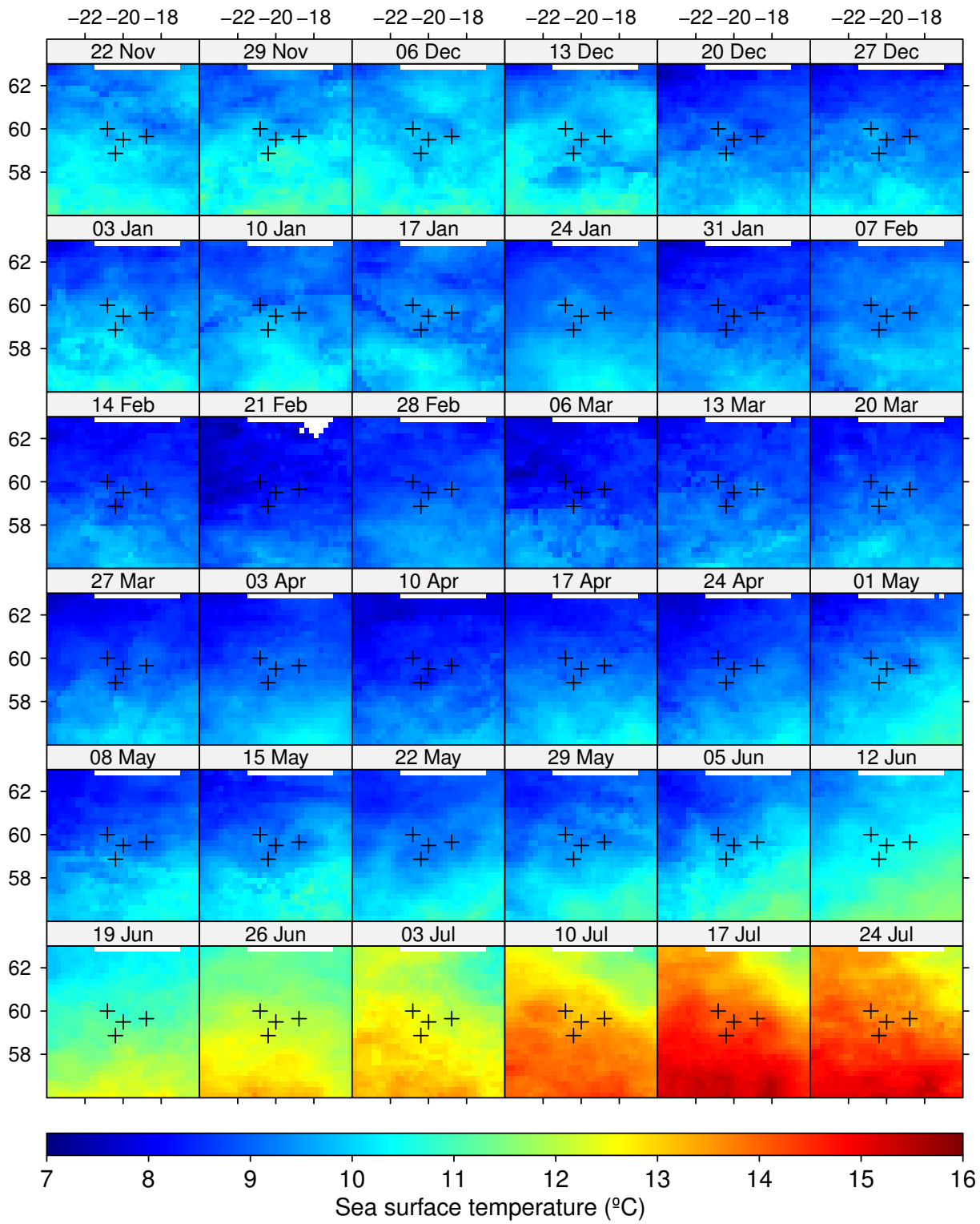

Figure 5.20 – Weekly composite maps of sea surface temperature. Trap locations are marked with black crosses.

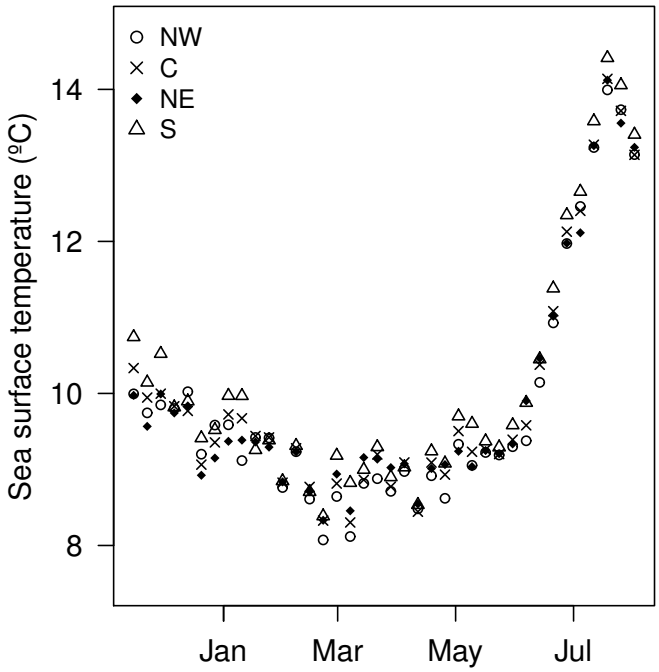

Figure 5.21 – Time-series of mean weekly SST in a $1° \times 0.8°$area above each trap.

keeping with other results from the north-east Atlantic (*Waniek et al.* 2005; *Honjo et al.* 2008; *Lampitt et al.* 2010). While diatoms dominate the annual spring bloom in the North Atlantic (*Sieracki et al.* 1993; *Henson et al.* 2006; *Leblanc et al.* 2009), and are thought to contribute substantially to the annual particle export in the region (*Billett et al.* 1983; *Buesseler et al.* 1992; *Henson et al.* 2006), coccolithophore blooms are regularly found there in summer (*Holligan et al.* 1993; *Brown and Yoder* 1994), and coccolithophores can also contribute significantly to, or even dominate, the phytoplankton community during non-bloom conditions (*Leblanc et al.* 2009; *Poulton et al.* 2010). Additionally, large numbers of Foraminifera and occasional fragments of pteropods were found in some of the trap samples, although the relative contribution of heterotrophic (Foraminifera, pteropods) *versus* autotrophic (coccolithophore) $CaCO_3$ was not assessed. Given the importance of coccolithophores in the surface plankton community one might expect them to contribute much of the $CaCO_3$, although the relative magnitude of coccolithophore *versus* foraminiferan $CaCO_3$ flux to sediments globally remains a matter of debate and has recently been suggested to be ∼1:1 (*Broecker and Clark* 2009).

The values of ^{230}Th content in the present samples fall well within the range of values reported elsewhere (*Bacon et al.* 1985; *Scholten et al.* 2001; *Yu et al.* 2001; *Scholten et al.* 2005), although the fluxes tended to be lower in the present samples, owing to the overall low mass fluxes. Other studies of ^{230}Th flux generally found strong relationships between ^{230}Th flux and mass flux (*Bacon et al.* 1985; *Colley et al.* 1995), although this was not the case for a 500 m north-east Atlantic trap (*Scholten et al.* 2001). Such a relationship was less pronounced in the present case, but the range of ^{230}Th fluxes reported by *Bacon et al.* (1985) and *Colley et al.* (1995) was also several-fold greater than that found here, with a much larger number of

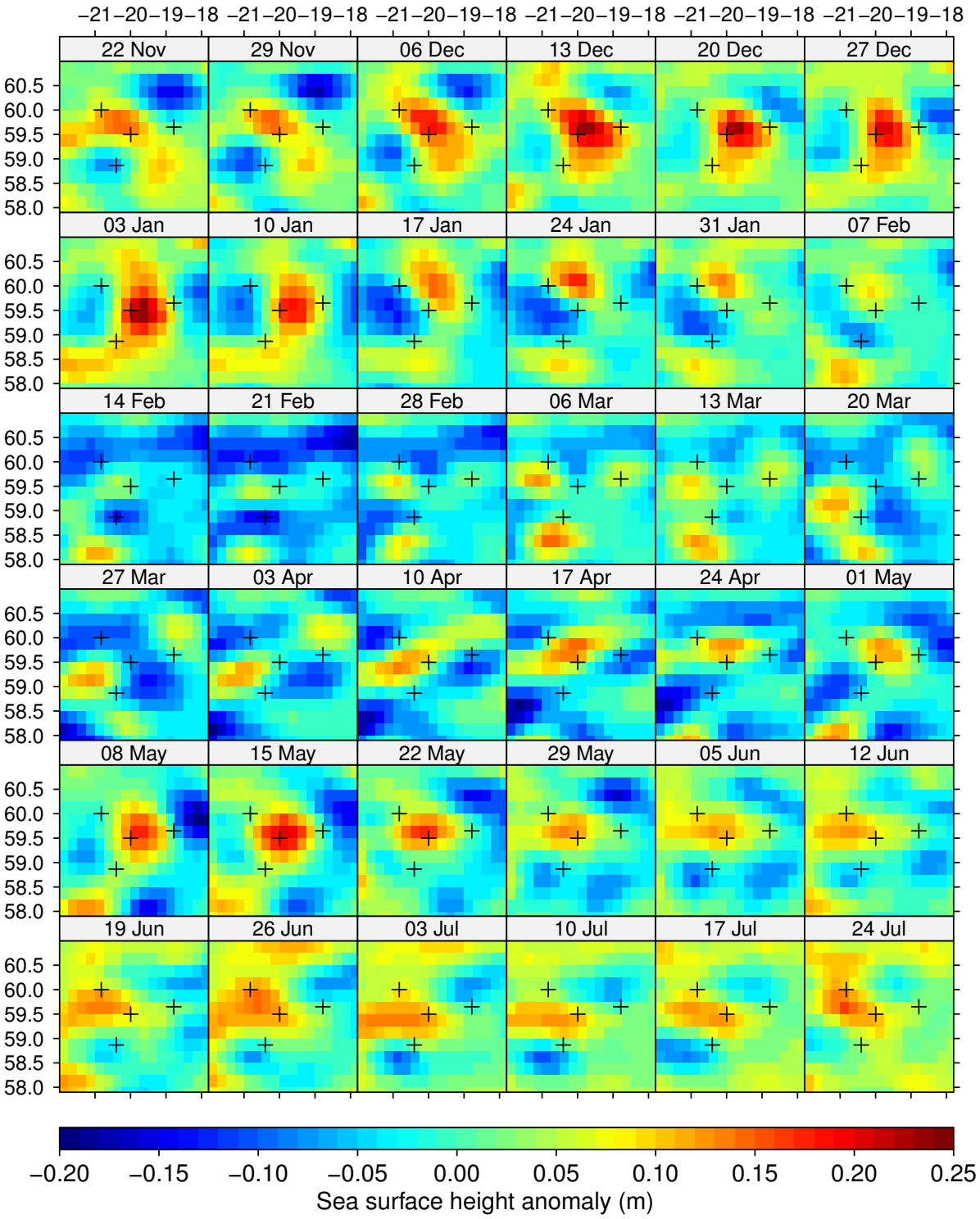

Figure 5.22 – Weekly composite maps of sea surface height anomaly. Trap locations are marked with black crosses.

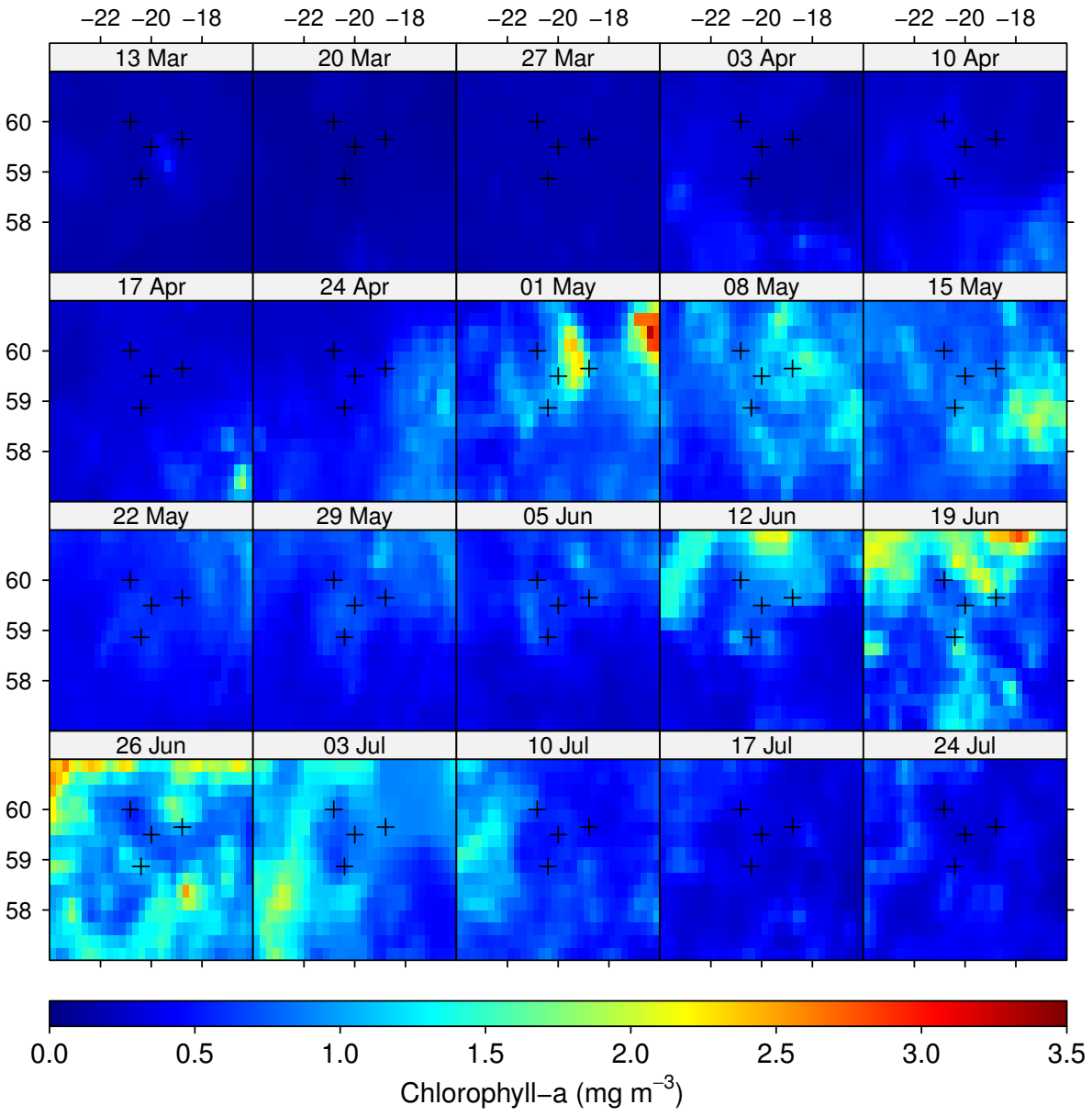

Figure 5.23 – Weekly composite maps of surface chlorophyll-*a* concentration. Trap locations are marked with black crosses. Data coverage was very poor prior to 13 March due to cloud cover, hence these plots are omitted

samples. However, Figure 5.12 shows three clear outliers with high ^{230}Th flux but very low mass flux, and thus overall the ^{230}Th content was not constant with mass flux. Rather, it appears as though ^{230}Th content was strongly reduced in spring and summer, presumably as a result of the relatively rapid sinking of large particles carrying little ^{230}Th. *Chase et al.* (2003) suggested that ^{230}Th is scavenged primarily by small, suspended particles, and thus ^{230}Th flux would be controlled by aggregation of the suspended particle stock (which is likely to offer a far greater surface area, a key factor controlling Th scavenging; *Bacon and Anderson* 1982). This hypothesis could explain the observations presented here.

5.5 Conclusions

While the seasonal cycle in particle flux was virtually identical in the four sediment traps, differences between traps of >2-fold were found for many of the individual 14 d collection periods. Over the entire deployment period, the cumulative mass flux differed by up to 30% without a corresponding difference in the cumulative flux of ^{230}Th, implying genuine mesoscale variability in cumulative flux. In contrast, the southern trap caught only half the cumulative ^{230}Th flux found in the other traps, chiefly due to lower flux during winter, implying that the lower mass flux in this trap was due to less efficient trapping. SSH and SST data revealed no obvious link to the lower fluxes in Trap S, such as persistent eddy influence. To what extent the short-term variability in flux between traps was caused by differences in trapping efficiency, *versus* representing genuine mesoscale variability cannot be deduced from this data-set, although there was pronounced patchiness in surface chlorophyll-*a* concentration during spring and summer. Overall, there was a significant inverse association between current speed during each sample collection interval and the relative rank of mass flux between traps. However, Trap S, which evidently did under-collect significantly relative to the other traps, did not experience a higher current regime either in terms of mean current speed or in terms of the number of peaks of very high speed.

Chapter 6

Conclusions

Chapters 2 and 3 focussed on export and mesopelagic particle flux in two very different ecological settings. The diatom bloom studied in Chapter 2 proceded until $Si(OH)_4$ was reduced to $\leq 1\,\mu mol\,L^{-1}$, and then produced a large pulse of particle flux that consisted largely of diatom detritus and sank approximately $100\,m\,d^{-1}$. While this material appeared to be chemically (and biologically) relatively fresh, and was thus presumably quite labile, it had a high transfer efficiency to at least 750 m. This contrasts with suggestions that high-latitude diatom-dominated systems are characterised by low T_{eff} due to the ballasting capacity of opal and / or the lability of diatom phytodetritus (*François et al.* 2002; *Ragueneau et al.* 2006), but agrees with the analysis of *Buesseler and Boyd* (2009) specific to export during a diatom bloom. It is, of course, possible that high-latitude diatom-dominated regions have low annual mean T_{eff} compared to $CaCO_3$-dominated regions, but the data in Chapter 2 suggest that this is would be due to the phytoplankton community shifting away from the initial diatom-dominated state. Sedimentation of phytodetritus out of diatom blooms can thus contribute large pulses of POC flux that have high T_{eff} through the mesopelagic.

The discovery of large numbers of diatom resting spores together with TEP in the sinking material is consistent with mass diatom sinking being an adaptive response and proceding via TEP-mediated aggregation. This would require that significant numbers of spores manage to dissociate in the mesopelagic and cease their rapid descent; a hypothesis that could be investigated in future by looking at mesopelagic particle stocks and spore populations after a diatom bloom and during the summer.

Chapter 2 further shows that particle flux can probably change quite dramatically over just a few days during bloom conditions. This would present obvious methodological problems in trying to sample such flux pulses accurately, as even small gaps in observations could introduce large uncertainties the overall flux estimates.

In contrast, the LohaFEX bloom (Chapter 3) consisted primarily of small phytoplankton and experienced substantial grazing pressure by copepods, probably with a lot of re-processing of sinking particles by copepods. Under these conditions, phytoplankton biomass remained relatively low despite high primary production, and particle flux consisted primarily of faecal

material and unrecognisable matter that was probably degraded faecal material; intact cells contributed only a very minor portion of the flux.

Despite alleviation of Fe limitation and the presence of high NO_3^- and PO_4^{3-}, the plankton community remained a recycling one, with control apparently exercised largely by the copepod community. Following the contrast made by *Smetacek et al.* (2004) between the export characteristics of Fe-limited and Fe-replete systems in the Southern Ocean, the LohaFEX results indicate that Fe levels may initially "set the scene" by allowing one or the other type of system to be established, but that ecological interactions between phyto- and zooplankton can then maintain the system even if Fe-limitation is alleviated. It is possible that although $Si(OH)_4$ was low, copepod grazing exerted the dominant control on diatom biomass and thus export; future iron-fertilisation experiments should hence also study the zooplankton community and grazing pressure thoroughly, as the export potential after alleviating Fe-limitation may not only be controlled by the $Si(OH)_4$ concentration.

From a methodological point of view, both the North Atlantic bloom study and LohaFEX were able to overcome the difficulties of temporal decoupling between production and export, and the different integration time-scales of methods assessing production, export, and mesopelagic flux. Both cruises were Lagrangian, tracking a particular water mass over time and thus allowing the temporal developments in the biology and biogeochemistry to be measured. In the case of LohaFEX, the cruise duration was long enough to enable a meaningful comparison between ^{234}Th-based export measurements and O_2:Ar-based NCP measurements. In future, this combination of measurements should be used more routinely during "export-oriented" biogeochemical cruises to overcome the problems inherent in comparing seasonal new production estimates based on nutrient budgets to ^{234}Th and sediment trap measurements.

Chapter 4 presented clear evidence that acantharian cysts can contribute significantly to the bathypelagic particle flux, at least in the Iceland Basin. While their contribution to POM flux was minor compared to the annual cumulative flux, they contributed very significantly during that particular period. Identical cysts were also found in the PELAGRA catches in Chapter 2, where celestite contributed up to at least 10% of mass flux. It was speculated in Chapter 4 that deep sedimentation was a strategy to allow juvenile Acantharia to exploit the seasonal export of fresh phytodetritus; this could be tested in future by taking bathypelagic and benthic samples in the Iceland basin in late spring or early summer and searching for juvenile Acantharia. Moreover, more measurements of Sr in bottom-tethered annual sediment traps would cast light on the geographic distribution of deep acantharian fluxes (and such measurements are technically easy); judging by published Sr profiles the North Pacific might be a promising area in which to search.

Finally, Chapter 5 reported one of very few assessments of mesoscale variability in bathypelagic particle fluxes, and was able to investigate to a degree the putative link between horizontal current speed and sediment trap collection efficiency. Regarding mesoscale variability, there was evidence for variation by up to 30% in the cumulative flux over eight months between traps ∼100 km apart, and this variability could not be attributed to differences in trapping efficiency. However, over any given collection period the flux varied several-fold between traps. Because ^{230}Th is only useful for assessing collection efficiency over longer time-scales, it was

not possible to determine to what extent this variability was genuine — although the surface chlorophyll-*a* concentrations were very patchy, suggesting that export was probably patchy, too. Some additional work would be warranted to address this question, although the results suggest that regional comparisons of annual bathypelagic particle flux (*e.g. Honjo et al.* 2008) are unlikely to be significantly biased by mesoscale variability.

Appendix A

Sampling Methods

A.1 Sediment traps

While many different methods have been used to measure the BCP, sediment traps are the only way of both quantifying particle flux and retrieving representative samples of sinking particles for laboratory analysis. Sediment traps of various designs have been used for decades and have yielded important insights into temporal, regional, and vertical trends in particle flux. However, it quickly became clear that sediment traps can suffer from significant biases that are very difficult to correct for or mitigate. This was recently reviewed comprehensively by *Buesseler et al.* (2007a), and the two main problems (hydrodynamics and "swimmers") are summarised below. Both are most acute at depths shallower than 1000 m, and for work in the mesopelagic neutrally buoyant traps have hence been developed recently (*Valdes and Price* 2000; *Lampitt et al.* 2008b; *Sherman et al.* 2011).

The first problem applies to sediment traps that are tethered either to the seafloor or to drifting surface buoys. Such traps invariably experience horizontal currents, and surface-tethered traps may additionally be moved vertically due to waves moving the surface buoy (*Gust et al.* 1994). Horizontal currents in particular have been linked to reduced "efficiency" of trapping (*i.e.* under-collecting downward particle flux relative to the true flux; *Gardner* 1980a,b, 1985; *Butman et al.* 1986; *Gardner and Zhang* 1997). While the *in situ* experiments by *Baker et al.* (1988) are sometimes cited as evidence that horizontal current speeds $<12\,\mathrm{cm\,s^{-1}}$ do not introduce substantial biases, trapping efficiency is an outcome of very complex interactions between current speeds, particle type, and trap geometry (*Gardner* 1980a; *Butman et al.* 1986). This has precluded discovery a simple relationship between current speed and trapping efficiency — indeed, *Gardner et al.* (1997) found no effect of horizontal currents on trapping efficiency — and the problem of under-trapping thus remains largely unsolved (*Buesseler et al.* 2007a).

On balance, it appears as though funnel-shaped traps tend to under-trap, with cylindrical traps collecting more accurately (*Gardner* 1980a; *Butman et al.* 1986), but funnel-shaped traps may be improved by adding baffles across the top (*Gardner* 1980a). The best that can currently be done is to try and assess the trapping efficiency for any individual deployment by measuring the flux of natural radionuclides into the trap, the true flux of which can be determined inde-

pendently and compared with the trap results (see Appendices B.5.1, B.6.1) — but it remains unclear whether the trapping efficiency of radionuclides really does apply equally to all other phases, such as POC (*Buesseler et al.* 2007a). Such "trap calibration" studies using the flux of ^{230}Th and ^{231}Pa have concluded that sediment traps below 1000–1500 m tend to perform reasonably well (*Scholten et al.* 2001; *Yu et al.* 2001). But trapping efficiency even at these depths can be as low as 20% (*Scholten et al.* 2001), so traps below 1000 m are by no means guaranteed to yield accurate samples.

The second major problem with sediment traps is that live zooplankton invariably enter the collection cups; these are referred to as "swimmers". If no poison / fixative is added to the collection cups, swimmers might feed off collected particles and / or defecate in the samples. Swimmers entering poisoned samples will quickly die, preventing the sample from being altered substantially, but then need to be removed from the sample before chemical analysis, otherwise the results can be substantially biased (*Lee et al.* 1988; *Karl and Knauer* 1989; *Buesseler et al.* 2007a). Unsurprisingly, the problem is greatest the shallower the trap is deployed, and surface-tethered traps suffer particularly — animals may actually be attracted to the mooring line above the traps (*Lee et al.* 1988). While some trap designs have been developed to minimise the swimmer problem (*e.g.* the "Labyrinth of Doom", *Coale* 1990), swimmers are not fully excluded even from those samples, necessitating methods of removing swimmers post-collection.

A common way of removing swimmers is to screen samples through a mesh small enough to retain most swimmers, but large enough to allow most particles to pass through. This approach has the advantages of allowing samples to be processed faster (thus potentially reducing particle dissolution artefacts, see *Lamborg et al.* 2008), and allowing less scope for contamination if trace elements are to be measured. However, some swimmers may pass through the mesh (*Michaels et al.* 1990), while some large particles that are genuinely part of the flux may be removed. A method that is probably better, and was used for the present work, is to manually remove swimmers under a dissecting microscope with tweezers and pipettes ("swimmer picking"). While tedious at the time, swimmers are probably more reliably removed this way (especially small copepods and nauplii), and can also be carefully cleaned in the process, thus minimising the loss of entangled particles. However, not all swimmers are easily recognised under a microscope, and the contribution by such "cryptic swimmers" (primarily gelatinous zooplankton and any feeding structures that they might have actively carried into the trap) can be significant (*Michaels et al.* 1990). Swimmer picking is also somewhat subjective (*Buesseler et al.* 2007a).

It is also possible to over-correct by removing all zooplankton: if an animal dies and sinks, it becomes a genuine part of the passive flux, and such individuals get caught in sediment traps as well. It is possible to retain any individuals that look visibly decayed (*e.g.* copepods lacking most internal organs; such individuals were retained in the present work, but were very rare), but that only works for individuals that have been dead for relatively long. *Sampei et al.* (2009) suggested an elegant way of distinguishing copepods that entered the trap alive from those that entered dead based on the posture of their appendages; while they found that only $<5\%$ of copepods collected in a sediment trap were part of the passive flux, they contributed 36% of POC flux. Such a criterion could not be employed in the present work, but if it were shown that

their method applied generally to copepods, not just the Arctic species they tested, it might allow copepod swimmers to be dealt with more accurately.

Neutrally buoyant sediment traps are thought to fare better than surface-tethered traps regarding both these biases, but whether they really do collect more accurate samples than surface-tethered traps is unfortunately difficult to answer. For the "NBST" trap (*Valdes and Price* 2000), a comparison with surface-tethered traps under low-current conditions off Bermuda showed some differences between traps, but it was not evident that one type was superior to the other (*Stanley et al.* 2004). *Lamborg et al.* (2008) concluded that the NBST performed better than a surface-tethered trap during one deployment in the sub-polar North Pacific, but that there was no difference during another deployment. For the PELAGRA traps used in the present work, *Lampitt et al.* (2008b) argued that they agreed with export estimates based on ^{234}Th, and in the present work they yielded results that were qualitatively and quantitatively consistent with the other approaches employed (Chapters 2, 3; PELAGRA has not yet been compared to surface-tethered traps). Overall, it seems that neutrally-buoyant traps yield relatively accurate results, better than surface-tethered traps, but independent methods of assessing particle flux should ideally be employed in conjunction with traps.

A.1.1 PELAGRA traps

PELAGRA traps (Particle Export measurements using a LAGRAngian trap; *Lampitt et al.* 2008b) have four separate collection funnels (0.115 m^{-2} each) arranged around an APEX float (Webb Research Corporation, USA). The APEX float has an in-built CTD sensor and a buoyancy engine: a hydraulic pump inflates or deflates an oil-filled bladder, thus changing the float's density and allowing it to reach a pre-programmed target position in the water-column. PELAGRA is shown in Figure A.1.

Each funnel leads to a separate 500 mL Nalgene collection jar that can be filled with a preservative of choice. During previous studies (*Lampitt et al.* 2008b; *Salter et al.* 2007) the collection cups were open under the funnels during trap deployment, and closed via a spring-loaded mechanism before the trap ascended at the end of its mission (the mechanism slides the cups away from the funnels and they are then covered by the plastic base-plate of the traps). This was unsatisfactory on two counts: (a) it was not known when exactly the traps started collecting particles, and the collection start time was simply assumed to be the time at which the trap stabilised at its target depth; and (b) any contamination from the ship that fell into the funnels during deployment ended up in the samples (*e.g.* specks of rust and paint). The traps were therefore modified before the work presented here was started such that the traps are deployed with the cups rotated away from the funnels (*i.e.* cups are closed and cannot be contaminated by any debris falling off the ship during deployment), the rotation mechanism then slides the cups underneath the funnels at a pre-programmed time to start collecting, and then closes the cups again before the trap ascends. Traps ascend by jettisoning a ballast weight (a 2 kg steel bar), and once at the surface transmit their positions via satellite to the ship.

The APEX float permits two modes of operating the trap, either isobaric or isopycnal. The former means that the trap targets a particular depth horizon and then remains there, while

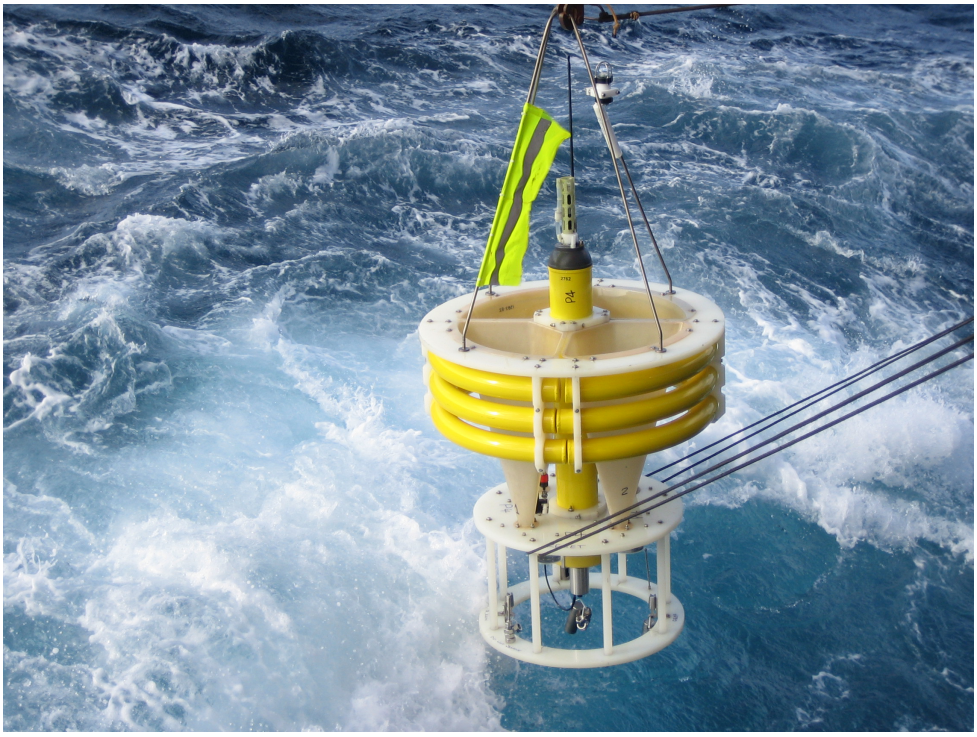

Figure A.1 – A PELAGRA trap being deployed.

the latter means that the trap targets a horizon of potential density (and remains there with a tolerance of ±0.01 sigma-theta). Traps were operated in isopycnal mode in this as in previous studies, as it was considered to lead to less movement of the trap relative to the surrounding water when internal waves pass. Whether this makes a difference in practice, and what velocities PELAGRA actually attains relative to the surrounding water is as yet unclear.

To deploy PELAGRA, a CTD profile at the deployment location needs to be taken first. The potential density at the target depth is then calculated and programmed into the APEX float together with the deployment duration, the trap is ballasted for the target density using pre-weighed steel bars and nuts (nominally to within 10 g), and the timer is programmed to open and close the cups, and jettison the ballast at the desired time. In this study, traps were always given 18–24 h to stabilise their position in the water column before opening the cups, and collection periods ranged from 18 h to 6 d.

PELAGRA is a technology that is still under active development. Deploying PELAGRA is complicated and labour-intensive, and technical problems invariably arise and cause several deployments during a cruise to fail. However, improvements are being made continually, and deployment is likely to become more routine, with a high success rate, over the coming years.

A.1.2 Bottom-tethered sediment traps

Bottom-tethered sediment traps have long been an "off-the-shelf" item manufactured commercially — producing and operating a tethered sediment trap is technically far easier than a

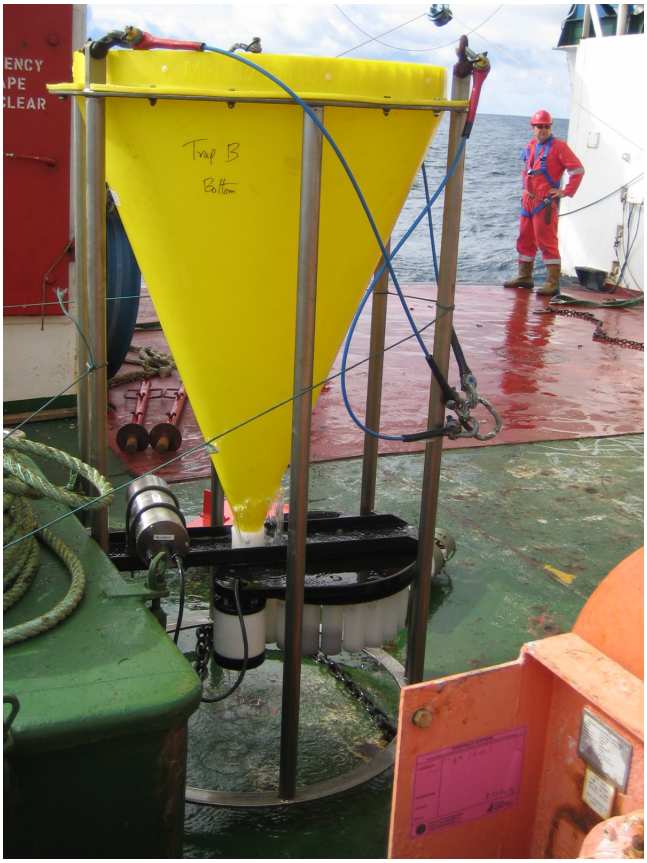

Figure A.2 – Bottom-tethered sediment trap upon recovery in the Iceland Basin in August 2007.

neutrally buoyant one. The tethered traps used in this study were Parflux Mark 78H-21 traps (McLane Research Laboratories, USA; Figure A.2), and were attached to mooring lines equipped with an acoustic release below, a current meter at trap depth, and buoyancy spheres above. They are time-series traps, *i.e.* they have a single collection funnel ($0.5\,m^2$), and a carousel of 21 collection cups, which are rotated below the funnel on pre-determined dates and are all filled with a preservative solution before deployment (see below).

A.2 Sediment trap preservative

Four different preservatives have been commonly used in sediment trap studies: formaldehyde, mercuric chloride, sodium azide, and chloroform, each of which is mixed with seawater and frequently some NaCl to increase the density of the solution. Preservatives are needed to stop microbial and zooplankton activity in the samples while the trap is collecting (*Lee et al.* 1992; *Gardner et al.* 1983), although no one of these preservatives has proven clearly superior to the others (*Lamborg et al.* 2008; *Hedges et al.* 1993; *Lee et al.* 1992).

Formaldehyde was chosen for this study as it is less hazardous than chloroform and because it is a fixative rather than just a poison. The bodies of zooplankton swimmers hence become

rigid and can be removed without breaking apart, which would contaminate the sample. The preservative was mixed as follows, using analytical reagent grade chemicals:

- Add 5 g sodium tetraborate ($Na_2B_4O_7{*}10\,H_2O$) to 1 L concentrated formalin solution (37% formaldehyde), shake and leave overnight
- Pour the borate-buffered formalin into 19 L particle-free seawater (either filtered or from several hundred metres depth)
- Add 100 g NaCl and mix thoroughly

A.3 Sediment trap sample handling

Sample handling after collection differed in specific details between the cruises, as described in the individual chapters. Briefly, samples were divided with either a Folsom splitter or one of two types of rotary splitter (each yielding eight splits), and swimmers were removed manually from any splits used for chemical analyses. The splitters (Figure A.3) divide the samples into representative sub-samples, so any quantitative measurement performed on a sub-sample can be converted to a flux by accounting for the split size (Appendix A.4). In the case of PELAGRA samples, splits for chemical work were then filtered onto an appropriate filter type and analysed. With the moored sediment traps, five splits (from a total of eight splits) were filtered together onto a single cellulose nitrate filter, the material scraped off the filter with a PTFE-coated spatula, freeze-dried in clean glass vials and crushed with a small stainless steel spatula. Chemical analyses were then conducted on aliquots of the powder weighed on a microbalance.

The procedure for the moored sediment traps was adopted due to the presence of large numbers of Foraminifera in some samples, and the desire to retain some material from each sample as an undisturbed archive. While the rotary splitter is considered to have a replication error $<3\%$ in terms of the volume of each split (*R. Lampitt*, pers. comm.), the variability of large, heavy particles such as Foraminifera was found to be considerably larger during preliminary splitting experiments (see below). For chemical measurements, the smallest uncertainties would be achieved by filtering down each sample completely, drying, weighing, and homogenising the particles, and performing the measurements on weighed aliquots of this material. However, it was decided that three sub-samples of each sample should be retained undisturbed to allow additional work in future; given the low quantity of particles in many samples, it was hence decided to split each sample once with a rotary splitter, and use only five $\frac{1}{8}$ splits for chemical measurements. Re-combining, drying, and crushing these five splits allowed an exactly appropriate quantity of material to be used for each analysis (^{230}Th required much more material than the other analyses), and allowed many measurements to be taken in triplicate. Such a procedure was not deemed necessary for the PELAGRA samples, because all measurements could be conducted on similar quantities of material, and because the PELAGRA samples contained greater quantities of material suspended in a greater volume of preservative solution.

Preliminary splitting experiments were conducted (together with Christopher Beer, NOCS) using a sample of Foraminifera taken from a sediment core. 200–500 mg of Foraminifera were

(a) Rotary splitter used for samples from the tethered sediment traps and PELAGRA samples from the North Atlantic bloom study.

(b) Rotary splitter used for PELAGRA samples collected during LohaFEX.

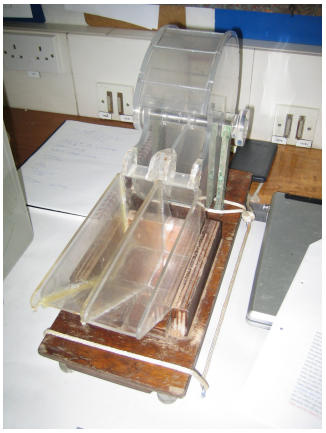

(c) Folsom splitter used for splitting PELAGRA samples during the North Atlantic bloom study.

Figure A.3 – The three models of sample splitters used.

mixed with 250 mL water (the volume of a sediment trap cup) and split with the rotary splitter exactly as for sediment trap samples. Each split was then filtered onto a pre-weighed GF/F filter, dried overnight at 50 °C, and weighed again (on a Mettler Toledo analytical balance with 0.0001 g readability). In three trials, the relative standard deviation of the weight of the eight splits was 18%, 20%, and 27%, which was deemed unacceptably high. The experiment was hence repeated four times (with 400 mg of Foraminifera), but with recombining five of the splits for each run. The dry weight of these combined splits differed by 3.6%, 5.2%, 6%, and 4% from the "correct" value of 250 mg ($\frac{5}{8} * 400 = 250$). As the splitting uncertainty for the samples could not be directly quantified, it was assumed to be 5% based on this experiment (this is hence also the uncertainty assumed for the dry weight fluxes, as the weighing error on the microbalance was negligible).

A.4 Calculation of fluxes

Daily fluxes were calculated for all sediment trap samples based on the known duration of sample collection, the area of the sediment trap funnel opening, and the split size of the sample. For example, POC flux in the deep, moored sediment traps (Chapter 5) was calculated from the measured concentration of POC in the dried sediment (mg POC [mg sediment]$^{-1}$) as follows:

$$\text{POC flux (mg m}^{-2}\text{d}^{-1}) = (\text{POC conc.}) * (\text{DW}) * \frac{1}{(\text{split size})} * \frac{1}{(\text{days})} * \frac{1}{(\text{area})} \tag{A.1}$$

where the split size is $\frac{5}{8}$ of the collected sample (Section A.3), DW is the dry weight of particles in the $\frac{5}{8}$ split, and days and area are the number of days over which the sample was collected (14 in this case) and the funnel collection area ($0.5\,\text{m}^2$).

In the PELAGRA samples, POC flux was calculated from the quantity of POC in a known split (in mg) as:

$$\text{POC flux} = (\text{POC in split}) * \frac{1}{(\text{split size})} * \frac{1}{(\text{days})} * \frac{1}{(\text{area})} \tag{A.2}$$

where "POC in split" is the quantity of POC in the analysed split (in mg), split size ranged from $\frac{1}{8}$ to $\frac{1}{32}$, and days and area are as in Equation A.1 (albeit with different values).

Fluxes of other components (*e.g.* PIC, BSi, Th) were calculated in the same manner.

A.5 Propagation of errors

Errors were propagated through all calculations as standard deviations using the basic equations:

$$SD_{(x+y)} = \sqrt{SD_x^2 + SD_y^2} \tag{A.3}$$

for addition/subtraction, and

$$SD_{(x*y)} = (x * y)\sqrt{\left(\frac{SD_x}{x}\right)^2 + \left(\frac{SD_y}{y}\right)^2} \tag{A.4}$$

for multiplication/division, where SD_x is the standard deviation of x.

Appendix B

Analytical Methods

The following sections present an overview of the principal analytical methods employed or developed during this study. Additional analyses were undertaken in some cases, and those are described in the individual chapters. All chemicals were of analytical reagent grade purity (either from Fisher Scientific or VWR) unless otherwise indicated. All weighing was done on a Sartorius ME-5 microbalance with precision of approximately $\pm 1\,\mu g$. All reagent solutions were made up with MilliQ water ($18.2\,M\Omega\,cm^{-1}$) unless otherwise stated.

B.1 Dry weight, POC, and PON

For PELAGRA samples, splits were filtered onto 25 mm pre-weighed, pre-combusted (550 °C for 4 h) Whatman GF/F filters. They were then dried at 40 °C for 24 h and weighed again to determine total dry weight flux. For deep, moored traps, the total quantity of freeze-dried sediment was weighed before crushing it.

PIC was then removed by treatment with HCl. PELAGRA samples were fumed with concentrated HCl vapour for 24 h in a plastic desiccator following *Hedges and Stern* (1984). Filters were then dried again at 40 °C for 24 h to remove residual acid vapours, then wrapped in pre-combusted (550 °C for 4 h) 30 mm aluminium disks (Elemental Microanalysis, UK), and pelletted using a custom-made sample press. For the deep, moored sediment traps, aliquots of 0.6–5 mg of freeze-dried sediment were weighed into pre-combusted (550 °C for 4 h) silver capsules (Elemental Microanalysis, UK) and acidified *in situ* with $2\,mol\,L^{-1}$ HCl on a hotplate at approximately 70 °C. During initial attempts it was noticed that the silver capsules had become very brittle during pre-combustion, as HCl solution leaked out of the cups, probably causing a loss of POC and PON (see also *Nieuwenhuize et al.* 1994). Therefore, each cup was placed on a pre-combusted (550 °C for 4 h) 12 mm diameter silver weighing pan (Elemental Microanalysis, UK) on the hotplate during acidification: although some acid did leak out of the cups into the weighing pans, the acid then quickly evaporated in the centre of the weighing pan without leaking out onto the hotplate. The cups were then crimped, rolled into the appropriate weighing pan, and pelletted.

POC and PON were then measured on a Flash 1112 Elemental Analyser (Thermo Finnigan) based at the Plymouth Marine Laboratory. The analyser works by combusting the sample at 1030 °C in presence of O_2 and passing it through a Cr_2O_3 catalyst, thus converting C to CO_2 and N to N_2. He is used as a carrier gas at 130 mL min^{-1}, and the (now gaseous) sample is passed through a water trap ($Mg(ClO_4)_2$) and then onto a Porapak QS gas chromatography column that separates CO_2 and N_2. Detection is then via a thermal conductivity (so-called "hot-wire") detector at 60 °C. The signals recorded from the samples (as peak area) are calibrated against acetanilide standards measured with each run.

The instrument has a dynamic range for C from blank levels (10–30 µg for GF/F filters; ∼1 µg for silver capsules) to around 3 mg and analytical precision of ≤1%. Procedural blanks were always analysed alongside the samples (described in the relevant chapters) and contributed <10% (and mostly ∼1%) of the signal for either element.

Blanks were prepared by either rinsing a GF/F filter with MilliQ and then processing exactly like a sample, including acid-fuming (Chapter 2), or first filtering blank sediment trap preservative through a GF/F filter, rinsing with MilliQ, and processing like a sample (Chapter 3). For the deep, moored trap samples, blanks were prepared from empty silver cups + weighing pans with acid added as for samples (Chapters 4, 5). Blank filters that were prepared with sediment trap preservative were not higher than blanks rinsed just with MilliQ.

POC and PON were analysed in triplicate in most samples from the deep, moored sediment traps, with RSDs mostly <10%. During the LohaFEX experiment (Chapter 3) PELAGRA samples could only be analysed singly, as sub-samples were shared with other groups to allow for additional analyses. Uncertainties on the LohaFEX flux estimates are likely to be close to those determined during the North Atlantic bloom study (Chapter 2).

B.2 PIC

PIC was estimated from Ca measurements via inductively-coupled plasma optical emission spectrometry (ICP OES). Samples (PELAGRA samples were filtered onto 25 mm 0.4 µm pore-size polycarbonate filters, for the deep, moored sediment traps 0.5–5 mg aliquots of freeze-dried sediment were used) were leached overnight in 1 mol L^{-1} acetic acid to dissolve biogenic carbonate. The leachate was then filtered through a 0.4 µm syringe filter into an autosampler tube and Ca and Na measured on a PerkinElmer Optima 4300DV ICP OES. In PELAGRA samples, Sr was also measured to determine the celestite flux. 1 mol L^{-1} acetic acid was chosen in favour of 0.4 mol L^{-1} HNO_3 as being a more benign leach, and thus less likely to attack lithogenic carbonate. Leaches were prepared volumetrically using autopipettors, as the inherent uncertainties associated with sediment trap studies do not warrant gravimetric preparation of samples.

PELAGRA samples were leached in new LDPE bottles with 10–20 mL acid, while the deep, moored sediment trap samples were leached with 10 mL acid in pre-used polypropylene centrifuge tubes that were cleaned by soaking in 10% HCl for 1 week and rinsing with MilliQ water. Procedural blanks contributed negligibly (typically ∼1%) to the signal for all three elements. Blanks were prepared from polycarbonate filters either rinsed just with MilliQ (Chapter 2) or

first with blank sediment trap preservative (Chapter 3), or, for the deep, moored trap samples, by just adding acetic acid to centrifuge tubes (Chapter 5).

PELAGRA samples from LohaFEX (Chapter 3) were size-fractionated to determine coccolith and foraminiferan/pteropod carbonate separately according to a method adapted from *Bairbakhish et al.* (1999). Filters were placed in acid-cleaned HDPE bottles and digested for ∼2 h with 10 mL 5% NaOCl and 10 mL >30% H_2O_2 to oxidise organic matter. Samples were shaken and sonicated for 5 s several times during digestion. The size-fractions were separated with a 30 µm metal sieve (Endecotts, UK) using alkaline MilliQ to rinse the samples through the sieve (1 L MilliQ + 3 drops concentrated NH_4OH). After a small aliquot had been taken from the small size-fractions for polarised light microscopy and scanning electron microscopy, both fractions were filtered onto 25 mm diameter 0.4 µm polycarbonate filters and leached as described above. The same procedure was applied to the blanks.

The instrument was set up such that the sample was converted into an aerosol in a nebuliser, passed through a baffled, cyclonic spray chamber (which substantially reduces matrix effects; *Green et al.* 2003), and into the plasma. The plasma excites electrons of the atoms in the sample to higher energy levels, and as these transition back to their ground state, they emit photons at wavelengths characteristic of the atom. Electrons in any element may undergo a number of different such transitions, thus emitting photons at several characteristic wavelengths. Photons emitted from the plasma are separated according to wavelength, and the intensity of each beam is measured by appropriately positioned detectors. Na and Sr were measured at only one wavelength, Ca was measured at 3–5 wavelengths and the results averaged.

External calibration standards were prepared gravimetrically from commercially available ICP standard solutions. The second-highest concentration standard was run every ten samples as a drift monitor preceded by an acid-blank (instrument drift was found to be negligible).

B.3 BSi

The method for sediment trap BSi measurements was established at NOC by *Salter* (2007) and is based on the wet alkaline digestion by *Mortlock and Froelich* (1989). Opaline silica in the sample is dissolved in 5 mL 0.2 mol L^{-1} NaOH in polypropylene centrifuge tubes heated to 90 °C in a waterbath. Samples were digested for 3 h following *Salter* (2007), and shaken vigorously every hour. The digests were then neutralised with 0.2 mol L^{-1} HCl, diluted with saline solution (40 g NaCl in 1 L MilliQ) depending on the expected Si concentration in each digest, and Si measured on a SEAL QuAATro autoanalyser. PELAGRA samples were filtered onto polycarbonate filters as for PIC analysis and then digested; for the deep, moored sediment traps 0.5–5 mg of dried sediment was weighed and digested. Procedural blanks (which contributed negligibly to the total signal) were prepared as for PIC analysis (Appendix B.2), though obviously omitting the size-fractionation step used for LohaFEX PIC samples.

The autoanalyser works by reacting dissolved Si to form a yellow silicomolybdate complex. Oxalic acid is then added to reduce excess molybdate (preventing phosphomolybdate and arsenomolybdate, which are also blue, from forming). Silicomolybdate is then reduced

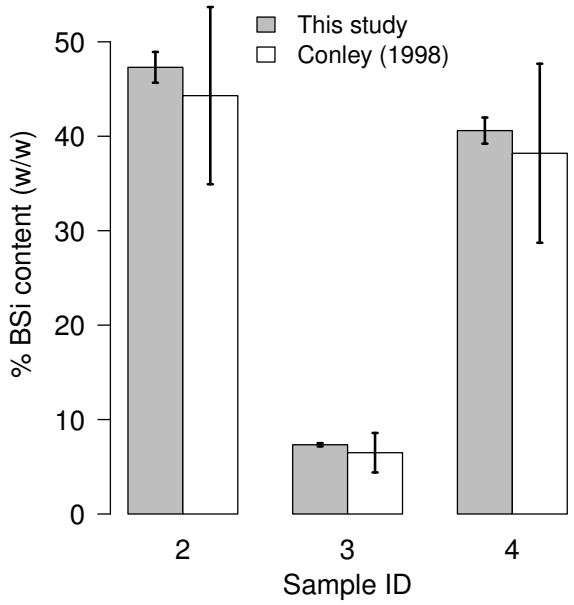

Figure B.1 – Results from BSi analysis of three samples used in the *Conley* (1998) inter-laboratory comparison of BSi methods. Data for this study are mean ± standard deviation of $n = 4$ replicate analyses. Data for *Conley* (1998) show the overall mean ± standard deviation from all 30 laboratories that participated in the study.

with ascorbic acid to yield a more stable blue-coloured compound, and the absorbance of the solution is then measured and quantified as peak height.

Standards were prepared from solid sodium fluorosilicate (Na_2SiF_6) dissolved in a fixed volume of MilliQ, and further diluted in saline solution. The highest concentration standard was run every ten samples as a drift monitor followed by two saline solution blanks to assess carry-over. Both drift and carry-over were found to be negligible.

The method was initially tested on three samples used in the *Conley* (1998) inter-laboratory comparison, which were also analysed by *Salter* (2007). Four replicate sub-samples from each sample were weighed and digested and analysed as described above, and results are shown in Figure B.1. In each case, the method employed here yielded results slightly higher than the overall mean BSi content reported in *Conley* (1998); this was also the case for *Salter* (2007), and attributed partly to dissolution of lithogenic Si. However, the inter-comparison samples were lake sediments, and thus probably had a higher lithogenic content than open-ocean particle samples; for the present study the possibility of a slight over-estimate in analysing the *Conley* (1998) samples was hence not deemed problematic.

Opal content of each sample was calculated from the measured Si values assuming 10% water content (*Salter et al.* 2007; *Mortlock and Froelich* 1989).

B.4 Transparent exopolymer particles (TEP)

TEP were measured using a modified version of the dye-binding assay of *Passow and Alldredge* (1995b). The method works by staining TEP in the sample with Alcian Blue and measuring the quantity of stain bound to TEP, which is then compared to the quantity of stain that binds to known weights of a standard substance, Gum Xanthan. The content of TEP in the sample is then expressed as grams of Gum Xanthan equivalents (g GX eq.).

TEP content in the samples was measured using aliquots between $\frac{1}{1600}$ and $\frac{1}{370}$ of the original sample. For each sample, two dilutions were prepared with a saline solution (35 g NaCl in 1 L MilliQ), and triplicate lots of 1 mL were filtered onto 25 mm 0.4 µm polycarbonate filters. Each filter was stained for ∼2 s with 0.5 mL of a 0.02% Alcian Blue solution prepared according to *Passow and Alldredge* (1995b) that was pre-filtered through a 0.2 µm syringe filter. The filter was then rinsed with 1 mL MilliQ to remove excess stain and soaked in 6 mL 80% H_2SO_4 for 2 h in polypropylene centrifuge tubes. Samples were gently agitated 2–3 times during acid treatment, and the absorbance of the acid was measured on a Hitachi U-2800 spectrophotometer at 787 nm against MilliQ as a reference. Blanks were prepared from stained, rinsed blank polycarbonate filters. The absorbance of unstained particles in these samples (tested by filtering and dissolving samples without staining them) was found to be zero. All filtration was conducted at a pressure of 200 mBar.

Different batches of Alcian Blue stain have different binding capacities, so the absorbance of a sample will be different if it is measured with different batches of dye solution (*Passow and Alldredge* 1995b), for instance due to gradual self-coagulation of the stain (the reason why the stain must be pre-filtered through a syringe filter on the day of usage). Therefore, the stain must be calibrated whenever new TEP measurements are taken, which is done by preparing a solution of Gum Xanthan, staining known quantities thereof, and measuring their absorption. The Gum Xanthan solution was prepared by gradually adding a few 10s mg of Gum Xanthan powder (SigmaAldrich, UK) to around 400 mL MilliQ while swirling the solution around. The solution was then shaken vigorously and ground three times in a 55 mL glass tissue grinder.

According to the original protocol of *Passow and Alldredge* 1995b, dry weights and absorbance of the Gum Xanthan solution are measured separately. For dry weights, replicate aliquots of 0.5–3 mL of the solution are filtered onto pre-weighed polycarbonate filters, dried, and re-weighed. The Alcian Blue binding capacity is then measured by filtering more replicate aliquots of 0.5–3 mL of the solution onto polycarbonate filters, and staining and measuring their absorbance as described above. For each volume, the average absorbance is plotted against the average dry weight, and a calibration curve fit by linear regression.

However, despite several attempts, no good calibration could be established using this method, because the variation in dry weight and absorbance between replicates was relatively high and the relationship deteriorated above 5–10 µg Gum Xanthan (a representative plot is shown in Figure B.2a). Varying the concentration of the Gum Xanthan solution, and grinding it more or less thoroughly did not solve this problem. It was also noticed that the weight of the Whatman polycarbonate filters used for this work could decrease by up to 3 µg if they were

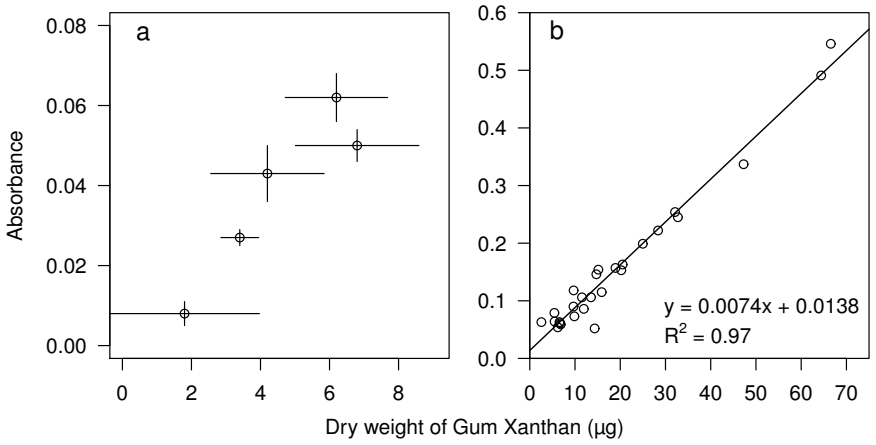

Figure B.2 – (a) Calibration of Alcian Blue solution using the original protocol of *Passow and Alldredge* 1995b; (b) calibration using the modified protocol described here. Note that the calibration in (b) extends to much higher values than in (a), but remains linear.

simply rinsed with MilliQ. Therefore, the protocol was modified as follows to allow both the dry weight and the absorbance of the Gum Xanthan solution to be measured on each filter.

All filters (25 mm 0.4 µm polycarbonate filters) were first rinsed with a few mL MilliQ, dried overnight at 60 °C, and pre-weighed. 0.5–6 mL aliquots of Gum Xanthan solution (three replicates per volume) were filtered, stained as in the original protocol, and then dried at 60 °C overnight. Filters were weighed, soaked in 6 mL 80% H_2SO_4 for 2 h, and the absorbance at 787 nm measured. The filter dry weights then had to be corrected for the mass of Alcian Blue: 10–200 mL aliquots of dye solution (for which the mass of Alcian Blue could be calculated from the concentration of the dye solution) were mixed with 80% H_2SO_4 and the absorbance measured after 2 h. The relationship between absorbance and mass of Alcian Blue (Figure B.3) was used to correct the dry weight of each stained filter. This correction was critical, as the calculated weight of Alcian Blue contributed 20–60% of the change in filter weight after filtering and staining the Gum Xanthan. The resulting calibration is shown in Figure B.2b. The relationship between absorbance and mass of Gum Xanthan was linear over a range of absorbances that exceeded the sample absorbances with $R^2 = 0.97$.

Three tests established that the stain is stable at 60 °C. First, ten replicate 3 mL lots of Gum Xanthan solution were filtered and stained, and either soaked directly in H_2SO_4, or dried overnight at 60 °C and then soaked in H_2SO_4, and the absorbance of each solution measured (Figure B.4a). Second, this experiment was repeated with stained blank polycarbonate filters (five replicates for each treatment), as the variance in the first experiment was high. The results are shown in Figure B.4b. Third, ten replicate 40 µL aliquots of the Alcian Blue solution were either added directly into 6 mL 80% H_2SO_4, or first dried overnight at 60 °C in polypropylene centrifuge tubes and then dissolved in acid, and the absorbances measured (Figure B.4c). Drying had no significant effect on absorbance (Wilcoxon-Mann-Whitney tests, all $p > 0.25$). One dried 40 µL aliquot had an absorbance of 0.088; as this was clearly distinct from the other

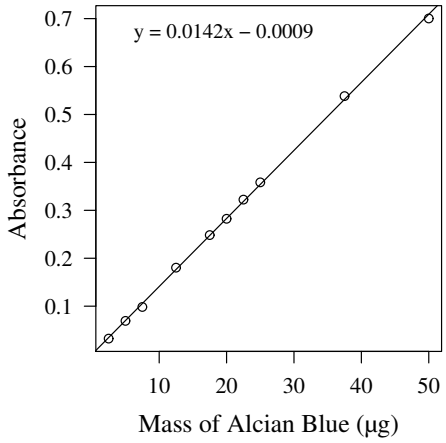

Figure B.3 – Relationship between mass of absorbance at 787 nm and mass of Alcian Blue used to correct Gum Xanthan dry weight measurements.

replicates in the treatment it was omitted from the analysis and from Figure B.4c (this was probably caused by a pipetting error).

B.5 ^{234}Th

B.5.1 Rationale

^{234}Th is a short-lived nuclide ($t_{1/2}$ = 24.1 days, decaying by β-decay to ^{234m}Pa) produced *in situ* by α-decay of ^{238}U. U is dissolved and conservative in seawater, with a mean oceanic residence time of 200,000–400,000 years (*Ku et al.* 1977; *Chen et al.* 1986). Th, in contrast, is highly particle-reactive and adsorbs to all types of marine particulate matter. Because ^{234}Th is so short-lived, while ^{238}U has $t_{1/2}$ = 4.468 billion years, the number of ^{234}Th atoms in a parcel of water reaches a constant value over time (termed secular equilibrium, where the activities of ^{238}U and ^{234}Th are equal) according to the equation:

$$\mathrm{N}_{234} = \left(\frac{\lambda_{238}}{\lambda_{234} - \lambda_{238}}\right) \mathrm{N}_{238} \left(e^{-\lambda_{238} t} - e^{-\lambda_{234} t}\right) + \mathrm{N}_{234_0} e^{-\lambda_{234} t}, \tag{B.1}$$

where N_{234} and N_{238} are the numbers of atoms of ^{234}Th and ^{238}U, λ_{234} and λ_{238} are the decay constants of ^{234}Th and ^{238}U (where $\lambda = \frac{\ln(2)}{t_{1/2}}$), t is time, and N_{234_0} is the number of ^{234}Th atoms present initially. Secular equilibrium in a sample is almost attained within six half-lives of ^{234}Th, so in the absence of any particle transport for ∼145 d the ^{234}Th:^{238}U activity ratio would be uniformly 1 throughout the water column. However, when particles sink over time-scales much shorter than the time taken to reach equilibrium, the downward removal on particles depletes ^{234}Th relative to ^{238}U in surface waters. The resulting radioactive disequilibrium is proportional to the amount of downward particle flux, and thus the downward ^{234}Th flux can be calculated from vertical profiles of ^{234}Th activity (described in Appendix B.5.4). ^{234}Th can be readily measured in water samples of 2–10 L, and because ^{238}U is dissolved and conservative,

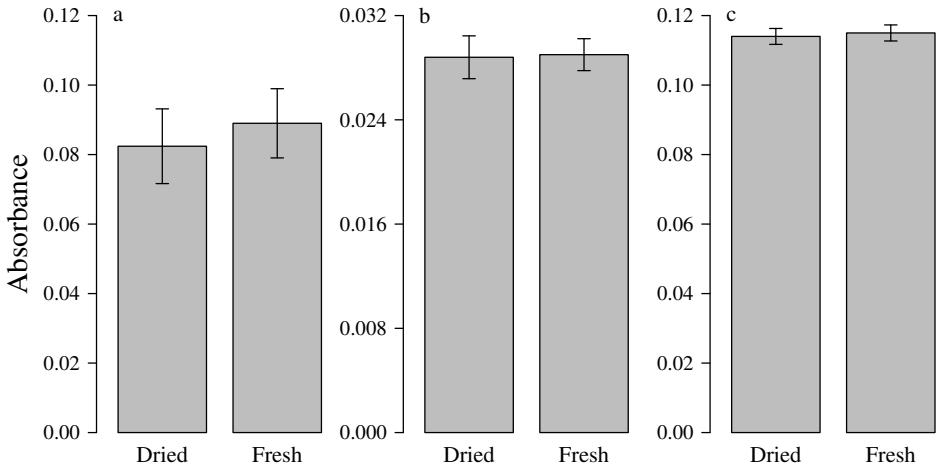

Figure B.4 – Results of experiments testing whether the absorbance of Alcian Blue is affected by drying at 60 °C. (a) Absorbances of 3 mL aliquots of Gum Xanthan solution either dried overnight, or measured fresh (10 replicates per treatment). (b) Absorbances of blank, stained polycarbonate filters either dried overnight, or measured fresh (5 replicates per treatment). (c) Absorbances of 40 µL aliquots of Alcian Blue solution in 6 mL 80% H_2SO_4 either dried overnight or measured fresh (10 replicates per treatment).

its activity can be calculated from salinity following *Chen et al.* (1986), based on a ^{238}U activity of 2.40 dpm L^{-1} at salinity 35 and 3.3% error:

$$A_{238} = 0.0686 \pm 0.00226 * salinity \tag{B.2}$$

Being such a short-lived isotope, the concentration of ^{234}Th in seawater in terms of mass is very low, typically 10–50 ag kg^{-1} (1 ag = 10^{-18}g). Mass spectrometric determination is therefore out of the question, also because (a) much of the activity would have decayed by the time a sample was back on land, and (b) because ^{234}U is several million times more abundant in seawater than ^{234}Th and would thus cause a major isobaric interference. However, the short half-life means that the little ^{234}Th that there is in seawater has a radioactivity of typically 0.5–2.5 dpm kg^{-1}, which is very easily measurable by β-counting. Moreover, because of this relatively high activity, no particularly great care needs to be taken to avoid contamination, unless high-activity β sources were being handled nearby.

B.5.2 Large volume method

During the North Atlantic Bloom study (Chapter 2), total ^{234}Th (dissolved + particulate) was measured using a 10 L MnO_2 co-precipitation technique (*Thomalla et al.* 2006; *Rutgers van der Loeff and Moore* 1999). Seawater was sampled from the CTD, exactly 10 L were measured out with a volumetric flask into clean HDPE carboys, and amended with three drops of concentrated NH_4OH solution, 125 µL concentrated $KMnO_4$ solution, and 50 µL of concentrated $MnCl_2$ solution. In seawater with slightly elevated pH, $KMnO_4$ and $MnCl_2$ react to form a precipitate of MnO_2, which co-precipitates many actinides, including thorium, but not uranium.

The precipitate was allowed to grow for 8 h and then filtered under pressure onto 142 mm 0.8 µm polycarbonate filters, rinsed with MilliQ, air-dried, and folded reproducibly into $18 \times 18\,\mathrm{mm}^2$ parcels wrapped in Mylar foil. ^{234}Th activity was measured in these as described below. The extraction efficiency (*i.e.* the percentage of ^{234}Th in the sample extracted onto the filter) was measured by retaining the filtrate of nine samples and repeating the precipitation, and was found to be $100 \pm 3\%$. Counting efficiency was quantified by measuring ^{234}Th in five samples from 1000 m, where ^{234}Th is expected to be in secular equilibrium with ^{238}U, and was found to be $24.7 \pm 0.9\%$.

^{234}Th in sinking particles was measured in sub-samples from PELAGRA collections, filtered and folded as for water column samples. POC:^{234}Th ratios were then calculated from the POC and ^{234}Th fluxes in each trap.

All labware was cleaned with a solution of $1.2\,\mathrm{mol\,L^{-1}}$ HCl + $0.1\,\mathrm{mol\,L^{-1}}$ H_2O_2 in between samples.

All ^{234}Th samples were then counted on a Risø National Laboratory GM-25-5A low-level β-counter in anti-coincidence mode, first within days of sampling and then repeatedly over the following six months to verify that the activity was decreasing according to the half-life of ^{234}Th. This was always the case, and a specimen decay curve obtained from one sample (plotted against time since sampling) is shown in Figure B.5a. After six half-lives, only ∼1.6% of the initial ^{234}Th activity remains.

To calculate the ^{234}Th activity at the time of sampling, a linear regression was fit to the natural log of the ^{234}Th activities against time after the activities had been background-corrected by subtracting the final (six months post-sampling) activity (Figure B.5b). The final activity measurement, instead of being subtracted from itself to give zero, was adjusted to such a value that the slope of the regression line became −0.02876, the decay-constant of ^{234}Th. The background-corrected activity at the time of sampling was then calculated as the y-intercept of the regression slope, and further corrected for in-growth from ^{238}U between the time of sampling and the mid-point of filtration (the time at which Th and U were separated).

The background count rates for samples after six months were typically around 0.35–0.45 counts per minute (cpm), significantly higher than the 0.15–0.21 cpm instrument background. *Benitez-Nelson et al.* (2001) showed that this background is primarily due to β-emission from the daughters of ^{226}Ra, which is scavenged by the MnO_2 (and β-counters do not discriminate between emissions from different elements). However, the background is stable over time (*Benitez-Nelson et al.* 2001).

B.5.3 Small-volume method

During the LohaFEX iron fertilisation experiment, total ^{234}Th was measured using a 4 L technique with recovery standard (*Pike et al.* 2005). Water was sampled from the CTD rosette into acid-cleaned HDPE bottles, acidified with 5 mL concentrated HNO_3, spiked with 39.3 pg ^{230}Th as the recovery standard, and allowed to equilibrate for 12 h. The pH was then raised to ∼8.3 with concentrated NH_4OH solution, and Th co-precipitated with MnO_2 as in Appendix B.5.2. Samples were then heated in a water-bath for 3 h following *Cai et al.* (2006) and filtered onto

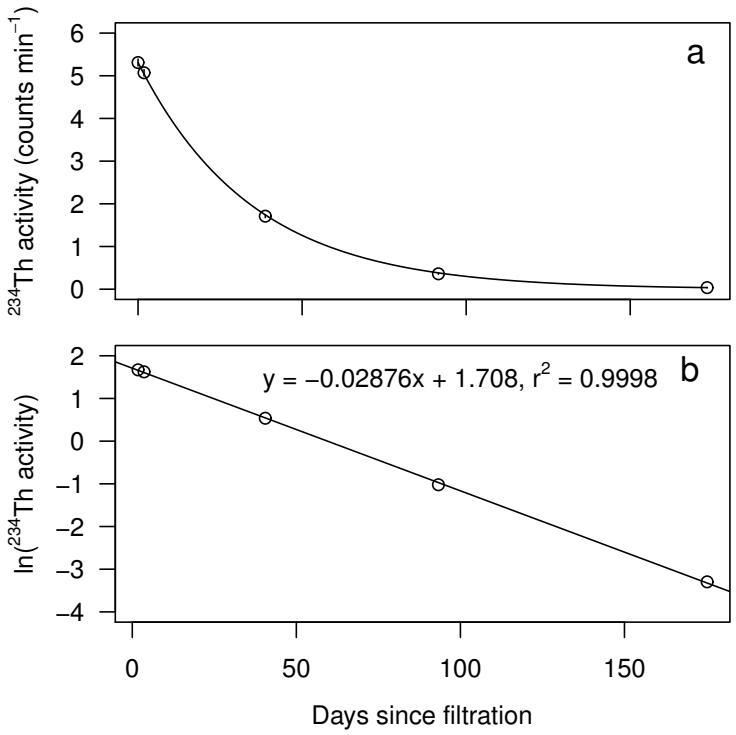

Figure B.5 – (a) Decay of β-activity in a specimen water-column ^{234}Th sample. Open symbols show background-corrected measured values (counting errors are smaller than the plotting symbols); the solid line shows the theoretical decay-curve of ^{234}Th with $\lambda = -0.02876$. (b) Natural log of the activities shown in (a) with a linear regression fitted to the data. The y-intercept of the regression line is the background-corrected ^{234}Th activity at the time of sampling.

25 mm Whatman QMA filters. Filters were air-dried, covered with one layer each of Mylar and aluminium foil, mounted onto Risø sample disks, and the activity of ^{234}Th counted on an anti-coincidence GM25-5 low-level β-counter. The background radiation of each sample was counted after six months.

All labware was cleaned with a solution of 1.2 mol L^{-1} HCl + 0.1 mol L^{-1} H_2O_2 in between samples.

Samples were then dismounted, the precipitate dissolved in 50% HNO_3 + 10% H_2O_2 with addition of 12.8 pg ^{229}Th, and Th purified on AG 1-X8 anion exchange resin. The purified fractions were then converted to a 2% HNO_3 matrix and the 229:230 ratio measured by inductively-coupled plasma mass spectrometry on a Thermo Element II to determine the yield during precipitation. Mass bias was corrected for using a natural uranium standard (from Physikalisch-Technische Bundesanstalt, Germany) (see Appendix B.6.7.1).

The background count rate was then subtracted from the initial count rate, the result corrected for the precipitation efficiency, and then decay-corrected to the time of sampling and corrected for the in-growth from ^{238}U between sampling and the mid-point of filtration.

The ^{238}U concentration was calculated from salinity as in Appendix B.5.2.

Particles for POC:^{234}Th ratios were collected with *in situ* pumps (ISPs) at 10 stations at 100 m depth. Particles were retained on a 53 µm Nitex screen in the ISPs, rinsed off the screen with filtered (0.2 µm) seawater, and filtered onto 25 mm pre-combusted (4 h at 450 °C) Whatman QMA filters. Filters were dried, mounted on Risø disks, and β-counted as for water samples. After background counting, filters were dismounted, acidified with 3–5 drops 0.1 mol L^{-1} HCl, oven-dried (60 °C overnight), pelletted in solvent-cleaned tin boats, and C and N measured on a Eurovector C/N Element analyser.

B.5.4 ^{234}Th flux calculations

The vertical profiles are then used to calculate the downward flux of ^{234}Th. The change in ^{234}Th activity over time (in dpm m^{-3} d^{-1}) in a given parcel of water can be calculated following *Coale and Bruland* (1985, 1987) as:

$$\frac{\partial A_{Th}}{\partial t} = \lambda A_U - \lambda A_{Th} - P + V \tag{B.3}$$

where A_{Th} and A_U are the activities of ^{234}Th and ^{238}U, λ is the decay-constant of ^{234}Th, P is the downward flux of ^{234}Th on particles, and V is the sum of advection and diffusion.

The simplest way of calculating P is to use a steady-state model, which assumes that the measured ^{234}Th concentrations are not changing over time (*i.e.* $\frac{\partial A_{Th}}{\partial t} = 0$). As physical transport (advection, diffusion) is generally very low outside of upwelling areas or coastal settings it can be neglected in open ocean studies (*Savoye et al.* 2006). The daily rate of ^{234}Th export at a given depth z can then be calculated by integrating the activity balance to the desired depth:

$$P = \int_0^z \lambda(A_U - A_{Th})dz \tag{B.4}$$

In practice, this is done by trapezoid integration of the measured ^{234}Th profile, *i.e.* using the mean of two measurements at successive depths as the ^{234}Th (or ^{238}U) concentration for that layer of the water column. P is thus calculated for each depth layer and then summed between 0 m and the depth of interest — generally the depth at which ^{234}Th and ^{238}U are again in radioactive equilibrium, typically at around 100 m.

Whether the deficit of ^{234}Th is changing or not can be assessed by measuring ^{234}Th profiles repeatedly in the same water mass, ideally over a period of around two weeks (*Savoye et al.* 2006;). Changes in ^{234}Th concentration are typically found during bloom conditions (*Buesseler et al.* 1992, 2005; *Cochran et al.* 2000; *Martin et al.* 2011), and P can be substantially underestimated if they are not taken into account. As ^{234}Th was measured during bloom conditions for Chapter 2, P was calculated using the non-steady-state model of *Buesseler et al.* (1992), which calculates the flux between two successive profiles. Although other formulations of non-steady-state ^{234}Th models have been proposed, these either require more profiles of ^{234}Th than could be taken (*Buesseler et al.* 2005), or a near-continuous record of ^{234}Th flux into sediment traps at around the depth at which P is to be calculated (*Cochran et al.* 2009). P was therefore calculated as:

$$P = P_{Th}^{p1} + \lambda \left[\frac{A_U \left(1 - e^{-\lambda t}\right) + A_{Th}^{p1} e^{-\lambda t} - A_{Th}^{p2}}{\left(1 - e^{-\lambda t}\right)} \right] \tag{B.5}$$

where superscript $p1$ and $p2$ denote activity/flux in at the first and second profile, respectively, t is the time-difference in days between the two profiles, and λ is the decay-constant of ^{234}Th. P is then the flux of ^{234}Th between the two profiles, which is assumed to be constant.

All errors were fully propagated through the calculations using the equations listed in Appendix A.5 (see also *Rutgers van der Loeff et al.* 2006; *Savoye et al.* 2006).

B.6 ^{230}Th

B.6.1 Rationale

^{230}Th is a long-lived nuclide ($t_{1/2} = 75,380$ years) produced *in situ* by α-decay of ^{234}U, which in turn is produced from decay of ^{238}U. Uranium is dissolved and conservative in seawater, with a mean residence time much longer than the time-scale of ocean mixing (*Ku et al.* 1977; *Chen et al.* 1986), although the ^{234}U:^{238}U ratio in seawater is elevated relative to secular equilibrium, with δ^{234}U of 146.8‰ throughout the oceans (*Andersen et al.* 2010). Due to the particle-reactive chemistry of Th in seawater, its residence-time in the ocean is typically ≤30 y, as it is scavenged by sinking particles throughout the water column and removed to the sediments (*Henderson and Anderson* 2003). In 70% of the oceans, the downward flux of ^{230}Th to the sediments is within 30% of the annual production from ^{234}U in the overlying water column, with boundary scavenging at ocean margins thought to be significantly less pronounced than for other particle-reactive elements (*Anderson et al.* 1983; *Lao et al.* 1993; *Henderson et al.* 1999).

Over an annual cycle, the downward flux of ^{230}Th in most open ocean settings should therefore be equal to the annual production of ^{230}Th in the overlying water column. ^{230}Th is therefore a very useful tool to investigate the trapping efficiency of bathypelagic sediment traps: any substantial deviation of the annual cumulative ^{230}Th flux from the annual ^{230}Th production is taken as an indication of under- or over-trapping relative to the true particle flux (*Brewer et al.* 1980; *Bacon et al.* 1985; *Scholten et al.* 2001; *Yu et al.* 2001).

A refinement of this approach was introduced by *Bacon et al.* (1985) to account for the fraction of ^{230}Th that is exported horizontally rather than downwards to the sediment (via horizontal advection and boundary scavenging). This method involves measuring both ^{230}Th and ^{231}Pa in the sediment traps (^{231}Pa is produced *in situ* from ^{235}U, but is less particle reactive than ^{230}Th), and the expected downward flux of ^{230}Th can then be calculated following *Anderson et al.* (1983) from the ratio of ^{230}Th:^{231}Pa in the traps, the ratio of ^{230}Th:^{231}Pa in the overlying water column, and the production of ^{230}Th and ^{231}Pa from U.

The approach using ^{230}Th and ^{231}Pa is undoubtedly preferable, and ^{231}Pa measurements were hence attempted in the sediment trap samples. However, while good results were achieved for ^{230}Th and ^{232}Th, the data for ^{231}Pa were highly suspect and were therefore not used (see Chapter 5.2.3). While this was unfortunate, the ^{230}Th flux alone is still useful, as a comparison of relative efficiency between traps is possible, and also as it is unlikely that a major portion of the ^{230}Th production would be advected horizontally in this region (*Henderson et al.* 1999).

B.6.2 Overview of the approach

To measure ^{230}Th flux into the deep, moored sediment traps (Chapter 5), an isotope-dilution (ID) mass spectrometry method was set up based on the description by *Thomas* (2006) of the method used at the University of Oxford (Dept. of Earth Sciences). The method works by dissolving the samples completely, spiking with the artificial nuclide ^{229}Th, purifying Th by anion exchange chromatography, and then measuring the 230:229 ratio on a multi-collector inductively-coupled plasma mass spectrometer (MC ICP MS). The ^{229}Th is an internal standard that corrects both for losses during chromatography as well as for any short-term fluctuations in the instrument signal during measurement.

The ^{230}Th thus measured is mostly derived from scavenging out of the water column, but an additional portion is contributed by lithogenic particles, in which ^{230}Th is in equilibrium with lithogenic ^{238}U. This latter ("supported") fraction needs to be quantified and subtracted from the total ^{230}Th to yield the quantity of "unsupported", or excess, ^{230}Th, which is termed $^{230}Th_{xs}$. The obvious solution would be to measure U isotopes in the sample, but a potentially major fraction of U in marine particles is in fact authigenic U, either precipitated in reducing micro-environments within particles undergoing remineralization, or complexed to organic matter (*Anderson* 1982; note that the residence time of particles in the water column is much too short for significant in-growth of ^{230}Th from the authigenic U). The supported ^{230}Th fraction is therefore calculated from the measured ^{232}Th in the sample, which is thought to be overwhelmingly of lithogenic origin (*Brewer et al.* 1980), and the known ^{238}U:^{232}Th activity ratio

in crustal rocks of 0.8±0.2 (*Yu et al.* 2001):

$$^{230}\mathrm{Th}_{\mathrm{xs}} = \mathrm{A}_{230} - 0.8{\pm}0.2 * \mathrm{A}_{232},$$

where A_{230} and A_{232} are the total activities (in dpm) of ^{230}Th and ^{232}Th. Although the concentration of ^{232}Th in terms of mass is far greater than that of ^{230}Th, the activity of ^{232}Th is much smaller due to its far longer half-life, and thus the correction to these samples was relatively minor (<8.5%).

B.6.3 Laboratory procedures

All acids used were either purified by sub-boiling distillation, or were Romil s.p.a. grade (except acids for cleaning equipment, which were Fisher Trace Metal grade). All solutions were prepared gravimetrically by weighing the solutions (at least three replicate weighings each) on an analytical balance with 0.0001 g readability. Problems with static charge when weighing Teflon-ware were overcome successfully by using a Milty Zerostat anti-static gun, such that standard deviations of 3–5 replicate weighings rarely exceeded 0.0003 g.

Initial sample handling (swimmer picking, sample splitting, filtration, drying, and weighing) was performed in a regular laboratory environment, not under clean conditions (although all relevant labware was cleaned with 10% HCl and rinsed with MilliQ water). Subsequent work was conducted in a clean laboratory at NOCS kept under over-pressure with filtered air, except for the sample digestion step involving perchloric acid ($\mathrm{HClO_4}$), which could not be conducted in the clean laboratory owing to the additional safety features required of fumehoods for handling $\mathrm{HClO_4}$.

All ICP-MS measurements were made on a Thermo Neptune MC-ICP-MS equipped with a CETAC Aridus desolvating nebuliser (which offers around 10× higher sensitivity than a spray chamber, because a far greater proportion of the sample is introduced to the plasma). The instrument had two arrays of four Faraday cups each on either side of a central, or axial, detector. Either a Faraday cup or a secondary electron multiplier (SEM, an ion counter) could be used as the axial cup for any measurement. Faraday cups are suitable for measurements at higher concentrations (usually in the ng and upper pg range, e.g. ^{238}U and ^{232}Th), and work by recording the electrical current caused by an incoming ion beam. The SEM counts the arrival of individual ions, each of which triggers an electron multiplier cascade. It is extremely sensitive, readily measuring to concentrations in the fg g^{-1} range, but cannot be used for ion beams exceeding around 1 million counts per second.

B.6.4 Preparation and calibration of the ^{229}Th spike

Obtaining a solution of ^{229}Th that is both isotopically very pure (with no, or only trace contamination from ^{230}Th and ^{232}Th) and which has a well-known concentration is of fundamental importance. ^{229}Th is the only viable Th isotope for an ID spike, as its long half-life means that it is not very radioactive at the concentrations required (unlike ^{228}Th), and, being an

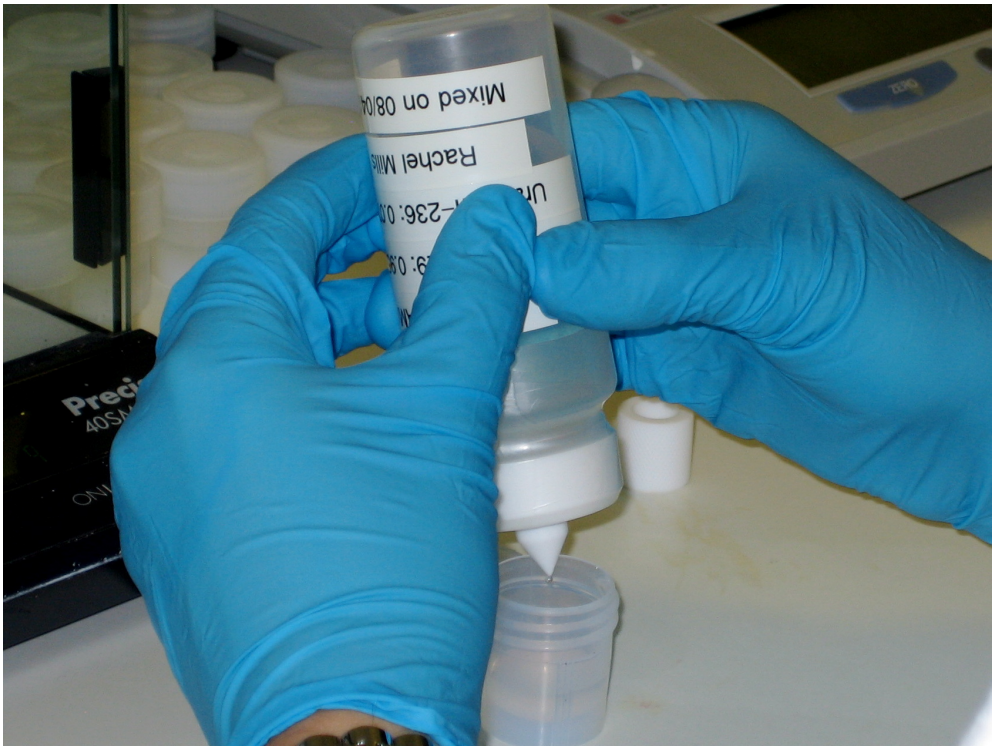

Figure B.6 – Teflon bottle for storage of the ^{229}Th + ^{236}U mixed spike with custom-made PTFE cap for dispensing.

artificial isotope, it is not contained in the sample. ^{232}Th cannot be used, as it is contained in comparatively very high concentrations in virtually any environmental sample.

As no well-calibrated ^{229}Th spike was available, a new spike was made from an existing stock solution at NOCS (∼26.5 Bq mL^{-1}). The stock solution was first mixed with a spike of ^{236}U to give a final molar U:Th ratio of ∼200, so that the spike could be used simultaneously for ^{238}U measurements in ocean sediments. It was then heavily diluted with 3 mol L^{-1} HNO_3. This spike is referred to as the "Southampton Mixed Spike" (SMS), and was stored in a 125 mL Teflon bottle with a custom-made PTFE cap (Figure B.6). The cap has a conical nozzle that is covered by a tightly-fitting push cap, and has a 0.3 mm diameter hole through which spike can be dispensed. This system allows spike to be dispensed through the nozzle without actually opening the bottle, and when the push-cap is forced back onto the nozzle any residual solution left in the nozzle is forced back into the bottle. Thus, evaporation of the spike over years of storage will be minimal.

The SMS was calibrated (*i.e.* the concentration of ^{229}Th determined) against a synthetic solution of ^{230}Th (product TZP10010 from HighTechnology Sources, UK), the concentration of which was certified to ±1.6% uncertainty at the 2σ level. Nine lots of SMS were mixed with ^{230}Th solution, but before the SMS was diluted with HNO_3, so that the concentrations were high enough to measure Th on Faraday cups. A tenth aliquot of SMS was removed to determine the level of ^{230}Th and ^{232}Th contamination. (to summarise: ^{229}Th stock was mixed with a small volume of ^{236}U solution, then nine aliquots were removed and mixed with ^{230}Th solution

for calibration measurements, a tenth aliquot was removed to determine isotopic purity, and then the ^{229}Th+^{236}U solution was diluted with HNO_3 to yield the final SMS). The ten aliquots were evaporated on a hotplate in Savillex Teflon pots and made up in a 2% HNO_3 matrix.

The concentration of ^{229}Th in the SMS was determined by measuring the 230:229 ratio of the calibration aliquots on a Thermo Neptune MC-ICP-MS in static mode on Faraday cups. An acid blank was run between each aliquot, and mass bias (Appendix B.6.7.1) was corrected for by measuring the 238:235 ratio in the natural uranium standard CRM-145 (New Brunswick Laboratory, USA) in static mode on Faraday cups. The corrected 229:230 ratio was then multiplied by the amount of ^{230}Th added to each aliquot and divided by the mass of SMS solution used, yielding nine replicate estimates of the ^{229}Th concentration in the SMS. The mean of these was taken as the real ^{229}Th concentration of the SMS. The error was calculated by combining the relative standard deviation of the nine measurements with the 1σ uncertainty in the ^{230}Th concentration (0.8%) using the standard error propagation formula. These values were then adjusted for the dilution of the SMS to its final concentration as described above. The final ^{229}Th concentration in the diluted SMS was determined as $129.27 \pm 1.04\,\mathrm{pg\,g^{-1}}$. ^{232}Th was present at only about 2% of the signal strength of ^{229}Th, so at $\leq 3\,\mathrm{pg\,g^{-1}}$, which is millions of times less than the ^{232}Th concentration in a sample.

B.6.5 Sample dissolution and spiking

Marine pelagic particles contain low quantities of ^{230}Th (typically a few tens of $\mathrm{pg\,g^{-1}}$; *Scholten et al.* 2001; *Yu et al.* 2001; *Fleisher and Anderson* 2003), and a preliminary calculation suggested that at least 100 mg per sample would be needed. Because many samples contained much less material, three composite samples were made for each trap to cover "winter" (22 November to 09 May), "spring" (09 May to 20 June), and "summer" (20 June to 18 July). Each composite sample was made by pooling either 6%, 12.5%, or 15.5% of each contributing sample. The composite samples ranged from 100–300 mg (Table B.1). Additionally, three Southern Ocean sediment samples from the CROZEX study were prepared (100 mg each), as these had been already analysed for Th in the University of Oxford, and thus provided a check on the reliability of the analyses conducted at NOCS (Gideon Henderson's laboratory in Oxford has extensive experience in analysing Th, U, and Pa isotopes in a range of sample types).

Samples were weighed onto discs of aluminium foil on a Sartorius ME-5 microbalance, and washed off the discs into 15 mL Savillex Teflon pots with MilliQ (wetting the sediment prevented loss due to static). The weighing error was thus <0.1%. Samples were then acidified by dropwise addition of concentrated HNO_3 to dissolve carbonates, evaporated on a hotplate, and refluxed overnight with concentrated HNO_3 on a hotplate at 100 °C. They were then evaporated, refluxed overnight with 5 mL aqua regia at 90 °C, evaporated, refluxed overnight with more aqua regia, and evaporated again. These initial steps were chosen to oxidise as much organic matter as possible before using perchloric acid. Samples were then refluxed overnight with 2.25 mL concentrated $HClO_4$ and 3 mL concentrated HF at 150 °C, evaporated to near-dryness, evaporated again after adding a further 5 mL concentrated $HClO_4$ (to ensure that any fluorides were driven off as HF). Repeated additions of 2–4 mL of $7.5\,\mathrm{mol\,L^{-1}}$ HNO_3 were then made,

with samples evaporated to dryness in between at 180 °C to drive off any remaining $HClO_4$. They were then brought up in 4 mL 7.5 mol L^{-1} HNO_3, and spiked with around 0.1 g SMS (around 13 pg ^{229}Th).

Two procedural blanks were prepared: the first was a simple procedural blank, starting from rinsing a blank aluminium disk with MilliQ into a Savillex pot, and treating the blank exactly like the samples. The second was a "lab blank" to test whether samples might have become contaminated during swimmer-picking in the non-clean particle flux laboratory. It was prepared by placing a clean glass Petri dish of the kind used for swimmer picking half-filled with MilliQ onto the extraction bench in the particle flux laboratory (where all swimmer picking was done). The dish was left there open for 48 h, but the MilliQ was refilled after 24 h. After 48 h the contents of the dish were rinsed with MilliQ into a Savillex pot, and the blank treated exactly like a sample.

B.6.6 Anion exchange chromatography

Anion exchange columns were filled with slurried Bio-Rad AG 1-X8 100–200 mesh chloride resin, which was then cleaned with MilliQ and 6 mol L^{-1} HCl, and conditioned with 7.5 mol L^{-1} HNO_3. Each sample was loaded onto one column in 7.5 mol L^{-1} HNO_3 and the column washed with 7.5 mol L^{-1} HNO_3. Th was then eluted with 6 mol L^{-1} HCl into Savillex Teflon beakers, and the purified fractions evaporated on a hotplate and stored in 7.5 mol L^{-1} HNO_3. This procedure purifies Th to a sufficient degree to allow a substantial part of each sample to be introduced into the mass spectrometer; otherwise the sample would be so rich in other dissolved constituents that the uptake capillary could clog, or the plasma be affected.

B.6.7 Th isotope measurement

The purified samples contained three Th isotopes, 229, 230, and 232, each of which needed to be measured. ^{232}Th was present in ng amounts, and thus needed to be measured on a Faraday cup, but samples contained only a few pg of ^{229}Th and ^{230}Th, so both needed to be measured on the SEM ion counter. As there was only one SEM a peak-jumping method was set up to alternately measure masses 229 and 230 in the SEM: the magnet was first set such that mass 229 fell into the SEM, then the magnet was jumped by 1 amu such that mass 230 entered the SEM. 50 such switches were made for each measurement and the mean and standard error calculated automatically. However, because of short-term fluctuations in the mass spectrometer (especially in the plasma, affecting the ionisation efficiency), the ratio of two alternately measured masses will be less accurate than if both masses were measured simultaneously. Therefore, Faraday cups were positioned such that ^{232}Th was measured in both steps of the peak-jump, but in different Faraday cups, and the ratio of $\frac{229}{230}$ calculated as the ratio of $\frac{229}{232}$ measured in Step 1 to $\frac{230}{232}$ measured in Step 2. Both $\frac{229}{232}$ and $\frac{230}{232}$ were first corrected for mass bias (Appendix B.6.7.1). The $\frac{229}{232}$ ratio was then further corrected for the SEM gain, which is ratio of SEM signal to the signal that a Faraday cup would measure given the identical ion beam, to obtain the correct ^{232}Th concentration. SEM gain was measured from the ^{235}U:^{238}U ratio in CRM-145 at low concentrations, with mass 235 entering the SEM, and correcting the $\frac{235}{238}$ ratio for mass

Trap-Cup	Weight used (mg)	% of sample	Weight of composite (mg)	Trap-Cup	Weight used (mg)	% of sample	Weight of composite (mg)
42-1	38.00	12.4	227.26	44-1	54.30	12.5	220.02
42-2	41.44	12.5		44-2	29.56	12.5	
42-3	41.29	12.5		44-3	6.90	12.5	
42-4	34.65	12.5		44-4	18.50	12.5	
42-5	9.025	12.5		44-5	4.81	12.5	
42-6	16.22	12.5		44-6	7.74	12.5	
42-7	6.62	12.4		44-7	19.62	12.5	
42-8	3.54	12.5		44-8	16.39	12.5	
42-9	5.32	12.4		44-9	7.63	12.5	
42-10	24.30	12.5		44-10	7.97	12.5	
42-11	1.63	12.6		44-11	25.98	12.5	
42-12	5.22	12.5		44-12	20.61	12.5	
42-13	42.11	12.5	169.42	44-13	75.76	6.2	225.11
42-14	110.19	12.5		44-14	117.64	6.3	
42-15	17.12	12.5		44-15	31.71	6.3	
42-16	21.64	12.5	190.92	44-16	39.04	12.5	142.06
42-17	65.31	12.5		44-17	28.02	12.5	
42-18	103.97	12.5		44-18	75.00	12.5	
43-1	50.89	12.5	218.64	45-1	14.17	12.6	104.44
43-2	34.19	12.5		45-2	25.05	15.6	
43-3	26.73	12.5		45-3	17.60	15.6	
43-4	25.42	12.5		45-4	7.45	15.6	
43-5	7.02	12.5		45-5	3.81	15.6	
43-6	15.28	12.5		45-6	2.78	15.6	
43-7	17.20	12.5		45-7	8.93	15.6	
43-8	12.93	12.5		45-8	8.03	15.6	
43-9	7.27	12.5		45-9	4.56	15.7	
43-10	3.13	12.5		45-10	3.45	15.6	
43-11	2.30	12.5		45-11	2.03	15.7	
43-12	6.28	12.5		45-12	6.57	15.7	
43-13	44.17	12.5	289.61	45-13	41.44	12.5	251.03
43-14	172.62	12.5		45-14	132.40	12.5	
43-15	72.82	12.5		45-15	77.19	12.5	
43-16	72.29	12.5	132.19	45-16	21.52	12.5	134.11
43-17	18.97	12.5		45-17	65.37	12.5	
43-18	40.93	12.5		45-18	47.22	12.5	

Table B.1 – Weights of sediment in the composite samples from the deep, moored sediment traps used for ^{230}Th analysis.

bias assessed with a higher-concentration CRM-145 solution (where 235 and 238 could both be measured on Faraday cups). Note that a gain correction was not necessary for the $\frac{229}{230}$ ratio, as the gain correction cancels out in the calculation. The gain of the Faraday cups is automatically calibrated approximately once every week by applying a constant voltage to all cups and correcting for any differences in signal between cups.

The concentration of ^{230}Th and ^{232}Th in each sample was then calculated from the corrected $\frac{230}{229}$ and $\frac{232}{229}$ ratios, the known quantity of ^{229}Th added to each sample, and the dry weight of each sample. To calculate the $^{230}Th_{xs}$ in each sample, the total ^{230}Th content was corrected for lithogenic ^{230}Th as described in Appendix B.6.2.

The total ^{230}Th content determined for the three sediment samples that had already been analysed in Oxford was 98.5±0.94%, 103±3.4%, and 99.1±3.2% of the values obtained in Oxford. Interestingly, the agreement for ^{232}Th was less good: values determined in Southampton were 88.3±2.1%, 93.1±3.1%, and 91.9±2.2% of the Oxford values. However, given the very small magnitude of the correction for ^{232}Th, and the large uncertainty associated with it, this under-estimation of ^{232}Th did not significantly impact the estimate of $^{230}Th_{xs}$.

Neither of the procedural blanks contained significant levels of ^{230}Th or ^{232}Th compared to the samples ($\leq$1.0% for ^{230}Th, and $<$1.3% for ^{232}Th).

B.6.7.1 Mass bias

The ratio of two isotopes measured in a mass spectrometer usually differs slightly from the true ratio in the sample because of mass bias. An ion beam in a mass spectrometer becomes depleted in the lighter isotope as the beam travels from the plasma to the detectors, and the measurement is hence biased heavy. This must be corrected for by measuring the isotopic ratio of a standard with an exactly known isotopic composition. Ideally, a standard of the element to be measured in the sample would be used, but because mass bias is caused mostly by physical factors, the natural uranium standard CRM-145 was used here (also used by *Thomas* 2006). CRM-145 has a very well-constrained 238:235 isotopic ratio of 137.88.

The most appropriate mass bias law for correcting measured isotopic ratios remains a matter of debate (*Thomas* 2006; *Meija et al.* 2009). However, the final propagated uncertainties in the measurements were going to be no smaller than several percent, while differences in mass bias laws change the result by much less than 1%, and thus a simple linear form was used:

$$R_t = \frac{R_m}{1 + \Delta M * f}, \tag{B.6}$$

where R_t and R_m are the true and measured isotopic ratios in the sample, respectively, ΔM is the mass difference between the isotopes (in amu), and f is the mass bias fractionation factor, calculated as:

$$f = \frac{\frac{Rs_m}{Rs_t} - 1}{\Delta M}, \tag{B.7}$$

where Rs_t and Rs_m are the true and measured isotopic ratios in the standard (here 238:235 ratios in CRM-145), and ΔM is the mass difference between the isotopes (in amu).

B.7 Net Community Production from O_2:Ar

Photosynthesis releases O_2 while respiration removes O_2. The concentration of O_2 in seawater is therefore partially a function of the balance between whole-community photosynthesis and respiration, which is termed net community production, NCP. However, three physical processes also affect the O_2 concentration significantly; these are bubble injection when waves break, temperature, and atmospheric pressure, and these factors must be accounted for in order to estimate NCP from O_2 data. This can be done if concomitant measurements of Ar are taken, following the theory developed by *Craig and Hayward* (1987). Ar is conservative, and thus its concentration is only a function of these physical processes, but furthermore, its solubility properties are very similar to those of O_2 — N_2, for instance, has rather different properties — and thus the deviation of the measured O_2:Ar ratio in seawater from the value it would have at equilibrium with the atmosphere (for the given temperature and salinity) can be taken as the biological O_2 saturation (*Craig and Hayward* 1987), BOS. A negative value of BOS would indicate net O_2 consumption, *i.e.* net heterotrophic conditions, and a positive value would indicate net O_2 production, *i.e.* net autotrophic conditions. NCP can then be calculated as the instantaneous biological air-sea O_2 flux following *Reuer et al.* (2007):

$$\mathrm{NCP}\ (\mathrm{mmol\,O_2\,m^{-2}\,d^{-1}}) = \left[\frac{\left(\frac{\mathrm{O_2}}{\mathrm{Ar}}\right)_{\mathrm{smpl}}}{\left(\frac{\mathrm{O_2}}{\mathrm{Ar}}\right)_{\mathrm{eq}}} - 1\right] [\mathrm{O_2}]_{\mathrm{eq}} k\rho, \tag{B.8}$$

where $\left(\frac{\mathrm{O_2}}{\mathrm{Ar}}\right)_{\mathrm{smpl}}$ is the measured O_2:Ar ratio, $\left(\frac{\mathrm{O_2}}{\mathrm{Ar}}\right)_{\mathrm{eq}}$ is the ratio that the measured water would have at equilibrium with the atmosphere, $[\mathrm{O_2}]_{\mathrm{eq}}$ is the O_2 concentration at equilibrium with the atmosphere ($\mathrm{mmol\,kg^{-1}}$), k is the gas transfer velocity ($\mathrm{m\,d^{-1}}$; calculated from local wind-speed), and ρ is the water density ($\mathrm{kg\,m^{-3}}$); the term in square brackets is the BOS. The integration time-scale of the method is 1–2 weeks, depending on the value of k. O_2:Ar measurements can now be taken continuously throughout a cruise using mass spectrometers connected to a ship's underway surface seawater supply (*Kaiser et al.* 2005; *Cassar et al.* 2009).

Two factors may significantly bias the O_2:Ar method, causing NCP to be under-estimated, and are discussed more in Section 3.4.3. The first is that any upward transport of (O_2-undersaturated) water across the thermocline would lower the BOS. However, as LohaFEX was not located in an upwelling region, it is unlikely that this introduced significant errors. A greater problem would be respiration by biofilms in the tubing of underway seawater supplies (*Juranek et al.* 2010). While this error is very difficult to quantify, it is also significantly temperature-dependent, and as surface water temperatures during LohaFEX were consistently below 10 °C, this was hopefully no major source of error — but it cannot be ruled out that NCP was significantly under-estimated.

Bibliography

Al-Mutairi, H., and M. R. Landry (2001), Active export of carbon and nitrogen at Station ALOHA by diel migrant zooplankton, *Deep-Sea Research Part II-Topical Studies in Oceanography*, *48*, 2083–2103.

Alldredge, A. L., and C. C. Gotschalk (1989), Direct observations of the mass flocculation of diatom blooms — Characteristics, settling velocities and formation of diatom aggregates, *Deep-Sea Research Part A-Oceanographic Research Papers*, *36*, 159–171.

Alldredge, A. L., and G. A. Jackson (1995), Aggregation in marine systems — Preface, *Deep-Sea Research Part II-Topical Studies in Oceanography*, *42*, 1–7.

Alldredge, A. L., U. Passow, and B. E. Logan (1993), The abundance and significance of a class of large, transparent organic particles in the ocean, *Deep-Sea Research Part I-Oceanographic Research Papers*, *40*, 1131–1140.

Alldredge, A. L., C. Gotschalk, U. Passow, and U. Riebesell (1995), Mass aggregation of diatom blooms: insights from a mesocosm study, *Deep-Sea Research Part II-Topical Studies in Oceanography*, *42*(1), 9–27.

Amon, R. M. W., H.-P. Fitznar, and R. Benner (2001), Linkages among the bioreactivity, chemical composition, and diagenetic state of marine dissolved organic matter, *Limnology & Oceanography*, *46*(2), 287–297.

Andersen, M. B., C. H. Stirling, B. Zimmermann, and A. N. Halliday (2010), Precise determination of the open ocean $^{234}U/^{238}U$ composition, *Geochemistry Geophysics Geosystems*, *11*(12), doi:10.1029/2010GC003318.

Anderson, R. F. (1982), Concentration, vertical flux, and remineralization of particulate uranium in seawater, *Geochimica et Cosmochimica Acta*, *46*, 1293–1299.

Anderson, R. F., M. P. Bacon, and P. G. Brewer (1983), Removal of ^{230}Th and ^{231}Pa at ocean margins, *Earth and Planetary Science Letters*, *66*, 73–90.

Antia, A. N., E. Bauerfeind, B. von Bodungen, and U. Zeller (1993), Abundance, encystment and sedimentation of Acantharia during autumn 1990 in the East Greenland Sea, *Journal of Plankton Research*, *15*, 99–114.

Aramaki, T., Y. Nojiri, and K. Imai (2009), Behaviour of particulate materials during iron fertilization experiments in the Western Subarctic Pacific (SEEDS and SEEDS II), *Deep-Sea Research Part II-Topical Studies in Oceanography*, *56*, 2875–2888.

Archer, D. E., and E. Maier-Reimer (1994), Effect of deep-sea sedimentary calcite preservation on atmospheric CO_2 concentration, *Nature*, *367*, 260–264.

Armstrong, R. A., C. Lee, J. I. Hedges, S. Honjo, and S. G. Wakeham (2002), A new, mechanistic model for organic carbon fluxes in the ocean based on the quantitative association of POC with ballast minerals, *Deep-Sea Research Part II-Topical Studies in Oceanography*, *49*, 219–236.

Aumont, O., and L. Bopp (2006), Globalizing results from ocean in situ iron fertilization studies, *Global Biogeochemical Cycles*, *20*, doi:10.1029/2005GB002591.

Azam, F., T. Fenchel, J. G. Field, J. S. Gray, L. A. Meyer-Reil, and F. Thingstad (1983), The ecological role of water-column microbes in the sea, *Marine Ecology Progress Series*, *10*, 257–263.

Azetsu-Scott, K., and U. Passow (2004), Significance of transparent exopolymer particles (TEP) in the upper ocean, *Limnology & Oceanography*, *49*, 741–748.

Backhaus, J. O., E. N. Hegseth, H. Wehde, X. Irigoien, K. Hatten, and K. Logemann (2003), Convection and primary production in winter, *Marine Ecology Progress Series*, *251*, 1–14.

Bacon, M. P., and R. F. Anderson (1982), Distribution of thorium isotopes between dissolved and particulate forms in the deep sea, *Journal of Geophysical Research*, *87*(C3), 2045–2056.

Bacon, M. P., C.-A. Huh, A. P. Fleer, and W. G. Deuser (1985), Seasonality in the flux of natural radionuclides and plutonium in the deep Sargasso Sea, *Deep-Sea Research*, *32*(3), 273–286.

Bagniewski, W., K. Fennel, M. J. Perry, and E. A. D'Asaro (2011), Optimizing models of the North Atlantic spring bloom using physical, chemical and bio-optical observations from a Lagrangian float, *Biogeosciences*, *8*, 1291–1307.

Bairbakhish, A. N., J. Bollmann, C. Sprengel, and H. R. Thierstein (1999), Disintegration of aggregates and coccospheres in sediment trap samples, *Marine Micropaleontology*, *37*, 219–223.

Baker, E. T., H. B. Milburn, and D. A. Tennant (1988), Field assessment of sediment trap efficiency under varying flow conditions, *Journal of Marine Research*, *46*, 573–592.

Barker, S., J. A. Higgins, and H. Elderfield (2003), The future of the carbon cycle: review, calcification respone, ballast and feedback on atmospheric CO_2, *Philosophical Transactions of the Royal Society A-Mathematical Physical and Engineering Sciences*, *361*, 1977–1999, doi:10.1089/rsta.2003.1238.

Bathmann, U. V., T. T. Noji, and B. von Bodungen (1991), Sedimentation of pteropods in the Norwegian Sea in autumn, *Deep-Sea Research*, *38*, 1341–1360.

Baudoux, A.-C., M. J. W. Veldhuis, H. J. Witte, and C. P. D. Brussaard (2007), Viruses as mortality agents of picophytoplankton in the deep chlorophyll maximum layer during IRONAGES III, *Limnology & Oceanography*, *52*(6), 2519–2519.

Beaulieu, S. E. (2002), Accumulation and fate of phytodetritus on the sea floor, *Oceanography and Marine Biology: An Annual Review*, *40*, 171–232.

Beers, J. R., and G. L. Stewart (1970), Micro-zooplankters in the plankton communities of the upper waters of the eastern tropical Pacific, *Deep-Sea Research*, *18*, 861–883.

Bence, J. R. (1995), Analysis of short time series: correcting for autocorrelation, *Ecology*, *76*(2), 628–639.

Benitez-Nelson, C. R., K. O. Buesseler, M. Rutgers van der Loeff, J. Andrews, L. Ball, G. Crossin, and M. A. Charette (2001), Testing a new small-volume technique for determining ^{234}Th in seawater, *Journal of Radioanalytical and Nuclear Chemistry*, *248*(3), 795–799.

Berelson, W. M. (2001), The flux of particulate organic carbon into the ocean interior: a comparison of four U.S. JGOFS regional studies, *Oceanography*, *14*(4), 59–67.

Berelson, W. M. (2002), Particle settling rates increase with depth in the ocean, *Deep-Sea Research Part II-Topical Studies in Oceanography*, *49*, 237–251.

Bernstein, R. E., and R. H. Byrne (2004), Acantharians and marine barite, *Marine Chemistry*, *86*, 45–50, doi:10.1016/j.marchem.2003.12.003.

Bernstein, R. E., P. R. Betzer, R. A. Feely, R. H. Byrne, M. F. Lamb, and A. F. Michaels (1987), Acantharian fluxes and strontium to chlorinity ratios in the North Pacific Ocean, *Science*, *237*, 1490–1494.

Bernstein, R. E., R. H. Byrne, P. R. Betzer, and A. M. Greco (1992), Morphologies and transformations of celestite in seawater — the role of acantharians in strontium and barium geochemistry, *Geochimica et Cosmochimica Acta*, *56*, 3273–3279.

Bernstein, R. E., R. H. Byrne, and J. Schijf (1998), Acantharians: a missing link in the oceanic biogeochemistry of barium, *Deep-Sea Research Part I-Oceanographic Research Papers*, *45*, 491–505.

Bernstein, R. E., S. A. Kling, and D. Boltovskoy (1999), Acantharia, in *South Atlantic Zooplankton*, vol. 1, edited by D. Boltovskoy, pp. 75–147, Backhuys Publishers, Leiden.

Biddanda, B., and R. Benner (1997), Carbon, nitrogen, and carbohydrate fluxes during the production of particulate and dissolved organic matter by marine phytoplankton, *Limnology & Oceanography*, *42*(3), 506–518.

Bidigare, R. R., K. L. Hanson, K. O. Buesseler, S. G. Wakeham, K. H. Freeman, R. D. Pancost, F. J. Millero, P. Steinberg, B. N. Popp, M. Latasa, M. R. Landry, and E. A. Laws (1999), Iron-stimulated changes in ^{13}C fractionation and export by equatorial Pacific phytoplankton: toward a paleogrowth rate proxy, *Paleoceanography*, *14*(5), 589–595.

Bidle, K. D., and F. Azam (1999), Accelerated dissolution of diatom silica by marine bacterial assemblages, *Nature*, *397*, 508–512.

Bidle, K. D., and F. Azam (2001), Bacterial control of silicon regeneration from diatom detritus: significance of bacterial ectohydrolases and species identity, *Limnology & Oceanography*, *46*(7), 1606–1623.

Billett, D. S. M., R. S. Lampitt, A. L. Rice, and R. F. C. Mantoura (1983), Seasonal sedimentation of phytoplankton to the deep-sea benthos, *Nature*, *302*, 520–522.

Billett, D. S. M., B. J. Bett, C. L. Jacobs, I. P. Rouse, and B. D. Wigham (2006), Mass deposition of jellyfish in the deep Arabian Sea, *Limnology & Oceanography*, *51*(5), 2077–2083.

Bishop, J. K. B., and T. Wood (2008), Particulate matter chemistry and dynamics in the twilight zone at VERTIGO ALOHA and K2 sites, *Deep-Sea Research Part I-Oceanographic Research Papers*, *55*, 1684–1706.

Bishop, J. K. B., T. J. Wood, R. E. Davis, and J. T. Sherman (2004), Robotic observations of enhanced carbon biomass and export at 55 °S during SOFeX, *Science*, *304*, 417–420, doi:10.1126/science.1087717.

Blain, S., B. Quéguiner, L. Armand, S. Belviso, B. Bombled, L. Bopp, A. Bowie, C. Brunet, C. Brussaard, F. Carlotti, U. Christaki, A. Corbière, I. Durand, F. Ebersbach, J.-L. Fuda, N. Garcia, L. Gerringa, B. Griffiths, C. Guigue, C. Guillerm, S. Jacquet, C. Jeandel, P. Laan, D. Lefèvre, C. L. Monaco, A. Malits, J. Mosseri, I. Obernosterer, Y.-H. Park, M. Picheral, P. Pondaven, T. Remenyi, V. Sandroni, G. Sarthou, N. Savoye, L. Scouarnec, M. Souhaut, D. Thuiller, K. Timmermans, T. Trull, J. Uitz, P. van Beek, M. Veldhuis, D. Vincent, E. Viollier, L. Vong, and T. Wagener (2007), Effect of natural iron fertilization on carbon sequestration in the Southern Ocean, *Nature*, *446*, 1070–1074, doi:10.1038/nature05700.

Bottazzi, E. M., and M. G. Andreoli (1982), Distribution of adult and juvenile Acantharia (Protozoa, Sarcodina) in the Atlantic Ocean, *Journal of Plankton Research*, *4*, 757–777.

Boyd, P. W., and P. P. Newton (1999), Does planktonic community structure determine downward particulate organic carbon flux in different oceanic provinces?, *Deep-Sea Research Part I-Oceanographic Research Papers*, *46*, 63–91.

Boyd, P. W., and T. W. Trull (2007), Understanding the export of biogenic particles in oceanic waters: is there consensus?, *Progress in Oceanography*, *72*, 276–312, doi:10.1016/j.pocean.2006.10.007.

Boyd, P. W., R. Strzepek, S. Takeda, G. Jackson, C. S. Wong, R. M. McKay, C. Law, H. Kiyosawa, H. Saito, N. Sherry, K. Johnson, J. Gower, and N. Ramaiah (2005), The evolution and termination of an iron-induced mesoscale bloom in the northeast subarctic Pacific, *Limnology & Oceanography*, *50*(6), 1872–1886.

Boyd, P. W., T. Jickells, C. S. Law, S. Blain, E. A. Boyle, K. O. Buesseler, K. H. Coale, J. J. Cullen, H. J. W. de Baar, M. Follows, M. Harvey, C. Lancelot, M. Levasseur, N. P. J. Owens, R. Pollard, R. B. Rivkin, J. Sarmiento, V. Schoemann, V. Smetacek, S. Takeda, A. Tsuda, S. Turner, and A. J. Watson (2007), Mesoscale iron enrichment experiments 1993-2005: synthesis and future directions, *Science*, *315*, 612–617.

Bratbak, G., J. K. Egge, and M. Heldal (1993), Viral mortality of the marine alga *Emiliania huxleyi* (Haptophyceae) and termination of algal blooms, *Marine Ecology Progress Series*, *93*, 39–48.

Brewer, P. G., Y. Nozaki, D. W. Spencer, and A. P. Fleer (1980), Sediment trap experiments in the deep North Atlantic: isotopic and elemental fluxes, *Journal of Marine Research*, *38*, 703–728.

Broecker, W., and E. Clark (2009), Ratio of coccolith $CaCO_3$ to foraminifera $CaCO_3$ in late Holocene deep sea sediments, *Paleoceanography*, *24*, doi:10.1029/2009PA001731.

Brown, C. W., and J. A. Yoder (1994), Coccolithophorid blooms in the global ocean, *Journal of Geophysical Research*, *99*(C4), 7467–7482.

Buesseler, K. O. (1998), The decoupling of production and particulate export in the surface ocean, *Global Biogeochemical Cycles*, *12*, 297–310.

Buesseler, K. O., and P. W. Boyd (2009), Shedding light on processes that control particle export and flux attenuation in the twilight zone of the open ocean, *Limnology & Oceanography*, *54*, 1210–1232.

Buesseler, K. O., M. P. Bacon, J. K. Cochran, and H. D. Livingston (1992), Carbon and nitrogen export during the JGOFS North-Atlantic Bloom Experiment estimated from Th-234:U-238 disequilibria, *Deep-Sea Research Part A-Oceanographic Research Papers*, *39*, 1115–1137.

Buesseler, K. O., L. Ball, J. Andrews, J. K. Cochran, D. J. Hirschberg, M. P. Bacon, A. Fleer, and M. Brzezinski (2001), Upper ocean export of particulate organic carbon and biogenic silica in the Southern Ocean along 170°W, *Deep-Sea Research Part II-Topical Studies in Oceanography*, *48*, 4275–4297, doi: 10.1016/S0967-0645(01)00089-3.

Buesseler, K. O., J. E. Andrews, S. M. Pike, and M. A. Charette (2004), The effects of iron fertilization on carbon sequestration in the Southern Ocean, *Science*, *304*, 414–417, doi:10.1126/science.1086895.

Buesseler, K. O., J. E. Andrews, S. M. Pike, M. A. Charette, L. E. Goldson, M. A. Brzezinski, and V. P. Lance (2005), Particle export during the Southern Ocean Iron Experiment (SOFeX), *Limnology & Oceanography*, *50*(1), 311–327.

Buesseler, K. O., C. R. Benitez-Nelson, S. B. Moran, A. Burd, M. Charette, J. K. Cochran, L. Coppola, N. S. Fisher, S. W. Fowler, W. Gardner, L. D. Guo, O. Gustafsson, C. Lamborg, P. Masque, J. C. Miquel, U. Passow, P. H. Santschi, N. Savoye, G. Stewart, and T. Trull (2006), An assessment of particulate organic carbon to thorium-234 ratios in the ocean and their impact on the application of Th-234 as a POC flux proxy, *Marine Chemistry*, *100*, 213–233.

Buesseler, K. O., A. N. Antia, M. Chen, S. W. Fowler, W. D. Gardner, O. Gustafsson, K. Harada, A. F. Michaels, M. Rutgers van der Loeff, M. Sarin, D. K. Steinberg, and T. Trull (2007a), An assessment of the use of sediment traps for estimating upper ocean particle fluxes, *Journal of Marine Research*, *65*, 345–416.

Buesseler, K. O., C. H. Lamborg, P. W. Boyd, P. J. Lam, T. W. Trull, R. R. Bidigare, J. K. B. Bishop, K. L. Casciotti, F. Dehairs, M. Elskens, M. Honda, D. M. Karl, D. A. Siegel, M. W. Silver, D. K. Steinberg, J. Valdes, B. Van Mooy, and S. Wilson (2007b), Revisiting carbon flux through the ocean's twilight zone, *Science*, *316*, 567–570.

Buesseler, K. O., C. Lamborg, P. Cai, R. Escoube, R. Johnson, S. Pike, P. Masque, D. McGillicuddy, and E. Verdeny (2008), Particle flux associated with mesoscale eddies in the Sargasso Sea, *Deep-Sea Research Part II-Topical Studies in Oceanography*, *55*, 1426–1444, doi:10.1016/j.dsr2.2008.02.007.

Buesseler, K. O., S. Pike, K. Maiti, C. H. Lamborg, D. A. Siegel, and T. W. Trull (2009), Thorium-234 as a tracer of spatial, temporal and vertical variability in particle flux in the North Pacific, *Deep-Sea Research Part I-Oceanographic Research Papers*, *56*, 1143–1167, doi:10.1016/j.dsr.2009.04.001.

Bury, S. J., P. W. Boyd, T. Preston, G. Savidge, and N. J. P. Owens (2001), Size-fractionated primary production and nitrogen uptake during a North Atlantic phytoplankton bloom: implications for carbon export estimates, *Deep-Sea Research Part I-Oceanographic Research Papers*, *48*, 689–720.

Butman, C. A., W. D. Grant, and K. D. Stolzenbach (1986), Predictions of sediment trap biases in turbulent flows: a theoretical analysis based on observations from the literature, *Journal of Marine Research*, *44*, 601–644.

Cadée, G. C. (1985), Macroaggregates of *Emiliania huxleyi* in sediment traps, *Marine Ecology Progress Series*, *24*, 193–196.

Cai, P., M. Dai, D. Lv, and W. Chen (2006), An improvement in the small-volume technique for determining thorium-234 in seawater, *Marine Chemistry*, *100*, 282–288.

Cai, P., M. Rutgers van der Loeff, I. Stimac, E.-M. Nöthig, K. Lepore, and S. B. Moran (2010), Low export flux of particulate organic carbon in the central Arctic Ocean as revealed by ^{234}Th:^{238}U disequilibrium, *Journal of Geophysical Research*, *115*, doi:10.1029/2009JC005595.

Cardinal, D., N. Savoye, T. W. Trull, L. André, E. E. Kopczynska, and F. Dehairs (2005), Variations of carbon remineralisation in the Southern Ocean illustrated by the Ba_{xs} proxy, *Deep-Sea Research Part I-Oceanographic Research Papers*, *52*, 355–370.

Caron, D. A., L. P. Madin, and J. J. Cole (1989), Composition and degradation of salp fecal pellets: implications for vertical flux in oceanic environments, *Journal of Marine Research*, *47*, 829–850.

Caron, D. A., A. F. Michaels, N. R. Swanberg, and F. A. Howse (1995), Primary productivity by symbiont-bearing planktonic sarcodines (Acantharia, Radiolaria, Foraminifera) in surface waters near Bermuda, *Journal of Plankton Research*, *17*, 103–129.

Casey, R. E. (1971), Distribution of polycystine Radiolaria in the oceans in relation to physical and chemical conditions, in *The Micropalaeontology of the Oceans*, edited by B. M. Funnel and W. R. Riedel, pp. 151–159, Cambridge University Press.

Cassar, N., B. A. Barnett, M. L. Bender, J. Kaiser, R. C. Hamme, and B. Tilbrook (2009), Continuous high-frequency dissolved O_2/Ar measurements by equilibrator inlet mass spectrometry, *Analytical Chemistry*, *81*, 1855–1864.

Chase, Z., R. F. Anderson, M. Q. Fleisher, and P. W. Kubik (2003), Scavenging of ^{230}Th, ^{231}Pa and ^{10}Be in the Southern Ocean (SW Pacific sector): the importance of particle flux, particle composition and advection, *Deep-Sea Research Part II-Topical Studies in Oceanography*, *50*, 739–768.

Checkley, D. M., R. E. Davis, A. W. Herman, G. A. Jackson, B. Beanlands, and L. A. Regier (2008), Assessing plankton and other particles in situ with the SOLOPC, *Limnology & Oceanography*, *53*(5/2), 2123–2136.

Chen, J. H., R. L. Edwards, and G. J. Wasserburg (1986), ^{238}U, ^{234}U and ^{232}Th in seawater, *Earth and Planetary Science Letters*, *80*, 241–251.

Cho, B. C., and F. Azam (1988), Major role of bacteria in biogeochemical fluxes in the ocean's interior, *Nature*, *332*, 441–443.

Christian, J. R., M. R. Lewis, and D. M. Karl (1997), Vertical fluxes of carbon, nitrogen, and phosphorus in the North Pacific Subtropical Gyre near Hawaii, *Journal of Geophysical Research*, *102*(C7), 15,667–15,677.

Cleveland, W. S., and S. J. Devlin (1988), Locally weighted regression: an approach to regression analysis by local fitting, *Journal of the American Statistical Association*, *83*(403), 596–610.

Coale, K. H. (1990), Labyrinth of doom: a device to minimize the "swimmer" component in sediment trap collections, *Limnology & Oceanography*, *35*(6), 1376–1381.

Coale, K. H. (1991), Effects of iron, manganese, copper, and zinc enrichments on productivity and biomass in the subarctic Pacific, *Limnology & Oceanography*, *36*(8), 1851–1864.

Coale, K. H., and K. W. Bruland (1985), ^{234}Th:^{238}U disequilibria within the California Current, *Limnology & Oceanography*, *30*(1), 22–33.

Coale, K. H., and K. W. Bruland (1987), Oceanic stratified euphotic zone as elucidated by ^{234}Th:^{238}U disequilibria, *Limnology & Oceanography*, *32*(1), 189–200.

Coale, K. H., K. S. Johnson, F. P. Chavez, K. O. Buesseler, R. T. Barber, M. A. Brzezinski, W. P. Cochlan, F. J. Millero, P. G. Falkowski, J. E. Bauer, R. H. Wanninkhof, R. M. Kudela, M. A. Altabet, B. E. Hales, T. Takahashi, M. R. Landry, R. R. Bidigare, X. Wang, Z. Chase, P. G. Strutton, G. E. Friederich, M. Y. Gorbunov, V. P. Lance, A. K. Hilting, M. R. Hiscock, M. Demarest, W. T. Hiscock, K. F. Sullivan, S. J. Tanner, R. M. Gordon, C. N. Hunter, V. A. Elrod, S. E. Fitzwater, J. L. Jones, S. Tozzi, M. Kobližek, A. E. Roberts, J. Hernodon, J. Brewster, N. Ladizinsky, G. Smith, D. Cooper, D. Timothy, S. L. Brown, K. E. Selph, C. C. Sheridan, B. S. Twining, and Z. I. Johnson (2004), Southern Ocean iron enrichment experiment: carbon cycling in high- and low-Si waters, *Science*, *304*, 408–414, doi:10.1126/science.1089778.

Cochran, J. K., K. O. Buesseler, M. P. Bacon, H. W. Wang, D. J. Hirschberg, L. Ball, J. Andrews, G. Crossin, and A. Fleer (2000), Short-lived thorium isotopes (^{234}Th, ^{228}Th) as indicators of POC export and particle cycling in the Ross Sea, Southern Ocean, *Deep-Sea Research Part II-Topical Studies in Oceanography*, *47*, 3451–3490, doi:10.1016/S0967-0645(00)00075-8.

Cochran, J. K., J. C. Miquel, R. Armstrong, S. W. Fowler, P. Masqué, B. Gasser, D. Hirschberg, J. Szlosek, A. M. Rodriguez y Baena, E. Verdeny, and G. M. Stewart (2009), Time-series measurements of ^{234}Th in water column and sediment trap samples from the northwestern Mediterranean Sea, *Deep-Sea Research Part II-Topical Studies in Oceanography*, *56*, 1487–1501, doi:10.1016/j.dsr2.2008.12.034.

Colley, S., J. Thomson, and P. P. Newton (1995), Detailed ^{230}Th, ^{232}Th and ^{210}Pb fluxes recorded by the 1989/90 BOFS sediment trap time-series at 48°N, 20°W, *Deep-Sea Research Part I-Oceanographic Research Papers*, *42*(6), 833–848.

Conley, D. J. (1998), An interlaboratory comparison for the measurement of biogenic silica in sediments, *Marine Chemistry*, *63*, 39–48.

Conte, M. H., N. Ralph, and E. H. Ross (2001), Seasonal and interannual variability in deep ocean particle fluxes at the Oceanic Flux Program (OFP)/Bermuda Atlantic Time Series (BATS) site in the western Sargasso Sea near Bermuda, *Deep-Sea Research Part II-Topical Studies in Oceanography*, *48*, 1471–1505.

Copin-Montegut, C., and G. Copin-Montegut (1983), Stoichiometry of carbon, nitrogen, and phosphorus in marine particulate matter, *Deep-Sea Research*, *30*(1), 31–46.

Craig, H., and T. Hayward (1987), Oxygen supersaturation in the ocean: biological versus physical contributions, *Science*, *235*, 199–202.

Cullen, J. J. (1982), The deep chlorophyll maximum: comparing vertical profiles of chlorophyll *a*, *Canadian Journal of Fisheries and Aquatic Sciences*, *39*, 791–803.

Dam, H. G., and D. T. Drapeau (1995), Coagulation efficiency, organic-matter glues and the dynamics of particles during a phytoplankton bloom in a mesocosm study, *Deep-Sea Research Part II-Topical Studies in Oceanography*, *42*, 111–123.

D'Asaro, E. A. (2008), Convection and the seeding of the North Atlantic bloom, *Journal of Marine Systems*, *69*, 233–237.

Davoll, P. J., and M. Y. Youngbluth (1990), Heterotrophic activity on appendicularian (Tunicata: Appendicularia) houses in mesopelagic regions and their potential contribution to particle flux, *Deep-Sea Research*, *37*(2), 285–294.

de Baar, H. J. W., P. W. Boyd, K. H. Coale, M. R. Landry, A. Tsuda, P. Assmy, D. C. E. Bakker, Y. Bozec, R. T. Barber, M. A. Brzezinski, K. O. Buesseler, M. Boyé, P. L. Croot, F. Gervais, M. Y. Gorbunov, P. J. Harrison, W. T. Hiscock, P. Laan, C. Lancelot, C. S. Law, M. Levasseur, A. Marchetti, F. J. Millero, J. Nishioka, Y. Nojiri, T. van Oijen, U. Riebesell, M. J. A. Rijkenberg, H. Saito, S. Takeda, K. R. Timmermans, M. J. W. Veldhuis, A. M. Waite, and C.-S. Wong (2005), Synthesis of iron fertilization experiments: from the Iron Age in the Age of Enlightenment, *Journal of Geophysical Research*, *110*, doi:10.1029/2004JC002601.

De Deckker, P. (2004), On the celestite-secreting Acantharia and their effect on seawater strontium to calcium ratios, *Hydrobiologia*, *517*, 1–13.

De La Rocha, C. L., and U. Passow (2007), Factors influencing the sinking of POC and the efficiency of the biological carbon pump, *Deep-Sea Research Part II-Topical Studies in Oceanography*, *54*, 639–658.

De La Rocha, C. L., N. Nowald, and U. Passow (2008), Interactions between diatom aggregates, minerals, particulate organic carbon, and dissolved organic matter: Further implications for the ballast hypothesis, *Global Biogeochemical Cycles*, *22*, doi:10.1029/2007gb003156.

de Villiers, S. (1999), Seawater strontium and Sr/Ca variability in the Atlantic and Pacific oceans, *Earth and Planetary Science Letters*, *171*, 623–634.

d'Ovidio, F., S. De Monte, S. Alvain, Y. Dandonneau, and M. Lévy (2010), Fluid dynamical niches of phytoplankton types, *Proceedings of the National Academy of Sciences of the United States of America*, *107*(43), 18,366–18,370, doi:10.1073/pnas.1004620107.

Dugdale, R. C., and J. J. Goering (1967), Uptake of new and regenerated forms of nitrogen in primary productivity, *Limnology & Oceanography*, *12*(2), 196–206.

Dugdale, R. C., F. P. Wilkerson, and H. J. Minas (1995), The role of a silicate pump in driving new production, *Deep-Sea Research Part I-Oceanographic Research Papers*, *42*(5), 697–719.

Dunne, J. P., J. L. Sarmiento, and A. Gnanadesikan (2007), A synthesis of global particle export from the surface ocean and cycling through the ocean interior and on the seafloor, *Global Biogeochemical Cycles*, *21*, doi:10.1029/2006GB002907.

Dutkiewicz, S., M. J. Follows, P. Heimbach, and J. Marshall (2006), Controls on ocean productivity and air-sea carbon flux: An adjoint model sensitivity study, *Geophysical Research Letters*, *33*, doi:10.1029/2005GL024987.

Ebersbach, F., and T. W. Trull (2008), Sinking particle properties from polyacrylamide gels during the KErguelen Ocean and Plateau compared Study (KEOPS): Zooplankton control of carbon export in an area of persistent natural iron inputs in the Southern Ocean, *Limnology & Oceanography*, *53*(1), 212–224.

Engel, A. (2000), The role of transparent exopolymer particles (TEP) in the increase in apparent particle stickiness (alpha) during the decline of a diatom bloom, *Journal of Plankton Research*, *22*, 485–497.

Eppley, R. W., and B. J. Peterson (1979), Particulate organic matter flux and planktonic new production in the deep ocean, *Nature*, *282*, 677–680.

Falkowski, P. G., R. T. Barber, and V. Smetacek (1998), Biogeochemical controls and feedbacks on ocean primary productivity, *Science*, *281*, 200–206.

Fenchel, T. (2008), The microbial loop — 25 years later, *Journal of Experimental Marine Biology and Ecology*, *366*, 99–103, doi:10.1016/j.jembe.2008.07.013.

Fischer, G., and G. Karakaş (2009), Sinking rates and ballast composition of particles in the Atlantic Ocean: implications for the organic carbon fluxes to the deep ocean, *Biogeosciences*, *6*, 85–102.

Fleisher, M. Q., and R. F. Anderson (2003), Assessing the collection efficiency of Ross Sea sediment traps using ^{230}Th and ^{231}Pa, *Deep-Sea Research Part I-Oceanographic Research Papers*, *50*, 693–712.

François, R., S. Honjo, R. Krishfield, and S. Manganini (2002), Factors controlling the flux of organic carbon to the bathypelagic zone of the ocean, *Global Biogeochemical Cycles*, *16*, doi:10.1029/2001GB001722.

Frankignoulle, M., and C. Canon (1994), Marine calcification as a source of carbon dioxide: positive feedback of increasing atmospheric CO_2, *Limnology & Oceanography*, *39*(2), 458–462.

Friedlingstein, P., R. A. Houghton, G. Marland, J. Hackler, T. A. Boden, T. J. Conway, J. G. Canadell, M. R. Raupach, P. Ciais, and C. Le Quéré (2010), Update on CO_2 emissions, *Nature Geoscience*, *3*, 811–812.

Gärdes, A., M. H. Iversen, H.-P. Grossart, U. Passow, and M. S. Ullrich (2011), Diatom-associated bacteria are required for aggregation of *Thalassiosira weissflogii*, *The ISME Journal*, *5*, 436–445, doi:10.1038/ismej.2010.145.

Gardner, W. D. (1980a), Sediment trap dynamics and calibration: a laboratory evaluation, *Journal of Marine Research*, *38*, 17–39.

Gardner, W. D. (1980b), Field assessment of sediment traps, *Journal of Marine Research*, *38*, 41–52.

Gardner, W. D. (1985), The effect of tilt on sediment trap efficiency, *Deep-Sea Research*, *32*(3), 349–361.

Gardner, W. D., and Y. Zhang (1997), The effect of brine on the collection efficiency of cylindrical sediment traps, *Journal of Marine Research*, *55*, 1029–1048.

Gardner, W. D., K. R. Hinga, and J. Marra (1983), Observations on the degradation of biogenic material in the deep ocean with implications on accuracy of sediment trap fluxes, *Journal of Marine Research*, *41*, 195–214.

Gardner, W. D., P. E. Biscaye, and M. J. Richardson (1997), A sediment trap experiment in the Vema Channel to evaluate the effect of horizontal particle fluxes on measured vertical fluxes, *Journal of Marine Research*, *55*, 995–1028.

Gilg, I. C., L. A. Amaral-Zettler, P. D. Countway, S. Moorthi, A. Schnetzer, and D. A. Caron (2010), Phylogenetic affiliations of mesopelagic acantharia and acantharian-like environmental 18S rRNA genes off the southern California coast, *Protist*, *161*(2), 197–211.

González, H. E., and V. Smetacek (1994), The possible role of the cyclopoid copepod *Oithona* in retarding vertical flux of zooplankton faecal material, *Marine Ecology Progress Series*, *113*, 233–246.

González, H. E., V. C. Ortiz, and M. Sobarzo (2000), The role of faecal material in the particulate organic carbon flux in the northern Humbolt Current, Chile (23°S), before and during the 1997–1998 El Niño, *Journal of Plankton Research*, *22*(3), 499–529.

González, H. E., D. Hebbeln, J. L. Iriarte, and M. Marchant (2004), Downward fluxes of faecal material and microplankton at 2300 m depth in the oceanic area of Coquimbo (30°S), Chile, during 1993–1995, *Deep-Sea Research Part II-Topical Studies in Oceanography*, *51*, 2457–2474, doi:10.1016/j.dsr2.2004.07.027.

Gordon, L. I., J. C. Jennings, A. A. Ross, and J. M. Krest (1994), *A suggested protocol for continuous flow automated analysis of seawater nutrients (phosphate, nitrate, nitrite, and silicic acid) in the WOCE Hydrographic Program and the Joint Global Ocean Fluxes Study. WHP Operations and Methods*, WOCE Hydrographic Program Office, methods manual 19-1 ed.

Gorsky, G., M. Picheral, and L. Stemmann (2000), Use of the Underwater Video Profiler for the study of aggregate dynamics in the North Mediterranean, *Estuarine, Coastal and Shelf Science*, *50*, 121–128.

Gowing, M. M., and K. F. Wishner (1998), Feeding ecology of the copepod *Lucicutia* aff. *L. grandis* near the lower interface of the Arabian Sea oxygen minimum zone, *Deep-Sea Research Part II-Topical Studies in Oceanography*, *45*, 2433–2359.

Green, D. R. H., M. J. Cooper, C. R. German, and P. A. Wilson (2003), Optimization of an inductively coupled plasma-optical emission spectrometry method for the rapid determination of high-precision Mg/Ca and Sr/Ca in foraminiferal calcite, *Geochemistry Geophysics Geosystems*, *4*(6), doi:10.1029/2002GC000488.

Guidi, L., L. Stemmann, L. Legendre, M. Picheral, L. Prieur, and G. Gorsky (2007), Vertical distribution of aggregates ($> 110\,\mu m$) and mesoscale activity in the northeastern Atlantic: Effects on the deep vertical export of surface carbon, *Limnology & Oceanography*, *52*, 7–18.

Guieu, C., M. Roy-Barman, N. Leblond, C. Jeandel, M. Souhaut, B. Le Cann, A. Dufour, and C. Bournot (2005), Vertical particle flux in the northeast Atlantic Ocean (POMME experiment), *Journal of Geophysical Research*, *110*, doi:10.1029/2004JC002672.

Gust, G., A. F. Michaels, R. Johnson, W. G. Deuser, and W. Bowles (1994), Mooring line motions and sediment trap hydrodynamics: *in situ* intercomparison of three common deployment designs, *Deep-Sea Research Part I-Oceanographic Research Papers*, *41*(5-6), 831–857.

Gustafsson, Ö., P. Andersson, P. Roos, Z. Kukulska, D. Broman, U. Larsson, S. Hajdu, and J. Ingri (2004), Evaluation of the collection efficiency of upper ocean sub-photic-layer sediment traps: a 24-month in situ calibration in the open Baltic Sea using ^{234}Th, *Limnology & Oceanography: Methods*, *2*, 62–74.

Hamm, C. E. (2002), Interactive aggregation and sedimentation of diatoms and clay-sized lithogenic material, *Limnology & Oceanography*, *47*(6), 1790–1795.

Harvey, M. J., C. S. Law, M. J. Smith, J. A. Hall, E. R. Abraham, C. L. Stevens, M. G. Hadfield, D. T. Ho, B. Ward, S. D. Archer, J. M. Cainey, K. I. Currie, D. Devies, M. J. Ellwood, P. Hill, G. B. Jones, D. Katz, J. Kuparinen, B. Macaskill, W. Main, A. Marriner, J. McGregor, C. McNeil, P. J. Minnett, S. D. Nodder, J. Peloquin, S. Pickmere, M. H. Pinkerton, K. A. Safi, R. Thompson, M. Walkington, S. W. Wright, and L. A. Ziolkowski (2010), The SOLAS air-sea gas exchange experiment (SAGE) 2004, *Deep-Sea Research Part II-Topical Studies in Oceanography*, doi:10.1016/j.dsr2.2010.10.015.

Hedges, J. I., and R. G. Keil (1995), Sedimentary organic matter preservation — an assessment and speculative synthesis, *Marine Chemistry*, *49*(2-3), 81–115.

Hedges, J. I., and J. H. Stern (1984), Carbon and nitrogen determinations of carbonate-containing solids, *Limnology & Oceanography*, *29*(3), 657–663.

Hedges, J. I., C. Lee, S. G. Wakeham, P. J. Hernes, and M. L. Peterson (1993), Effects of poisons and preservatives on the fluxes and elemental compositions of sediment trap materials, *Journal of Marine Research*, *51*, 651–668.

Hedges, J. I., J. A. Baldock, Y. Gélinas, C. Lee, M. Peterson, and S. G. Wakeham (2001), Evidence for non-selective preservation of organic matter in sinking marine particles, *Nature*, *409*, 801–804.

Henderson, G. M., and R. F. Anderson (2003), The U-series toolbox for paleoceanography, in *Reviews in Mineralogy and Geochemistry*, vol. 52, pp. 493–531, Mineralogical Society of America, doi:10.2113/0520493.

Henderson, G. M., C. Heinze, R. F. Anderson, and A. M. E. Winguth (1999), Global distribution of the ^{230}Th flux to ocean sediments constrained by GCM modelling, *Deep-Sea Research Part I-Oceanographic Research Papers*, *46*, 1861–1893.

Henjes, J., P. Assmy, C. Klaas, and V. Smetacek (2007), Response of the larger protozooplankton to an iron-induced phytoplankton bloom in the Polar Frontal Zone of the Southern Ocean (EisenEx), *Deep-Sea Research Part I-Oceanographic Research Papers*, *54*, 774–791, doi:10.1016/j.dsr.2007.02.005.

Henson, S. A., R. Sanders, C. Holeton, and J. T. Allen (2006), Timing of nutrient depletion, diatom dominance and a lower-boundary estimate of export production for Irminger Basin, North Atlantic, *Marine Ecology Progress Series*, *313*, 73–84.

Henson, S. A., J. P. Dunne, and J. L. Sarmiento (2009), Decadal variability in North Atlantic phytoplankton blooms, *Journal of Geophysical Research-Oceans*, *114*, doi:10.1029/2008JC005139.

Henson, S. A., R. Sanders, E. Madsen, P. J. Morris, F. Le Moigne, and G. D. Quartly (2011), A reduced estimate of the strength of the ocean's biological carbon pump, *Geophysical Research Letters*, *38*, doi:10.1029/2011GL046735.

Hillebrand, H., C.-D. Dürselen, D. Kirschtel, U. Pollinger, and Z. Tamar (1999), Biovolume calculation for pelagic and benthic microalgae, *Journal of Phycology*, *35*, 403–424.

Hollande, A., J. Cachon, and M. Cachon-Enjumet (1965), Les modalités de l'enkystement présporogénétique chez les acanthaires, *Protistologica*, *1*, 91–112.

Holligan, P. M., E. Fernández, J. Aiken, W. M. Balch, P. Boyd, P. H. Burkill, M. Finch, S. B. Groom, G. Malin, K. Muller, D. A. Purdie, C. Robinson, C. C. Trees, S. M. Turner, and P. van der Wal (1993), A biogeochemical study of the coccolithophore, *Emiliania huxleyi*, in the North Atlantic, *Global Biogeochemical Cycles*, *7*(4), 879–900.

Honjo, S. (1976), Coccoliths: production, transportation and sedimentation, *Marine Micropaleontology*, *1*, 65–79.

Honjo, S., and S. J. Manganini (1993), Annual biogenic particle fluxes to the interior of the North Atlantic Ocean; studied at 34°N 21°W and 48°N 21°W, *Deep-Sea Research Part II-Topical Studies in Oceanography*, *40*, 587–607.

Honjo, S., S. J. Manganini, R. A. Krishfield, and R. François (2008), Particulate organic carbon fluxes to the ocean interior and factors controlling the biological pump: A synthesis of global sediment trap programs since 1983, *Progress in Oceanography*, *76*, 217–285.

Ingalls, A. E., C. Lee, S. G. Wakeham, and J. I. Hedges (2003), The role of biominerals in the sinking flux and preservation of amino acids in the Southern Ocean along 170 degrees W, *Deep-Sea Research Part II-Topical Studies in Oceanography*, *50*, 713–738.

IPCC (2007), *Climate Change 2007: The Physical Science Basis. Contribution of Working Group I to the Fourth Assessment Report of the Intergovernmental Panel on Climate Change*, Cambridge University Press.

Iversen, M. H., and L. K. Poulsen (2007), Coprorhexy, coprophagy, and coprochaly in the copepods *Calanus helgolandicus*, *Pseudocalanus elongatus*, and *Oithona similis*, *Marine Ecology Progress Series*, *350*, 79–89, doi:10.3354/meps07095.

Jackson, G. A. (1993), Flux feeding as a mechanim for zooplankton grazing and its implications for vertical particulate flux, *Limnology & Oceanography*, *38*(6), 1328–1331.

Jacquet, S. H. M., J. Henjes, F. Dehairs, A. Worobiec, N. Savoye, and D. Cardinal (2007), Particulate Babarite and acantharians in the Southern Ocean during the European Iron Fertilization Experiment (EIFEX), *Journal of Geophysical Research*, *112*, doi:04010.01029/02006JG000394.

Jiao, N., G. J. Hendl, D. A. Hansell, R. Benner, G. Kattner, S. W. Wilhelm, D. L. Kirchman, M. G. Weinbauer, T. Luo, F. Chen, and F. Azam (2010), Microbial production of recalcitrant dissolved organic matter: long-term carbon storage in the global ocean, *Nature Reviews Microbiology*, *8*, 593–599, doi:10.1038/nrmicro2386.

Jickells, T. D., P. P. Newton, P. King, R. S. Lampitt, and C. Boutle (1996), A comparison of sediment trap records of particle fluxes from 19 to 48°N in the northeast Atlantic and their relation to surface water productivity, *Deep-Sea Research Part I-Oceanographic Research Papers*, *43*(7), 971–986.

Juranek, L. W., R. C. Hamme, J. Kaiser, R. Wanninkhof, and P. D. Quay (2010), Evidence of O_2 consumption in underway seawater lines: implications for air-sea O_2 and CO_2 fluxes, *Geophysical Research Letters*, *37*, doi:10.1029/2009GL040423.

Kahl, L. A., A. Vardi, and O. Schofield (2008), Effects of phytoplankton physiology on export flux, *Marine Ecology Progress Series*, *354*, 3–19.

Kaiser, J., M. K. Reuer, B. Barnett, and M. L. Bender (2005), Marine productivity estimates from continuous O_2/Ar ratio measurements by membrane inlet mass spectrometry, *Geophysical Research Letters*, *32*, doi: 10.1029/2005GL023459.

Karl, D. M., and G. A. Knauer (1989), Swimmers: a recapitulation of the problem and a potential solution, *Oceanography*, *2*(1), 32–35.

Karl, D. M., R. Letelier, D. Hebel, L. Tupas, J. Dore, J. Christian, and C. Winn (1995), Ecosystem changes in the North Pacific subtropical gyre attributed to the 1991–1992 El Niño, *Nature*, *373*, 230–234.

Kemp, A. E. S., J. Pike, R. B. Pearce, and C. B. Lange (2000), The "Fall dump" — a new perspective on the role of a "shade flora" in the annual cycle of diatom production and export flux, *Deep-Sea Research Part II-Topical Studies in Oceanography*, *47*, 2129–2154.

Kiørboe, T., J. L. S. Hansen, A. L. Alldredge, G. A. Jackson, U. Passow, H. G. Dam, D. T. Drapeau, A. Waite, and C. M. Garcia (1996), Sedimentation of phytoplankton during a diatom bloom: Rates and mechanisms, *Journal of Marine Research*, *54*, 1123–1148.

Kiørboe, T., P. Tiselius, B. Mitchell-Innes, J. L. S. Hansen, A. W. Visser, and X. Mari (1998), Intensive aggregate formation with low vertical flux during an upwelling-induced diatom bloom, *Limnology & Oceanography*, *43*, 104–116.

Klaas, C., and D. E. Archer (2002), Association of sinking organic matter with various types of mineral ballast in the deep sea: Implications for the rain ratio, *Global Biogeochemical Cycles*, *16*, doi:10.1029/2001GB001765.

Kobari, T., A. Shinada, and A. Tsuda (2003), Functional roles of interzonal migrating mesozooplankton in the western subarctic Pacific, *Progress in Oceanography*, *57*, 279–298.

Kobari, T., D. K. Steinberg, A. Ueda, A. Tsuda, M. W. Silver, and M. Kitamura (2008), Impacts of ontogenetically migrating copepods on downward carbon flux in the western subarctic Pacific Ocean, *Deep-Sea Research Part II-Topical Studies in Oceanography*, *55*, 1648–1660, doi:10.1016/j.dsr2.2008.04.016.

Kranck, K., and T. G. Milligan (1988), Macroflocs from diatoms: in situ photography of particles in Bedford Basin, Nova Scotia, *Marine Ecology Progress Series*, *44*, 183–189.

Ku, T.-L., K. G. Knauss, and G. G. Mathieu (1977), Uranium in open ocean: concentration and isotopic composition, *Deep-Sea Research*, *24*, 1005–1017.

Kuwata, A., T. Hama, and M. Takahashi (1993), Ecophysiological characterization of 2 life forms, resting spores and resting cells, of a marine planktonic diatom, *Chaetoceros pseudocurvisetus*, formed under nutrient depletion, *Marine Ecology Progress Series*, *102*, 245–255.

Kwon, E. Y., F. Primeau, and J. L. Sarmiento (2009), The impact of remineralization depth on the air-sea carbon balance, *Nature Geoscience*, *2*, 630–635, doi:10.1038/NGEO612.

Lam, P. J., and J. K. B. Bishop (2007), High biomass, low export regimes in the Southern Ocean, *Deep-Sea Research Part II-Topical Studies in Oceanography*, *54*, 601–638.

Lamborg, C. H., K. O. Buesseler, J. Valdes, C. H. Bertrand, R. Bidigare, S. Manganini, S. Pike, D. K. Steinberg, T. Trull, and S. Wilson (2008), The flux of bio- and lithogenic material associated with sinking particles in the mesopelagic "twilight zone" of the northwest and north central Pacific Ocean, *Deep-Sea Research Part II-Topical Studies in Oceanography*, *55*, 1540–1563.

Lampitt, R. S. (1985), Evidence for the seasonal deposition of detritus to the deep-sea floor and its subsequent resuspension, *Deep-Sea Research Part A-Oceanographic Research Papers*, *32*, 885–897.

Lampitt, R. S., and A. N. Antia (1997), Particle flux in deep seas: regional characteristics and temporal variability, *Deep-Sea Research Part I-Oceanographic Research Papers*, *44*, 1377–1403.

Lampitt, R. S., T. Noji, and B. von Bodungen (1990), What happens to zooplankton faecal pellets? Implications for material flux, *Marine Biology*, *104*(1), 15–23, doi:10.1007/BF01313152.

Lampitt, R. S., K. F. Wishner, C. M. Turley, and M. V. Angel (1993), Marine snow studies in the Northeast Atlantic Ocean: distribution, composition and role as a food source for migrating plankton, *Marine Biology*, *116*, 689–702.

Lampitt, R. S., E. P. Achterberg, T. R. Anderson, J. A. Hughes, M. D. Iglesias-Rodriguez, B. A. Kelly-Gerreyn, M. Lucas, E. E. Popova, R. Sanders, J. G. Shepherd, D. Smythe-Wright, and A. Yool (2008a), Ocean fertilization: a potential means of geoengineering?, *Philosophical Transactions of the Royal Society A-Mathematical Physical and Engineering Sciences*, *366*, 3919–3945.

Lampitt, R. S., B. Boorman, L. Brown, M. Lucas, I. Salter, R. Sanders, K. Saw, S. Seeyave, S. J. Thomalla, and R. Turnewitsch (2008b), Particle export from the euphotic zone: Estimates using a novel drifting sediment trap, Th-234 and new production, *Deep-Sea Research Part I-Oceanographic Research Papers*, *55*, 1484–1502.

Lampitt, R. S., I. Salter, and D. Johns (2009), Radiolaria: Major exporters of organic carbon to the deep ocean, *Global Biogeochemical Cycles*, *23*, doi:1010.1029/2008GB003221.

Lampitt, R. S., I. Salter, B. A. de Cuevas, S. Hartman, K. E. Larkin, and C. A. Pebody (2010), Long-term variability of downward particle flux in the deep northeast Atlantic: Causes and trends, *Deep-Sea Research Part II-Topical Studies in Oceanography*, *57*, 1346–1361, doi:10.1016/j.dsr2.2010.01.011.

Lancelot, C. (1979), Gross excretion rates of natural marine phytoplankton and heterotrophic uptake of excreted products in the southern North Sea, as determined by short-term kinetics, *Marine Ecology Progress Series*, *1*, 179–186.

Landry, M. R., M. E. Ondrusek, S. J. Tanner, S. L. Brown, J. Constantinou, R. R. Bidigare, K. H. Coale, and S. Fitzwater (2000), Biological response to iron fertilization in the eastern equatorial Pacific (IronEx II). I. Microplankton community abundances and biomass, *Marine Ecology Progress Series*, *201*, 27–42.

Lao, Y., R. F. Anderson, W. S. Broecker, H. J. Hofmann, and W. Wolfli (1993), Particulate fluxes of ^{230}Th, ^{231}Pa, and ^{10}Be in the northeastern Pacific Ocean, *Geochimica et Cosmochimica Acta*, *57*, 205–217.

Laws, E. A. (1991), Photosynthetic quotients, new production and net community production in the open sea, *Deep-Sea Research*, *38*(1), 143–167.

Laws, E. A., P. G. Falkowski, W. O. Smith, H. Ducklow, and J. J. McCarthy (2000), Temperature effects on export production in the open ocean, *Global Biogeochemical Cycles*, *14*(4), 1231–1246.

Le Fèvre, J., L. Legendre, and R. B. Rivkin (1998), Fluxes of biogenic carbon in the Southern Ocean: roles of large microphagous zooplankton, *Journal of Marine Systems*, *17*, 325–345.

Le Quéré, C., C. Rödenbeck, E. T. Buitenhuis, T. J. Conway, R. Langenfels, A. Gomez, C. Labuschagne, M. Ramonet, T. Nakazawa, N. Metzl, N. Gillett, and M. Heimann (2007), Saturation of the Southern Ocean CO_2 sink due to recent climate change, *Science*, *316*, 1735–1738, doi:10.1126/science.1136188.

Leblanc, K., A. Leynaert, C. Fernandez, I. Rimmelin, T. Moutin, P. Raimbault, J. Ras, and B. Quéguiner (2005), A seasonal study of diatom dynamics in the North Atlantic during the POMME experiment (2001): evidence for Si limitation of the spring bloom, *Journal of Geophysical Research*, *110*, doi:10.1029/2004JC002621.

Leblanc, K., C. E. Hare, Y. Feng, G. M. Berg, G. R. DiTullio, A. Neeley, I. Benner, C. Sprengel, A. Beck, S. A. Sanudo-Wilhelmy, U. Passow, K. Klinck, J. M. Rowe, S. W. Wilhelm, C. W. Brown, and D. A. Hutchins (2009), Distribution of calcifying and silicifying phytoplankton in relation to environmental and biogeochemical parameters during the late stages of the 2005 North East Atlantic spring bloom, *Biogeosciences*, *6*, 2155–2179.

Lee, C., S. G. Wakeham, and J. I. Hedges (1988), The measurement of oceanic particle flux — are "swimmers" a problem?, *Oceanography*, *1*(2), 34–36.

Lee, C., J. I. Hedges, S. G. Wakeham, and N. Zhu (1992), Effectiveness of various treatments in retarding microbial activity in sediment trap material and their effects on the collection of swimmers, *Limnology & Oceanography*, *37*(1), 117–130.

Lee, C., M. L. Peterson, S. G. Wakeham, R. A. Armstrong, J. K. Cochran, J. C. Miquel, S. W. Fowler, D. Hirschberg, A. Beck, and J. Xue (2009), Particulate organic matter and ballast fluxes measured using time-series and settling velocity sediment traps in the northwestern Mediterranean Sea, *Deep-Sea Research Part II-Topical Studies in Oceanography*, *56*, 1420–1436, doi:10.1016/j.dsr2.2008.11.029.

Lenton, T. M., and N. E. Vaughan (2009), The radiative forcing potential of different climate geoengineering options, *Atmospheric Chemistry and Physics*, *9*, 5539–5561, doi:10.5194/acp-9-5539-2009.

Lochte, K., H. W. Ducklow, M. J. R. Fasham, and C. Stienen (1993), Plankton succession and carbon cycling at 47-Degrees-N-20-Degrees-W during the JGOFS North-Atlantic Bloom Experiment, *Deep-Sea Research Part II-Topical Studies in Oceanography*, *40*, 91–114.

Logan, B. E., and A. L. Alldredge (1989), Potential for increased nutrient-uptake by flocculating diatoms, *Marine Biology*, *101*, 443–450.

Logan, B. E., U. Passow, A. L. Alldredge, H. P. Grossart, and M. Simon (1995), Rapid formation and sedimentation of large aggregates is predictable from coagulation rates (half-lives) of transparent exopolymer particles (TEP), *Deep-Sea Research Part II-Topical Studies in Oceanography*, *42*, 203–214.

Loh, A. N., and J. E. Bauer (2000), Distribution, partitioning and fluxes of dissolved and particulate organic C, N and P in the eastern North Pacific and Southern Oceans, *Deep-Sea Research Part I-Oceanographic Research Papers*, *47*, 2287–2316.

Lutz, M., R. Dunbar, and K. Caldeira (2002), Regional variability in the vertical flux of particulate organic carbon in the ocean interior, *Global Biogeochemical Cycles*, *16*(3), doi:10.1029/2000GB001383.

Mackenzie, F. T. (1964), Strontium content and variable strontium-chlorinity relationship of Sargasso sea water, *Science*, *146*, 517–518.

Maiti, K., C. R. Benitez-Nelson, Y. Rii, and R. Bidigare (2008), The influence of a mature cyclonic eddy on particle export in the lee of Hawaii, *Deep-Sea Research Part II-Topical Studies in Oceanography*, *55*, 1445–1460, doi:10.1016/j.dsr2.2008.02.008.

Maiti, K., C. R. Benitez-Nelson, and K. O. Buesseler (2010), Insights into particle formation and remineralization using the short-lived radionuclide, Thorium-234, *Geophysical Research Letters*, *37*, doi:10.1029/2010GL044063.

Malej, A., and R. P. Harris (1993), Inhibition of copepod grazing by diatom exudates — a factor in the development of mucus aggregates, *Marine Ecology Progress Series*, *96*, 33–42.

Mari, X., and T. Kiørboe (1996), Abundance, size distribution and bacterial colonization of transparent exopolymeric particles (TEP) during spring in the Kattegat, *Journal of Plankton Research*, *18*, 969–986.

Martin, A. P., I. P. Wade, K. J. Richards, and K. J. Heywood (1998), The PRIME eddy, *Journal of Marine Research*, *56*, 439–462.

Martin, J. H. (1990), Glacial to interglacial CO_2 change: the iron hypothesis, *Paleoceanography*, *5*, 1–13.

Martin, J. H., and S. E. Fitzwater (1988), Iron deficiency limits phytoplankton growth in the northeast Pacific subarctic, *Nature*, *331*, 341–343.

Martin, J. H., G. A. Knauer, D. M. Karl, and W. W. Broenkow (1987), VERTEX - Carbon cycling in the Northeast Pacific, *Deep-Sea Research Part A-Oceanographic Research Papers*, *34*, 267–285.

Martin, P., J. T. Allen, M. J. Cooper, D. G. Johns, R. S. Lampitt, R. Sanders, and D. A. Teagle (2010), Sedimentation of acantharian cysts in the Iceland Basin: Strontium as a ballast for deep ocean particle flux, and implications for acantharian reproductive strategies, *Limnology & Oceanography*, *55*(2), 604–614.

Martin, P., R. S. Lampitt, M. J. Perry, R. Sanders, C. Lee, and E. D'Asaro (2011), Export and mesopelagic particle flux during a North Atlantic spring bloom, *Deep-Sea Research Part I-Oceanographic Research Papers*, *58*, 338–349, doi:10.1016/j.dsr.2011.01.006.

Martin-Jézéquel, V., M. Hildebrand, and M. A. Brzezinski (2000), Silicon metabolism in diatoms: Implications for growth, *Journal of Phycology*, *36*, 821–840.

McGillicuddy, D. J., A. R. Robinson, D. A. Siegel, H. W. Jannasch, R. Johnson, T. D. Dickey, J. McNeil, A. F. Michaels, and A. H. Knap (1998), Influence of mesoscale eddies on new production in the Sargasso Sea, *Nature*, *394*, 263–266.

McQuoid, M. R., and L. A. Hobson (1996), Diatom resting stages., *Journal of Phycology*, *32*, 889–902.

Meija, J., L. Yang, R. Sturgeon, and Z. Mester (2009), Mass bias fractionation laws for multi-collector ICPMS: assumptions and their experimental verification, *Analytical Chemistry*, *81*, 6774–6778, doi:10.1021/ac9008435.

Menden-Deuer, S., and E. J. Lessard (2000), Carbon to volume relationship for dinoflagellates, diatoms, and other protist plankton, *Limnology & Oceanography*, *45*(569-579).

Michaels, A. F. (1988), Vertical distribution and abundance of Acantharia and their symbionts, *Marine Biology*, *97*, 559–569.

Michaels, A. F. (1991), Acantharian abundance and symbiont productivity at the VERTEX seasonal station, *Journal of Plankton Research*, *13*, 399–418.

Michaels, A. F., M. W. Silver, M. M. Garcia, and G. A. Knauer (1990), Cryptic zooplankton "swimmers" in upper ocean sediment traps, *Deep-Sea Research*, *37*(8), 1285–1296.

Michaels, A. F., D. A. Caron, N. R. Swanberg, F. A. Howse, and C. M. Michaels (1995), Planktonic sarcodines (Acantharia, Radiolaria, Foraminifera) in surface waters near Bermuda — abundance, biomass and vertical flux, *Journal of Plankton Research*, *17*, 131–163.

Millero, F. J., S. Sotolongo, and M. Izaguirre (1987), The oxidation kinetics of Fe(II) in seawater, *Geochimica et Cosmochimica Acta*, *51*, 793–801.

Moran, S. B., M. A. Charette, J. A. Hoff, R. L. Edwards, and W. M. Landing (1997), Distribution of ^{230}Th in the Labrador Sea and its relation to ventilation, *Earth and Planetary Science Letters*, *150*, 151–160.

Morris, P. J., R. Sanders, R. Turnewitsch, and S. Thomalla (2007), ^{234}Th-derived particulate organic carbon export from an island-induced phytoplankton bloom in the Southern Ocean, *Deep-Sea Research Part II-Topical Studies in Oceanography*, *54*, 2208–2232, doi:10.1016/j.dsr2.2007.06.002.

Mortlock, R. A., and P. N. Froelich (1989), A simple method for the rapid-determination of biogenic opal in pelagic marine sediments, *Deep-Sea Research Part A-Oceanographic Research Papers*, *36*, 1415–1426.

Nelson, D. M., D. J. DeMaster, R. B. Dunbar, and W. O. Smith (1996), Cycling of organic carbon and biogenic silica in the Southern Ocean: Estimates of water-column and sedimentary fluxes on the Ross Sea continental shelf, *Journal of Geophysical Research-Oceans*, *101*, 18,519–18,532.

Neuer, S., V. Ratmeyer, R. Davenport, G. Fischer, and G. Wefer (1997), Deep water particle flux in the Canary Island region: seasonal trends in relation to long-term satellite derived pigment data and lateral sources, *Deep-Sea Research Part I-Oceanographic Research Papers*, *44*(8), 1451–1466.

Newton, P. P., R. S. Lampitt, T. D. Jickells, P. King, and C. Boutle (1994), Temporal and spatial variability of biogenic particle fluxes during the JGOFS northeast Atlantic process studies at 47°N, 20°W, *Deep-Sea Research Part I-Oceanographic Research Papers*, *41*, 1617–1642.

Nieuwenhuize, J., Y. E. M. Maas, and J. J. Middelburg (1994), Rapid analysis of organic carbon and nitrogen in particulate materials, *Marine Chemistry*, *45*, 217–224.

Nodder, S. D., and A. M. Waite (2001), Is Southern Ocean organic carbon and biogenic silica export enhanced by iron-stimulated increases in biological production? Sediment trap results from SOIREE, *Deep-Sea Research Part II-Topical Studies in Oceanography*, *48*, 2681–2701.

Noji, T. T., K. W. Estep, F. Macintyre, and F. Norrbin (1991), Image analysis of faecal mterial grazed upon by three species of copepods: evidence for coprorhexy, coprophagy, and coprochaly, *Journal of the Marine Biological Association of the United Kingdom*, *71*, 465–480.

Oku, O., and A. Kamatani (1995), Resting spore formation and phosphorus composition of the marine diatom *Chaetoceros pseudocurvisetus* under various nutrient conditions, *Marine Biology*, *123*, 393–399.

Pacala, S., and R. Socolow (2004), Stabilization Wedges: solving the climate problem for the next 50 years with current technologies, *Science*, *305*, 968–972, doi:10.1126/science.1100103.

Pace, M. L., G. A. Knauer, D. M. Karl, and J. H. Martin (1987), Primary production, new production, and vertical flux in the eastern Pacific Ocean, *Nature*, *325*, 803–804.

Parekh, P., S. Dutkiewicz, M. J. Follows, and T. Ito (2006), Atmospheric carbon dioxide in a less dusty world, *Geophysical Research Letters*, *33*, doi:10.1029/2005GL025098.

Passow, U. (2002), Transparent exopolymer particles (TEP) in aquatic environments, *Progress in Oceanography*, *55*, 287–333.

Passow, U. (2004), Switching perspectives: Do mineral fluxes determine particulate organic carbon fluxes or vice versa?, *Geochemistry Geophysics Geosystems*, *5*, doi:10.1029/2003gc000670.

Passow, U., and A. L. Alldredge (1994), Distribution, size and bacterial-colonization of transparent exopolymer particles (TEP) in the ocean, *Marine Ecology Progress Series*, *113*, 185–198.

Passow, U., and A. L. Alldredge (1995a), Aggregation of a diatom bloom in a mesocosm - the role of transparent exopolymer particles (TEP), *Deep-Sea Research Part II-Topical Studies in Oceanography*, *42*, 99–109.

Passow, U., and A. L. Alldredge (1995b), A dye-binding assay for the spectrophotometric measurement of transparent exopolymer particles (TEP), *Limnology & Oceanography*, *40*, 1326–1335.

Passow, U., and C. L. De La Rocha (2006), Accumulation of mineral ballast on organic aggregates, *Global Biogeochemical Cycles*, *20*, doi:10.1029/2005gb002579.

Passow, U., and R. Peinert (1993), The role of plankton in particle flux: two case studies from the northeast Atlantic, *Deep-Sea Research Part II-Topical Studies in Oceanography*, *40*(1-2), 573–585.

Passow, U., A. L. Alldredge, and B. E. Logan (1994), The role of particulate carbohydrate exudates in the flocculation of diatom blooms, *Deep-Sea Research Part I-Oceanographic Research Papers*, *41*, 335–357.

Passow, U., R. F. Shipe, A. Murray, D. K. Pak, M. A. Brzezinski, and A. L. Alldredge (2001), The origin of transparent exopolymer particles (TEP) and their role in the sedimentation of particulate matter, *Continental Shelf Research*, *21*, 327–346.

Passow, U., J. Dunne, J. W. Murray, L. Balistrieri, and A. L. Alldredge (2006), Organic carbon to Th-234 ratios of marine organic matter, *Marine Chemistry*, *100*, 323–336.

Peinert, R., and J.-C. Miquel (1994), The significance of frontal processes for vertical particle fluxes: a case study in the Alboran Sea (SW Mediterranean Sea), *Journal of Marine Systems*, *5*, 377–389.

Peinert, R., A. Antia, E. Bauerfeind, B. von Bodungen, O. Haupt, M. Krumbholz, I. Peeken, R. O. Ramseier, M. Voss, and B. Zeitzschel (2001), Particle flux variability in the polar and Atlantic biogeochemical provinces of the Nordic seas, in *The Northern North Atlantic: A Changing Environment*, edited by P. Schäfer, W. Ritzrau, M. Schlüter, and J. Thiede, pp. 53–68, Springer.

Peloquin, J., J. Hall, K. Safi, W. O. Smith, S. Wright, and R. van den Enden (2010), The response of phytoplankton to iron enrichment in Sub-Antarctic HNLCLSi waters: results from the SAGE experiment, *Deep-Sea Research Part II-Topical Studies in Oceanography*, doi:10.1016/j.dsr2.2010.10.021.

Phillips, B., P. Kremer, and L. P. Madin (2009), Defecation by *Salpa thompsoni* and its contribution to vertical flux in the Southern Ocean, *Marine Biology*, *156*, 455–467, doi:10.1007/s00227-008-1099-4.

Pike, S. M., K. O. Buesseler, J. Andrews, and N. Savoye (2005), Quantification of ^{234}Th recovery in small volume sea water samples by inductively coupled plasma-mass spectrometry, *Journal of Radioanalytical and Nuclear Chemistry*, *263*(2), 355–360.

Pollard, R. T., I. Salter, R. J. Sanders, M. I. Lucas, C. M. Moore, R. A. Mills, P. J. Statham, J. T. Allen, A. R. Baker, D. C. E. Bakker, M. A. Charette, S. Fielding, G. R. Fones, M. French, A. E. Hickman, R. J. Holland, J. A. Hughes, T. D. Jickells, R. S. Lampitt, P. J. Morris, F. H. Nédélec, M. Nielsdóttir, H. Planquette, E. E. Popova, A. J. Poulton, J. F. Read, S. Seeyave, T. Smith, M. Stinchcombe, S. Taylor, S. Thomalla, H. J. Venables, R. Williamson, and M. V. Zubkov (2009), Southern Ocean deep-water carbon export enhanced by natural iron fertilization, *Nature*, *457*, 577–580, doi:10.1038/nature07716.

Poulton, A. J., A. Charalampopoulou, J. R. Young, G. A. Tarran, M. I. Lucas, and G. D. Quartly (2010), Coccolithophore dynamics in non-bloom conditions during late summer in the central Iceland Basin (July–August 2007), *Limnology & Oceanography*, *55*(4), 1601–1613.

Ragueneau, O., N. Dittert, P. Pondaven, P. Treguer, and L. Corrin (2002), Si/C decoupling in the world ocean: is the Southern Ocean different?, *Deep-Sea Research Part II-Topical Studies in Oceanography*, *49*, 3127–3154.

Ragueneau, O., S. Schultes, K. Bidle, P. Claquin, and B. Moriceau (2006), Si and C interactions in the world ocean: Importance of ecological processes and implications for the role of diatoms in the biological pump, *Global Biogeochemical Cycles*, *20*, doi:10.1029/2006gb002688.

Ramaswamy, V., M. M. Sarin, and R. Rengarajan (2005), Enhanced export of carbon by salps during the northeast monsoon period in the northern Arabian Sea, *Deep-Sea Research Part II-Topical Studies in Oceanography*, *52*, 1922–1929, doi:10.1016/j.dsr2.2005.05.005.

Read, J. F., and R. T. Pollard (2001), A long-lived eddy in the Iceland Basin 1998, *Journal of Geophysical Research*, *106*(C6), 11,411–11,421.

Redfield, A. C., B. H. Ketchum, and F. A. Richards (1963), The influence of organisms on the composition of sea water, in *The Sea*, vol. 2, edited by M. N. Hill, pp. 26–77, Interscience, New York.

Reigstad, M., and P. Wassmann (2007), Does *Phaeocystis* spp. contribute significantly to vertical export of organic carbon?, *Biogeochemistry*, *83*, 217–234.

Reuer, M. J., B. A. Barnett, M. L. Bender, P. G. Falkowski, and M. B. Hendricks (2007), New estimates of Southern Ocean biological production rates from O_2/Ar ratios and the triple isotope composition of O_2, *Deep-Sea Research Part I-Oceanographic Research Papers*, *54*, 951–974, doi:10.1016/j.dsr.2007.02.007.

Richardson, A. J., A. W. Walne, A. W. G. John, T. D. Jonas, J. A. Lindley, D. W. Sims, D. Stevens, and M. Witt (2006), Using continuous plankton recorder data, *Progress in Oceanography*, *68*, 27–74.

Röthlisberger, R., M. Bigler, E. W. Wolff, F. Joos, E. Monnin, and M. A. Hutterli (2004), Ice core evidence for the extent of past atmospheric CO_2 change due to iron fertilisation, *Geophysical Research Letters*, *31*, doi:10.1029/2004GL020338.

Rothman, D. H., and D. C. Forney (2007), Physical model for the decay and preservation of marine organic carbon, *Science*, *316*, 1325–1328.

Rutgers van der Loeff, M., I. Vöge, and H. Lilienthal (2004), Automatisiertes Filtrationsverfahren und Filtrationssystem zur Verfahrensdurchführung, Patent Nr. 102004040248, Germany.

Rutgers van der Loeff, M., M. M. Sarin, M. Baskaran, C. Benitez-Nelson, K. O. Buesseler, M. Charette, M. Dai, Ö. Gustafsson, P. Masque, P. J. Morris, K. Orlandini, A. Rodriguez y Baena, N. Savoye, S. Schmidt, R. Turnewitsch, I. Vöge, and J. T. Waples (2006), A review of present techniques and methodological advances in analyzing ^{234}Th in aquatic systems, *Marine Chemistry*, *100*, 190–212.

Rutgers van der Loeff, M. M., and W. S. Moore (1999), Determination of natural radioactive tracers, in *Methods of Seawater Analysis*, edited by K. Grasshoff, M. Ehrhardt, and K. Kremling, pp. 365–397, Verlag Chemie, Weinheim.

Sabine, C. L., R. A. Feely, N. Gruber, R. M. Key, K. Lee, J. L. Bullister, R. Wanninkhof, C. S. Wong, D. W. R. Wallace, B. Tilbrook, F. J. Millero, T.-H. Peng, A. Kozyr, T. Ono, and A. F. Rios (2004), The oceanic sink for anthropogenic CO_2, *Science*, *305*, 367–371, doi:10.1126/science.1097403.

Salter, I. (2007), Particle fluxes in the north-east Atlantic and Southern Ocean, Ph.D. thesis, University of Southampton.

Salter, I., R. S. Lampitt, R. Sanders, A. Poulton, A. E. S. Kemp, B. Boorman, K. Saw, and R. Pearce (2007), Estimating carbon, silica and diatom export from a naturally fertilised phytoplankton bloom in the Southern Ocean using PELAGRA: A novel drifting sediment trap, *Deep-Sea Research Part II-Topical Studies in Oceanography*, *54*, 2233–2259.

Sampei, M., H. Sasaki, H. Hattori, A. Forest, and L. Fortier (2009), Significant contribution of passively sinking copepods to the downward export flux in Arctic waters, *Limnology & Oceanography*, *54*(6), 1894–1900.

Sanders, R., L. Brown, S. Henson, and M. Lucas (2005), New production in the Irminger Basin during 2002, *Journal of Marine Systems*, *55*, 291–310, doi:10.1016/j.jmarsys.2004.09.002.

Sanders, R., P. J. Morris, M. Stinchcombe, S. Seeyave, H. Venables, and M. Lucas (2007), New production and the f ratio around the Crozet Plateau in austral summer 2004–2005 diagnosed from seasonal changes in inorganic nutrient levels, *Deep-Sea Research Part II-Topical Studies in Oceanography*, *54*, 2191–2207, doi:10.1016/j.dsr2.2007.06.007.

Sanders, R., P. J. Morris, A. J. Poulton, M. C. Stinchcombe, A. Charalampopoulou, M. I. Lucas, and S. J. Thomalla (2010), Does a ballast effect occur in the surface ocean?, *Geophysical Research Letters*, *37*, doi:10.1029/2010GL042574.

Sarmiento, J. L., and N. Gruber (2006), *Ocean Biogeochemical Dynamics*, Princeton University Press, Princeton, USA.

Savidge, G., P. Boyd, A. Pomroy, D. Harbour, and I. Joint (1995), Phytoplankton production and biomass estimates in the Northeast Atlantic-Ocean, May to June 1990, *Deep-Sea Research Part I-Oceanographic Research Papers*, *42*, 599–617.

Savoye, N., C. Benitez-Nelson, A. B. Burd, J. K. Cochran, M. Charette, K. O. Buesseler, G. A. Jackson, M. Roy-Barman, S. Schmidt, and M. Elskens (2006), Th-234 sorption and export models in the water column: A review, *Marine Chemistry*, *100*, 234–249.

Savoye, N., T. W. Trull, S. H. M. Jacquet, J. Navez, and F. Dehairs (2008), ^{234}Th-based export fluxes during a natural iron fertilization experiment in the Southern Ocean (KEOPS), *Deep-Sea Research Part II-Topical Studies in Oceanography*, *55*, 841–855, doi:10.1016/j.dsr2.2007.12.036.

Schewiakoff, W. T. (1926), Die Acantharia, *Fauna e Flora del Golfo di Napoli*, *37*.

Schneider, B., R. Schlitzer, G. Fischer, and E. M. Nöthig (2003), Depth-dependent elemental compositions of particulate organic matter (POM) in the ocean, *Global Biogeochemical Cycles*, *17*, doi:10.1029/2002GB001871.

Scholten, J. C., J. Fietzke, S. Vogler, M. M. Rutgers van der Loeff, A. Mangini, W. Koeve, J. Waniek, P. Stoffers, A. Antia, and J. Kuss (2001), Trapping efficiencies of sediment traps from the deep Eastern North Atlantic: the ^{230}Th calibration, *Deep-Sea Research Part II-Topical Studies in Oceanography*, *48*, 2383–2408.

Scholten, J. C., J. Fietzke, A. Mangini, P. Stoffers, T. Rixen, B. Gaye-Haake, T. Blanz, V. Ramaswamy, F. Sirocko, H. Schulz, and V. Ittekot (2005), Radionuclide fluxes in the Arabian Sea: the role of particle composition, *Earth and Planetary Science Letters*, *230*, 319–337, doi:10.1016/j.epsl.2004.11.003.

Sherman, A. D., B. W. Hobson, P. R. McGill, R. E. Davis, M. C. McClune, and K. L. Smith (2011), Lagrangian sediment traps for sampling at discrete depths beneath free-drifting icebergs, *Deep-Sea Research Part II-Topical Studies in Oceanography*, doi:10.1016/j.dsr2.2010.11.008.

Siegel, D. A., and R. A. Armstrong (2002), Corrigendum to: "Trajectories of sinking particles in the Sargasso Sea: modeling of statistical funnels above deep-ocean sediment traps" [Deep-Sea Research I 44, 1519-1541], *Deep-Sea Research Part I-Oceanographic Research Papers*, *49*, 1115–1116.

Siegel, D. A., and W. G. Deuser (1997), Trajectories of sinking particles in the Sargasso Sea: modeling of statistical funnels above deep-ocean sediment traps, *Deep-Sea Research Part I-Oceanographic Research Papers*, *44*(9-10), 1519–1541.

Siegel, D. A., T. C. Granata, A. F. Michaels, and T. D. Dickey (1990), Mesoscale eddy diffusion, particle sinking, and the interpretation of sediment trap data, *Journal of Geophysical Research*, *95*(C4), 5305–5311.

Siegel, D. A., E. Fields, and K. O. Buesseler (2008), A bottom-up view of the biological pump: modeling source funnels above ocean sediment traps, *Deep-Sea Research Part I-Oceanographic Research Papers*, *55*, 108–127, doi:10.1016/j.dsr.2007.10.006.

Sieracki, M. E., P. G. Verity, and D. K. Stoecker (1993), Plankton community response to sequential silicate and nitrate depletion during the 1989 North-Atlantic spring bloom, *Deep-Sea Research Part II-Topical Studies in Oceanography*, *40*, 213–225.

Smayda, T. J. (1970), The suspension and sinking of phytoplankton in the sea, *Oceanography and Marine Biology: An Annual Review*, *8*, 353–414.

Smetacek, V., and S. W. A. Naqvi (2008), The next generation of iron fertilization experiments in the Southern Ocean, *Philosophical Transactions of the Royal Society A-Mathematical Physical and Engineering Sciences*, *366*, 3947–3967.

Smetacek, V., P. Assmy, and J. Henjes (2004), The role of grazing in structuring Southern Ocean pelagic ecosystems and biogeochemical cycles, *Antarctic Science*, *16*(4), 541–558, doi:10.1017/S0954102004002317.

Smetacek, V. S. (1985), Role of sinking in diatom life-history cycles — ecological, evolutionary and geological significance, *Marine Biology*, *84*, 239–251.

Smith, D. C., M. Simon, A. L. Alldredge, and F. Azam (1992), Intense hydrolytic enzyme activity on marine aggregates and implications for rapid particle dissolution, *Nature*, *359*, 139–142.

Smith, W. O., and R. B. Dunbar (1998), The relationship between new production and vertical flux on the Ross Sea continental shelf, *Journal of Marine Systems*, *17*(445-457).

Spindler, M., and K. Beyer (1990), Distribution, abundance and diversity of Antarctic acantharian cysts, *Marine Micropaleontology*, *15*, 209–218.

Stanley, R. H. R., K. O. Buesseler, S. J. Manganini, D. K. Steinberg, and J. R. Valdes (2004), A comparison of major and minor elemental fluxes collected in neutrally buoyant and surface-tethered sediment traps, *Deep-Sea Research Part I-Oceanographic Research Papers*, *51*, 1387–1395, doi:10.1016/j.dsr.2004.05.010.

Steinberg, D. K. (1995), Diet of copepods (*Scopalatum vorax*) associated with mesopelagic detritus (giant larvacean houses) in Monterey Bay, California, *Marine Biology*, *122*, 571–584.

Steinberg, D. K., B. A. S. Van Mooy, K. O. Buesseler, P. W. Boyd, T. Kobari, and D. M. Karl (2008), Bacterial vs. zooplankton control of sinking particle flux in the ocean's twilight zone, *Limnology & Oceanography*, *53*(4), 1327–1338.

Suess, E. (1980), Particulate organic carbon flux in the oceans — surface productivity and oxygen utilisation, *Nature*, *288*, 260–263.

Sutherland, K. R., L. P. Madin, and R. Stocker (2010), Filtration of submicrometer particles by pelagic tunicates, *Proceedings of the National Academy of Sciences of the United States of America*, *107*(34), 15,129–15,134, doi:10.1073/pnas.1003599107.

Suttle, C. A. (2007), Marine viruses — major players in the global ecosystem, *Nature Reviews Microbiology*, *5*, 801–812, doi:10.1038/nrmicro1750.

Takahashi, T., S. C. Sutherland, C. Sweeney, A. Poisson, N. Metzl, B. Tilbrook, N. Bates, R. Wanninkhof, R. A. Feely, C. Sabine, J. Olafsson, and Y. Nojiri (2002), Global sea-air CO_2 flux based on climatological surface ocean pCO_2, and seasonal biological and temperature effects, *Deep-Sea Research Part II-Topical Studies in Oceanography*, *49*, 1601–1622.

Taucher, J., and A. Oschlies (2011), Can we predict the direction of marine primary production change under global warming?, *Geophysical Research Letters*, *38*, doi:10.1029/2010GL045934.

Thomalla, S., R. Turnewitsch, M. Lucas, and A. Poulton (2006), Particulate organic carbon export from the North and South Atlantic gyres: The Th-234/U-238 disequilibrium approach, *Deep-Sea Research Part II-Topical Studies in Oceanography*, *53*, 1629–1648.

Thomalla, S. J., A. J. Poulton, R. Sanders, R. Turnewitsch, P. M. Holligan, and M. I. Lucas (2008), Variable export fluxes and efficiencies for calcite, opal, and organic carbon in the Atlantic Ocean: a ballast effect in action?, *Global Biogeochemical Cycles*, *22*, doi:10.1029/2007GB002982.

Thomas, A. L. (2006), Variations in past and present ocean circulation assessed with U-series nuclides, Ph.D. thesis, University of Oxford.

Thornton, D. C. O. (2002), Diatom aggregation in the sea: mechanisms and ecological implications, *European Journal of Phycology*, *37*, 149–161.

Turner, J. T. (2002), Zooplankton fecal pellets, marine snow and sinking phytoplankton blooms, *Aquatic Microbial Ecology*, *27*, 57–102.

Tyrrell, T. (1999), The relative influences of nitrogen and phosphorus on oceanic primary production, *Nature*, *400*, 525–531.

Utermöhl, H. (1958), Zur Vervollkommnung der quantitativen Phytoplankton-Methodik, *Mitteilungen/Internationale Vereinigung für Theoretische und Angewandte Limnologie*, *9*, 1–38.

Valdes, J. R., and J. F. Price (2000), A neutrally buoyant, upper ocean sediment trap, *Journal of Atmospheric and Oceanic Technology*, *17*, 62–68.

Van Mooy, B. A. S., and A. H. Devol (2008), Assessing nutrient limitation of emphProchlorococcus in the North Pacific subtropical gyre by using an RNA capture method, *Limnology & Oceanography*, *53*(1), 78–88.

Verdeny, E., P. Masqué, K. Maiti, J. Garcia-Orellana, J. M. Bruach, C. Mahaffey, and C. R. Benitez-Nelson (2008), Particle export within cyclonic Hawaiian lee eddies derived from ^{210}Pb-^{210}Po disequilibrium, *Deep-Sea Research Part II-Topical Studies in Oceanography*, *55*, 1461–1472, doi:10.1016/j.dsr2.2008.02.009.

Vogler, S., J. Scholten, M. Rutgers van der Loeff, and A. Mangini (1998), ^{230}Th in the eastern North Atlantic: the importance of water mass ventilation in the balance of ^{230}Th, *Earth and Planetary Science Letters*, *156*, 61–74.

Volk, T., and M. I. Hoffert (1985), Ocean carbon pumps: analysis of relative strengths and efficiencies in ocean-driven atmospheric CO_2 changes, in *The carbon cycle and atmospheric CO_2: Natural variations Archean to Present*, edited by E. T. Sundquist and W. S. Broecker, pp. 99–110, AGU, Washington D.C.

von Bodungen, B. (1986), Phytoplankton growth and krill grazing during spring in the Bransfield Strait, Antarctica — Implications from sediment trap collections, *Polar Biology*, *6*, 153–160.

von Bodungen, B., U. Bathmann, M. Voss, and M. Wunsch (1990), Vertical particle flux in the Norwegian Sea — resuspension and interannual variability, in *Sediment Trap Studies in the Nordic Countries Symposium Proceedings*, vol. 2, edited by P. Wassmann, A.-S. Heiskanen, and O. Lindahl, pp. 116–136.

Waniek, J., W. Koeve, and R. D. Prien (2000), Trajectories of sinking particles and the catchment areas above sediment traps in the northeast Atlantic, *Journal of Marine Research*, *58*, 983–1006.

Waniek, J. J., D. E. Schulz-Bull, J. Kuss, and T. Blanz (2005), Long time series of deep water particle flux in three biogeochemical provinces of the northeast Atlantic, *Journal of Marine Systems*, *56*, 391–415, doi: 10.1016/j.jmarsys.2005.03.001.

Wassmann, P. (1998), Retention versus export food chains: processes controlling sinking loss from marine pelagic systems, *Hydrobiologia*, *363*, 29–57.

Weber, T. S., and C. Deutsch (2010), Ocean nutrient ratios governed by plankton biogeography, *Nature*, *467*, 550–554, doi:10.1038/nature09403.

Welling, L. A., N. G. Pisias, E. S. Johnson, and J. R. White (1996), Distribution of polycystine radiolaria and their relation to the physical environment during the 1992 El Niño and following cold event, *Deep-Sea Research Part II-Topical Studies in Oceanography*, *43*, 1413–1434.

Yebra, L., C. Almeida, and S. Hernández-León (2005), Vertical distribution of zooplankton and active flux across an anticyclonic eddy in the Canary Island waters, *Deep-Sea Research Part I-Oceanographic Research Papers*, *52*, 69–83, doi:10.1016/j.dsr.2004.08.010.

Yu, E.-F., R. François, M. P. Bacon, S. Honjo, A. P. Fleer, S. J. Manganini, M. M. Rutgers van der Loeff, and V. Ittekot (2001), Trapping efficiency of bottom-tethered sediment traps estimated from the intercepted fluxes of ^{230}Th and ^{231}Pa, *Deep-Sea Research Part I-Oceanographic Research Papers*, *48*, 865–889.

Zeebe, R. E., and D. Archer (2005), Feasibility of ocean fertilization and its impact on future atmospheric CO_2 levels, *Geophysical Research Letters*, *32*, doi:10.1029/2005GL022449.